Biocatalytic synthesis of statin side-chain precursors

Švarc, Anera

University of Zagreb

FACULTY OF CHEMICAL ENGINEERING AND TECHNOLOGY

Anera Švarc

BIOCATALYTIC SYNTHESIS OF STATIN SIDE-CHAIN PRECURSORS

DOCTORAL THESIS

Zagreb, 2020

SVEUČILIŠTE U ZAGREBU
FAKULTET KEMIJSKOG INŽENJERSTVA I TEHNOLOGIJE

Kandidatkinja Anera Švarc
predala je dana: 28. listopada 2019. doktorski rad izrađen pod mentorstvom prof. dr. sc. Ane Vrsalović Presečki, Fakultet kemijskog inženjerstva i tehnologije Sveučilišta u Zagrebu.

Povjerenstvo za ocjenu doktorskog rada u sastavu:

Prof. dr. sc. Zvjezdana Findrik Blažević, Fakultet kemijskog inženjerstva i tehnologije Sveučilišta u Zagrebu
Prof. emerita Đurđa Vasić-Rački, Fakultet kemijskog inženjerstva i tehnologije Sveučilišta u Zagrebu
Prof. dr. sc. Anett Schallmey, Institute for Biochemistry, Biotechnology and Bioinformatics, Technische Universität Braunschweig

pozitivno je ocijenilo doktorski rad doktorandice Anere Švarc, a Fakultetsko vijeće Fakulteta kemijskog inženjerstva i tehnologije Sveučilišta u Zagrebu na sjednici održanoj dana 16. prosinca 2019. prihvatilo je ocjenu i odobrilo obranu doktorskog rada pred povjerenstvom u istom sastavu.

Obrana doktorskog rada održana je dana 13. ožujka 2020.

D e k a n

Prof. dr. sc. Tomislav Bolanča

Sveučilište u Zagrebu

FAKULTET KEMIJSKOG INŽENJERSTVA I TEHNOLOGIJE

Anera Švarc

BIOKATALITIČKA SINTEZA PREKURSORA BOČNIH LANACA STATINA

DOKTORSKI RAD

Zagreb, 2020.

University of Zagreb

FACULTY OF CHEMICAL ENGINEERING AND TECHNOLOGY

Anera Švarc

BIOCATALYTIC SYNTHESIS OF STATIN SIDE-CHAIN PRECURSORS

DOCTORAL THESIS

Supervisor: Prof. Ana Vrsalović Presečki, PhD

Zagreb, 2020

Sveučilište u Zagrebu

FAKULTET KEMIJSKOG INŽENJERSTVA I TEHNOLOGIJE

Anera Švarc

BIOKATALITIČKA SINTEZA PREKURSORA BOČNIH LANACA STATINA

DOKTORSKI RAD

Mentor: prof. dr. sc. Ana Vrsalović Presečki

Zagreb, 2020.

BIBLIOGRAPHIC FACTS

UDK: 66.011:544.473:577.15:615.2(043.3)=111
Scientific area: Technical Sciences
Scientific field: Chemical Engineering
Scientific branch: Reaction Engineering
Institution: University of Zagreb, Faculty of Chemical Engineering and Technology**,** Department of Reaction Engineering and Catalysis
Supervisor: Prof. Ana Vrsalović Presečki, PhD
Number of pages: 194
Number of figures: 86
Number of tables: 36
Number of appendixes: 23
Number of references: 216

Date of defense: March 13th, 2020

The thesis defense committee members:

1. Prof. emer. Đurđa Vasić-Rački, PhD, Faculty of Chemical Engineering and Technology, University of Zagreb, Croatia
2. Prof. Zvjezdana Findrik Blažević, PhD, Faculty of Chemical Engineering and Technology, University of Zagreb, Croatia
3. Prof. Anett Schallmey, PhD, Institute for Biochemistry, Biotechnology and Bioinformatics, Technische Universität Braunschweig, Germany

The dissertation is stored at:

1. National and University Library in Zagreb, Hrvatske bratske zajednice bb, Zagreb
2. Faculty of Chemical Engineering and Technology Library, University of Zagreb, Marulićev trg 20, Zagreb
3. University of Rijeka Library, Dolac 1, Rijeka
4. University of Split Library, Livanjska 5, Split
5. University of Osijek Library, Europska avenija 24, Osijek

Dissertation topic was accepted on 218th session of Council of the Faculty of Chemical Engineering and Technology, University of Zagreb held on September 24th, 2018, and approved at 6th session of Senate of University of Zagreb held on January 22nd, 2019 in 350th academic year (2018/2019).

This thesis was done in the frame of the “CarbaZymes” project that has received funding from European Union's Horizon 2020 Research and Inovation Programme under Grant Agreement No 635595.

INFORMATION ABOUT THE SUPERVISOR

Ana Vrsalović Presečki [redacted] She started her studies at The Faculty of Chemical Engineering and Technology, University of Zagreb (FCET) in 1993. During her studies, she received two Rector's Awards for her scientific work (1994 and 1996). She graduated in 1999 and in January 2000 she started to work at the Department of Reaction Engineering and Catalyst, FCET, as an assistant. She got her master's degree in 2003 and her PhD in the field of chemical engineering in 2006. In 2009 she became an assistant professor at the Department of Reaction Engineering and Catalysis, FCET, Zagreb, in 2013 an associate professor, and in 2018 a full professor. In 2008 she received the Vera Johanides Award of Croatian Academy of Engineering. She has been trained at several foreign institutions: in 2001 (two months) and 2007 (one month) at Forschungszentrum Jülich, Institute für Biotechnologie 2, Germany, in 2005 (two weeks) at the Faculty of Chemistry and Chemical Engineering in Maribor, Slovenia and in 2008 and 2010 (two weeks) in Veszprem, Hungary at the Research Institute of Chemical and Process Engineering.

The area of scientific interest of prof. Vrsalović Presečki is applied biocatalysis and includes use of isolated enzymes or whole cells as biocatalysts, fermentation technology, studying biotransformations in batch or continuously operated enzyme membrane reactors. When studying biotransformations, she applies the chemical engineering methodology which includes mathematical modelling and process optimization – tools that are especially valuable in multi-enzyme reaction systems.

Her research results have been published in twenty-five scientific publications in CC and SCI indexed journals, while one scientific paper was cited in a secondary publication. She published three papers in proceedings from international scientific conferences, four papers in proceedings of other scientific conferences, and three papers in proceedings of national conference. She has given sixty-six presentations at international and national conferences. She was an associate of five national and seven international projects, and she was the principal investigator of the Croatian-Slovenian bilateral project Applied Biocatalysis – Integrated Catalytic Processes (2009 – 2010).

In the last five years she has been involved as an associate in the following projects: Horizon 2020: CarbaZymes – Sustainable industrial processes based on a C-C bond-forming enzyme platform (2015 – 2019; coordinator: Prof. Wolf-Dieter Fessner, PhD; principal

investigator: Prof. Zvjezdana Findrik Blažević, PhD) and HRZZ Installation Research Project: Synthesis and Target Application of Metallic Nanoparticles (2015 – 2017; principal investigator: Assoc. Prof. Iva Rezić).

She reviewed over thirty scientific articles in international scientific journals.

She teaches several courses in the field of technical science: undergraduate studies (Mass and Energy Balance, Biochemical Engineering, Introduction to Environmental Engineering), graduate studies (Biochemical Engineering, Bioreaction technique, Industrial Biotransformation, Environmental Engineering Laboratory) and PhD studies (Biochemical Engineering). She was a supervisor of seventeen BSc theses, sixteen MSc theses and one PhD thesis. She is currently a supervisor of three PhD theses.

She participated in the organization of twelve scientific and professional conferences, and she was an editor of seven proceedings and book of abstracts. She is a member of the Croatian Society of Chemical Engineers and Technologists and the Croatian Society for Biotechnology.

ACKNOWLEDGEMENTS

This PhD thesis was supported by the Horizon 2020 CarbaZymes project: Sustainable industrial processes based on a C-C bond-forming enzyme platform, with grant agreement number 635595. I would additionally like to acknowledge the support from the COST organization and the COST Action CM1303 - Systems Biocatalysis.

Thanks to the CarbaZymes project my PhD was an amazing journey that enriched my life and made me grow in every aspect!

I could not have imagined having a better advisor and mentor than my mentor Prof. Ana Vrsalović Presečki, PhD. I am proud to acknowledge that because of her knowledge, dedication, hard work, and sincere interest in the enzyme catalysis I was inspired to grow in the area of biocatalysis. I could not be more humbled that she was my mentor during two of my previous research projects awarded with a Dean's Awards, my Master's Thesis and now – my PhD Thesis. I am grateful for her continuous support of my PhD study and related research, for her motivation, for sharing her immense knowledge, for all the suggestions, insights and discussions. Her guidance helped me while researching and writing this thesis. I am thankful to her for always supporting my ideas and giving me the freedom to be me.

I would like to express my sincere gratitude towards Prof. Zvjezdana Findrik Blažević, PhD, our CarbaZymes PI, for taking me on her CarbaZymes team. Thanks to her and the CarbaZymes project, I was able to thrive, learn and deepen my skills and knowledge. If it was not for her support, I would not be able to acquaint renowned scientists, be up-to-date with the cutting edge of biocatalysis and widen my knowledge in the same area through summer schools and national and international conferences.

I am thankful to Prof. emer. Đurđa Vasić-Rački, PhD, for showing high interest in my work and progress. I am very honored for all her efforts expressed during the duration of the project on the topic of my PhD, her encouraging comments on my results, her openness towards strong discussions, and for sharing her enviable knowledge on the enzyme catalysis – and way beyond.

My sincere thanks also go to Prof. Anett Schallmey, PhD, who provided me with an opportunity to join her team in 2016 as a PhD Research Assistant Intern and for giving me access to the laboratory and research facilities. Without her support, it would not be possible to

conduct certain parts of this research. I am also thankful to her team for their openness, amicability, support, and for making me feel at home.

During the research, I was challenged at certain points. Thanks to Melinda Fekete, PhD, from Enzymicals, our project partner, I managed to overcome the encountered challenges and thus learn. Our discussions and her suggestions and organic chemistry insights were extremely helpful by enabling me to circumvent certain laborious work. I must admit that whenever we met in person, we had great fun, and I am happy to say I made a good friend for life!

I would like to thank my colleagues at the Department of Organic Chemistry at my Faculty: Irena, Ivana, Andrea, Andrijana, and Silvija, among the rest of their Department, for always being welcoming, offering suggestions in the aspect of organic chemistry when asked, and for letting me be part of the Department whenever I needed.

I thank my fellow labmates: Lela, Morana, Martin, Dino, Nevena, and Marina, for all the fun we have had in the last four years. My sincere appreciation also goes to my Faculty colleagues who have contributed to this thesis and supported me in any way.

I would also like to thank Milica, Emerik, Jelena, and Kristina for their contribution as well as for the fun we had during our experimenting.

A big thank you goes to my loving friends, Tanja and Tea, as well as to Ana, Anita, Antonella, Gloria, Hrvoje, Igor, Kristian, Maja S., Maja Š., Matea, Matej Š., Matija S., Matija Š., Matija T., and Zina, for all the deep and meaningful conversations, ultimate understanding, spiritual support, warm encouragements, and all the shared joy. I am also grateful for being surrounded by good friends who are not mentioned here but are worthy to me.

Finally, my special thank you goes to my family: my mom, dad, Ruth, Martin, and my late grandma, for always sticking with me, their endless patience with me, unconditional love and the enormous trust they put into me! I am so happy and proud that my accomplishments are theirs as well.

If it was not for you all, I would not be who and where I am today. Thank you for that!

Nothing in life is to be feared. It is only to be understood.

Marie Skłodowska Curie (1867 – 1934)

To my family

BIOCATALYTIC SYNTHESIS OF STATIN SIDE-CHAIN PRECURSORS

ABSTRACT

Statins, also known as 3-hydroxy-3-methylglutaryl coenzyme A (HMG-CoA) reductase inhibitors, are the most widely prescribed lipid-lowering drugs in the world. Even though well-established chemical approaches for the production of statins are employed, they are time-consuming and require a large number of steps. The increasing commercial demand for statins and requirements for their high chemical and stereochemical purity have led to immense efforts to find a more efficient and economical production of chiral statin side-chain precursors. Due to the nature of enzymes to perform highly stereoselective attacks under mild conditions, biocatalysis represents the most attractive alternative.

The objective of this thesis was the development of two enzymatic cascades for the synthesis of two distinctive statin side-chain precursors. The kinetics of each elementary reaction within the multi-enzyme system and the impact of all present compounds (organic compounds: substrates and products) on the enzyme stability were determined. The developed mathematical models were validated in different reactor types (batch, repetitive batch, and fed-batch reactor). Using the validated models, the reaction conditions were optimized with respect to production of optimum quantity of key molecules and volume productivity.

The research was based on the following hypotheses:

1. The kinetic models and enzyme stability properties will enable determination of the most suitable strategy for the implementation of a multi-enzyme process.
2. The mathematical models will enable determination of optimal reaction conditions.
3. The optimized multi-enzyme process for the synthesis of statin side-chain precursors will become an attractive alternative to chemical methods.

Two different routes towards the production of statin side-chain precursors were examined, which differed in starting materials and used enzymes. The first statin side-chain precursor was obtained by conducting a reaction that involved a 2-deoxyribose-5-phosphate aldolase (DERA), an NAD(P)-dependent dehydrogenase (DH), and a halohydrin dehalogenase

(HHDH), while the second precursor was synthesized by carrying out a tandem reaction consisting of DERA and DH, whereby different genetically modified DERA and DH variants were tested, using inexpensive, easily-accessible aldehydes. To make the DH-catalyzed reactions economically feasible, for each reaction an *in situ* $NAD(P)^+$ regeneration system was examined using an NAD(P)H-dependent oxidase (NOX).

The influence of different pH, buffers and organic compounds (substrates and products) on the activity and/or stability of all applied enzymes was investigated. The kinetic data of each elementary reaction within the multi-enzyme system was obtained applying the initial reaction rate method. The developed kinetic models and the data obtained from the enzyme stability measurements enabled the determination of the most suitable strategy for the implementation of a multi-enzyme process. The mathematical models were developed for different reactor modes and the proposed models were experimentally validated. The possibility of running multi-enzyme one-pot reactions was examined as well. It was experimentally proven that all cascade reactions could be conducted in a sequential multi-step one-pot manner with an integrated coenzyme regeneration system working as simultaneous one-pot in order to obtain industrially relevant metrics. The validated mathematical models were used for further optimization of reaction conditions. Based on the obtained results and calculated metrics, optimal reaction setups and enzymes were found. The validated mathematical models represent a valuable basis for future application in the examined multi-enzyme-catalyzed synthesis of statin side-chain precursors.

Key words: aldolase, cascade reaction, dehydrogenase, enzyme kinetics, halohydrin dehalogenase, mathematical modelling, optimization, statins.

BIOKATALITIČKA SINTEZA PREKURSORA BOČNIH LANACA STATINA

PROŠIRENI SAŽETAK

Uvod i cilj rada

Statini spadaju u najčešće propisivane lijekove današnjice za snižavanje lipida u krvi. Iako se za njihovu proizvodnju primjenjuju dobro uhodane kemijske metode, one su dugotrajne i sastoje se od velikog broja koraka. Zbog sve veće potražnje za statinima i zbog zahtjeva za njihovom visokom kemijskom i stereokemijskom čistoćom ulažu se veliki napori u pronalaženju učinkovitih i ekonomski prihvatljivih procesa proizvodnje kiralnih prekursora bočnog lanca statina. Iz tog razloga razvijaju se biokatalitički procesi njihove sinteze. Naime, primjena enzima predstavlja vrlo atraktivnu alternativu kemijskim procesima zbog činjenice da kataliziraju stereoselektivne reakcije pri vrlo blagim reakcijskim uvjetima koje rezultiraju proizvodnjom produkata visoke enantiočistoće.

Cilj istraživanja bio je razvoj dviju enzimskih kaskada u svrhu proizvodnje dvaju prekursora statina. Određena je kinetika svake pojedine reakcije unutar postavljenih višeenzimskih sustava te utjecaj svih prisutnih komponenata reakcija (organskih spojeva: supstrata i produkata) na stabilnost enzima. Razvijeni matematički modeli reakcija validirani su u različitim izvedbama reaktora (šaržni reaktor, ponovljivi šaržni reaktor, šaržni reaktor s dotokom). Primjenom validiranih matematičih modela optimirani su reakcijski uvjeti s ciljem proizvodnje optimalne količine ključnih molekula i postizanje visoke volumne produktivnosti.

Istraživanje se temeljilo na hipotezama kako će kinetički modeli i informacije o stabilnosti enzima omogućiti definiranje najprikladnije strategije implementacije višeenzimskog sustava, da će se primjenom matematičkog modeliranja utvrditi optimalni reakcijski uvjeti te će optimirani višeenzimski sustav za proizvodnju prekursora bočnih lanaca statina biti atraktivna alternativa trenutno zastupljenim kemijskim metodama.

Istraživane kaskade razlikovale su se u polaznim molekulama (supstratima) i primijenjenim enzimima. Supstrati koji su se koristili za potrebu sinteza prekursora bili su ekonomski prihvatljivi i lako dostupni aldehidi, a reakcije su bile katalizirane kombinacijom enzima različitih skupina. Supstrati prve rute bili su kloroacetaldehid (CAA) i acetaldehid (AA),

dok su supstrati druge rute bili *N*-(3-oksopropil)-2-fenilacetamid (OPA) i AA. Prva se kaskada sastojala od enzima 2-deoksiriboza-5-fosfat-aldolaze (DERA), NAD(P)-ovisne dehidrogenaze (DH) i halogenhidrin-dehalogenaze (HHDH^{001}), dok se druga sastojala od enzima DERA i DH, pri čemu su bile korištene različite genetički modificirane varijante enzima DERA i DH. S obzirom na to da su određeni stupnjevi reakcija bili katalizirani enzimom DH, ispitana je mogućnost primjene regeneracije koenzima NAD(P)$^+$ *in situ* primjenom NAD(P)H-ovisne oksidaze (NOX).

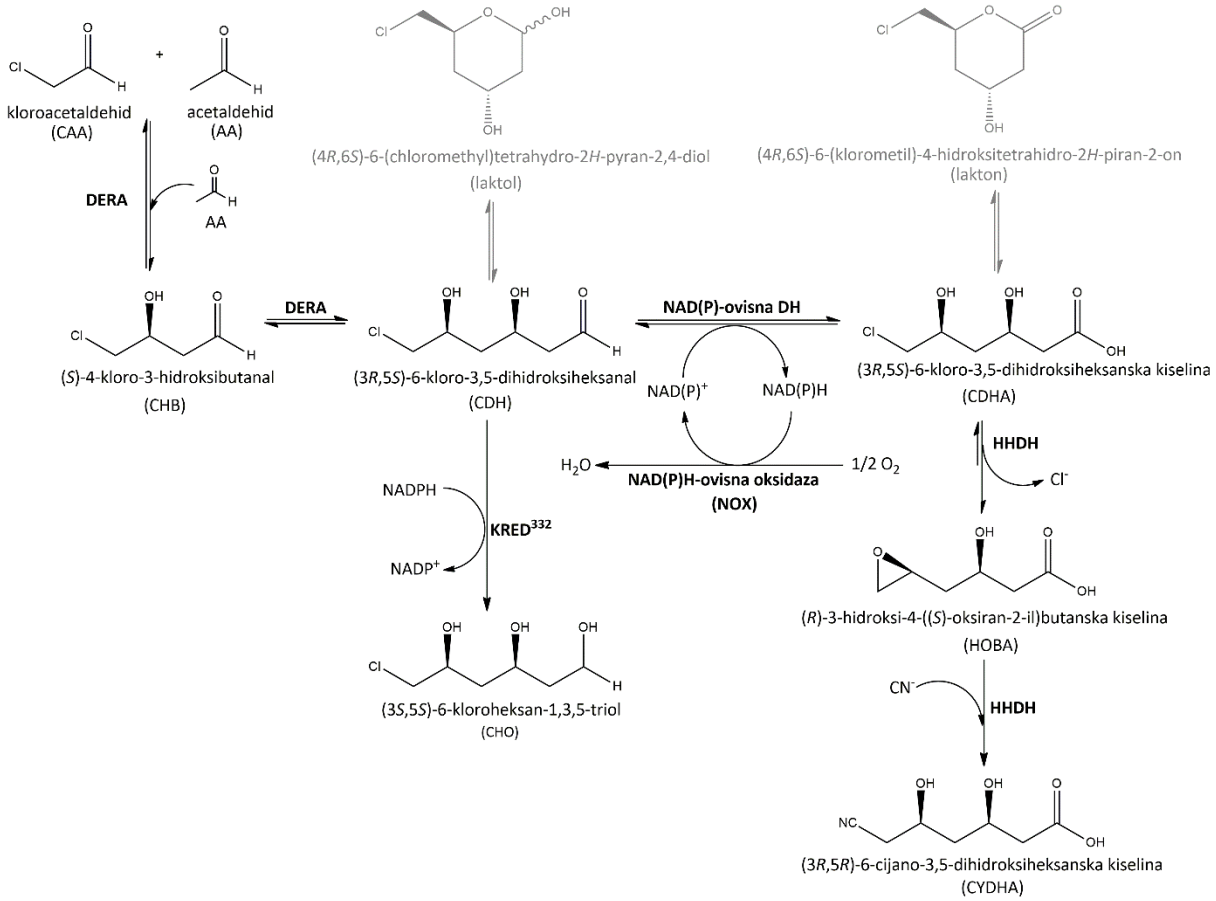

Slika 1. Višeenzimska (kaskadna) reakcija sinteze prvog prekursora bočnog lanca statina. Reakcija se sastojala od aldolne reakcije katalizirane enzimom DERA (DERA^{Tm} ili DERA^{024}), reakcije oksidacije katalizirane NAD(P)-ovisnom DH (AlDH ili KRED^{332}) uz regeneraciju koenzima NAD(P)$^+$ *in situ* primjenom NAD(P)H-ovisne DH (NOX), te reakcija kataliziranih enzimom HHDH (HHDH^{001}): dehalogenacije i otvaranja prstena epoksida u prisustvu nukleofila (CN^-).

Prva reakcijska ruta (slika 1.) sastojala se od dvostruke aldolne adicije, oksidacije te od dehalogenacije i otvaranja prstena epoksida u pristustvu jakoga nukleofila. Dvostruka aldolna adicija bila je katalizirana enzimom DERA (DERA^{Tm} ili DERA^{024}). Prva aldolna adicija AA na CAA rezultirala je nastajanjem međuprodukta 4-kloro-3-hidroksibutanala (CHB), dok je adicijom druge molekule AA na međuprodukt CHB dobiven konačni aldolni produkt 6-kloro-

3,5-dihidroksiheksanal (CDH). Oksidacija dobivenog aldehida CDH-a u 6-kloro-3,5-dihidroksiheksansku kiselinu (CDHA) provedena je primjenom enzima DH. U tu svrhu ispitana su dva različita enzima: NAD-ovisna aldehid dehidrogenaza (AlDH) i NADP-ovisna ketoreduktaza (KRED^{332}). Regeneracija koenzima NAD^+ provedena je implementacijom regeneracijskog sustava *in situ* uvođenjem enzima NADH-ovisne oksidaze (NOX^{009}), koja kao kosupstrat zahtjeva kisik. Treći, a ujedno posljednji stupanj kaskade, bila je reakcija katalizirana enzimom HHDH (HHDH^{001}). Enzim HHDH^{001} katalizira reakciju dehalogenacije CDHA-a, čime se na mjestu klorida fomira epoksid te nastaje konačni produkt 3-hidroksi-4-(oksiran-2-il)-butanska kiselina (HOBA). Ukoliko se reakcija provodi uz dodatak jakog nukleofila, poput kalijeva cijanida, enzim HHDH^{001} katalizira dvostupnjevitu reakciju nastanka 6-cijano-3,5-dihidroksiheksanske kiseline (CYDHA) preko gore spomenutog međuprodukta HOBA.

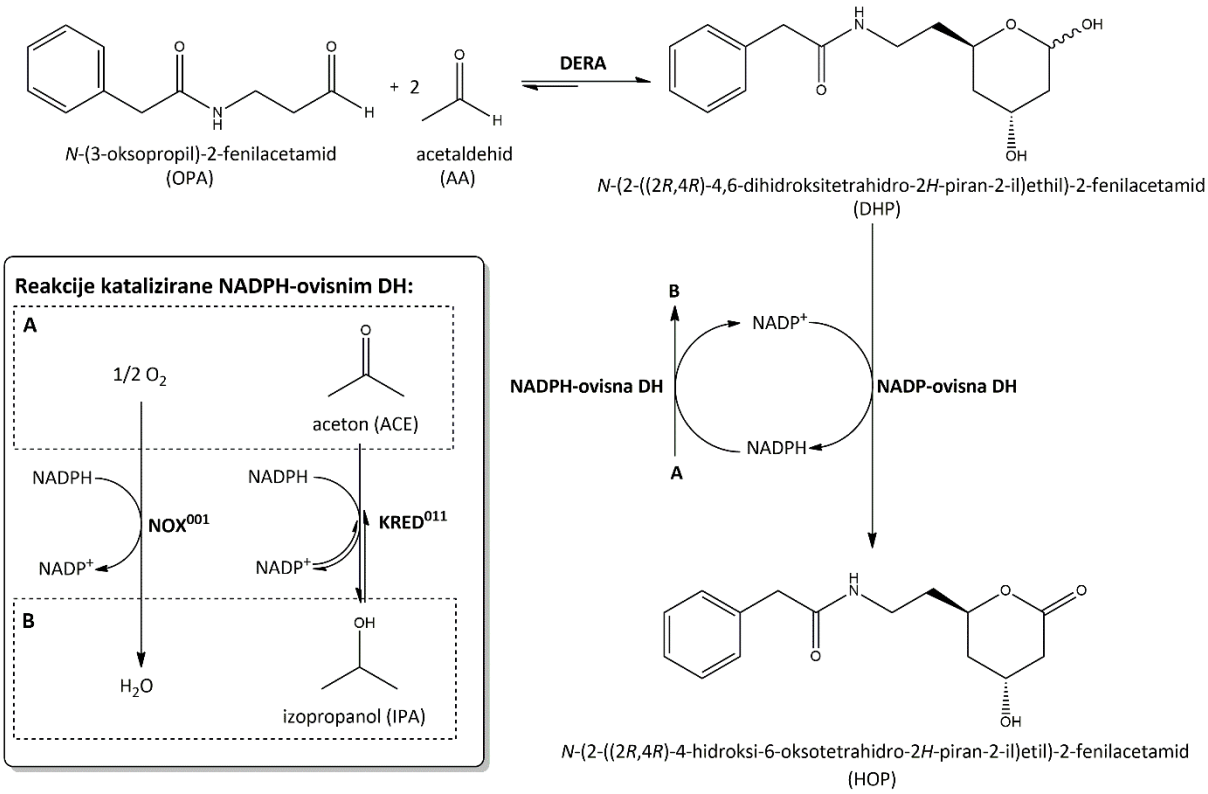

Slika 2. Višeenzimska (kaskadna) reakcija sinteze drugog prekursora bočnog lanca statina. Reakcija se sastojala od aldolne reakcije katalizirane enzimom DERA (DERA^{062}) i reakcije oksidacije katalizirane NADP-ovisnom DH (KRED^{354}) uz regeneraciju koenzima $NADP^+$ *in situ* primjenom NAD(P)H-ovisne DH (NOX^{001} ili KRED^{011}).

Druga reakcijska ruta (slika 2.) sastojala se od dvostruke aldolne adicije i oksidacije nastalog aldolnog produkta. Dvostruke aldolne adicije bila je katalizirana enzimom DERA^{062}, dok je oksidacija aldola bila katalizirana NADP-ovisnom DH (KRED^{354}). Reakcija katalizirana enzimom DERA^{062} rezultirala je produktom *N*-(2-((2*R*,4*R*)-4,6-dihidroksitetrahidro-2*H*-piran-

2-il)etil)-2-fenilacetamidom (DHP). Nastali aldehid DHP bio je enzimski oksidiran u *N*-(2-((2*R*,4*R*)-4-hidroksi-6-oksotetrahidro-2*H*-piran-2-il)ethil)-2-fenilacetamid (HOP). Ispitana je mogućnost regeneracije koenzima $NADP^+$ implementacijom regeneracijskog sustava *in situ* uvođenjem enzima NADPH-ovisne DH. Kao mogući enzimi ispitani su NOX^{001}, enzim koji kao kosupstrat zahtjeva kisik, i $KRED^{011}$, enzim koji kao kosupstrat zahtjeva aceton (ACE).

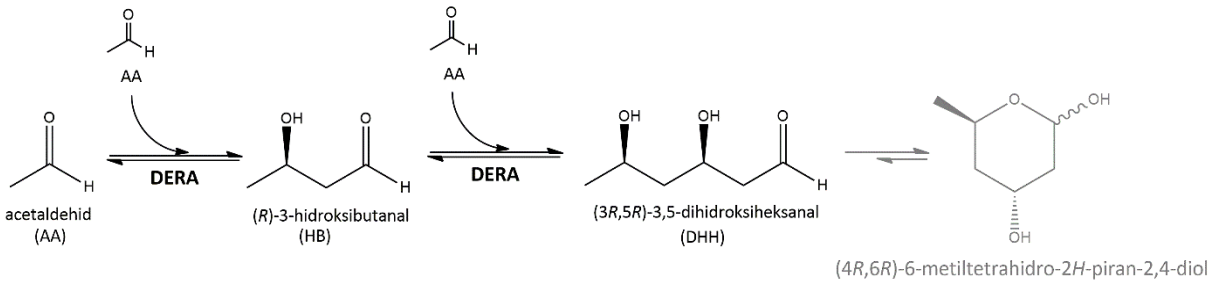

Slika 3. Sporedna reakcija dvostruke aldolne samoadicije acetaldehida katalizirana enzimom DERA ($DERA^{Tm}$, $DERA^{024}$ ili $DERA^{062}$).

S obzirom na to da enzim DERA prihvaća AA ujedno kao donor i akceptor, reakcija dvostruke aldolne samoadicije AA rezultira nastankom konačnog produkta 3,5-dihidroksiheksanala (DHH) preko međuprodukta 3-hidroksibutanala (HB) (slika 3.).

Razlog provedbe oksidacije u oba slučaja bio je prevođenje konačnog produkta (aldehidi CDH i DHP) u svoj stabilniji oblik (kiseline CDHA i HOP). U slučaju prve rute, oksidacija CDH-a je također bila nužna iz razloga što karbonilni spojevi (aldehidi i ketoni) kemijski reagiraju s cijanidom (CN^-) čime dolazi do cijanohidrinske reakcije. Time bi nastali neželjeni nusprodukti, a reakcija bi rezultirala sa smanjenim prinosom na konačnom produktu (prekursoru bočnog lanca statina).

Metodologija

Analitičke metode

Uzorci uzeti iz reakcijske otopine analizirani su primjenom tekućinske kromatografije na kromatografu Shimadzu HPLC (Kyoto, Japan).

Aktivnosti svih enzima utvrđene su primjenom eksperimentalno definiranih spektrofotometrijskih testova na spektrofotometru Shimadzu UV-1601 (Kyoto, Japan).

Optimalni pH i temperatura

Utjecaj različitih pufera, pH i temperature na aktivnost i stabilnost svih korištenih enzima određeni su provedbom spektrofotometrijskih mjerenja. Pošto enzimi DH kataliziraju reakcije pri jednom pH (čime nastaje glavni produkt oksidacije), a regeneracija koenzima odvija se pri drugom pH, pronađen je kompromisan pH temeljem dostupne literature i prikupljenih eksperimentalnih rezultata.

Stabilnost enzima

Stabilnost enzima određena je miješanjem enzima s različitim koncentracijama supstrata ili produkta, u optimalnom puferu pri optimalnoj temperaturi. Tijekom definiranog razdoblja uzimani su uzorci i mjerena je aktivnost enzima. Iz dobivenih rezultata procijenjene su konstante deaktivacije enzima u prisutnosti svakog pojedinog ispitanog spoja.

Regeneracija koenzima

Regeneracija koenzima provođena je ili uvođenjem novog enzima u reakcijski sustav (NADH-ovisna NOX) ili primjenom istoga enzima koji katalizira glavnu reakciju oksidacije (NADPH-ovisna KRED), ovisno o enzimu koji katalizira glavnu reakciju oksidacije, odnosno njegovoj specifičnosti prema vrsti upotrijebljenog kofaktora. Količina regeneriranog koenzima praćena je spektrofotometrijski pri 340 nm, s obzirom na to da koenzim NAD(P)H apsorbira svjetlost pri toj valnoj duljini.

Kinetička mjerenja

Za svaki pojedini biokatalitički stupanj unutar promatranog sustava provedena su nezavisna mjerenja praćenjem ovisnosti početne reakcijske brzine o koncentracijama pojedinih komponenti reakcijskog sustava, to jest primjenom metode početnih reakcijskih brzina. Dobiveni eksperimentalni podaci korišteni su za procjenu kinetičkih parametara. Mjerenja su provedena ili primjenom spektrofotometrijskoga testa ili praćenjem reakcije u vremenu mjerenjem koncentracije supstrata ili produkta primjenom tekućinske kromatografije.

Jednostupanjske reakcije

Sve reakcije uključene u sintezu prekursora bočnog lanaca statina provedene su u barem jednom od sljedećih reaktora: šaržnom reaktoru (BR), ponovljivom šaržnom reaktoru (RBR) ili šaržnom reaktoru s dotokom (FBR). Kada se reakcija provodila u RBR-u, dodavana je svježa

količina supstrata ili enzima jednaka onoj početnoj u onome trenutku kada je koncentracija ili aktivnost pala na nulu. Kod reakcija koje su provedene u FBR-u, supstrati i/ili enzimi dovođeni su u reaktor pomoću klipnih pumpi (PHD 4400 Syringe Pump Series, Harvard Apparatus, SAD).

Višeenzimski sustavi

Nakon što su ispitane sve jednostupanjske reakcije uključene u sintezu prekursora, provedene su kaskadne reakcije. Višeenzimski sustavi sastojali su se od kombinacije različitih enzima u svrhu pojednostavljenja procesa sinteze bez pada produktivnosti. Reakcije su provedene ili u jednom reaktoru ili kao slijedne reakcije u odabranom tipu reaktora. Kod reakcija provedenih u jednom reaktoru, na početku eksperimenta dodani su svi supstrati, enzimi i koenzimi, a kod reakcija provođenih kao niz slijednih reakcija, svaki se sintetski korak gledao kao samostalna reakcija, što znači su se samo najnužniji supstrati, enzimi i koenzimi dodali prije sljedećeg sintetskog koraka, ali bez prethodnog pročišćavanja nastalih (među)produkata.

Matematičko modeliranje, validacija i simulacije modela

Matematički modeli sastoje se od kinetičkih i bilančnih jednadžbi, a razvijeni su na temelju reakcijske sheme, procijenjenih kinetičkih parametara i bilančnih jednadžbi za odabrani tip reaktora te su validirani na nezavisnom skupu eksperimentalnih podataka prikupljenih iz podataka prikupljenih u odgovarajućem tipu reaktora. Razvijeni modeli poslužili su u simulacijama i optimizaciji početnih parametara reakcije u svrhu dobivanja optimalne koncentracije glavnoga produkta i postizanja volumne produktivnosti.

Obrada podataka

Za procjenu kinetičkih parametara i konstante operacijske stabilnosti enzima korištene su simpleks-metoda i metoda najmannjih kvadrata primjenom računalnog programa *Scientist* (MicroMath), pri čemu se kao funkcija cilja koristila suma kvadrata odstupanja. Za potrebe simulacije primijenjen je algoritam *Episode* za rješavanje skupa diferencijalnih jednadžbi. Standardna devijacija i koeficijenti determinacije izračunati su primjenom statističkih funkcija ugrađenih u *Scientist*.

Rezultati, rasprava i zaključci

Da bi se utvrdili optimalni pufer i pH za provedbu enzimskih reakcija, ispitan je utjecaj različitih pufera i pH-vrijednosti na aktivnost i stabilnost enzima. Eksperimentalno je utvrđeno

kako je optimalni pufer za provedbu reakcije aldolne adicije AA na CAA katalizirane DERA^{Tm}-om 0.1 M pufer TEA-HCl, pH 7, dok je za istu reakciju kataliziranu DERA^{024}-om najbolji 0.1 M fosfatni pufer, pH 6. Za reakciju oksidacije CDH-a katalizirane enzimom AlDH odabran je 0.1 M fosfatni pufer, pH 8. Za reakciju aldolne adicije AA na OPA katalizirane enzimom DERA^{062} utvrđeno je kako je optimalni pufer 0.1 M fosfatni pufer, pH 7, dok je za slijednu reakciju kataliziranu KRED^{354} optimalni isti pufer, ali pH 8.

Ispitan je utjecaj temperature na aktivnost i stabilnost enzima DERA^{Tm}. Rezultati su potvrdili kako aktivnost enzima raste s porastom temperature u skladu s Arrheniusovom jednadžbom. Pomoću prikupljenih eksperimentalnih podataka određeni su parametri jednadžbe. Enzim je pokazao vrlo dobru termostabilnost zadržavši 87 % inicijalne aktivnosti nakon tri dana inkubacije pri temperaturi 20 – 25 °C.

Kako bi se uspješno postavili matematički modeli, bilo je potrebno odrediti utjecaj organskih spojeva (supstrata i produkata) na stabilnost enzima te odrediti kinetiku enzima u reakcijama koje kataliziraju.

Konstanta deaktivacije enzima u prisustvu organskih spojeva za svaki pojedini enzim procijenjena je pomoću eksperimentalnih podataka vremenskih promjena aktivnosti enzima za svaku pojedinu koncentraciju pojedinačnog aldehida primjenom kinetike drugoga reda. Procijenjene konstante deaktivacije su potom prikazane kao ovisnost konstante deaktivacije o pojedinoj koncentraciji svakog ispitivanog spoja, te opisane polinomom. Rezultati ispitivanja utjecaja organskih spojeva na stabilnost enzima potvrdili su kako je nužno odrediti optimalne početne koncentracije supstrata te izbjeći akumulaciju spojeva koji imaju destabilizirajući učinak na enzime odabirom prikladne konfiguracije reaktora.

Primjenom metode početnih brzina određena je kinetika svih enzima u svakoj pojedinoj reakciji unutar postavljenog višeenzimskog sustava. Kinetika svake pojedine enzimski katalizirane reakcije opisana je jednosupstratnom ili dvosupstratnom Michaelis-Menteničinom kinetikom. Ukoliko je bilo eksperimentalno utvrđeno, kinetičke jednadžbe bile su proširene članovima koji su se uključivali inhibicije uzrokovane supstratom i/ili produktom reakcije. Svi parametri Michaelis-Menteničine kinetike bili su procijenjeni primjenom nelinearne regresije programskog paketa *Scientist* (MicroMath). Uzimajući vrijednosti kinetičkih parametara u obzir, enzimi su se pogodnim katalizatorima istraživanih reakcija, međutim zaključeno je kako je za dvostruku aldolnu adiciju AA na CAA prikladniji enzim DERA^{024} nego enzim DERA^{Tm}, a kako je za oksidaciju CDH-a prikladniji enzimski sustav kojeg čine AlDH/NOX^{009} nego

enzim KRED^{332}. U slučaju druge reakcijske rute, vezano uz regeneraciju koenzima $NADP^+$ *in situ*, oba bi se enzima mogla uspješno koristiti u svrhu njegove regeneracije, pri čemu primjena enzima NOX^{001} pokazuje određene prednosti nad KRED^{011}.

Temeljem prikupljenih podataka ovisnosti stabilnosti enzima o prisustvu organskih spojeva u reakcijskoj otopini i razvijenih kinetičkih modela predloženi su matematički modeli za odgovarajući tip reaktora. Razvijeni matematički modeli validirani su u odgovarajućem reaktoru provedbom jednoenzimskih i višeenzimskih (kaskadnih) reakcija.

Služeći se validiranim matematičkim modelima, optimirani su reakcijski uvjeti promatranih enzimski kataliziranih reakcija s ciljem proizvodnje industrijski relevantne količine ključnih molekula. U tu svrhu, kao mjerilo uspješnosti, poslužili su relevantni industrijski zahtjevi za proizvodnju finih kemikalija, poput količine proizvedenog produkta (> 50 g/L), konverzije supstrata (> 95 %, 24 h), iskorištenje biokatalizatora (> 10 $g_{produkt}/g_{enzim}$) i produktivnost (> 100 g/(L·dan)).

Kaskadne reakcije bile su provedene u odgovarajućem reaktoru na simultani (ako je uključivalo regeneraciju koenzima) i/ili sekvencijalni (ako su produkti prethodne reakcije bili supstrati sljedeće reakcije bez prethodne alternacije reakcijske otopine) način. Na temelju prikupljenih eksperimentalnih podataka, potvrđeno je kako je moguće pojednostaviti promatrane reakcijske sustave provedbom kaskadnih reakcija i time dobiti veće količine željenog produkta. Iako nije bilo moguće simultano provesti kaskadne reakcije koje uključuju enzime DERA i DH, iz razloga što enzimi DH neselektivno oksidiraju aldehide, eksperimentalno je potvrđeno kako je moguće provesti kaskadne reakcije na sekvencijalan način. Tako je provedbom sekvencijalne kaskade, koja uključuje prisustvo DERA^{024}-e i AlDH/NOX^{009}-a, reakcija rezultirala zadovoljavanjem industrijski značajnih procesnih veličina, u usporedbi s kaskadnom reakcijom provedenom u prisustvu DERA^{024}-e i KRED^{332}-a. Spomenute kaskade provedene su u šaržnom reaktoru, pri čemu su aldolne reakcije provedene s dodacima supstrata i enzima a reakcije oksidacije s dodacima enzima u trenutcima kada su se supstrati u potpunosti potrošili, odnosno kada je preostala aktivnost enzima bila ispod 20 %. Iako zbog kemijske reakcije aldehida s cijanidom nije bilo moguće provesti kaskadnu reakciju katalizirane s HHDH^{001} na simultan način (AlDH, NOX^{009} i HHDH^{001} dodani u istom stupnju), reakcija je provedena na sekvencijalni (po završetku reakcije katalizirane enzimskim sustavom AlDH/NOX^{009} dodana je HHDH^{001}) način. Ta se kaskada sastojala od prvog stupnja (aldolna reakcija: DERA^{024}, ponovljivi šaržni reaktor), drugog stupnja (reakcija oksidacije:

AlDH/NOX^{009}, šaržni reaktor s dodatcima enzima) i trećeg stupnja (reakcija katalizirana s HHDH^{001}, u prisustvu KCN-a, šaržni reaktor), a demonstrirala je mogućnost uspješne provedbe kaskadne reakcije, kao i postizanje industrijskih zahtjeva za proizvodnju finih kemikalija.

Provedbom kaskadne reakcije na sekvencijalni način, sačinjene od enzima DERA^{062} u prvom reakcijskom stupnju i KRED^{354} i NOX^{001} ili KRED^{011} u drugom stupnju, pri optimalnim reakcijskim uvjetima, dobiveni rezultati upućuju kako se oba enzima (NOX^{001} i KRED^{011}) mogu uspješno koristiti u svrhu regeneracije koenzima $NADP^+$. Zbog jednostavnosti i neznatno boljih rezultata, preporučeni regeneracijski sustav je onaj kataliziran enzimom NOX^{001}. Eksperimentalno je utvrđeno da dolazi do raspada produkta oksidacije HOP-a, čime je dokazano kako nastala kiselina HOP nije stabilniji oblik aldehida DHP-a proizvedenog aldolnom adicijom. Time je dokazano kako oksidaciju trebalo provoditi simultano u prisustvu, na primjer, lipaze kako bi se zaobišao gubitak na produktu HOP, odnosno gubitak HOP-a kao supstrata sljedećeg, trećeg stupnja promatrane kaskade.

Ekperimenti provedeni na temelju validiranih matematičkih modela rezultirali su s industrijski značajnim vrijednostima. Ti modeli predstavljaju dragocjenu osnovu za buduću primjenu promatranih kaskadnih sustava u svrhu proizvodnje prekursora bočnog lanca statina.

Ključne riječi: aldolaza, dehidrogenaza, enzimska kinetika, halohydrin dehalogenaza, matematičko modeliranje, optimiranje, statini, višeenzimski sustav.

TABLE OF CONTENTS

1 INTRODUCTION

Biocatalysis is the use of enzymes (i.e. biocatalysts) for chemical synthesis [1, 2]. Their use, either as isolated enzymes or as whole-cell systems [1, 3, 4], due to the recent advances [5], has significantly expanded and has impacted the chemical synthesis in multiple industries, including the production of pharmaceuticals, agrochemicals, and food [1, 2, 4]. The application of enzymes shows remarkable advantages over classical chemical catalysis, due their nature to perform highly selective reactions while operating under mild conditions, for which reason they are considered as 'green' solutions with a minimized environmental impact [2 - 5]. Additionally, using recombinant DNA technology and protein engineering, it is possible to completely tailor the enzymes in order to adapt them for the given process [5], although it is still a challenging task to fully accomplish due to certain limitations [1 - 4]. Despite, the interest in enzyme application, especially in the pharmaceutical industry [1], is ever-growing [2] and thus some of the pharmaceutical companies are outsourcing the synthetic stages with a focus on the discovery and formulation [3].

As of today, several pharmaceutical companies are successfully producing valuable precursors for the production of active pharmaceutical ingredients[1] (APIs) using enzymes, some of them being statins, such as atorvastatin calcium (based on the aldol reactions) or pravastatin (based on the hydroxylation), among other APIs [2]. Statins are hypolipidemics, blockbuster drugs[2] used for prevention of cardiovascular diseases [6] and for lowering low-density lipoprotein cholesterol concentration in blood [7 - 9]. Due to challenges in the chemical synthesis, the production of the statin intermediates using enzyme-catalyzed reactions shows some notable advantages. Depending on the employed substrates in the statin precursor synthesis [5, 8, 10 - 13], the biocatalytic production of those intermediates circumvents the selective protective group addition that causes low yields and thus simplifies the production process, demonstrates high enantioselectivity ($ee \geq 98.5$ %) and operates under mild conditions, as opposed to harsh conditions during the chemical synthesis (metal catalysts or extreme temperatures) [10, 12, 14 - 18]. Also, the reason why they are appealing is that the formation of chiral centers, present in the statin molecule, is a laborious task applying the traditional

[1] Active pharmaceutical ingredient (API) is any substance in a finished pharmaceutical product [205].

[2] Blockbuster refers to pharmaceuticals with worldwide sales in excess of US$1 billion.

chemical methods [10, 11]. Therefore, the research and development (R&D) laboratories of the pharmaceutical (and biotechnological) industry, including Codexis, Pfizer, Bristol-Myers Squibb, Diversa Corporation, Dow Pharmaceutical Sciences, DSM Pharma Chemicals, Lek Pharmaceuticals, IMI TAMI (Institute for Research and Development Ltd.) [19], among others, have shifted their focus towards applying the biochemical catalysis for the production of statin intermediates.

The objective of this research was the production of two statin side-chain precursors by the application of multiple enzymes that were used as cell-free extracts (CFEs). Two different routes towards their production were examined that differed in starting materials and used enzymes. When possible, the process was optimized as (sequential and/or simultaneous) cascade one-pot systems. Since the conducted reactions involved NAD(P)-dependent dehydrogenases (DHs), they were combined with *in situ* coenzyme $NAD(P)^+$ regeneration through an enzyme-coupled regeneration system using NAD(P)H-dependent enzymes.

The first reaction route consisted of four reactions catalyzed by three different enzymes in the following order: (1) double-aldol addition reaction, (2) oxidation, (3) dehalogenation, and (4) epoxide ring-opening in presence of a strong nucleophile. The starting materials were acetaldehyde (AA) and chloroacetaldehyde (CAA). The aldol reaction, which was catalyzed by deoxyribose-phosphate aldolase ($DERA^{Tm}$, $DERA^{024}$), proceeded *via* the production of intermediate 4-chloro-3-hydroxybutanal (CHB) which further reacted with AA to form the final aldol product 6-chloro-3,5-dihydroxyhexanal (CDH). The following reaction was the NAD(P)-dependent DH-catalyzed (AlDH, $KRED^{332}$) oxidation of CDH into 6-chloro-3,5-dihydroxyhexanoic acid (CDHA). The AlDH-catalyzed oxidation was combined with coenzyme regeneration facilitated by H_2O-forming NADH-dependent oxidase (NOX^{009}). The third and the fourth step, and thus the final reactions of this route, were the reactions catalyzed by halohydrin dehalogenase ($HHDH^{001}$), which was responsible for the CDHA dehalogenation and its ring-opening in presence of a strong nucleophile: KCN (Figure 1) [20 - 24].

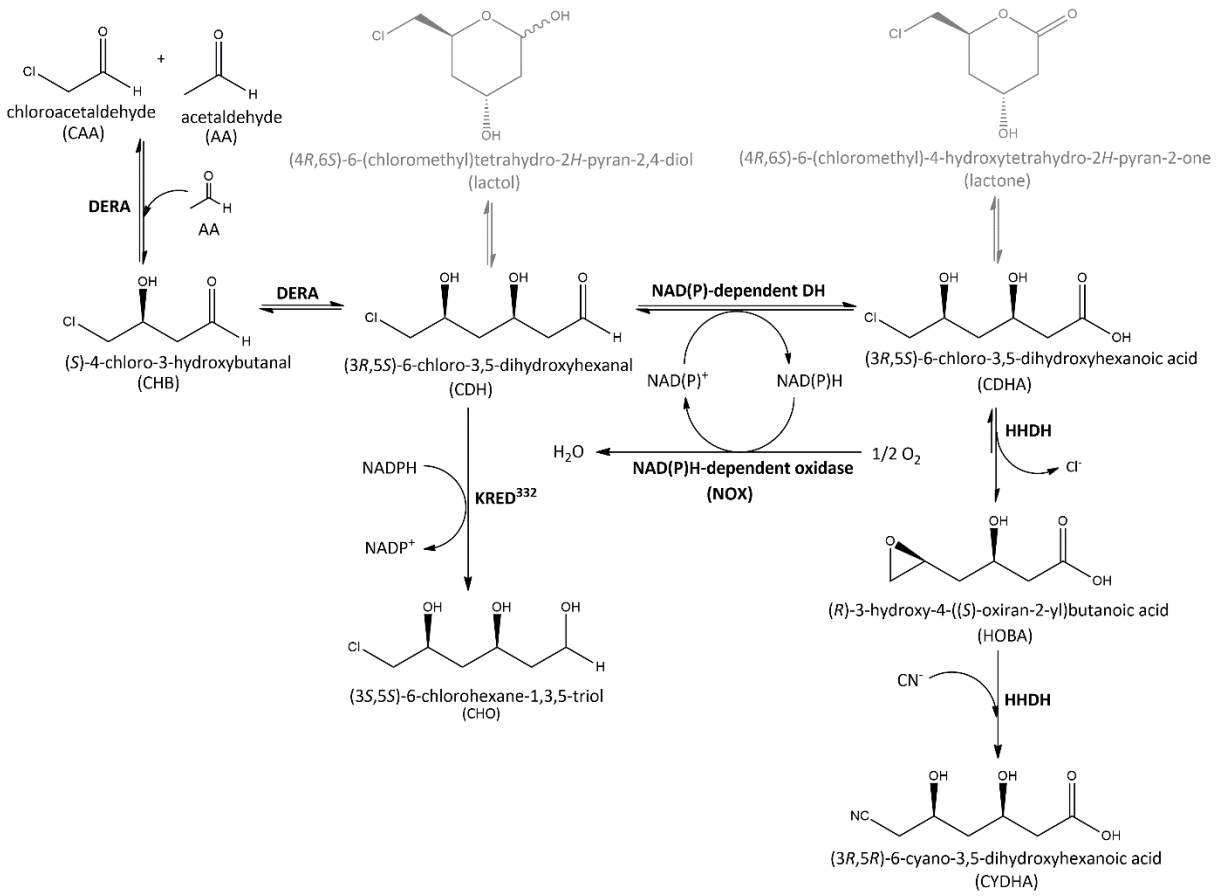

Figure 1 Reaction scheme of the first multi-enzyme reaction route. The full reaction route consists of the DERA-catalyzed aldol reaction (DERA^{Tm} or DERA^{024}), NAD(P)-dependent DH-catalyzed oxidation (AlDH or KRED^{332}) combined with *in situ* NOX-catalyzed NAD(P)$^+$ regeneration, and of HHDH^{001}-catalyzed dehalogenation and epoxide ring-opening with a nucleophile (CN^-).

The second reaction route consisted of (1) an aldol reaction catalyzed by DERA^{062} followed by (2) an oxidation catalyzed by NADP-dependent DH (KRED^{354}). The starting materials of the aldol reaction were *N*-(3-oxopropyl)-2-phenylacetamide (OPA) and AA. The aldol reaction resulted in the formation of *N*-(2-((2*R*,4*R*)-4,6-dihydroxytetrahydro-2*H*-pyran-2-yl)ethyl)-2-phenylacetamide (DHP) which was subsequently oxidized into *N*-(2-((2*R*,4*R*)-4-hydroxy-6-oxotetrahydro-2*H*-pyran-2-yl)ethyl)-2-phenylacetamide (HOP). The oxidation was paired with an NADP$^+$ regeneration system. Two different enzymes were examined for that purpose: the H_2O-forming NOX (NOX^{001}) and NADPH-dependent DH (KRED^{011}), in which case co-substrate acetone (ACE) was added (Figure 2).

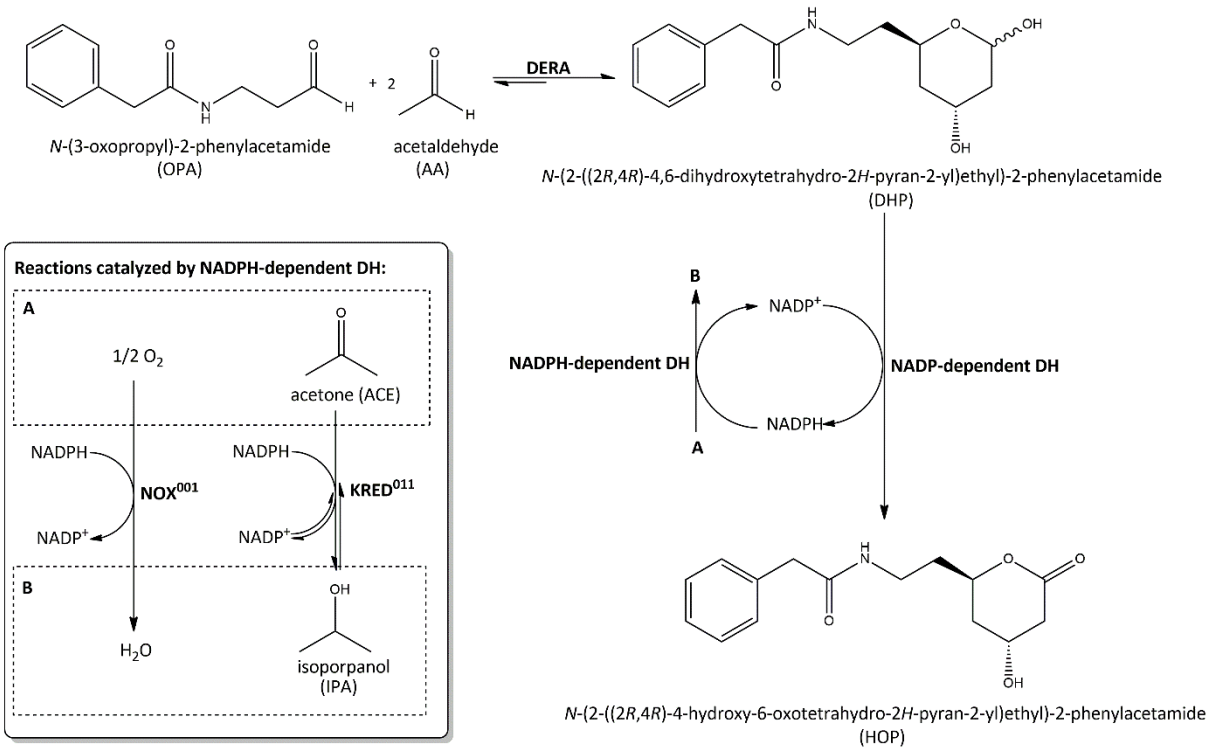

Figure 2 Reaction scheme of the second multi-enzyme reaction route. The full reaction route consists of the DERA-catalyzed aldol reaction (DERA^{062}) followed by a NADP-dependent DH-catalyzed oxidation (KRED^{354}) combined with *in situ* NADPH-dependent DH-catalyzed NADP$^+$ regeneration (KRED^{011} or NOX^{001}).

Since DERA accepts AA as both donor and acceptor, a DERA-catalyzed side reaction of self-aldol addition of AA occurred. The reaction was a two-step reaction in which two molecules of AA reacted to form the side intermediate 3-hydroxybutanal (HB) which further reacted with the third molecule of AA to form the final side product 3,5-dihydroxyhexanal (DHH) (Figure 3).

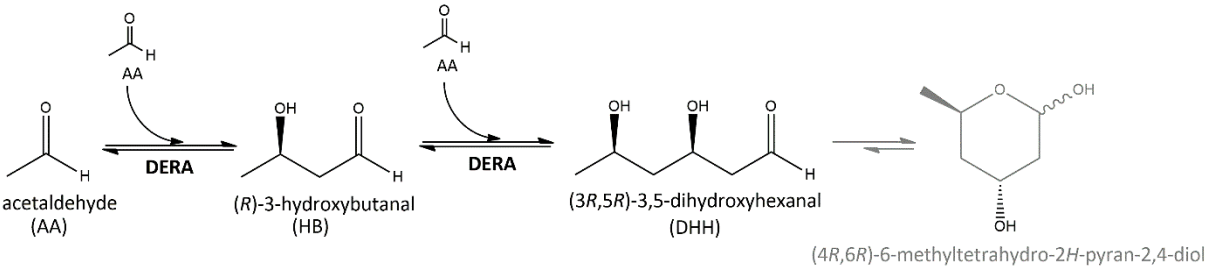

Figure 3 Reaction scheme of the side reaction of AA self-aldol addition catalyzed by DERA^{Tm}, DERA^{024} or DERA^{062}.

In both reaction routes, the oxidation was conducted to convert the aldehyde product into its more stable acid form [8, 11, 12, 25 - 28]. In case of the first reaction route, the CDH oxidation was also necessary because aldehydes (and ketones) chemically react with a cyanide

anion or a nitrile to form a cyanohydrin. This would have caused unwanted side-products, while the reaction would result in lowered yield of the final product (statin side-chain precursor).

The examined reactions were conducted as single- and multi-enzyme reaction systems. While the single-enzyme catalysis refers to a reaction in which only one enzyme participates, the multi-enzyme catalysis refers to a reaction in which a number of enzymes work together in a multi-step (cascade) fashion so that the product of one enzyme is the substrate of the other [29].

Both examined routes (Figure 1 – 3) were explored to be conducted in a cascade mode as one-pot systems run either in a sequential or simultaneous one-pot format. The sequential one-pot reaction is a reaction in which the reactants and enzymes are added into the reactor after the previous chemoenzymatic step was successfully completed without prior or additional work-up, whilst the simultaneous one-pot reaction is a reaction in which all the reactants and all the enzymes are added into the reactor at the beginning of the reaction.

The application of multi-enzyme cascade systems shows a promising direction for the production of optically active chemicals. That way, the process results in higher yields, spends fewer chemicals, and saves time, especially when an unstable intermediate does not need to be isolated. Moreover, process conducted in this manner results in significant reduction of both waste and production costs on the industrial scale [30]. The main drawback, which can be overcome by applying mathematical modelling, is finding optimal process conditions. Therefore, when finding the most cost-effective mode for the statin side-chain biosynthesis, especially for further industrial use, it is of great importance to understand the mechanisms and kinetics of the enzyme systems [31]. For this purpose, mathematical modelling, as reaction engineering tool, is used and has an important role in the study of enzymatic reactions [31]. Despite its undeniable importance, for each of the synthetic steps towards the production of statin side-chain building blocks, the available literature offers very little or virtually no kinetic data obtained based on kinetic models. Although the kinetic data concerning other reactions catalyzed by NAD(P)-dependent oxidoreductase are available [32], the data concerning aldolase-catalyzed reactions are scarce [14, 33, 34], and for now only two were found concerning mathematical modelling of the reaction towards statin side-chain production [14]. In addition to the apparent lack of aldolase kinetic data, the data related to halohydrin dehalogenase and the reaction of statin side-chain production is even less available [27], especially data obtained based on a simple and robust mathematical model but in no relation to

the statin side-chain production [35]. It should be noted that, for the time being, the catalytic data for the biocatalytic epoxide-ring opening in the presence of strong nucleophiles were not estimated and thus no mathematical models were developed, although those reactions are of scientific interest [8, 22, 24, 36].

2 THEORETICAL BACKGROUND

2.1. Green chemistry

The well-being of modern society is unimaginable without the countless products of the organic synthesis and the quality of our life is strongly dependent on the products of the pharmaceutical industry. The success of the modern pharmaceutical industry is firmly built on the remarkable successes in the organic synthesis over the last century, however many of the recognized and trusted synthetic methodologies were developed at the time when the toxic properties of reagents and solvents were less known and the issues of waste minimization and sustainability were largely unheard of. In the last three decades, it became increasingly clear that the chemical and allied industries are faced with substantial environmental issues. Many of the classical synthetic methodologies have a broad scope but generate extensive amounts of waste and the chemical industry has been subjected to increasing pressure to minimize or even eliminate the waste [5].

In the mid-1990s Anastas and coworkers at the United States Environmental Protection Agency [37 - 40] developed the concept of 'benign by design', which stands for designing environmentally benign products and processes to address the environmental issues caused by both chemical products and the processes by which they are produced [5]. It incorporated the concepts of atom economy (synthetic methods should be designed to maximize the incorporation of all materials used in the process into the final product) and E factor (actual amount of waste produced in the process, defined as kilogram of waste per kilogram of desired product) and ultimately became a guiding principle of the Green Chemistry concept, embodied in the 12 Principles of Green Chemistry [5, 39, 41 - 45]. Green Chemistry is based on prevention rather than appliance of end-of-pipe solutions, it utilizes (preferably renewable) raw materials, applies safer solvents and auxiliaries and designs safer chemicals while preserving functional efficacy, thus less hazardous chemical syntheses. The syntheses obeying the Green Chemistry principles are shortened and circumvent derivatization procedures, usually used as protection/deprotection methods [16], i.e. as temporary modifications during syntheses, and successfully apply catalytic reagents (as selective as possible) that are superior to stoichiometric reagents [39, 40, 42 - 48].

More recently, 12 Principles of Green Engineering were proposed [49], which contain the same underlying features but from an engineering standpoint. Poliakoff and coworkers [40]

proposed a mnemonic PRODUCTIVELY, an acronym based on the 12 Principles of Green Chemistry that should allow rapid understanding of the Green Chemistry idea.

When designing a process based on Green Chemistry, it is impossible to meet all twelve principles at the same time but it should be attempted to apply as many principles as possible during certain stages of the synthesis [42, 43, 50 - 52].

2.2 Industrial biotechnology

The industrial biotechnology, also called the white biotechnology, comprises the production of a variety of different chemical compounds, materials, and energy through the application of microorganisms and enzymes [53 - 57]. Biotechnology is considered variously as ‘the science of genetic manipulation or the technology of industrial exploitation of biochemical systems’, genetically modified or not [57]. A bioprocess is typically made up of three steps: pretreatment (sorting, sieving, comminution, hydrolysis, medium formulation, sterilization), bioreaction (biomass production, metabolite biosynthesis, biocatalysis) and downstream processing (filtration, centrifugation, sedimentation, flocculation, cell disruption, extraction, ultrafiltration, precipitation, crystallization, evaporation, drying, packaging, etc.) [57].

Although running biochemical reactions is similar to running chemical reactions, it requires additional multidisciplinary skills such as from biology and biochemistry along with chemical and engineering sciences, which are essential features of biochemical engineering [57]. There is a consensus among the stakeholders that white biotechnology will be vital for helping specific economies build novel high-value products which have, so far, proved impossible to manufacture economically [55].

Biocatalysis is the catalysis conducted by enzymes and presents the key technology according to the green chemistry principles [41, 58]. It is perceived as an environmentally friendly process that can open new possibilities for the production of highly valued products from renewable resources with low energy input and minimization of (toxic) waste [3, 53]. The most powerful driver of white biotechnology is its ability to perform specific biochemical reactions which synthetic chemistry is not able to provide. According to the literature, enzymes present an irreplaceable tool for some specific industries [54, 56, 59, 60] and, more impressively, almost any chemical reaction seems to be achievable through the biocatalysis [61, 62]. Since naturally occurring enzymes are often not suitable for the desired biocatalytic

processes, they are further tailored or redesigned in order to be fine-tuned for the substrate specificity or activity [63].

Robins and coworkers [64] described how biocatalysis reached its present industrially proven level through the technological research and innovations, leading to the application of enzymes for the manufacture of chiral synthons, such as atorvastatin or sitagliptin [58, 64, 65]. But, despite these reactions running on an industrial scale, the potential of biocatalysis is not yet fully realized [64, 65]. Although the enzyme-catalyzed production of natural and non-natural intermediates as well as APIs does exist, biocatalysis still represents the second choice [3,66,67] or is applied only when it is challenging to produce the desired product by traditional methods [67]. Over the years biocatalysis has begun to establish itself primarily in the pharmaceutical industry [3, 66], albeit the process remains a slow uphill battle with classic organic chemical synthesis, which continues to be the most common approach [62]. The main disadvantages of biocatalysis are manifested through a limited toolbox with commercially available enzymes [62], low substrate solubility in aqueous systems, poor productivities, insufficient stabilities [68] or the question of economic feasibility for its implementation [3].

Table 1 Industrial requirements for an economically feasible biocatalytic process using isolated enzymes [8, 15, 19, 69, 70].

Parameter	Value
Substrate concentration, g/L	> 100
Enzyme concentration, g/L	≤ 5
Conversion (within 24 hours)	> 95
Enantiomeric excess, %	> 99.5
Substrate-to-enzyme ratio[3] (BY), g/g	> 10
Cofactor concentration, g/L	< 0.5
Space-time yield (STY), g/(L·day)	> 100
Production volume, t/year	> 1000
Final product concentration, g/L	> 50

The pharmaceutical processes are run on a smaller scale compared to chemical processes. For the biocatalysis to be run at an industrial scale as compared to the academic research, the process requires significant substrate concentrations of at least 5 - 10 % *w*/*w*. With respect to biocatalyst usage, conversion and optical purity, some general rules of thumb for a feasible enzyme-catalyzed process can be roughly defined (Table 1) [8, 15, 69, 70]. The main problem

[3] This can also be referred to as 'biocatalyst yield'. When using immobilized enzymes, the metrics suggest > 50 g/g for high value products (e.g. pharmaceuticals), > 100 g/g for medium value products (e.g. flavors), or > 10 000 g/g for low value products (e.g. biofuels) [214].

for the industrial implementation of biocatalysis lies in the transfer of the biocatalytic process from laboratory to a larger scale, which can cause a loss in productivity and product quality [15], but can be overcome by getting insight in the reaction characteristics on a laboratory scale [3, 15]. Despite the before-mentioned obstacles, the list of companies who successfully apply biocatalysis on an industrial scale is ever-growing [41].

2.3 Enzymes: the driving force of biocatalysis

Enzymes are products of living cells and are defined as high molecular weight complex proteins composed of amino acid chains linked together by peptide bonds [53 - 57].

Although the potential use of enzymes suffers from some common prejudices, such as being sensitive, expensive or only active on their natural substrate [61], the application of enzymes indeed shows to be advantageous to common chemical catalysis.

Below are listed key benefits of enzyme application and enzyme-catalyzed reactions:

1. **EFFICIENCY**. Enzymes catalyze reactions 10^8 to 10^{10} times faster compared to non-catalyzed reactions, which is unachievable by the application of chemical catalysts [61]. Also, chemical catalysts are generally employed in concentrations of 0.1 to 1 % *n*/*n*, whereas most enzymatic reactions can be performed at rates of 10^{-3} to 10^{-4} % *n*/*n* of catalyst, making them even more effective [61, 71].
2. **ENVIRONMENT-FRIENDLY.** Enzymes are generally considered to be natural products [72] and can be completely degraded in the environment [58, 71, 73], in contrast to the usual chemical catalyst, such as heavy metals or hazardous and toxic catalysts [61].
3. **MILD CONDITIONS.** Enzymes operate under mild, near-ambient reaction conditions: pH ranging from 5 to 8 (typically around pH 7) and temperature ranging from 20 to 40 °C (usually around 30 °C) [41, 56, 61, 71, 72, 74].
4. **COMPATIBILITY.** Since enzymes generally function under same or similar conditions, they are compatible with each other within certain ranges [61, 73]. Therefore, some biocatalytic reactions can be carried out as sequential or simultaneous one-pot cascade systems [58, 61]. This approach yields new advantages, such as the production of chiral compounds from racemic mixtures or it can facilitate the down-stream processing [30, 73].

5. **SUBSTRATE SCOPE.** Enzymes exhibit high substrate tolerance by accepting a large variety of non-natural substances [56, 61].
6. **MEDIUM SCOPE.** If it is beneficial for the process, the aqueous medium can often be replaced by an organic solvent [61], which can affect the stereoselectivity [74]. Enzymes, just like chemical catalysts, can only accelerate reactions and have no impact on the position of the reaction's thermodynamic equilibrium [61]. In principle, enzyme-catalyzed reactions can be run in both directions [61]. Thus, there is an enzyme-catalyzed process equivalent to almost every type of organic reaction [61].
7. **SELECTIVITY.** Enzymes display four major types of selectivities: chemo-, regio-, diastereo- and enantioselectivity [41, 58, 61, 71, 74, 75]. Chemoselectivity is regarded as the ability of an enzyme to 'react with one group or atom in a molecule in preference to another group or atom present in the same molecule' [74, 76]; regioselectivity as 'the preference of one direction of chemical bond making or breaking over all other possible directions' [74]; diastereoselectivity as an ability to perform a reaction in which 'one diastereomer is formed in preference to another' [74]; while enantioselectivity is regarded as the 'selectivity of a reaction towards one of a pair of enantiomers' [74]. Stereoselectivity and enantioselectivity represent the most important properties of an enzyme because of their asymmetric exploitation [74], whose significance Fisher already recognized more than 120 years ago [61].

2.3.1 Enzyme classification

Enzymes are classified by the Enzyme Commission Number (the EC number), which is a numerical classification scheme that divides enzymes into six distinctive groups according to the chemical reaction they catalyze [41, 56] (Table 2).

Table 2 Enzyme classification according to EC numbers [41, 61].

EC number	Enzyme class	General reaction
EC 1	Oxidoreductases	Oxidation or reduction
EC 2	Transferases	Transfer of a functional group from one substance to another
EC 3	Hydrolases	Bond hydrolysis
EC 4	Lyases	Synthesis or cleavage of a covalent bond, without ATP consumption
EC 5	Isomerases	Intramolecular rearrangement (isomerization)
EC 6	Ligases	Bond synthesis between two molecules, with ATP consumption

The EC numbers are assigned by the Nomenclature Committee of the International Union of Biochemistry and Molecular Biology [72, 77]. The EC number consists of letters 'EC'

followed by four numbers separated by periods. The first digit defines the general type of reaction catalyzed by the enzyme (ranging from 1 to 6), the second indicates the subclass, the third the sub-subclass, and the fourth figure is the serial identifier [41, 61, 72].

2.3.2 Oxidoreductases (EC 1)

Oxidoreductases (EC 1) are enzymes that catalyze oxidations and reductions in which the transfer of electrons, hydrogen or oxygen atoms is involved [72]. They act in the central metabolic pathways of the cell and are strictly intracellular enzymes [72]. Under this class, there are 22 sub-classes [72]. Among them, several sub-classes are of technological importance, such as the dehydrogenases [72]. Those enzymes are used as catalysts due to their reduction-oxidation (redox) capabilities [78] and find practical use in the chiral synthesis [78, 79]. To be catalytically active, these enzymes require the presence of coenzymes, such as NAD, NADP, FAD or FMN, whose role is the transmission of hydride ions or electrons *via* the enzyme's catalytic center [69, 72, 80]. Some of those coenzymes, such as FAD, are bound to the enzyme, while others, like NAD(P), mostly exist as a soluble component of the enzyme [80]. Over the years the interest in the application of oxidoreductases to produce fine chemicals and APIs has significantly grown [41, 81].

2.3.2.1 NAD(P)-dependent dehydrogenases (EC 1.2.1)

Dehydrogenases (DHs) are extremely useful catalysts in organic chemistry for the production of chiral compounds. They can be divided into different groups according to used donors (substrates) and acceptors (coenzymes) [80].

Figure 4 Oxidation catalyzed by NAD(P)-dependent dehydrogenases.

Throughout the literature names such as alcohol dehydrogenases (ADHs), ketoreductases (KREDs), carbonyl reductases (CRs) or more specific names, such as shikimate (shikimic acid) dehydrogenase, are frequently but interchangeably used and can be unified and generalized under the name 'dehydrogenases' [82]. There are approximately 300 different DH sub-classes [82]. DHs that belong to the EC 1.2.1 class are enzymes that catalyze reversible oxidation of aldehydes, or oxo groups, as donors in presence of a $NAD(P)^+$ as an acceptor (Figure 4) [69, 77].

These enzymes are mostly used for reduction of prochiral compounds but find important applications in the oxidation and therefore are considered as a useful tool for large-scale production of chiral compounds [80].

2.3.2.2 NAD(P)H oxidases: H_2O-forming (EC 1.6.3.2)

The NAD(P)H oxidases (NOX, EC 1.6.3) can be either H_2O_2- (EC 1.6.3.1) or H_2O-forming (EC 1.6.3.2) enzymes that act on the reduced form of the pyridine nucleotide coenzyme, NAD(P)H, by using the molecular oxygen (O_2) as an acceptor [77]. The reaction results in the reduction of oxygen into either hydrogen peroxide (H_2O_2), in a two-electron reduction, or in water (H_2O), in a four-electron reduction (EC 1.6.3.2) (Figure 5) [83 - 85].

a) $2\ NAD(P)H + 2\ H^+ + O_2 \xrightarrow{NOX} 2\ NAD(P)^+ + 2H_2O$

b) $NADH + H^+ + O_2 \xrightarrow{NOX} NAD^+ + H_2O_2$

Figure 5 NOX-catalyzed NAD(P)H oxidation which results in a) hydrogen peroxide or b) water formation.

Since most of the enzymes deactivate upon exposure to hydrogen peroxide, the application of H_2O-forming NOXs shows superiority over H_2O_2-forming NOXs when utilizing multi-enzyme systems [81], despite a catalase, a common enzyme that catalyzes the decomposition of hydrogen peroxide into water and oxygen, can be additionally added to the system [69]. But, by adding a new enzyme into the process the complexity of the system increases, due to the necessity to adjust optimal operating conditions for all of the present enzymes [81].

Those H_2O-forming NOX enzymes find use, most often, for cofactor recycling, since oxidoreductases, especially DHs, depend on the stoichiometric use of cofactors [80, 81].

2.3.3 Aldolases: carbon-carbon lyases (EC 4.1)

The aldol reaction has long been considered a fundamental reaction in organic chemistry since it results in the formation of new carbon-carbon bonds [14, 15, 28, 67, 86 - 91]. Aldol reactions have been recognized as one of the most powerful strategies towards the production of enantiopure multifunctional molecules, such as new valuable structures accessible for investigations in drug discovery [92, 93].

The aldol reaction is *in vivo* catalyzed by aldolases [28, 86, 89] exhibit high regioselectivity and stereoselectivity under mild conditions [14, 15, 28, 87, 91, 94, 93]. Aldolases catalyze the stereoselective addition of a ketone or aldehyde donor to an aldehyde acceptor [18, 77, 86, 95]. In the cell, the aldol reactions, i.e. carbon-carbon bond formation and cleavage, are catalyzed by these enzymes and represent essential steps in the anabolism and catabolism of a wide variety of carbohydrates and keto-acids [95].

To date, over 30 different aldolases have been identified and classified into two major groups according to their catalytic mechanism: class I, found in animals and higher plants, and class II, found in bacteria and fungi [86, 93, 95]. With only a few exceptions, the stereoselectivity in both types of aldolases is controlled by the enzyme and does not depend on the structure or stereochemistry of the substrate, which allows highly predictable products containing newly formed stereocenters [86, 92, 93].

The aldolase-catalyzed stereoselective synthesis represents an attractive alternative to chemical aldol reactions. With the use of aldolases, it is possible to omit the application of protecting group procedures and strategies [14, 15, 28, 87, 91, 94]. However, the application of those enzymes shows some limits. Some enzymes and their substrates can be pricey and unstable; not all substrates are readily soluble in aqueous media; due to their ingrained specificity, the number of substrates and stereochemical outcomes being available is likely to be limited; and their intrinsic specificity has prevented them from becoming broad-based, general catalysts for asymmetric synthesis [67].

2.3.3.1 Deoxyribose-phosphate aldolase (EC 4.1.2.4)

The aldehyde-dependent aldolase family consists of only one enzyme: the deoxyribose-phosphate aldolase (or the 2-deoxyribose-5-phosphate aldolase, DERA, E.C. 4.1.2.4) [28, 67, 86, 90, 91, 96, 97]. *In vivo*, DERA catalyzes the conversion of 2-deoxy-D-ribose-5-phosphate (DRP) into glyceraldehyde-3-phosphate (GP) and acetaldehyde (AA), as shown in Figure 6 [77, 92, 93, 96, 98, 99].

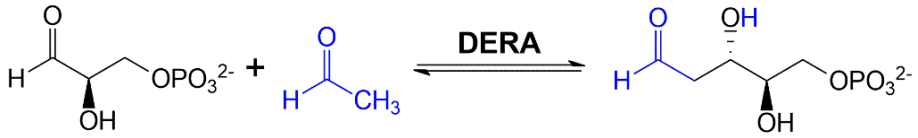

Figure 6 Natural reaction [100] [100]. The DERA-catalyzed reversible cleavage of DRP [77, 92, 96, 98, 99].

The DERA enzyme, which is a type I aldolase, is considered to be one of the most important enzymes for carbon-carbon bond formation [96]. The most attractive feature of that enzyme is its unique ability to catalyze self- and cross-aldol additions of acetaldehyde [92, 97] without the use of cofactors [28, 101]. The enzyme catalyzes a two-step acetaldehyde addition onto an aldehyde acceptor in a sequential, stereo-selective manner [14, 15, 67, 86, 87, 89, 96, 102 - 104]. It accepts a broad range of acceptor aldehydes [12, 28, 86, 87, 89, 91, 94, 99, 101, 105] and has a relatively large donor tolerance (with up to four carbon atoms) [12, 28, 86, 90, 94, 106]. The DERA enzyme, along with the fructose-6-phosphate aldolase (FSA, EC 4.1.2.–) enzyme, is the only known class I aldolase that catalyze an aldol reaction between two aldehydes that results in new aldehyde products containing two enantiopure chiral centers (Figure 7) [15, 28, 86, 89, 90, 94, 99, 105 - 108].

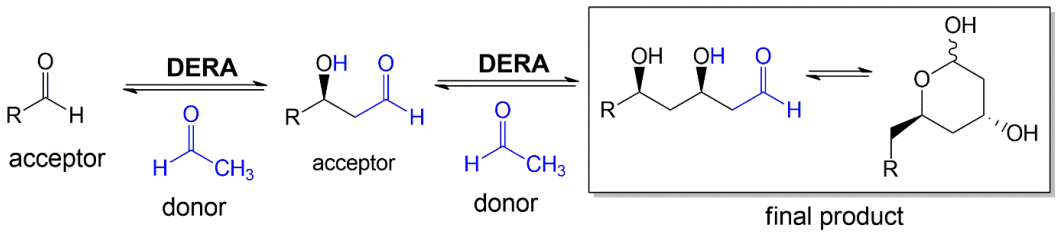

Figure 7 Engineered enzyme [100]. The aldol reaction is catalyzed in a two-step manner: first the donor (acetaldehyde, blue) reacts with the first acceptor forming a monoadduct intermediate which consecutively reacts with the same donor to produce the final product [14, 89], which spontaneously cyclize to form a six-membered hemiacetal (lactol) [8, 61, 109].

Due to the wide substrate scope and enantiomerically pure products which arise from the aldol reactions, DERA has been widely used as a biocatalyst to perform stereo-controlled aldol reactions [96, 106]. The most promising commercial application of the DERA enzyme is in the synthesis of valuable precursors that can be used as building blocks in the production of statin side-chains [14].

2.3.4 Dehalogenases: carbon-halide lyases (EC 4.5)

The carbon-halogen bond can be cleaved either by enzymatic dehalogenation, where the carbon-halogen bond cleavage is catalyzed by specific enzymes (dehalogenases) or through chemical dehalogenation [110]. Recently, the development of dehalogenating enzymes for the industrial application was limited but has significantly improved in the following years [75]. There are several different enzymatic dehalogenation mechanisms [75, 110], and three classes of enzymes have received much attention: haloalkanoic acid dehalogenases (EC 3.8.1.2), halohydrin dehalogenases (EC 4.5.1), and haloalkane dehalogenases (EC 3.8.1). These enzymes are applied to produce chiral intermediates, recycling of chlorinated by-products, chemical manufacturing, and selective treatment of process waste streams [75]. The application of dehalogenating enzymes for industrial biocatalysis is constantly increasing, but currently, only hydrolytic dehalogenases and halohydrin dehalogenases are being commercially utilized or are in development for industrial use [75].

2.3.4.1 Halohydrin dehalogenases (EC 4.5.1. –)

Halohydrin dehalogenases, also called haloalcohol dehalogenases, haloalcohol/halohydrin epoxidases or hydrogen-halide lyases (HHDHs, EC. 4.5.1.-.) [111 - 114], were reported and described for the first time in the 1970s as catalysts in the reaction of epoxide formation from vicinal halohydrins [20, 75, 110, 111, 115, 116]. They were the first to be proposed for the industrial application of dehalogenating enzymes for the conversion of halohydrins to epoxides [75]. Since these enzymes require neither cofactors nor oxygen to be catalytically active, the reaction mechanism proceeds *via* the intramolecular substitution [21, 75, 110].

These enzymes catalyze the nucleophilic displacement of a halogen by a vicinal hydroxyl group in halohydrins (α,β-halohydrins) yielding an epoxide, a proton and a halide ion [75, 111, 113]. They can also efficiently catalyze the reverse reaction: the halogenation of epoxides [21, 111, 112] and the halogenation of vicinal chlorocarbonyls to hydroxycarbonyls [112]. Besides, these enzymes can be also applied for the formation of novel carbon-carbon, carbon-nitrogen and carbon-oxygen bonds [24, 27, 111, 117]. Due to the promiscuous epoxide ring-opening activity strong nucleophiles such as cyanide, azide or nitrite are accepted in the ring-opening reaction leading to a diverse range of products [20, 21, 23, 27, 111], such as β-azido alcohols, β-hydroxynitriles, or optically pure cyano-substituted building blocks for the statin side-chain synthesis [20 - 24].

Figure 8 HHDH-catalyzed dehalogenation (removal of a halide, X^-). If a strong nucleophile (Nu^-) is present, the enzyme catalyzes both dehalogenation and nucleophile addition *via* epoxide formation [24, 61, 114].

The interest in the application of these enzymes increased when it was found that the reaction can proceed with high enantioselectivity, which made these enzymes favorable for the production of optically pure epoxides and halohydrins [21, 111, 112, 116]. Therefore, these enzymes are in active development for the manufacture of optically active halohydrins and epoxides, which find applications as chiral intermediates of pharmaceuticals and agrochemicals [75, 116]. Based on the current publications and patent activities, companies such as Daiso Co. Ltd. (Hyogo, Japan), Nitto Chemical Industry (Yokohama, Japan) and Hercules Inc. (now Ashland Inc.; Kentucky, US) have been developing HHDH-based processes at an industrial level [75].

2.4 Cascade systems

Cascade, tandem, domino or multi-enzyme reactions [73, 82] represent an appealing, yet attractive development in the area of white biotechnology [30, 73]. Biocatalytic cascade reactions are considered to be any reaction system in which two or more transformations are carried out in the same reaction vessel [73], referred to as a one-pot reaction concept [82]. The idea of performing such syntheses as either simultaneous or sequential one-pot systems, despite not being very new, has received a lot of attention in the previous years [30, 73].

Cascades represent a promising approach mainly due to some fundamental advantages, such as:

1. Intermediate extraction and purification steps can be reduced or even avoided. This is especially important when unstable or toxic intermediates are formed [30, 73, 118].
2. If the enzyme that catalyzes the desired reaction is coenzyme-dependent, the application of stoichiometric quantities of coenzymes can be circumvented [118], since it is possible to regenerate the coenzyme by applying an enzyme-based regeneration system.
3. Enzyme inactivation or inhibition due to side-product accumulation can be eliminated, e.g. by biocatalytic decomposition of hydrogen peroxide as a side-product of a coenzyme regeneration system [118].

4. Optically pure products can be obtained, e.g. deracemization reactions[4] [73].
5. An additional source for forming new carbon-carbon bonds [73].
6. The reaction system requires the use of fewer chemicals, e.g. no need for organic solvents which are required for intermediate (mid-step) extractions [118].
7. Consequently, less waste is produced, which implies lower production costs on the industrial scale [20] and no mid-step downstream processes [73].

Based on the above-mentioned features, this approach is viewed as environmentally acceptable and benign and makes the whole production process sustainable, hence falls into the concept of green chemistry [118].

The cascades can be systemized into for different layouts: linear, orthogonal, parallel, and cyclic (Figure 9) [73].

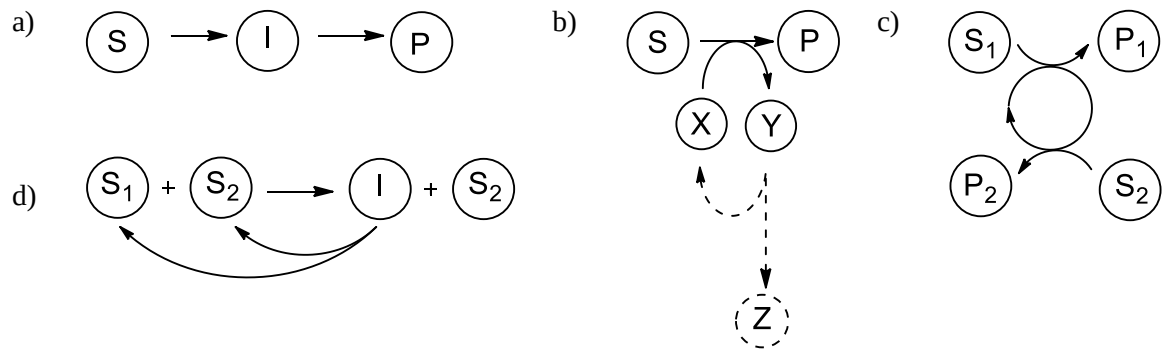

Figure 9 Four different cascade configurations: a) linear cascade, b) orthogonal cascade, c) parallel cascade, and d) cyclic cascade [73]. Legend: *S*, S_1, S_2 – substrate, *P* – product, *I* – intermediate, *X* – co-substrate, *Y* – co-product, *Z* – side-product.

The linear cascade, shown in Figure 9a, is a cascade in which a single substrate is converted into a single product through one or more intermediates in a multi-step one-pot fashion. The advantage of this design is that it saves time and reduces waste through the elimination of downstream processing steps. If the intermediate is toxic or unstable, it does not accumulate but is directly transformed into the (final) product. This leads to a safer process with reduced side reactions and better yields. Those linear cascades help in driving the reversible reaction into completion.

[4] Deracemization cascades are cascades applied for stereoselective deracemization of racemic compounds. One enantiomer of a racemic compound is converted into an enantiomer of opposite configuration *via* a prochiral intermediate which leads to an optically pure (or optically enriched) product.

The best example of an orthogonal cascade is coenzyme regeneration (Figure 9b). The cascade consists of an enzyme-catalyzed transformation of the main substrate into the main product coupled with another reaction to regenerate a coenzyme into its original oxidative state, to regenerate co-substrates, or to remove the unwanted by-products.

The parallel cascade consists of two substrates converted into two products by two distinct biocatalytic reactions, which are coupled through coenzymes or co-substrates (Figure 9c). The main difference between the orthogonal and parallel cascade is the economic value of the used substrates; in the parallel cascade, both products are considered to be valuable compounds, while in the orthogonal cascade the by-products are discarded.

In the cyclic cascade, shown in Figure 9d, one out of the mixture of substrates (S_1, Figure 9d) is selectively converted into an intermediate which is then transformed back into starting materials. Repetition of this cycle leads to the accumulation of the compound which is left behind in the first transformation. This design is mostly used for deracemization of amino acids, hydroxyl acids, and amines.

In most cases, a true cascade may consist of a combination of before-mentioned cascade setups [73].

2.4.1 Cofactor regeneration

Traditionally, whole-cells have been preferred catalysts, as opposed to isolated enzymes [82]. Since some enzymes are cofactor-dependent, a whole-cell system has the intrinsic ability to recycle the biological cofactor by simple addition of an economically acceptable substrate, such as glucose [119], as external cofactor addition is not necessary [82]. Therefore, the application of whole-cells offers several advantages [61, 82, 119 - 121], like simplicity and low cost [119], since there is no need for tedious enzyme purification [82]. For that purpose usually non-growing, i.e. resting cells are applied [61, 119, 120], because working with living organisms shows several drawbacks, like low biocatalytic activity, which is linked to metabolic activity and therefore limits the space-time yield (STY) and the actual biotransformation time window [82, 119].

Since DHs are emerging as eco-friendly alternatives applied for oxidative reactions due to numerous advantages in comparison to chemical catalysts [63, 122], the main challenge for their commercial application represents their cofactor dependency. Most of the enzymes depend on the pyridine nucleotide coenzyme: 80 % on the NAD(H) and 10 % on the NADP(H) [61].

The main drawbacks of these pyridine nucleotide coenzymes are that they are relatively unstable and expensive if used in stoichiometric amounts but have to be applied in such quantities since the oxidative state of the coenzyme changes during the reaction (Figure 4) [82] [61]. However, while the coenzymes change their oxidative state, they do not change their remaining complex structure, meaning that they can be regenerated *in situ via* a second concurrent redox reaction that allows them to re-enter into the reaction cycle [61]. Thus, the expensive cofactor is then only needed in catalytic amounts, which leads to a drastic cost reduction.

Therefore, it is possible to make the whole process economically feasible by integrating an efficient coenzyme regeneration system. Besides making the process economically acceptable, *in situ* coenzyme regeneration adds additional advantages [74, 120]:

1. **ECONOMY.** By integrating the coenzyme regeneration system, there is no need for adding stoichiometric but catalytic amounts of the coenzyme into the process.
2. **BALANCE SHIFT.** The coenzyme regeneration shifts the balance of the biochemical reaction in the desired direction.
3. **PREVENT INHIBITION.** Due to the consumption of the state-changed coenzyme, the accumulation of the state-changed coenzyme and/or reaction by-products that may inhibit the forward reaction, are avoided.
4. **SIMPLIFY WORKUP.** Depending on the used co-substrate, the accumulation of by-products is reduced or even eliminated since lower quantities of the coenzymes are used, thus simplifying the reaction workup.

There are several different coenzyme regeneration methods that can be applied, which are divided into enzymatic and non-enzymatic methods [82, 119]. The enzymatic regeneration methods are the preferred approach, regarded as simple and efficient [123] [61]. So far, only the enzymatic approach has reached preparative relevance [69]. As a rule of thumb, using less than 0.1 % *n*/*n* of cofactor makes the regeneration system economically acceptable [69].

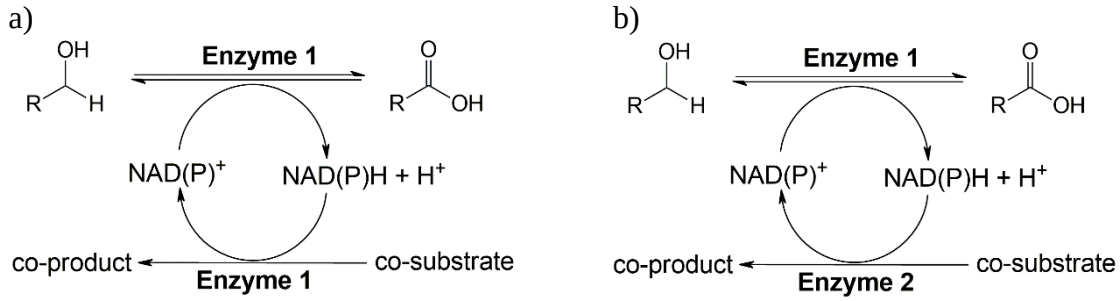

Figure 10 Enzymatic $NAD(P)^+$ regeneration set-ups: a) substrate-coupled $NAD(P)^+$ coenzyme regeneration, and b) enzyme-coupled $NAD(P)^+$ coenzyme regeneration.

There are two distinctive enzyme-based *in situ* setups (Figure 10), usually organized as orthogonal cascades (Figure 9b): the substrate- and the enzyme-coupled regeneration system [61, 124]. In the substrate-coupled approach, only one enzyme is applied: the same enzyme that catalyzes the main reaction catalyzes the coenzyme regeneration reaction as well, whereas in the enzyme-coupled approach two enzymes are applied: one enzyme that catalyzes the main reaction and a second enzyme that catalyzes the coenzyme regeneration reaction.

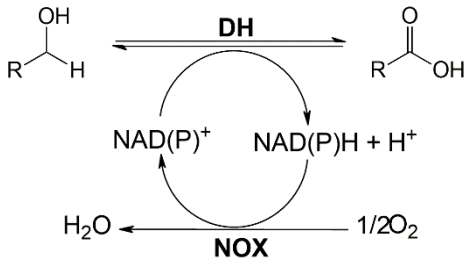

Figure 11 Enzyme-coupled NOX-catalyzed cofactor regeneration: the main reaction is catalyzed by a NAD(P)-dependent enzyme (DH) that catalyzes the main reaction, while the regeneration reaction is catalyzed by a NAD(P)H-dependent enzyme (NOX).

To have an efficient DH-catalyzed process, special attention must be paid to $NAD(P)^+$ regeneration and the enzyme's kinetic properties. The regeneration of $NAD(P)^+$ from NAD(P)H is problematic since organic oxidants in enzyme-catalyzed oxidations are unstable at higher pH values, that are required for maximal activity of the oxidations ($pH \approx 9$) [125]. In an appropriate regeneration system, co-product or unreacted co-substrate of the regeneration reaction should not interfere with the enzyme in the main reaction or with the method for the isolation of the desired product [125]. In general, glutamate dehydrogenase, lactate dehydrogenase, alcohol dehydrogenase, NAD(P)H oxidase (NOX), and NADH dehydrogenase are auxiliary enzymes used for the $NAD(P)^+$ regeneration [125], although the most attractive among them for $NAD(P)^+$ coenzyme regeneration is the H_2O-forming NOX enzyme. Its advantageous

application for coenzyme regeneration arises from the reaction it catalyzes: the enzyme accepts oxygen, which is present as dissolved gas in the media, and NAD(P)H, which is produced through the main DH-catalyzed oxidation. The NOX-catalyzed reaction results in the production of water, which does not negatively affect the reaction since the enzyme-catalyzed reactions are usually carried out in water-based (buffer) media, and $NAD(P)^+$, which is needed by the main DH enzyme (Figure 11) [83, 125, 126]. The main disadvantage of the NOX enzymes is their instability caused by the needed oxygen [125].

2.5 Biocatalysis in the pharmaceutical industry

Biocatalysis represents one of the most green technologies for the synthesis of complex, pharmaceutically relevant molecules due to the advantageous properties of enzymes, like smart insertion of chirality and selectivity with regard to regio- and stereochemistry in molecules, simple usage in technical production units, and catalysis under mild reaction conditions [3, 63, 122, 127]. The main challenge in the pharmaceutical industry, regarding the production of highly functionalized building blocks, is the complexity of molecules and the number of chiral centers needed to be produced [3, 60, 127], which reflects on the number of reaction steps combined with additional protection/deprotection of functional groups, thus regarded as difficult or tedious syntheses [16, 60, 127] that tend to increase even further with improving research [3, 122, 127].

The chiral pharmaceutical compounds are usually manufactured in a single enantiomeric form [3, 60], since the opposite enantiomer may have adverse effects [60]. However, if a drug has more than one chiral center, the single most active is usually marketed [128]. The current regulations demand proof that the non-therapeutic enantiomer is non-teratogenic [3, 60]. Because most drug effects are due to the interactions with chiral biological materials, each enantiomer may have different pharmacological properties [128]. The increasing understanding of the mechanisms of action led to the widespread awareness of the importance of chirality as the key to the efficiency of many drugs [127, 129]. The competition in the production of fine chemicals does not work through the pressure on the production cost, unlike the situation in bulk chemistry[5] [122].

[5] Bulk chemistry involves bulk chemicals or commodities, which are large-volume, low-price homogeneous and standardized chemicals produced in dedicated plants and used for a large variety of applications and priced typically less than US$1/kg.

For the production of chiral drug intermediates, different routes are employed [129], but the application and implementation of enzyme-based processes and their use in the pharmaceutical industry is seen as a great promise [60], since enzymes inherently satisfy the requirements expected for drug production. Hence, several pharmaceutical companies are now outsourcing the synthetic stages to focus on the discovery and formulation [60].

Despite the biocatalysis' potential is not being fully exploited; the recent developments have focused on two important areas [129]. The first area is the development of novel enzymes that catalyze reactions that are complicated to perform using traditional chemistry, such as asymmetric catalytic decarboxylation, asymmetric carbon-carbon bond formation in water and stereoselective oxidation, while the second area is the application of enzymes for deracemization of racemic mixtures to obtain a single enantiomer with a theoretical yield of 100 % [129]. Accordingly, based on the most recently published literature, the application of biocatalysis for the production of drug or drug intermediates has significantly increased in the past few years [58].

2.5.1 Bioproduction of statin precursors

While cholesterol is vital for the normal functioning of the body [9], it is also considered to be the main cause of coronary heart disease [7, 130]. Over the course of nearly a century of investigation, scientists have developed several lines of evidence that establish the causal relationship between blood cholesterol, atherosclerosis, and coronary heart disease [7]. Relying on those findings, scientists and the pharmaceutical industry have successfully developed a remarkably effective class of drugs called statins, which lower cholesterol levels in the blood and therefore reduce the frequency of heart attacks and illnesses related to high cholesterol levels [7 - 9]. Thus, statins belong to hypolipidemic drugs, which are lipid-lowering agents. They are medication prescribed for lowering low-density lipoprotein cholesterol (LDL-C) concentration by competitively inhibiting the enzyme 3-hydroxy-3-methylglutaryl coenzyme A (HMG-CoA) reductase. This enzyme plays the central role in the production of cholesterol in the liver [8, 11, 131 - 134] and, therefore, in presence of statins, the conversion of HMG-CoA to mevalonic acid does not occur [1, 8, 11, 135] (Figure 12).

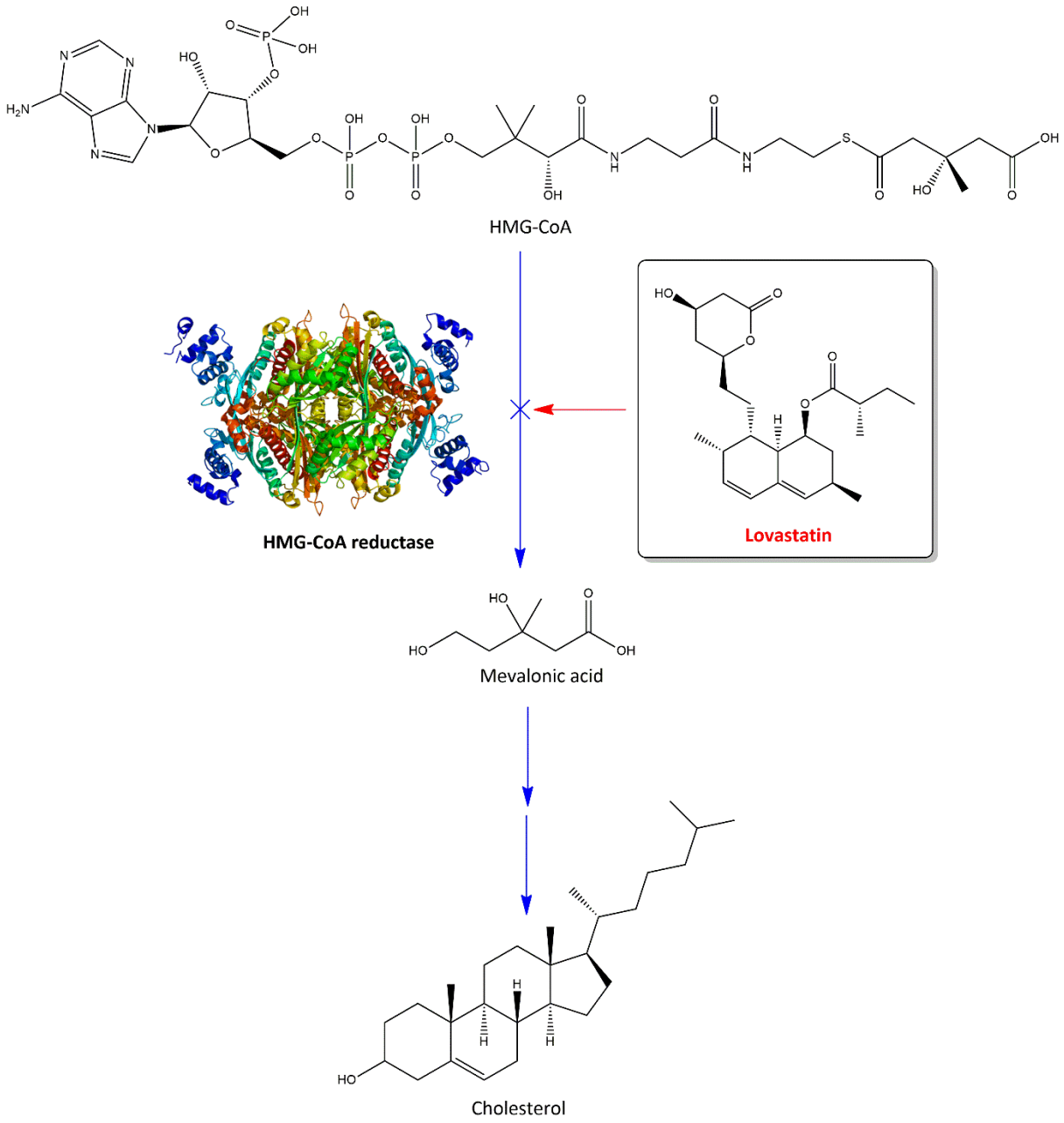

Figure 12 Simplified scheme of the mevalonate pathway. The HMG-CoA reductase catalyzes the conversion of HMG-CoA into mevalonic acid. In presence of statins (e.g. Lovastatin), the statin molecules occupy the HMG-CoA binding site of the enzyme [136], thus blocking the access of the HMG-CoA substrate to the enzyme's active site [135].

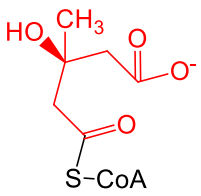

Figure 13 Simplified structure of HMG-CoA, an intermediate in the mevalonate and ketogenesis pathways [138, 139]; red-colored is the *syn*-3,5-dihydroxy carboxylate side-chain.

Statins are one of the most prescribed drugs today [8, 134] with worldwide annual sales exceeding 15 billion US dollars [8, 13, 16, 25, 27, 64, 88, 102, 137] making them blockbuster drugs [70]. As of now, a number of statins have been on the market, either as natural or synthetic products [16], with all having the pharmacophore *syn*-3,5-dihydroxy carboxylate side-chain in common (Figure 13) [11]. This side-chain resembles the HMG-CoA moiety (Figure 13), due to which all statins (examples, Figure 14) are biologically active as inhibitors of the HMG-CoA reductase (Figure 12) [8, 11, 12, 88, 131, 132, 134].

Besides lowering LDL-C levels, and therefore reducing the cardiovascular risk [6], it was reported that the use of statins has additional positive side effects such as the promotion of new blood vessel growth, stimulation of bone formation, offering protection against oxidative modification of LDL, and having anti-inflammatory effects [135, 138].

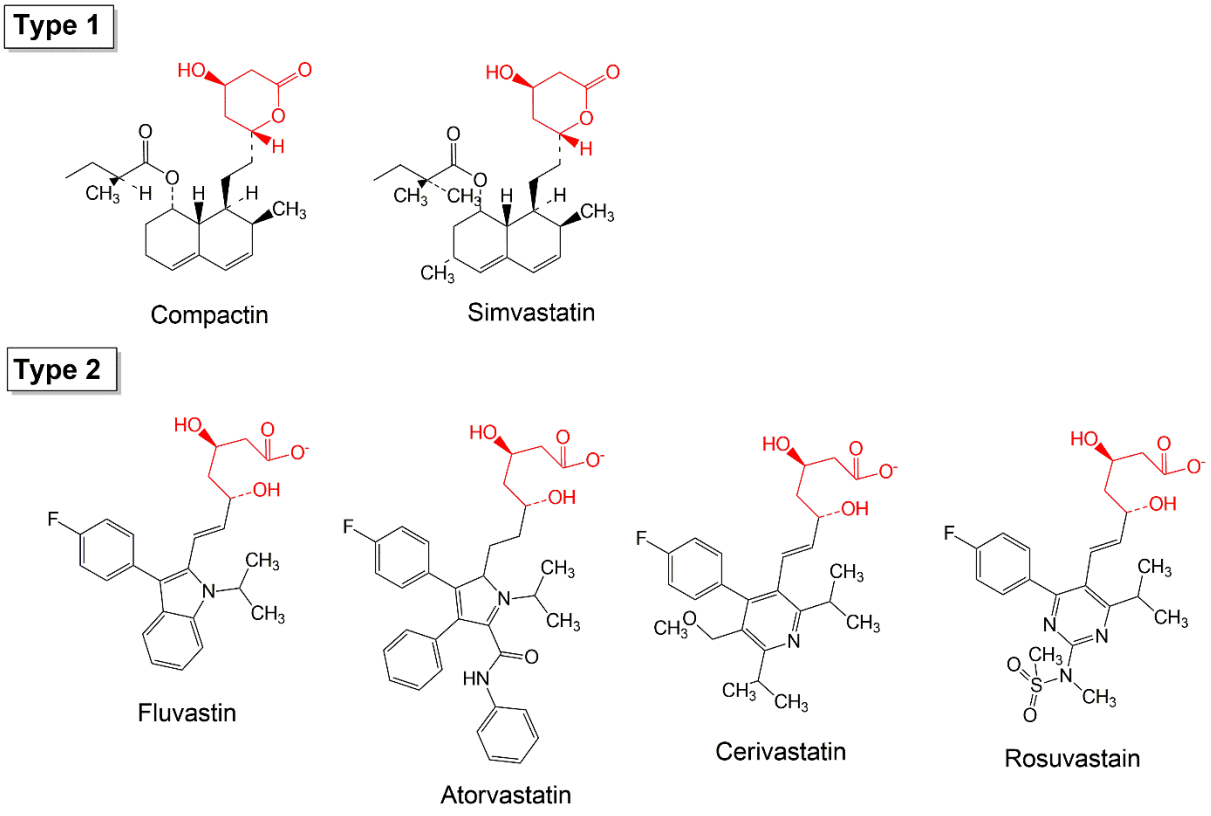

Figure 1 Structural formulas of several statin inhibitors [6, 8]. The HMG-like moiety, which is present in all statins, is red-colored [138].

Statins can be classified into three categories based on their generation. The first generation of statins includes simvastatin (Zocor), pravastatin (Pravachol) and lovastatin (Mevacor), which are fungal metabolites with similar chemical structure. The second generation includes synthetic and racemic fluvastatin (Lescol), while the third generation

includes synthetic enantiomerically pure compounds like atorvastatin (Lipitor), rosuvastatin (Crestor) and pitavastatin (Livazo) [6, 8]. These fully synthetic third-generation statins are frequently being addressed as super-statins [140]. Based on the HMG-CoA motive, the statins can be grouped into two categories according to the motive type (Figure 14) [140].

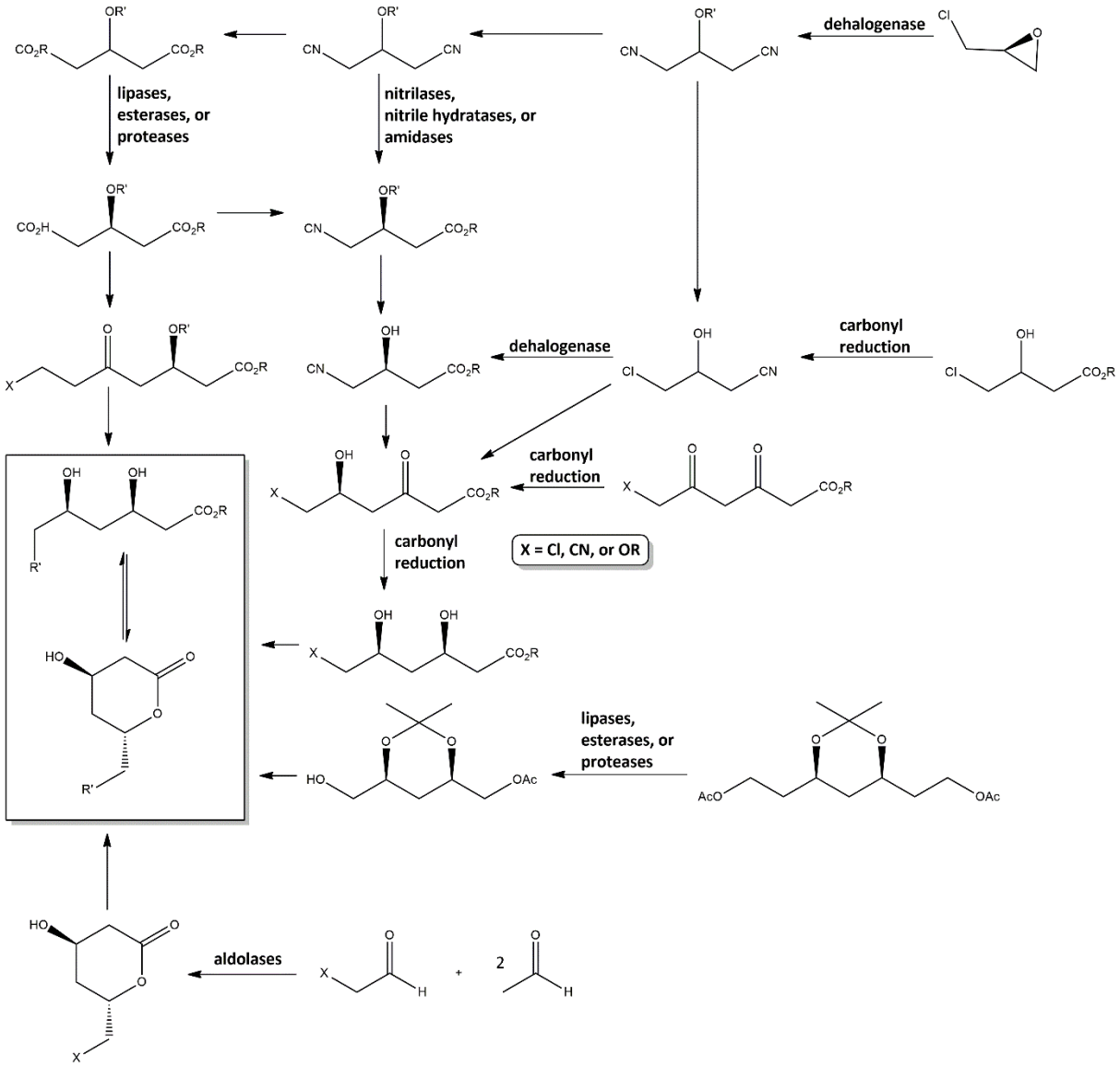

Figure 15 Examples of common routes for the production of the *syn*-3,5-dihydroxy carboxylate statin side-chain [5, 8, 11, 70].

Satins were discovered in the 1970s as fungal metabolites [7, 15, 25, 131] and since then many efforts were focused not only on their structural modification to make them more effective with less side effects [25, 131, 134, 140] but also to simplify their production process, since laborious chemical processes at harsh conditions are currently being employed [10, 12, 14 - 18]. Additionally, the two chiral centers present in the molecule are challenging to make by applying traditional chemical methods [10, 11].

The increasing commercial demand for statins and the need for a simple preparation on the industrial scale have led to immense efforts towards finding a more efficient and economical process to produce statin intermediates [12, 15, 25, 70, 134, 141]. Driven by the requirements of high chemical and stereochemical purity, considering the trend in the pharmaceutical companies towards the biocatalysis as a source for enantio- and diastereopurities [8], a variety of biocatalytic routes involving different classes of enzymes and starting materials have been developed for the enantioselective synthesis of the statin side-chain precursors [5, 8, 10 - 13]. The most common biocatalytic methods towards the production of statin intermediates are covered in Figure 15 [5, 8, 11, 13, 25, 137], whereby those biocatalytic approaches can be broadly grouped into two strategies [10, 27].

The first strategy involves the synthesis of the key chiral precursor ethyl (*R*)-4-cyano-3-hydroxybutyrate on which the second stereocenter is introduced at a later step (Figure 16a). Most of the biocatalytic methods fall under this strategy [10], although, according to some literature, the usage of nitrilases is classified as a separate third strategy [25, 64]. The second strategy involves the generation of both chiral centers in a single step using aldolases that catalyze the aldol reaction, which results in a more advanced six-carbon statin side-chain intermediate (Figure 16b) [10, 27].

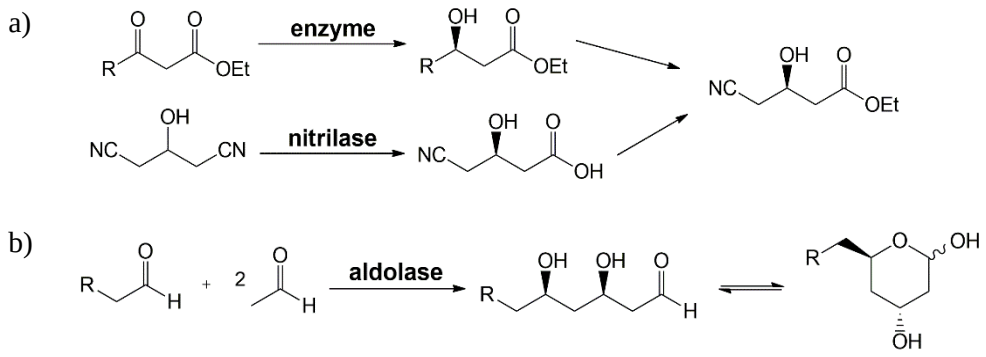

Figure 16 Biocatalytic strategies towards the production of statin side-chain intermediates. a) The first strategy results in the formation of ethyl (*R*)-4-cyano-3-hydroxybutyrate [10, 27], while b) the second strategy is based on an aldol reaction that results in the formation of a six-carbon intermediate [10, 12].

2.5.1.1 DERA-catalyzed statin side-chain intermediate production

Although different biocatalytic approaches have been developed, the ever-growing attention is being shifted towards a simplified reaction containing fewer reaction steps with a high atom economy in which the generation of both chiral centers is done in a single step by using DERA (Figure 16b) [10, 12, 16, 25, 28, 134]. By using achiral substrates [15, 131] DERA

catalyzes the sequential aldol addition, that yields an enantiomerically pure lactol, a cyclized 2,4,6-trideoxyhexose [8, 11, 25, 26, 89, 99, 101, 142] (Figure 17). The lactol is a valuable chiral synthon [87, 88, 99] that is used for the production of statin intermediates [28, 87 - 89, 101 - 105, 142]. The preparation of the chiral 2,4,6-trideoxyhexose has provoked extensive activities towards its production, because of its extremely high market price and particular pharmaceutical requirements (Table 3) [14, 88, 131]. Due to the challenges present in the chemical synthesis of statin intermediates, the use of DERA presents one of the most attractive and most promising routes [12, 14, 15, 86, - 88, 91, 102, 105, 131, 134, 141, 143].

Table 3 Example of the value-added chain in the chemical industry for atorvastatin (Lipitor by Pfizer) [127].

Parameter	**Bulk chemicals**		**Fine chemicals**			**Specialty**
			Intermediates		**API**[a]	
Example	**Methanol**	**Acetic acid**	**(I)**	**(II)**	**(III)**	**Lipitor**
Molecular formula	CH_4O	$C_2H_4O_2$	$C_7H_{11}NO_3$	$C_{14}H3_0NO_4$	$C_{33}H_{35}FN_2O_5$	N/A
Molecular weight	32.04	60.05	157.17	269.34	558.65	N/A
Applications	> 100	> 50	10	1	1	N/A
Price indication (US$/kg)	0.2	1.00	100	200	2,000	80,000
Production (tons/year)	$32 \cdot 10^6$	$8 \cdot 10^6$	200	300	400	400
Producers	100	25	10	5	1[a]	1[a]
Customers	100	50	1	1	1[a]	Millions
Plant type [b]	D, C	D, C	M, B	M, B	M, B	N/A
Manufacturing steps	1	2	5	15	20	+2

[a] Active pharmaceutical ingredient (API)
[b] Ex-patent holder; several generic producers have launched in the meantime (B – batch, C – continuous, D – dedicated, M – multipurpose)
Fine chemicals:
(I) or ethyl(*R*)-4-cyano-3-hydroxybutanoate (or 'hydroxynitrile')
(II) or *tert*-butyl(4*R*,6*R*)-2-[6-(aminoethyl)-2,2-dimethyl-1,3-dioxan-4-yl] acetate
(III) or 2-(4-fluorophenyl)-*β*,*δ*-dihydroxy-5-(1-methylethyl)-3-phenyl-4-[(phenylamino)carbonyl]-1-*H*-pyrrole-heptanoic acid (or atorvastatin)
Note: Figures are indicative only.

An example of the value-added chain extending from bulk through fine chemicals to APIs is shown in Table 3, blockbuster Lipitor (atorvastatin) used as an example. The value-added chain extends from a C_1 molecule (methanol) all the way to a C_{33} molecule (atorvastatin). Methanol and acetic acid are typical commodities: low-price, multi-usage products manufactured in large quantities by many companies. Three examples of fine chemicals used

for the manufacture of atorvastatin are listed: the advanced intermediates (1) ethyl 4-chloro-3-hydroxy butanoate and (2) tert-butyl (4*R*,6*R*)-2-[6-(2-aminoethyl)-2,2-dimethyl-1,3-dioxan-4-yl] acetate, and the API itself: (3) atorvastatin. As long as atorvastatin, 2-(4-fluorophenyl)-*β*,*δ*-dihydroxy-5-(1-methylethyl)-3-phenyl-4-[(phenylamino)-carbonyl]-1*H*-pyrrole-heptanoic acid, is sold according to specifications, it is a fine chemical. In the pharmaceutical industry, the chemical synthesis of an API is also referred to as primary manufacturing. The secondary manufacturing comprises the formulation of the API into the final delivery form (FDF). The API is compounded by recommended bulkiness, stability, color, and taste. Once atorvastatin is tableted, packed, and sold as the anti-cholesterol prescription drug Lipitor, it becomes a specialty. The price difference between the API and the package sold in the drugstore is very substantial, which is evident from Table 3 [127].

Although the application of DERA shows great potential in the production of statin intermediates, the enzyme shows some major drawbacks for its practical application, such as poor resistance to high aldehyde concentrations or the requirement of large quantities of the enzyme to obtain industrially useful product yields [8, 12, 88, 131, 133, 141]. Due to the high interest in the application of DERA for the mentioned synthesis, the enzyme is being continuously re-engineered and cloned for better performance and stability under otherwise harsh industrial conditions [10, 25, 26, 88, 99, 141].

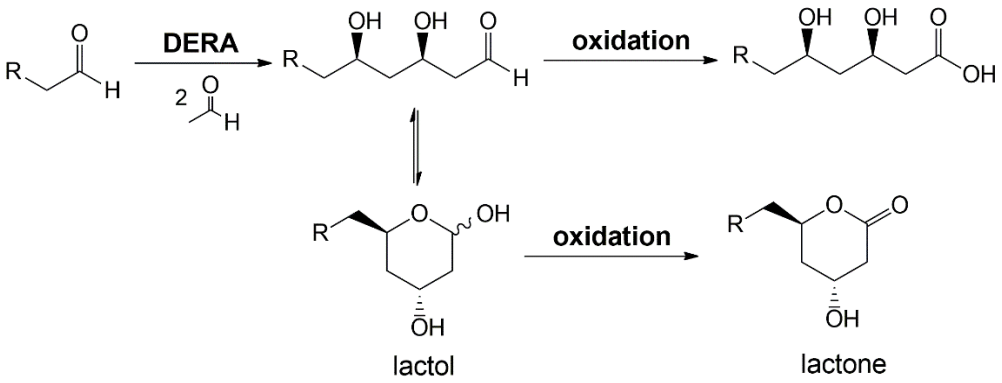

Figure 17 DERA-catalyzed 3,5-dihydroxy carboxylate side-chain synthesis followed by an oxidation. Depending on the oxidation method or the enzyme substrate specificity, the oxidation of the appropriate substrate-form occurs [12].

The DERA-based strategy is almost by default coupled with an oxidation step in which the lactol is further oxidized into a lactone (Figure 17), such as the cyclized 3,5-dihydroxyhexanoic acid, which is a more stable form of lactol [144]. For that reason, the lactone presents a key product in the synthesis of statin intermediates [8, 11, 12, 25 - 28] (Figure 17).

The significance of those reactions is evident also in the industry: DSM Pharma Chemicals [145, 146] and Diversa [143, 147] operate the DERA-catalyzed aldol reaction followed by a chemical oxidation of the produced lactol [8, 13, 143, 145, 146], while Lek Pharmaceuticals patented the DERA-catalyzed reaction followed by DH-catalyzed oxidation, which results in a more economic process: reduced number of synthetic steps, improved and simplified reaction, etc. [148].

By studying the available literature, it is evident that there are only a few known suitable ways for chemical oxidation of the enzymatically produced lactol [12, 88, 134, 143], whereas investigations on the enzymatic lactol oxidations remain rare [25, 134]. This is especially interesting considering that the chemical oxidation of the DERA-produced lactols is done with the excess of harsh chemicals, while the biocatalytic oxidation uses oxygen as a co-substrate and produces water as a by-product, which classifies the latter approach in the area of green chemistry [25].

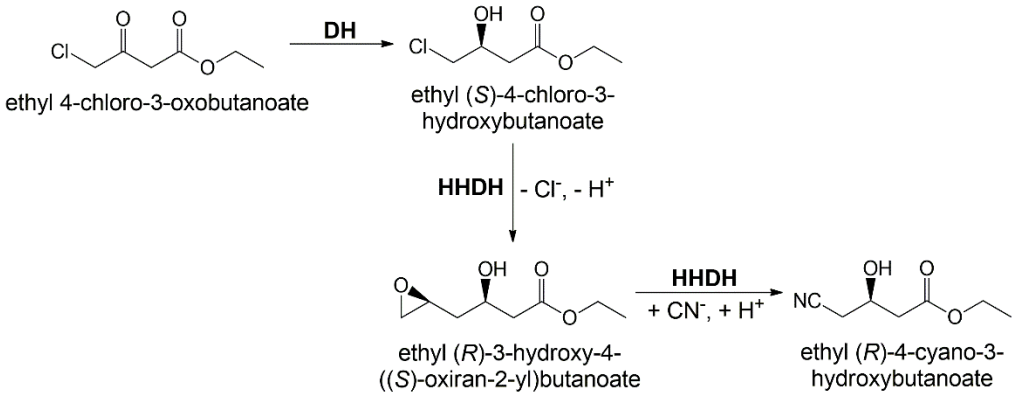

Figure 18 DH-catalyzed oxidation of ethyl 4-chloro-3-oxobutanoate followed by HHDH-catalyzed conversion of ethyl (*S*)-4-chloro-3-hydroxybutyrate into ethyl (*R*)-4-cyano-3-hydroxybutyrate [5, 27, 149]. The change in stereo-configuration from the substrate to the final product is caused by a switch in priority of the substituents at the chiral center according to the Cahn-Ingold-Prelog (CIP) priority rules [149].

Based on the accessible literature, an interesting route towards the statin side-chain intermediate production seems to be a multi-enzyme process consisting of DHs and HHDHs, where the HHDHs are used for their ability to replace the halide group with a strong nucleophile containing nitrogen, such as nitrile [5]. The application of HHDHs is classified under the first statin side-chain strategy that results in the production of ethyl (*R*)-4-cyano-3-hydroxybutyrate (Figure 18) [5, 21, 27, 149].

A similar reaction of statin intermediate synthesis was patented by Codexis, who demonstrated a two-step three-enzyme catalyzed reaction involving two DHs, where one is responsible for the substrate oxidation and the other for coenzyme regeneration, and an HHDH enzyme applied for the dehalogenation reaction and cyano-group addition [150]. They filed a new successive patent in which they expanded the substrate scope and applied newly engineered enzymes [151]. Similar reactions were claimed by DSM Pharma Chemicals who are using HHDH enzymes to synthesize epoxides, lactones, alcohols, and other intermediates in the preparation of APIs, in particular of statins [152]. In their patent, they also claim a completely chemoenzymatic pathway towards the production of the desired lactone by combining DERA and HHDH enzymes.

2.6 Mathematical modeling of enzymatic reactions

The main goal of enzyme reaction engineering is a high space-time yield at a high degree of substrate conversion under the conditions of high chemical and enantiomeric selectivity [41]. The goal of reactor design is the description of the behavior of both the pertinent degree of conversion X ($0 \leq X \leq 100$ %) and of selectivity σ ($0 \leq \sigma \leq 1$) over the reaction time [41].

Biocatalytic processes are quite similar to chemical processes in many aspects, where the most significant difference is that enzyme kinetics and enzyme stability must be taken into account [153]. A few years ago modeling of enzyme-catalyzed reactions was not considered to be an important industrial practice, but nowadays the situation changed with the need for rapid and effective scale-up combined with the aim of conducting economically feasible production of fine chemicals [3, 4, 154]. This can be achieved with the use of miniaturized experimentation or by applying mathematical modeling [3, 153]. Albeit there are four classification areas regarding mathematical modeling [155], the strategy of mathematical modeling based on the observed kinetics incorporated with mass balance equations for every participating component in an appropriate reactor type seems not only to be promising but has already been successfully applied for large-scale production optimization [153].

In order to choose the best enzyme reactor for the observed process, it is necessary to determine the reaction kinetics. Consequently, particular attention should be applied to the system features (pH, temperature, substrate, product and enzyme concentration), reaction aspects (thermodynamic and kinetic constants), enzyme characteristics (mechanical properties, activity, stability, and molecular mass), and their interdependence and influence on the process as whole [31, 41, 156].

Model development consists of enzyme kinetic modeling and reactor modeling that connects enzyme kinetics with mass balance equations in an appropriate reactor type [153].

To successfully develop a model, the following steps should be performed [41, 153, 157]:

1. Characterization of enzyme activity and stability dependence on pH, temperature, substrate and product concentrations.
2. Acquiring experimental data using the initial reaction rate method which is a steady-state approximation where the initial reaction rates are measured at different substrate concentrations.
3. Mathematical evaluation of the obtained results and the development of an adequate reaction rate equation.
4. Estimation of kinetic parameters using non-linear regression analysis and optimization using an optimization algorithm. The numerical values of the parameters are evaluated by fitting the model to the experimental data. The model equations are solved numerically by an algorithm such as the fourth order Runge-Kutta. The calculated data is then compared to the experimental data, recalculated in the optimization routine and fed again to the integration step until minimal errors between experimental and integrated values are achieved. The residual sum of squares is defined as a measure of discrepancy between the experimental data and the data obtained based on the model.
5. Model validation by comparing experimental data with simulations under identical conditions, where the experimental data (validation set) is different from the experimental data (training set) used for identifying kinetic parameters.

Once the model was successfully validated, it can be further used:

6. Using validated mathematical models for computer simulations which will help in optimization of reaction conditions, such as the appropriate concentration of enzyme(s), substrate(s) and/or reactor type.

2.6.1 Reaction kinetics

The reaction kinetics have to be found under conditions relevant to the process, which are different than the values published in literature since they refer to optimal values of pH and temperature for the enzyme in question and are mainly for low substrate concentrations [41]. To develop a meaningful reaction kinetics model, the influence of all the substrates, products, and inhibitors has to be known [41]. Also, the thermodynamics of an enzyme reaction must be

integrated into the kinetic model, since an enzyme can catalyze both the forward and reverse reaction [41]. The kinetic parameters, such as maximum rate of reaction (V_m) or Michaelis constant (K_m^S) for the Michaelis-Menten kinetic models, should be determined by using non-linear regression models [41].

The Michaelis-Menten kinetics is one of the best-known models of enzyme kinetics, due to being based on the simplest enzyme reaction mechanism consisting of a binding and a catalytic step (Equation 1) [41, 153, 158 - 160].

$$S + E \underset{k_2}{\overset{k_1}{\rightleftarrows}} ES \overset{k_3}{\rightarrow} P + E \qquad \text{Equation 1}$$

In Equation 1 *S* denotes the free substrate, *E* and *ES* denote the free and bound enzyme, respectively, and *P* the product. The k_1 is the rate constant of the enzyme-substrate complex formation, k_2 the rate constant of the enzyme-substrate complex dissociation, while k_3 is the catalytic constant.

The Michaelis-Menten kinetics is based on the findings of Michaelis and Menten who published 1913 an equation that incorporates the reaction rate with substrate and enzyme concentration, which they supported by numerous experimental data [161]. They suggested that the free enzyme first binds to the substrate forming the enzyme-substrate complex, which is a fast but reversible reaction. The dissociation of the enzyme-substrate complex into the free enzyme and product is a slow reaction and hence the rate-limiting step. Throughout the reaction, the total concentration of the enzyme will be the sum of the concentration of total free enzyme and concentration of total enzyme bound with the substrate [41, 160 - 162]. The rate of product formation, i.e. the reaction rate of the enzyme-catalyzed reaction can be described by single-substrate Michaelis-Menten kinetics expressed as

$$r = \frac{\mathrm{d}c_P}{\mathrm{d}t} = \frac{V_m \cdot c_s}{K_m^s + c_s} \qquad \text{Equation 2}$$

where *r* is the reaction rate (mmol/mL·min), c_P the product concentration (mmol/mL), *t* the time (min), V_m the maximum rate achieved by the system at the saturating substrate concentration (mmol/mL·min), c_S is the substrate concentration (mmol/mL), K_m^S is the Michaelis constant (mmol/mL), which equals the substrate concentration at which the reaction rate is half of V_m.

Biochemical reactions involving a single substrate are often assumed to follow Michaelis-Menten kinetics, without regard to the model's underlying assumptions. The key parameters in

the Michaelis-Menten equation are K_m^S and V_m where V_m depends upon the enzyme concentration (Equation 3), whereas K_m^S on the constants given by Equation 4. The V_m is the rate of reaction at which the enzyme is saturated with substrate. The K_m^S, which is an inverse measure of affinity, is the concentration of the substrate when the reaction rate is equal to one half of the maximal rate (V_m) for the reaction (Equation 5). An enzyme with a high K_m^S has a low affinity for its substrate and requires a greater concentration of substrate to reach V_m [160, 163].

$$V_m = k_3 \cdot E_0 \qquad \text{Equation 3}$$

$$K_m^s = \frac{k_1 + k_3}{k_2} \qquad \text{Equation 4}$$

$$K_m^s = \frac{1}{2} \cdot V_m \qquad \text{Equation 5}$$

When plotting the rate of the enzyme-catalyzed reaction as a function of substrate concentration, the curve takes on the characteristic hyperbolic shape (Figure 19). At low substrate concentration, the reaction rate linearly depends on substrate concentration and can be approximated as first-order kinetics. At high substrate concentration, the reaction rate does not depend on the substrate concentration and therefore can be approximated as zero-order kinetics. The area between those two areas is called the Michaelis-Menten area [164].

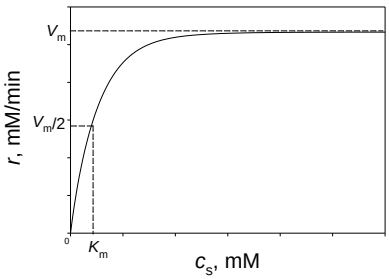

Figure 19 Typical Michaelis-Menten kinetics plot.

Most enzyme-catalyzed reactions are multi-substrate systems, usually consisting of at least two substrates Equation 6). In case of a DH-catalyzed reaction, the second substrate is usually a coenzyme [164]. The Michaelis-Menten equation is then extended, and in case of a double-substrate system, it is described as per Equation 7.

$$S_1 + S_2 \rightarrow P_1 + P_2 \qquad \text{Equation 6}$$

$$r = \frac{V_m \cdot c_{s_1} \cdot c_{s_2}}{\left(K_m^{s_1} + c_{s_1}\right) \cdot \left(K_m^{s_2} + c_{s_2}\right)}$$ Equation 7

Biocatalytic reactions often show a change in enzyme activity over time which is manifested as rate deceleration. These substances that reduce the activity of an enzyme-catalyzed reaction are known as inhibitors, which cause reversible or irreversible enzyme inhibition [160]. The inhibitors act either directly or indirectly by influencing the catalytic properties of the active site [159] and can be a substrate, a product, or both [160]. There are four types of reversible inhibition: competitive (Equation 8), non-competitive (Equation 9), uncompetitive (Equation 10), and mixed inhibition [159, 160].

$$r = \frac{V_m \cdot c_s}{K_m^s \cdot \left(1 + \frac{c_i}{K_i}\right) + c_s}$$ Equation 8

$$r = \frac{V_m \cdot c_s}{\left(K_m^s + c_s\right) \cdot \left(1 + \frac{c_i}{K_i}\right)}$$ Equation 9

$$r = \frac{V_m \cdot c_s}{K_m^s + c_s \cdot \left(1 + \frac{c_i}{K_i}\right)}$$ Equation 10

In Equation 8 – 10 K_i represents the inhibition constant (mM), while c_i the concentration of the inhibiting compound (mM).

Competitive inhibitors compete with the substrate at the substrate binding site [160]. One of the characteristics of competitive inhibitors is that they can be displaced from the active site if high concentrations of the substrate are used, thereby restoring the enzyme activity. Thus, competitive inhibitors increase the K_m^S of a reaction because they increase the concentration of the substrate required to saturate the enzyme. However, they do not change the V_m [159, 160].

Non-competitive inhibitors react with the enzyme at a site different from the active site. Therefore, the binding of the inhibitor does not physically block the substrate-binding site, but it does prevent the subsequent reaction [160]. Most non-competitive inhibitors are chemically unrelated to the substrate, and their inhibition cannot be overcome by increasing the substrate concentration. Such inhibitors reduce the concentration of the active enzyme in solution, thereby reducing the V_m of the reaction, but do not change the value of K_m^S [159].

The uncompetitive inhibitor binds only to the enzyme-substrate complex, meaning the binding of the substrate creates the binding site for the inhibitor; therefore, the binding of the

inhibitor is promoted by the presence of the substrate. Both V_m and the K_m^S decrease [159] [160, 165]. A special case of uncompetitive inhibition is substrate inhibition whereby the substrate itself blocks enzyme activity at high concentrations. This is caused by more than one substrate molecule binding to the active site of the enzyme meant for just one substrate molecule, e.g., different parts of the substrate molecule bind to different parts of the enzyme active site [160].

Mixed inhibition is a combination of competitive and uncompetitive inhibition [159, 160].

Another reason for the decrease of the reaction rate is the loss of enzyme activity during a reaction due to its instability in the present system which is referred to as the decay of enzyme activity. It is usually described using the first- (Equation 11) or second-order (Equation 12) kinetics [166].

$$\frac{\mathrm{d}V_m}{\mathrm{d}t} = -k_d \cdot V_m \qquad \text{Equation 11}$$

$$\frac{\mathrm{d}V_m}{\mathrm{d}t} = -k_d \cdot V_m^2 \qquad \text{Equation 12}$$

2.6.2 Ideal enzyme reactors

The reactor design is one of the fundamental elements of chemical reaction engineering [167]. The reactor model of ideal reactors is based on a simplified perception of a reactor system, such as the assumption of ideal flow or ideal mixing [167, 168], thus belonging to ideal flow models [167]. Based on this, the reactant and the product concentration inside the reactor are considered to be uniform and are therefore observed as homogeneous systems, combined with the assumptions of constant temperature (isotherm conditions) and constant volume (isochoric conditions), pressure and pH [167].

As of operation modes of chemical reactors for the industrial application are concerned, they can run as either batch, continuous or semi-batch (or semi-continuous) models [167]. Reactors operating under batch mode are referred to as batch reactors (Figure 20a) [167]. When carrying out the reaction under the batch mode, all feeds are loaded into the reactor at the very beginning of the reaction [167]. After a certain period of reaction time when, for example, the desired conversion was achieved, the whole content of the reactor is unloaded. Accordingly, there is no input or output of the reaction materials meaning no material flow [167]. A batch

reaction is an unsteady process and therefore the composition inside the reactor does change with time. The reaction rate of an ideal batch reactor can be expressed as follows

$$-r_s \cdot V = \frac{\mathrm{d}n_s}{\mathrm{d}t} \qquad \text{Equation 13}$$

where $V$is the reaction volume (mL) and n_S is the amount of substrate (mol) that equals

$$n_s = c_S \cdot V \qquad \text{Equation 14}$$

Since the batch process is considered to be an isochoric process, Equation 13 can be expressed as

$$r_s = -\frac{\mathrm{d}c_s}{\mathrm{d}t} \qquad \text{Equation 15}$$

An interesting upgrade of a batch operating mode is running a reaction as a repetitive batch mode. This mode is especially interesting for obtaining higher product concentrations or for increasing the substrate conversion [169]. In big part, the operating mode resembles a standard batch mode, but instead of unloading and starting a new cycle, a fresh feed, often of same as the initial, is loaded into the reactor once the previous load was spent, i.e. once substrate concentration dropped to zero or enzyme does not show any residual activity. This repetitive technique has been shown to be very effective and easy to handle [170] when the synthesized products do not have a negative impact on the applied enzymes.

In case of running a reaction in a continuous mode, the feedstock is continuously fed (supplied) into the reactor and simultaneously the product is removed from the reactor [167]. Reactors operating under such mode are called continuous or flow reactors [167]. Most reactors that operate under a continuous mode are under steady state, since at any specific location in the reaction system parameters, like the substrate or product concentration, do not change with time. Thus, the general model for a continuous reactor can be expressed as given in Equation 16. If the reactor operates in steady-state ($q_0 = q_t = q = const.$) and if V, $\rho = const.$, it can be expressed as *per* Equation 17.

$$q_0 \cdot c_{S,0} - q_t \cdot c_{S,t} - V \cdot r = \frac{\mathrm{d}n_S}{\mathrm{d}t} \qquad \text{Equation 16}$$

$$r = \frac{c_{S,0} - c_S}{V} \cdot q \qquad \text{Equation 17}$$

In Equations 16 and 17 $c_{(s,0)}$ denotes the initial concentration of a substrate (mM), while q denotes the volumetric flow rate (mL/min).

If a reactor is operated with at least one reactant (or enzyme) that is continuously fed into the reactor or if one product is leaving the reactor while other components are added to or removed from the reactor, the reactor is then being operated under a semi-batch mode, hence called a semi-batch reactor. When, during the reaction, nothing is removed from the reactor, but at least one substrate or enzyme is continuously fed into the reactor, then the reaction is being conducted under a fed-batch mode and is referred to as a fed-batch reactor [171, 172], but alternatively may be called a semi-batch reactor [172]. In such reactors, the resulting products remain in the reactor until the end of the run [172]. Based on the described, these reactors operate under non-steady state.

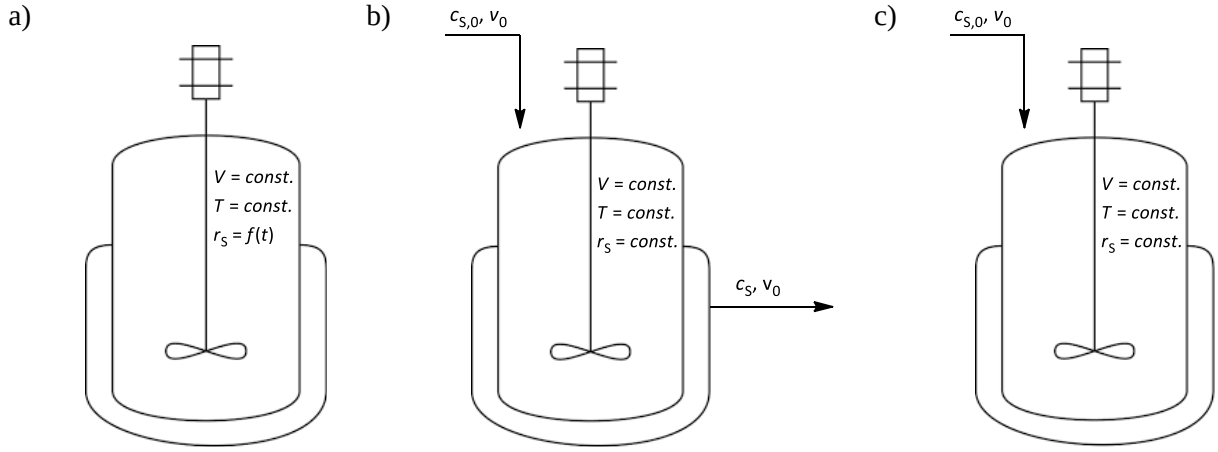

Figure 20 Scheme of an ideal a) batch, b) continuous, and c) fed-batch reactor [168, 173].

The application of a fed-batch reactor shows some notable advantages, such as avoidance of a substrate or product inhibition, or maintenance of appropriate enzyme activity [172]. The reaction rate in a semi-batch (fed-batch) reactor depends on the system set-up and the mass balance equation is expressed as given in Equation 16. If only one feed, i.e. one substrate supply exists without the removal of formed products, the reaction rate for a fed-batch reactor can be expressed as

$$r = \frac{c_{S,0} - c_S}{V} \cdot q - \frac{\mathrm{d}c_S}{\mathrm{d}t} \qquad \text{Equation 18}$$

The Equation 18 stays true if the volume change is considered equal to the volumetric in-flow rate [173].

Repetitive batch and fed-batch reactor modes are considered to be standard modes for decreasing enzyme consumption [174].

2.6.3 Kinetic data related to statin synthesis

Despite its certain importance for each of the synthetic steps towards the production of statin side-chain building blocks, the available literature offers very little or virtually no kinetic data obtained based on kinetic models.

The data concerning aldolase-catalyzed reactions are scarce [14, 33, 34], and for now, only few studies were found concerning mathematical modeling of the reaction towards statin side-chain production [14]. Švarc and coworkers (2019) have reported a mathematical model (consisting of a formal kinetic model that includes the data-driven or the empirical model which has less kinetic constants) validated in multiple reactor configurations. Using the developed model, process simulations were done, and optimal process design was proposed [175]. Ručigaj and Krajanc (2015) have reported a very complex model for the sequential aldol reaction involving acetyloxyacetaldehyde, acetaldehyde, and chloroacetaldehyde as substrates, which was catalyzed by crude DERA expressing culture lysate [14].

Regarding reactions catalyzed by NAD(P)-dependent DHs, for now, only few published research articles offer kinetic data for the enzymes used for the oxidation of the DERA-produced lactols, but without further model development that would help in process optimization and scale-up. A research was published in 2014, in which the kinetic data of the *E. coli* membrane-bound PQQ-dependent glucose dehydrogenase (GDH) was given [134]. The authors have used a DERA-GDH coupled system using a whole-cell catalyst, but despite performing a successful oxidation mediated by the PQQ-GDHs, the system resulted in a disadvantageous industrial application, due to the application of the PQQ as a cofactor and the low expression level of GDH as membrane protein [134]. This finding was followed by the research of the Xu group in 2016 [25] who carried the oxidation of the key lactol by a novel NADP-dependent aldehyde dehydrogenase (AlDH). Although they have published values of kinetic parameters, they have not developed a mathematical model which would be a basis for future application.

In addition to the obvious lack of aldolase and DH kinetic data, the data related to HHDHs and the reaction of statin side-chain production remains unavailable [11], especially data obtained based on a simple and robust mathematical model for statin side-chain production [22]. It should be noted that, for the time being, the catalytic data for the biocatalytic reaction of epoxide-ring opening in presence of strong nucleophiles was not estimated yet and thus no

mathematical models were developed, although these reactions are of scientific interest [8, 24, 22, 36].

3 SYNTHESIS OF THE FIRST STATIN SIDE-CHAIN PRECURSOR

3.2 Introduction

The first reaction route consisted of four reactions catalyzed by three different enzymes (Figure 1) in the following order:

1. DERA^{Tm}- or DERA^{024}-catalyzed double-aldol addition
2. AlDH- or KRED^{332}-catalyzed oxidation
3. HHDH^{001}-catalyzed dehalogenation
4. HHDH^{001}-catalyzed epoxide ring-opening in presence of a KCN

The starting materials were acetaldehyde (AA) and chloroacetaldehyde (CAA). The aldol reaction proceeded *via* the production of intermediate 4-chloro-3-hydroxybutanal (CHB) which further reacted with AA to form the final aldol product 6-chloro-3,5-dihydroxyhexanal (CDH).

The following reaction was the oxidation of CDH into 6-chloro-3,5-dihydroxyhexanoic acid (CDHA) catalyzed by either AlDH or KRED^{332}. The AlDH-catalyzed oxidation was combined with coenzyme regeneration facilitated by H_2O-forming NADH-dependent oxidase (NOX^{009}).

The third and fourth step were the reactions catalyzed by halohydrin dehalogenase (HHDH^{001}). HHDH^{001} catalyzes CDHA dehalogenation and its ring-opening in presence of KCN.

The DERA-catalyzed side reaction of self-aldol addition of AA is a two-step reaction (Figure 3) in which two molecules of AA reacted to form the side intermediate 3-hydroxybutanal (HB) which further reacted with the third molecule of AA to form the final side product 3,5-dihydroxyhexanal (DHH).

The substrate and product abbreviation list are presented in Table 4.

List of reactant and product abbreviations: acetaldehyde (**AA**), chloroacetaldehyde (**CAA**), 4-chloro-3-hydroxybutanal (**CHB**), 6-chloro-3,5-dihydroxyhexanal (**CDH**), 6-chloro-3,5-dihydroxyhexanoic acid (**CDHA**), 3-hydroxy-4(-oxiran-2-yl)butanoic acid (**HOBA**), 6-cyano-3,5-dihydroxyhexanoic acid (**CYDHA**), 3-hydroxybutanal (**HB**), 3,5-dihydroxyhexanal (**DHH**).

Table 1 Abbreviation list of compounds of the first statin side-chain reaction route.

Abbreviation	Full name of the compound
AA	Acetaldehyde
CAA	Chloroacetaldehyde
CHB	4-chloro-3-hydroxybutanal
CDH	6-chloro-3,5-dihydroxyhexanal
CDHA	6-chloro-3,5-dihydroxyhexanoic acid
HOBA	3-hydroxy-4(-oxiran-2-yl)butanoic acid
CYDHA	6-cyano-3,5- dihydroxyhexanoic acid
HB	3-hydroxybutanal
DHH	3,5-dihydroxyhexanal

3.3 Experimental part

3.3.1 Materials

In this thesis, following chemicals were used: ethyl acetate (EtOAc), hydrochloric acid, $NADP^+$, nitric acid, sulfuric acid (BDH Prolabo Chemicals, UK); chloroacetic acid, 1,3-dichloro-2-propanol, 2,4'-dibromoacetophenone, 2-deoxyribose 5-phosphate sodium salt (DRP), 3-hydroxybutanal (aldol, CHB), acetaldehyde (AA), chloroacetaldehyde (CAA), magnesium sulfate anhydrous, triosephosphate isomerase from rabbit muscle (TPI), α-glycerophosphate dehydrogenase from rabbit muscle (GDH), σ-benzylhydroxylamine hydrochloride (Merck, Germany); dipotassium phosphate, mercury(II) thiocyanate, methanol (MetOH), monopotassium phosphate, NAD^+, NADH, $NADP^+$, potassium cyanate, potassium hydroxide, propionaldehyde (PA), pyridine, triethanolamine hydrochloride (TEA-HCl), tris(hydroxymethyl)aminomethane (Tris), *O*-benzylhydroksylamine hydrochloride (Acros Organics, USA); acetic acid (T.T.T., Croatia); acetonitrile (ACN), ethanol absolute (EtOH), magnesium sulfate anhydrous, trifluoroacetic acid (TFA) (Fisher Scientific, UK); albumin from bovine serum (BSA) (Fluka Chemie, Germany); isopropyl alcohol (IPA), potassium hydroxide (Kemika, Croatia); ammonium iron(III) sulfate dodecahydrate, Coomassie brilliant blue G-250, sodium chloride, sodium sulfate anhydrous (Lach-Ner, Czech Republic); NADPH (AppliChem, Germany); sodium hydroxide (Gram-mol, Croatia).

The 2-deoxyribose-5-phosphate aldolases ($DERA^{Tm}$, $DERA^{024}$) and NAD(P)(H)-dependent dehydrogenases (AlDH, NOX^{009}, $KRED^{332}$) were expressed and supplied by Prozomix (UK), while the halohydrin dehalogenase ($HHDH^{001}$) was expressed and provided by Enzymicals (Germany). The enzymes were supplied as cell-free extracts (CFEs).

List of reactant and product abbreviations: acetaldehyde (**AA**), chloroacetaldehyde (**CAA**), 4-chloro-3-hydroxybutanal (**CHB**), 6-chloro-3,5-dihydroxyhexanal (**CDH**), 6-chloro-3,5-dihydroxyhexanoic acid (**CDHA**), 3-hydroxy-4(-oxiran-2-yl)butanoic acid (**HOBA**), 6-cyano-3,5-dihydroxyhexanoic acid (**CYDHA**), 3-hydroxybutanal (**HB**), 3,5-dihydroxyhexanal (**DHH**).

3.3.2 Apparatus

In this thesis the following apparatus were used: analytical scale (AUW 120, Shimadzu, Japan), centrifuge (Universal 320 R, Hettich, Germany), freeze dryer (FreeZone, Labconco, USA), fume hood (Flores Valles, Spain), high performance liquid chromatography (HPLC; degasser DGU-20A3; pumps LC-20AT and LC-10AT; injector SIL-20ACHT; UV-VIS detector SPD-10A; column oven CTO-20AC, communications bus module CBM-20A, Shimadzu, Japan), homogenizer (MS2 Minishaker, Ika-Combing, Germany), incubator/shaker (Innova 4330, New Brunswick Scientific, USA; orbital shaker PSU-10i, Biosan, Latvia; Tehtnica VibroMix 203 EVT, Slovenia), laboratory scale (EW 1500-2M, Kern & Sohn, Germany), magnetic stirrer (Rotamix S-10, Tehtnica, Slovenia), pH meter (Lab 860, Schott Instruments Analytics, Germany),refrigerator and freezer (Končar, Croatia), rotary evaporator (Hei-VAP Platinum 2, Heidolph, Germany), UV-Vis spectrophotometer (UV 1800, Shimadzu, Japan), syringe pumps (PHD 4400 Syringe Pump Series, Harvard Apparatus, USA), thermomixer (ThermoMixer C, Eppendorf, Germany), ultrapure water system (NIRO-VV-UV-UF, Nirosta, Croatia).

Additionally, Amicon ultra-centrifugal filter units (CFUs, 10 kDa, 0.5 mL and 15 mL; Merck Milipore, Ireland) were used.

3.3.3 Analytical methods

3.3.3.1 HPLC analysis

To follow aldehydes and carboxylic acids using HPLC on the Phenomenex Kinetex RP-HPLC column (C18, 5 μm, 250 x 4.6 mm, 100 Å), two different derivatization methods were introduced to make the compounds UV detectable, but also to enhance the chromatographic properties and to increase their stability [176].

The derivatization of aldehydes was done using the following procedure [107]: the sample (5 μL) was mixed with 0.05 mL of a stock solution of *O*-benzylhydroxylamine hydrochloride (0.02 g/mL in a mixture of pyridine, MetOH, and water in ratio 33:15:2) as the derivatization agent. After incubation on a shaker at 25 °C for 20 minutes, samples were diluted with MetOH (0.45 mL), centrifuged to remove any solid and analyzed by HPLC.

List of reactant and product abbreviations: acetaldehyde (**AA**), chloroacetaldehyde (**CAA**), 4-chloro-3-hydroxybutanal (**CHB**), 6-chloro-3,5-dihydroxyhexanal (**CDH**), 6-chloro-3,5-dihydroxyhexanoic acid (**CDHA**), 3-hydroxy-4(-oxiran-2-yl)butanoic acid (**HOBA**), 6-cyano-3,5-dihydroxyhexanoic acid (**CYDHA**), 3-hydroxybutanal (**HB**), 3,5-dihydroxyhexanal (**DHH**).

The derivatization of carboxylic acids was based on the following procedure [177]: the sample (0.01 mL) was mixed with 0.04 mL of stock solution of 2,4'-dibromoacetophenone (300 mM in ACN) as the derivatization agent, incubated at 60 °C for 60 minutes, diluted with MetOH (0.2 mL), centrifuged (14 000 rpm, 4 °C, 5 min) to remove any solid and analyzed by HPLC.

The developed method was used for monitoring derivatized aldehydes and carboxylic acids involved in the first reaction route (Method 1). The mobile phase consisted of solvent A (ACN, water and TFA in the ratio 80:20:0.1) and solvent B (0.1 % v/v TFA in water) with gradient elution from 90 to 28.4 % B for the first 10 minutes and from 28.4 to 90 % B from minute 14 to 16. The injection volume was 20 μL, the flow rate 1.5 mL/min, the column temperature was set at 30 °C, while the UV detection was at 215 nm. Examples of calibration curves are presented in the Appendix. The calibration curves of not commercially available compounds were made based on the experimental data using balance equations and corresponding reaction scheme. Examples of calibration curves are shown in the Appendix: AA (Appendix figure 1), CAA (Appendix figure 2), CHB (Appendix figure 3), CDH (Appendix figure 4), HB (Appendix figure 5), and CHH (Appendix figure 6), and CDHA (Appendix figure 7). The retention time of AA, CAA, CHB and CDH were 11.1, 12.9, 10.4 and 9.3 minutes, respectively. The retention time of HB was 9.1 minutes, while of DHH 8.3 minutes. The retention time of the CDHA acid was 9.9 minutes. Respective examples HPLC chromatograms are shown in Appendix. For the aldehydes in Appendix figure 17, while for CDHA in Appendix figure 18.

Since aldehydes CHB, CDH, HB and DHH are not commercially available at the moment, they were confirmed using LC-MS analysis. The LC-MS method is described in Appendix figure 23.

3.3.3.2 Spectrophotometric measurements

3.3.3.2.1 Quantitative determination of protein content

The total protein concertation was determined using the Bradford protein assay [178]. The samples (0.2 mL) were mixed with Bradford reagent (0.8 mL) and incubated for five minutes at 25 °C. The absorbance was measured at 595 nm. The calibration curve was made using the BSA. Example of a BSA calibration curve is shown in Appendix figure 8.

List of reactant and product abbreviations: acetaldehyde (**AA**), chloroacetaldehyde (**CAA**), 4-chloro-3-hydroxybutanal (**CHB**), 6-chloro-3,5-dihydroxyhexanal (**CDH**), 6-chloro-3,5-dihydroxyhexanoic acid (**CDHA**), 3-hydroxy-4(-oxiran-2-yl)butanoic acid (**HOBA**), 6-cyano-3,5-dihydroxyhexanoic acid (**CYDHA**), 3-hydroxybutanal (**HB**), 3,5-dihydroxyhexanal (**DHH**).

3.3.3.2.2 Quantitative determination of chloride ion content

The concentration of chloride ions present in the solution was measured using a colorimetric assay [114, 179]. The samples (0.2 mL), filtered through a filter syringe, were mixed with the halogen solution (0.8 mL) and immediately placed into the spectrophotometer to read the absorbance at 460 nm, according to the procedure described elsewhere [24]. The calibration curve was done using sodium chloride. Example of a NaCl calibration curve is shown in Appendix figure 9.

3.3.3.3 Enzyme assays

All enzymes used in this work were provided as CFEs and were used without further purification unless stated otherwise. All measurements were carried out in quartz cuvettes (10 mm path, 1 mL) at 25 °C.

The specific enzyme activity was calculated from the change in the absorbance over time, $\Delta ABS/t$ (min^{-1}) using the Equation 19 in which the extinction coefficient for NAD(P)H at 340 nm (ε_{340}) equals 6.22 1/(mM·cm), while d represents the light path length (cm) and γ_e the mass concentration of enzyme in solution (mg/cm^3).

$$A_S = \frac{1}{\varepsilon_{340} \cdot d \cdot \gamma_e} \cdot \frac{\Delta ABS}{\Delta t} \qquad \text{Equation 19}$$

3.3.3.3.1 DERA activity assays

To measure the DERA activity, two different assay methods were developed: the 2-deoxyribose 5-phosphate (DRP) Assay and the DERA HPLC assay.

The activities of $DERA^{Tm}$ and $DERA^{024}$ were determined by using the DRP Assay, which is based on the DRP cleavage activity of DERA by measuring the oxidation of NADH in a coupled assay using triosephosphate isomerase (TPI) and α-glycerophosphate dehydrogenase (GDH) enzymes [101, 103, 104]. The assay mixture contained 0.1 M TEA-HCl buffer pH 7, 0.1 mM NADH, 0.4 mM DRP, 11 U of TPI, 4 U of GDH, and diluted DERA (0.3 mg/mL). The reaction was initiated by the addition of DERA, and the subsequent decrease of NADH concentration was monitored at 340 nm. 1 U of DERA activity was defined as the amount of

List of reactant and product abbreviations: acetaldehyde (**AA**), chloroacetaldehyde (**CAA**), 4-chloro-3-hydroxybutanal (**CHB**), 6-chloro-3,5-dihydroxyhexanal (**CDH**), 6-chloro-3,5-dihydroxyhexanoic acid (**CDHA**), 3-hydroxy-4(-oxiran-2-yl)butanoic acid (**HOBA**), 6-cyano-3,5-dihydroxyhexanoic acid (**CYDHA**), 3-hydroxybutanal (**HB**), 3,5-dihydroxyhexanal (**DHH**).

enzyme required for cleavage of 1 μmol of NADH per minute in 0.1 M TEA-HCl buffer pH 7 at 25 °C.

The DERA^{Tm} and DERA^{024} activities in the aldol addition reaction were determined by monitoring the aldol reaction with 200 mM of AA and 100 mM of CAA in the indicated buffer (DERA HPLC Assay). The reaction was initiated by enzyme addition (1 mg/mL). Samples were withdrawn at regular time intervals during the first 10 minutes of the reaction, derivatized using the derivatization procedure for aldehydes, centrifuged to remove any solid (14 000 rpm, 4 °C, 5 min) and analyzed by HPLC Method 1. 1 U of DERA activity was defined as the amount of enzyme required to form 1 μmol of product per minute at 25 °C in 0.1 M TEA-HCl buffer pH 7 (DERA^{Tm}) or 0.1 M phosphate buffer pH 6 (DERA^{024}). The specific enzyme activity was calculated from the change in the concentration of the product over time (mM/min) using the Equation 20, in which V_{rn} represents the reaction volume (mL) and V_e volume of the added enzyme (mL).

$$A_S = \frac{V_{rn}}{V_e} \cdot \frac{\Delta c}{\Delta t} \qquad \text{Equation 20}$$

3.3.3.3.2 Activity assays for oxidoreductases

The AlDH activity mixture contained 50 mM PA, 10 mM NAD^+ and diluted AlDH enzyme (0.1 mg/mL) in 0.1 M phosphate buffer pH 8. The reaction was initiated by the addition of AlDH, and the subsequent increase of NADH concentration was monitored at 340 nm. 1 U of AlDH activity was defined as the amount of enzyme required for reduction of 1 μmol of NAD^+ per minute in 0.1 M phosphate buffer pH 8 at 25 °C.

The NOX^{009} activity mixture contained 0.1 mM NADH and diluted NOX^{009} enzyme (0.1 mg/mL) in 0.1 M phosphate buffer pH 7. The reaction was initiated by the addition of NOX^{009}, and the subsequent decrease of NADH concentration was monitored at 340 nm. 1 U of NOX^{009} activity was defined as the amount of enzyme required for oxidation of 1 μmol of NADH per minute 0.1 M phosphate buffer pH 7 at 25 °C.

The KRED^{332} activity mixture contained 1 mM chloroacetic acid, 0.06 mM NADPH and diluted KRED^{332} enzyme (0.2 mg/mL) in 0.1 M phosphate buffer pH 8. The reaction was initiated by the addition of KRED^{332}, and the subsequent increase of NADH concentration was

List of reactant and product abbreviations: acetaldehyde (**AA**), chloroacetaldehyde (**CAA**), 4-chloro-3-hydroxybutanal (**CHB**), 6-chloro-3,5-dihydroxyhexanal (**CDH**), 6-chloro-3,5-dihydroxyhexanoic acid (**CDHA**), 3-hydroxy-4(-oxiran-2-yl)butanoic acid (**HOBA**), 6-cyano-3,5-dihydroxyhexanoic acid (**CYDHA**), 3-hydroxybutanal (**HB**), 3,5-dihydroxyhexanal (**DHH**).

monitored at 340 nm. 1 U of KRED^{332} activity was defined as the amount of enzyme required for oxidation of 1 μmol of NADPH per minute 0.1 M phosphate buffer pH 8 at 25 °C.

3.3.3.3.3 HHDH^{001} activity assay

The HHDH^{001} assay was determined by carrying the reaction (1.2 mL) of chloride release from the 1,3-dichloro-2-propanol (10 mM) catalyzed by the HHDH^{001} enzyme (0.5 mg/mL) in phosphate buffer pH 8 at 25 °C. The experiments were conducted in locking microcentrifuge tubes (1.5 mL) used as batch reactors. During the first 5 minutes since the addition of the enzyme into the reactor, the samples were taken out at regular time intervals and filtered through a syringe filter to remove the enzyme. The release of the halide ion was monitored at 460 nm using the chloride assay (Chapter 3.3.3.2.2). 1 U of HHDH^{001} activity was defined as the amount of enzyme required to release of 1 μmol of chloride per minute 0.1 M phosphate buffer pH 8 at 25 °C.

3.3.4 Synthesis and purification of chemicals

3.3.4.1 Enzymatic synthesis of CDH

The aldol reaction (100 mL) of AA (200 mM) with CAA (100 mM) was catalyzed by DERA^{024} (5 mg/mL) in the 0.1 M phosphate buffer pH 6 (batch reactor, glass bottle, 200 mL; shaker, 150 rpm; 25 °C).

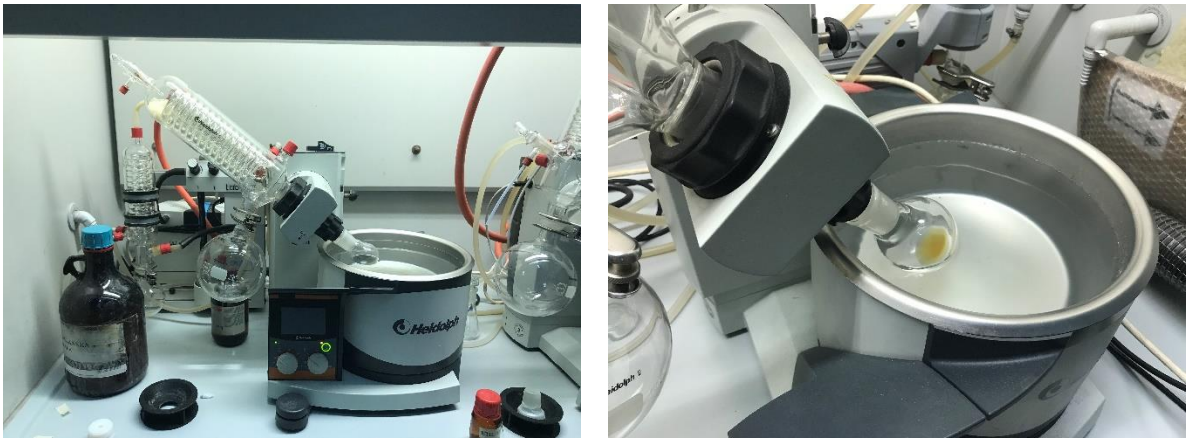

Figure 21 Removal of EtOAc under reduced pressure (Heidolph, Germany) to yield thick (viscous) CDH product.

During the reaction, the samples were periodically taken from the reactor, derivatized using the derivatization method for aldehydes and analyzed using the HPLC Method 1. After 8

List of reactant and product abbreviations: acetaldehyde (**AA**), chloroacetaldehyde (**CAA**), 4-chloro-3-hydroxybutanal (**CHB**), 6-chloro-3,5-dihydroxyhexanal (**CDH**), 6-chloro-3,5-dihydroxyhexanoic acid (**CDHA**), 3-hydroxy-4(-oxiran-2-yl)butanoic acid (**HOBA**), 6-cyano-3,5-dihydroxyhexanoic acid (**CYDHA**), 3-hydroxybutanal (**HB**), 3,5-dihydroxyhexanal (**DHH**).

hours from the beginning of the reaction, AA (50 mM) and DERA (5 mg/mL) were re-added into the reactor. The reaction was stopped after 28 hours from the beginning of the reaction by distributing the reaction solution (25 mL) into conical centrifuge tubes (50 mL) and adding EtOAc (25 mL) into each tube to carry out the liquid-liquid extraction (3 x 25 mL). The organic layer was dried using anhydrous magnesium sulfate and filtered. The solvent was removed under reduced pressure (55 °C, Figure 21). The obtained product was stored in a glass vial at -20 °C.

3.3.4.2 Enzymatic synthesis of CDHA

The AlDH-catalyzed oxidation of CDH (approx. 350 mM, 100 mL) in 0.1 M phosphate buffer pH 8. A glass bottle (200 mL) was used as batch reactor, which was placed on a shaker at 280 rpm and 25 °C. The reaction was started with the addition of NAD^+ (10 mM), AlDH and NOX^{009} (10 mg/mL each), where the addition of AlDH was the beginning of the reaction. During the reaction, the samples were periodically taken from the reactor, derivatized using the derivatization method for acids and analyzed using the HPLC Method 1. The reaction was conducted with multiple additions of fresh quantities of enzymes at 0 h (10 mg/mL AlDH and NOX^{009}, each), at 6 h (10 mg/mL AlDH and NOX^{009}, each), at 24 h (5 mg/mL AlDH and NOX^{009}, each) and at 52 h (7 mg/mL AlDH and NOX^{009}, each) after start of the reaction. At 52 h fresh amount of coenzyme NAD^+ (10 mM) was added into the reactor as well. Before the addition of enzymes into the reactor, they were desalted (100 mM phosphate buffer pH 7). To do that, centrifugal filter units (CFUs, 0.5 mL) were used (20 min, 14 000 rpm, 4 °C) [180]. During the reaction, the pH was frequently checked using a pH electrode (magnetic stirrer, 150 rpm, 25 °C). Because the pH decreased during the reaction, the pH was adjusted to pH 8 using the 5 M KOH solution.

The experiment was stopped after 74 h from the beginning of the reaction. The reaction mixture was distributed into conical centrifuge tubes (50 mL) to precipitate any present solid by centrifugation (15 min, 5 000 rpm, 4 °C). The decanted reaction mixture contained dissolved proteins that were separated using CFUs (15 mL) by centrifugation (120 min, 5 000 rpm, 4 °C). The filtrate, which contained the target CDHA molecule was distributed into multiple conical centrifuge tubes (15 mL) and stored at -80 °C overnight. The frozen samples were placed in the freeze dryer and lyophilized for 48 hours.

List of reactant and product abbreviations: acetaldehyde (**AA**), chloroacetaldehyde (**CAA**), 4-chloro-3-hydroxybutanal (**CHB**), 6-chloro-3,5-dihydroxyhexanal (**CDH**), 6-chloro-3,5-dihydroxyhexanoic acid (**CDHA**), 3-hydroxy-4(-oxiran-2-yl)butanoic acid (**HOBA**), 6-cyano-3,5-dihydroxyhexanoic acid (**CYDHA**), 3-hydroxybutanal (**HB**), 3,5-dihydroxyhexanal (**DHH**).

3.3.5 Influence of buffers on enzyme activity and stability

The influence of buffers of various pH on the activity and stability of DERA^{Tm} and DERA^{024} were examined at 25 °C using the following buffers: 0.1 M phosphate buffer (pH 5.4, 6, 7, 8), 0.1 TEA-HCl buffer (pH 7), 0.1 Tris-HCl buffer (pH pH 7, 8, 9) and glycine-NaOH buffer (pH 9, 10). To assess the influence of pH on the activity and stability of AlDH and NOX^{009} at 25 °C, 0.1 M phosphate buffer at pH 7, 7.4, 7.6, 7.8 and 8 were used.

The effects of buffers on the activities of DERA^{Tm} and DERA^{024} were tested by following the reaction of CHB production in the chosen buffer. The reactions (1 mL) were carried out in 1.5 mL-locking microcentrifuge tubes as batch reactors placed on a shaker at 1 000 rpm. The activities were measured using DERA HPLC Assay. The samples were taken at regular time intervals during the first 10 (DERA^{Tm}) or 15 (DERA^{024}) minutes from the beginning of the reaction.

The stabilities of both DERAs in different buffers of various pH were determined by dissolving 10 mg/mL DERA in the chosen buffer in a 1.5 mL-locking microcentrifuge tube by incubating it using a thermomixer (1 000 rpm, 25 °C) for 24 hours. The residual activities of DERAs were measured by applying the DRP Assay.

For evaluating the effects of pH on the activity of AlDH, the spectrophotometric test was carried out in 0.1 M phosphate buffer consisting of 0.7 mM CDH, 9.4 mM NAD^+ and 0.1 mg/mL AlDH. To measure the influence of pH on the activity of NOX^{009}, the spectrophotometric test was prepared in 0.1 M phosphate buffer containing 0.1 M NADH and 0.01 mg/mL NOX^{009}. The final volume of the spectrophotometric tests was 1 mL. The reaction was initiated by the addition of AlDH or NOX^{009}, and the subsequent change in NAD(H) concentration was monitored at 340 nm at 25 °C. 1 U of AlDH or NOX^{009} activity was defined as the amount of enzyme required for oxidation of 1 μmol of CDH or NADH, respectively, in 0.1 M phosphate buffer (AlDH: pH 8; NOX^{009}: pH 7) at 25 °C.

The effects of different pH on the stability of AlDH and NOX^{009} were examined by incubating the enzyme preparations in 0.1 M phosphate buffer (1 mg/mL, 1 mL) in locking microcentrifuge tubes (1.5 mL) and placing them on a shaker at 1 000 rpm and 25 °C for 24 (AlDH) or five (NOX^{009}) hours. The residual DH activity was measured using the appropriate DH assay.

List of reactant and product abbreviations: acetaldehyde (**AA**), chloroacetaldehyde (**CAA**), 4-chloro-3-hydroxybutanal (**CHB**), 6-chloro-3,5-dihydroxyhexanal (**CDH**), 6-chloro-3,5-dihydroxyhexanoic acid (**CDHA**), 3-hydroxy-4(-oxiran-2-yl)butanoic acid (**HOBA**), 6-cyano-3,5-dihydroxyhexanoic acid (**CYDHA**), 3-hydroxybutanal (**HB**), 3,5-dihydroxyhexanal (**DHH**).

3.3.6 Influence of temperature on DERA^{Tm} activity and stability

The influence of temperature on the activity and stability of DERA variants in the reaction of CDH production was examined on the DERA^{Tm} variant. The examined temperature interval was between 20 and 50 °C with a step of 5 °C. 10 mg/mL of DERA^{Tm} was incubated for five minutes at different temperatures after which residual activity was determined at 25 °C by using DRP Assay.

To assess the enzyme thermostability at different temperatures, 10 mg/mL of DERA^{Tm} was incubated in 0.1 M TEA-HCl buffer pH 7 for three days during which the residual activity was determined at appropriate intervals using the DRP Assay.

3.3.7 Influence of organic compound on enzyme stability

The influence of compounds on the stability of an enzyme was examined by placing the enzyme in a single-compound solution. The examined compounds were: AA, CAA, CHB, CDH and CDHA. The experiments were carried out in 1.5 mL-locking microcentrifuge tubes with a total reaction volume of 1 mL by placing the tube containing the enzyme dissolved in the solution on a shaker at 1 000 rpm and 25 °C for 3 h. During incubation, the samples were taken at regular time intervals to measure the residual activity using the appropriate assay. Prior to carrying out the activity measurements, the compound was removed using 0.5 mL-CFUs and the enzyme residue was diluted in the assay buffer. To determine the enzyme's operational stability decay rate constant the activities were measured using the same procedure.

The effects of AA, CAA, CHB and CDH on both DERA variants were examined by incubating 10 mg/mL of enzyme in working buffer in a single-aldehyde solution of defined concentration (up to 1000 mM). The working buffers for DERA^{Tm} and DERA^{024} were 0.1 M TEA-HCl buffer pH 7 and 0.1 M phosphate buffer pH 6, respectively.

The influence of AA, CAA, CHB, CDH and CDHA on the AlDH, KRED^{332} and NOX^{009} stability were measured by incubating the enzyme preparation in 0.1 M phosphate buffer pH 8 at different concentrations of aldehydes (up to 200 mM). The experiments with AlDH and KRED^{332} were carried out with 5 mg/mL of the enzyme, while the experiments with NOX^{009} were conducted with 1 mg/mL of the enzyme.

List of reactant and product abbreviations: acetaldehyde (**AA**), chloroacetaldehyde (**CAA**), 4-chloro-3-hydroxybutanal (**CHB**), 6-chloro-3,5-dihydroxyhexanal (**CDH**), 6-chloro-3,5-dihydroxyhexanoic acid (**CDHA**), 3-hydroxy-4(-oxiran-2-yl)butanoic acid (**HOBA**), 6-cyano-3,5-dihydroxyhexanoic acid (**CYDHA**), 3-hydroxybutanal (**HB**), 3,5-dihydroxyhexanal (**DHH**).

The influence of CDHA and KCN on $HHDH^{001}$ stability was examined in 0.1 M phosphate buffer pH 8 by placing 10 mg/mL of $HHDH^{001}$ in DCHA or KCN solution. The DHA concentration was varied up to 200 mM, while the KCN concentration up to 150 mM.

3.3.8 Enzyme kinetics

The kinetics of each of the applied enzymes was examined in the reactions which they catalyze using the initial reaction rate method. The initial reaction rate was measured so that, during the measurement, the concentration of the investigated substrate did not decrease by more than 10 %. The double-substrate kinetics was measured at constant enzyme concentration so that one substrate was kept constant at the saturating concentration (Figure 19), while the other substrate's concentration was varied. Then, the concentration of the second substrate was kept constant at saturating concentrations, while the concentration of the first substrate was varied.

The influence of products on the forward reaction was examined as well to evaluate the existence of product inhibition. In that case, the concentration of both substrates was kept constant at saturating concentrations, while the concentration of the product was varied. To evaluate the influence of co-substrates and co-products, the same approach was applied when the possibility of product inhibition was investigated.

All kinetic measurements concerning DERAs were measured by carrying the aldol reaction and following it using the HPLC Method 1. The measurements in which oxidoreductases were applied were carried out spectrophotometrically at 340 nm in 1 mL-quartz cuvettes (10 mm path). The $HHDH^{001}$ kinetic measurements were carried out by following the chloride release (Chapter 3.3.3.2.2) during the first 10 minutes of the reaction.

The kinetic equations (Chapter 3.6.4) were developed based on the reaction scheme (Figures 1 and 3) and experimental data (Chapter 3.6.4). Experimental conditions for measuring enzyme kinetics can be found in figure descriptions in shown in Chapter 3.6.4.

3.3.9 Reactor experiments: one-step biocatalysis

The reactions for the synthesis of the first statin side-chain precursor were carried out at 25 °C. The reactions were initiated by the addition of the enzyme which catalyzes the reaction. The reactions were monitored for a certain period, during which the samples were taken at

List of reactant and product abbreviations: acetaldehyde (**AA**), chloroacetaldehyde (**CAA**), 4-chloro-3-hydroxybutanal (**CHB**), 6-chloro-3,5-dihydroxyhexanal (**CDH**), 6-chloro-3,5-dihydroxyhexanoic acid (**CDHA**), 3-hydroxy-4(-oxiran-2-yl)butanoic acid (**HOBA**), 6-cyano-3,5-dihydroxyhexanoic acid (**CYDHA**), 3-hydroxybutanal (**HB**), 3,5-dihydroxyhexanal (**DHH**).

regular time intervals to determine the concentrations of substrates and products by HPLC Method 1. The residual enzyme activity was also measured by applying the appropriate assay procedure. Prior to assaying, to remove compounds such as substrates and products, the enzyme was separated from the reaction solution using 0.5 mL-CFUs by centrifugation (14 000 rpm, 4 °C, 5 min). The enzyme retained on the filter was resuspended with appropriate buffer respecting the enzyme concentration in the assay and used in the activity assay.

When DHs were applied, the coenzyme $NAD(P)^+$ was added into the reactor before the start of the oxidation. When needed, the pH was adjusted using the 5 M KOH solution, since the pH decreased during the CDH oxidation.

3.3.9.1 DERA-catalyzed aldol additions

The DERA-catalyzed tandem aldol addition of AA onto CAA (Figure 1 and Figure 3) was conducted in batch, repetitive-batch and fed-batch reactor modes. The $DERA^{Tm}$-catalyzed aldol reaction was carried out in 0.1 M TEA-HCl buffer pH 7, while the $DERA^{024}$-catalyzed reactions in 0.1 M phosphate buffer pH 6. The reactions were conducted at 25 °C. During all reactions, the samples were taken at regular time-intervals to evaluate the substrate and product concentration *via* HPLC and the residual enzyme activity by DRP assay.

The batch reactions were conducted in 2 mL-locking microcentrifuge tubes placed on a shaker at 1 000 rpm. The repetitive-batch reactions of total reaction volume of 4 mL were carried out in 5 mL-glass bottles used as a batch reactor placed on a shaker at 400 rpm. The substrates and the enzyme were re-added to the reactor after substrate concentration dropped to zero and the enzyme activity was below 20 %.

The aldol reactions in fed-batch reactor were conducted in a 10-mL glass bottle that was placed on a shaker at 400 rpm to which two feeds (syringe pumps; HD 4400 Syringe Pump Series, Harvard Apparatus, SAD) were connected. One was the substrate feed, while the other was the enzyme feed. In all carried aldol reactions, at the beginning of the reaction the reactor was filled with a certain amount of working buffer. The start of the pump, or pumps, was approximated as the start of the experiment. The experimental conditions are given in detail in figure descriptions: Figure 53 for $DERA^{Tm}$ and Figure 54 for $DERA^{024}$.

List of reactant and product abbreviations: acetaldehyde (**AA**), chloroacetaldehyde (**CAA**), 4-chloro-3-hydroxybutanal (**CHB**), 6-chloro-3,5-dihydroxyhexanal (**CDH**), 6-chloro-3,5-dihydroxyhexanoic acid (**CDHA**), 3-hydroxy-4(-oxiran-2-yl)butanoic acid (**HOBA**), 6-cyano-3,5-dihydroxyhexanoic acid (**CYDHA**), 3-hydroxybutanal (**HB**), 3,5-dihydroxyhexanal (**DHH**).

Figure 22 Fed-batch setup for the DERA^{Tm}- and DERA^{024}-catalyzed reaction.

3.3.9.2 DH-catalyzed oxidations

All reactions were conducted in a batch reactor (locking microcentrifuge tube, 2 mL) placed on a shaker at 1 000 rpm in 0.1 M phosphate buffer pH 8. The AlDH-catalyzed oxidation, AlDH-catalyzed CDH oxidation with NOX^{009}-catalyzed NAD$^+$ regeneration and KRED^{332}-catalyzed oxidation were conducted with purified CDH (Figure 1). During the experiment, the samples were taken at regular time-intervals and were analyzed *via* HPLC and spectrophotometer to assess the change of substrate and product concentration and residual enzyme activity, respectively. The experimental conditions for the conducted CDH oxidation reactions are given in detail in figure descriptions shown in Chapter 3.6.5.2.

3.3.9.3 HHDH^{001}-catalyzed reactions

The HHDH^{001}-catalyzed dehalogenation was carried out in 1.5 mL-locking microcentrifuge tube placed on shaker at 1 000 rpm. The reaction volume was 1.2 mL. The HHDH^{001}-catalyzed dehalogenation and epoxide ring-opening with KCN was conducted in 4 mL-glass bottle used as a batch reactor that was placed on a shaker at 300 rpm. The reactions were conducted at 25 °C with purified CHDA in 0.1 M phosphate buffer pH 8. Because with the addition of KCN the pH of the reaction solution increases, the pH was adjusted using the 9.2 M sulfuric acid solution. The samples were taken at regular time-intervals to quantify the change in substrate and product concentration *via* HPLC and to evaluate the residual enzyme activity using the appropriate assay procedure. The conditions at which the experiments were carried out are given in detail under figure descriptions in Chapter 3.6.5.3.

List of reactant and product abbreviations: acetaldehyde (**AA**), chloroacetaldehyde (**CAA**), 4-chloro-3-hydroxybutanal (**CHB**), 6-chloro-3,5-dihydroxyhexanal (**CDH**), 6-chloro-3,5-dihydroxyhexanoic acid (**CDHA**), 3-hydroxy-4(-oxiran-2-yl)butanoic acid (**HOBA**), 6-cyano-3,5-dihydroxyhexanoic acid (**CYDHA**), 3-hydroxybutanal (**HB**), 3,5-dihydroxyhexanal (**DHH**).

3.3.10 Reactor experiments: multi-step one-pot biocatalysis

The cascade reactions for the synthesis of the first statin side-chain precursor were carried out at 25 °C. The reactions were initiated by the addition of the enzyme which catalyzes the main reaction of the observed cascade. The reactions were monitored for a certain period, during which the samples were taken at regular time intervals to determine the concentrations of substrates and products by HPLC (Method 1). The residual enzyme activity was also measured by applying the appropriate assay procedure. Prior to assaying, to remove compounds such as substrates and products, the enzyme was separated from the reaction solution using 0.5 mL-CFUs by centrifugation (14 000 rpm, 4 °C, 5 min). The enzyme retained on the filter was resuspended with appropriate buffer and used in the activity assay, respecting the enzyme concentration in the assay procedure.

When DHs were applied, the coenzyme $NAD(P)^+$ was added into the reactor before the start of the oxidation. When needed, the pH was adjusted using the 5 M KOH solution, since the pH decreased during the CDH oxidation.

3.3.10.1 Cascade synthesis of CDHA

CDH was synthesized in the $DERA^{024}$-catalyzed aldol reaction in repetitive batch reactor mode in 0.1 M phosphate buffer pH 6. Once full substrate AA and CAA conversion were attained, the pH was adjusted using the 5 M KOH solution since the oxidation takes place at pH 8. Depending on the desired concentration of the crude CDH, the final $DERA^{024}$ reaction mixture was either used undiluted or diluted with 0.1 M phosphate buffer pH 8 to attain lower concentrations of crude CDH. To oxidize the obtained crude CDH, the AlDH and NOX^{009} or $KRED^{332}$ were added into the reactor containing the final $DERA^{024}$ reaction mixture. The reaction conditions are given in detail in Figure 47 (for $DERA^{024}$-catalyzed reaction), Figure 59 (for AlDH/NOX^{009}-catalyzed reaction) and Figure 60 (for $KRED^{354}$-catalyzed reaction).

3.3.10.2 Cascade synthesis of CYDHA

The sequential multi-step one-pot reaction of CYDHA production consisted of three consecutive reactions. The first reaction was the $DERA^{024}$-catalyzed production of CDH in a repetitive batch reactor in 0.1 M phosphate buffer pH 6. The second reaction was the CDH oxidation, in order to obtain the CDHA product, catalyzed by AlDH with NOX^{009}-catalyzed

List of reactant and product abbreviations: acetaldehyde (**AA**), chloroacetaldehyde (**CAA**), 4-chloro-3-hydroxybutanal (**CHB**), 6-chloro-3,5-dihydroxyhexanal (**CDH**), 6-chloro-3,5-dihydroxyhexanoic acid (**CDHA**), 3-hydroxy-4(-oxiran-2-yl)butanoic acid (**HOBA**), 6-cyano-3,5-dihydroxyhexanoic acid (**CYDHA**), 3-hydroxybutanal (**HB**), 3,5-dihydroxyhexanal (**DHH**).

NAD^+ regeneration system prior which the pH of the reaction mixture was adjusted to pH 8 using 5 M KOH. Once full CDH conversion into CDHA was achieved, KCN was added to the final AlDH/NOX^{009} reaction mixture and the pH was adjusted to pH 8 using the 9.2 M sulfuric acid solution, since KCN increases the pH of the reaction solution. The third reaction was initiated with the addition of HHDH^{001} into the reactor. The experimental conditions are given in detail in Figure 47 (for DERA^{024}-catalyzed reaction), Figure 59 (for AlDH/NOX^{009}-catalyzed reaction) and Figure 61 (HHDH^{001}-catalyzed reaction).

3.4 Mathematical modeling

The kinetic parameters were estimated from the dependence of the initial reaction rate on the concentrations of compounds in single- and multi-enzyme reactions. The mathematical models for all enzyme-catalyzed reactions. The mathematical model consisted of kinetic equations, mass balance equations in an appropriate reactor and operational stability decay equations. The model was developed using the estimated kinetic parameters and relevant reaction scheme.

3.4.1 DERA^{Tm}- and DERA^{024}-catalyzed aldol additions

The DERA^{Tm}- and DERA^{024}-catalyzed aldol reaction of AA with CAA is a two-step reaction in which one molecule of AA reacts with CAA (reaction rate r_1, Figure 23a) followed by the second addition of AA onto newly-formed intermediate CHB (reaction rate r_2, Figure 23b) resulting with the formation of CDH (Figure 1).

The reaction rate r_1 for the first DERA-catalyzed AA addition onto CAA was described by double-substrate Michaelis-Menten kinetics for DERA^{Tm} (Equation 21) and with non-competitive inhibition by CHB and CDH for DERA^{024} (Equation 22). The reaction rate r_2 for the second AA addition was described by the double-substrate Michaelis-Menten kinetics for DERA^{Tm} (Equation 23) and with uncompetitive substrate inhibition by CHB for DERA^{024} (Equation 24). The reaction rate r_3 for the DERA-catalyzed AA self-aldol addition (Figure 23c), which results in the formation of DHH, was described by the Michaelis-Menten kinetics with competitive inhibition by CAA and non-competitive inhibition by CHB (Equation 25).

List of reactant and product abbreviations: acetaldehyde (**AA**), chloroacetaldehyde (**CAA**), 4-chloro-3-hydroxybutanal (**CHB**), 6-chloro-3,5-dihydroxyhexanal (**CDH**), 6-chloro-3,5-dihydroxyhexanoic acid (**CDHA**), 3-hydroxy-4(-oxiran-2-yl)butanoic acid (**HOBA**), 6-cyano-3,5-dihydroxyhexanoic acid (**CYDHA**), 3-hydroxybutanal (**HB**), 3,5-dihydroxyhexanal (**DHH**).

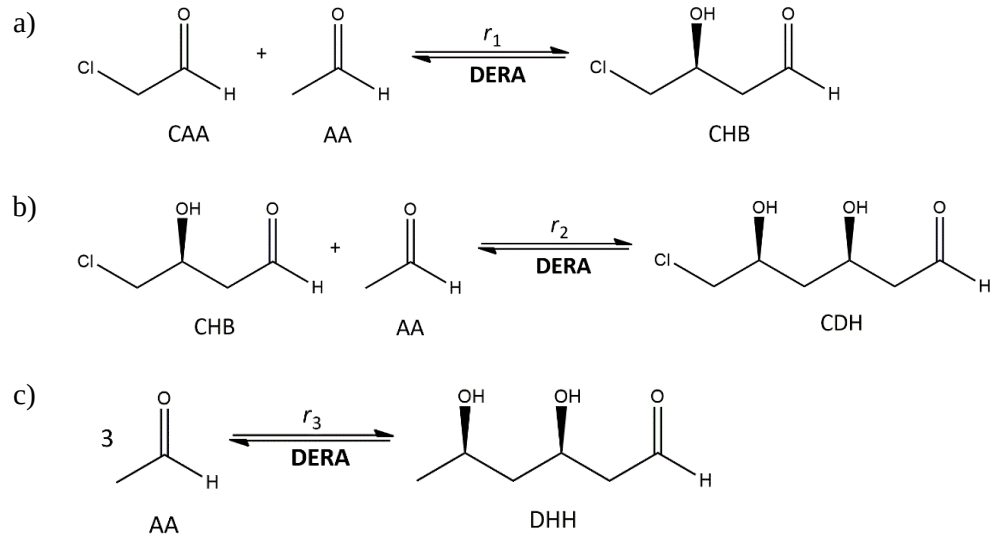

Figure 23 Reaction scheme of the DERA^{Tm}- or DERA^{024}-catalyzed a) AA addition onto CAA, b) AA addition onto CHB, and c) self-aldol AA addition.

$$r_1 = \frac{V_{m,1} \cdot \gamma_{DERA} \cdot c_{AA} \cdot c_{CAA}}{\left(K_{m,1}^{AA} + c_{AA}\right) \cdot \left(K_{m,1}^{CAA} + c_{CAA}\right)} \qquad \text{Equation 21}$$

$$r_1 = \frac{V_{m,1} \cdot \gamma_{DERA} \cdot c_{AA} \cdot c_{CAA}}{\left(K_{m,1}^{AA} + c_{AA}\right) \cdot \left(K_{m,1}^{CAA} + c_{CAA}\right) \cdot \left(1 + \frac{c_{CHB}}{K_{i,1}^{CHB}} + \frac{c_{CDH}}{K_{i,1}^{CDH}}\right)} \qquad \text{Equation 22}$$

$$r_2 = \frac{V_{m,2} \cdot \gamma_{DERATm} \cdot c_{AA} \cdot c_{CHB}}{\left(K_{m,1}^{AA} + c_{AA}\right) \cdot \left(K_{m,1}^{CHB} + c_{CHB}\right)} \qquad \text{Equation 23}$$

$$r_2 = \frac{V_{m,2} \cdot \gamma_{DERA024} \cdot c_{AA} \cdot c_{CHB}}{\left(K_{m,1}^{AA} + c_{AA}\right) \cdot \left[K_{m,1}^{CHB} + c_{CHB} \cdot \left(1 + \frac{c_{CHB}}{K_{i,2}^{CHB}}\right)\right]} \qquad \text{Equation 24}$$

$$r_3 = \frac{V_{m,3} \cdot \gamma_{DERA} \cdot c_{AA}^3}{\left(K_{m,3}^{AA} + c_{AA}\right)^2 \cdot \left[K_{m,3}^{AA} \cdot \left(1 + \frac{c_{CAA}}{K_{i,3}^{CAA}}\right) + c_{AA}\right] \cdot \left(1 + \frac{c_{CHB}}{K_{i,3}^{CHB}}\right)} \qquad \text{Equation 25}$$

The mass balances for reactants and products in the batch and repetitive batch reactor are presented by Equation 26 – 30. The activity decrease in the batch reactor was described by the second-order kinetics (Equation 31), while the operational stability decay rate constant was described by Equation 39.

$$\frac{\mathrm{d}c_{AA}}{\mathrm{d}t} = -r_1 - r_2 - 3 \cdot r_3 \qquad \text{Equation 26}$$

List of reactant and product abbreviations: acetaldehyde (**AA**), chloroacetaldehyde (**CAA**), 4-chloro-3-hydroxybutanal (**CHB**), 6-chloro-3,5-dihydroxyhexanal (**CDH**), 6-chloro-3,5-dihydroxyhexanoic acid (**CDHA**), 3-hydroxy-4(-oxiran-2-yl)butanoic acid (**HOBA**), 6-cyano-3,5-dihydroxyhexanoic acid (**CYDHA**), 3-hydroxybutanal (**HB**), 3,5-dihydroxyhexanal (**DHH**).

$$\frac{\mathrm{d}c_{CAA}}{\mathrm{d}t} = r_1 \quad \text{Equation 27}$$

$$\frac{\mathrm{d}c_{CHB}}{\mathrm{d}t} = r_1 - r_2 \quad \text{Equation 28}$$

$$\frac{\mathrm{d}c_{CDH}}{\mathrm{d}t} = r_2 \quad \text{Equation 29}$$

$$\frac{\mathrm{d}c_{DHH}}{\mathrm{d}t} = r_3 \quad \text{Equation 30}$$

$$\frac{\mathrm{d}\gamma_{DERA}}{\mathrm{d}t} = -k_d \cdot \gamma_{DERA}^2 \quad \text{Equation 31}$$

The mass balance equations for reactants AA and CAA and products CHB, CDH and CHH in the fed-batch reactor are presented by Equations 32 – 36. Equation 37 represents the change in reactor volume during the aldol reaction, where $q = q_1 + q_2$. The DERA^{Tm} and DERA^{024} operational stability decay was described by Equation 38 as second-order kinetics, while the operational stability decay rate constant was described by Equation 39.

$$\frac{\mathrm{d}c_{AA}}{\mathrm{d}t} = \frac{1}{V} \cdot \left(-c_{AA} \cdot \frac{\mathrm{d}V}{\mathrm{d}t} + c_{AA,0} \cdot q_1\right) - r_1 - r_2 - 3 \cdot r_3 \quad \text{Equation 32}$$

$$\frac{\mathrm{d}c_{CAA}}{\mathrm{d}t} = \frac{1}{V} \cdot \left(-c_{CAA} \cdot \frac{\mathrm{d}V}{\mathrm{d}t} + c_{CAA,0} \cdot q_1\right) - r_1 \quad \text{Equation 33}$$

$$\frac{\mathrm{d}c_{CHB}}{\mathrm{d}t} = \frac{1}{V} \cdot \left(-c_{CHB} \cdot \frac{\mathrm{d}V}{\mathrm{d}t}\right) + r_1 - r_2 \quad \text{Equation 34}$$

$$\frac{\mathrm{d}c_{CDH}}{\mathrm{d}t} = \frac{1}{V} \cdot \left(-c_{CDH} \cdot \frac{\mathrm{d}V}{\mathrm{d}t}\right) + r_2 \quad \text{Equation 35}$$

$$\frac{\mathrm{d}c_{\mathrm{DHH}}}{\mathrm{d}t} = \frac{1}{V} \cdot \left(-c_{DHH} \cdot \frac{\mathrm{d}V}{\mathrm{d}t}\right) + r_3 \quad \text{Equation 36}$$

$$\frac{\mathrm{d}V}{\mathrm{d}t} = q_1 + q_2 \quad \text{Equation 37}$$

$$\frac{\mathrm{d}\gamma_{DERA}}{\mathrm{d}t} = \frac{1}{V} \cdot \left(-\gamma_{DERA} \cdot \frac{\mathrm{d}V}{\mathrm{d}t} + \gamma_{DERA,0} \cdot q_2\right) - k_d \cdot \gamma_{DERA}^2 \quad \text{Equation 38}$$

The dependence of the operational stability decay rate constant on the concentration of AA, CAA and CHB was described by the second-order polynomial model that includes its dependency on the concentration of AA, CAA and CHB, as per Equation 39.

List of reactant and product abbreviations: acetaldehyde (**AA**), chloroacetaldehyde (**CAA**), 4-chloro-3-hydroxybutanal (**CHB**), 6-chloro-3,5-dihydroxyhexanal (**CDH**), 6-chloro-3,5-dihydroxyhexanoic acid (**CDHA**), 3-hydroxy-4(-oxiran-2-yl)butanoic acid (**HOBA**), 6-cyano-3,5-dihydroxyhexanoic acid (**CYDHA**), 3-hydroxybutanal (**HB**), 3,5-dihydroxyhexanal (**DHH**).

$$k_d^{DERA} = \sum_i \left(a_i \cdot c_i^2 + b_i \cdot c_i\right)$$ Equation 39

3.4.2 AlDH-catalyzed CDH oxidation with NAD^+ regeneration catalyzed by NOX^{009}

The reaction rate r_4 for the AlDH-catalyzed CDH oxidation into CDHA (Figure 24a) was described by double-substrate Michaelis-Menten kinetics with uncompetitive inhibition by substrate NAD^+ and competitive inhibition by product NADH (Equation 40).

$$r_4 = \frac{V_{m,4} \cdot \gamma_{AlDH} \cdot c_{CDH} \cdot c_{NAD^+}}{\left[K_{m,4}^{CDH} + c_{CDH}\right] \cdot \left[K_{m,4}^{NAD^+} \cdot \left(1 + \frac{c_{NADH}}{K_{i,4}^{NADH}}\right) + c_{NAD^+} \cdot \left(1 + \frac{c_{NAD^+}}{K_{i,4}^{NAD^+}}\right)\right]}$$ Equation 40

The reaction rate r_5 for the reverse reaction of CDH oxidation (Figure 24a) was described by second-order kinetics (Equation 41).

$$r_5 = k_5 \cdot \gamma_{AlDH} \cdot c_{CDHA} \cdot c_{NADH}$$ Equation 41

Due to the presence of NOX activity in the AlDH, which was used as CFE, the reaction rate r_6 of the NOX(AlDH)-catalyzed NADH oxidation (Figure 24a) was described by single-substrate Michaelis-Menten kinetics with competitive NAD^+ inhibition (Equation 42).

$$r_6 = \frac{V_{m,6} \cdot \gamma_{NOX(AlDH)} \cdot c_{NADH}}{K_{m,6}^{NADH} \cdot \left(1 + \frac{c_{NAD^+}}{K_{i,6}^{NAD^+}}\right) + c_{NADH}}$$ Equation 42

If the coenzyme was not regenerated by the action of the NOX^{009} enzyme (Figure 24b), the reaction rate r_6 of the NOX^{009}-catalyzed NADH oxidation (Equation 42) was upgraded with NADH, CDH and CDHA inhibition (r_7, Equation 43).

List of reactant and product abbreviations: acetaldehyde (**AA**), chloroacetaldehyde (**CAA**), 4-chloro-3-hydroxybutanal (**CHB**), 6-chloro-3,5-dihydroxyhexanal (**CDH**), 6-chloro-3,5-dihydroxyhexanoic acid (**CDHA**), 3-hydroxy-4(-oxiran-2-yl)butanoic acid (**HOBA**), 6-cyano-3,5-dihydroxyhexanoic acid (**CYDHA**), 3-hydroxybutanal (**HB**), 3,5-dihydroxyhexanal (**DHH**).

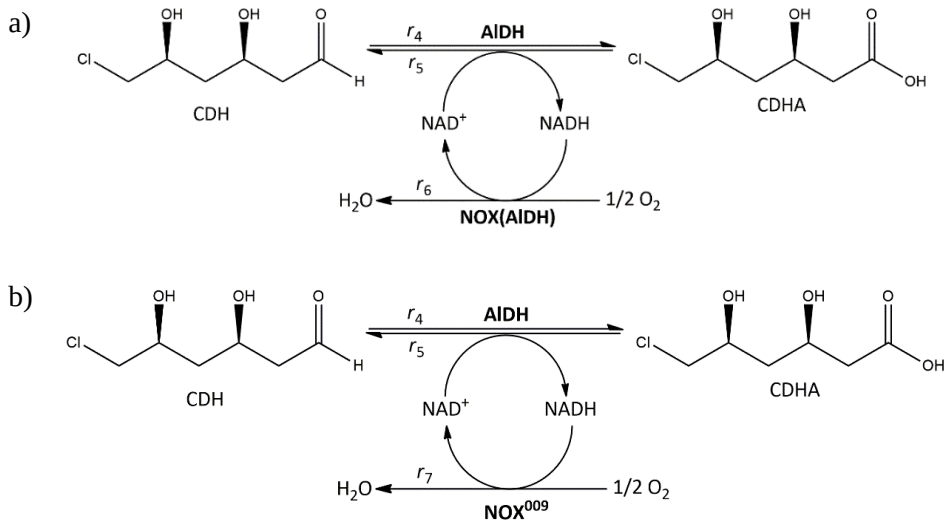

Figure 24 Reaction scheme of the AlDH-catalyzed CDH oxidation a) without NAD^+ regeneration and b) with NAD^+ regeneration catalyzed by NOX^{009}.

$$r_7 = \frac{V_{m,7} \cdot \gamma_{NOX009} \cdot c_{NADH}}{\left[K_{m,6}^{NADH} \cdot \left(1 + \frac{c_{NAD^+}}{K_{i,7}^{NAD^+}}\right) + c_{NADH}\right] \cdot \left(1 + \frac{c_{CDH}}{K_{i,7}^{CDH}} + \frac{c_{CDHA}}{K_{i,7}^{CDHA}}\right)} \qquad \text{Equation 43}$$

The mass balance equations for substrates and products in the AlDH-catalyzed oxidation of CDH into CDHA with NOX^{009}-catalyzed NADH oxidation conducted in the batch reactor were developed (Equation 44 – 47).

$$\frac{\mathrm{d}c_{CDH}}{\mathrm{d}t} = -r_4 + r_5 \qquad \text{Equation 44}$$

$$\frac{\mathrm{d}c_{CDHA}}{\mathrm{d}t} = r_4 - r_5 \qquad \text{Equation 45}$$

$$\frac{\mathrm{d}c_{NAD^+}}{\mathrm{d}t} = -r_4 + r_5 + r_6 + r_7 \qquad \text{Equation 46}$$

$$\frac{\mathrm{d}c_{NADH}}{\mathrm{d}t} = r_4 - r_5 - r_6 - r_7 \qquad \text{Equation 47}$$

The AlDH and NOX^{009} operational stability decay rates were described by second-order kinetics (Equations 48 and 49, respectively). The operational stability decay rate constant for NOX(AlDH) was assumed to be included under the operational stability decay rate constant of AlDH (Equation 48).

List of reactant and product abbreviations: acetaldehyde (**AA**), chloroacetaldehyde (**CAA**), 4-chloro-3-hydroxybutanal (**CHB**), 6-chloro-3,5-dihydroxyhexanal (**CDH**), 6-chloro-3,5-dihydroxyhexanoic acid (**CDHA**), 3-hydroxy-4(-oxiran-2-yl)butanoic acid (**HOBA**), 6-cyano-3,5-dihydroxyhexanoic acid (**CYDHA**), 3-hydroxybutanal (**HB**), 3,5-dihydroxyhexanal (**DHH**).

$$\frac{\mathrm{d}\gamma_{AlDH}}{\mathrm{d}t} = -k_d^{AlDH} \cdot \gamma_{AlDH}^2 \qquad \text{Equation 48}$$

$$\frac{\mathrm{d}\gamma_{NOX009}}{\mathrm{d}t} = -k_d^{NOX009} \cdot \gamma_{NOX}^2 \qquad \text{Equation 49}$$

During certain experiments, it was found that the operational stability of AlDH (Equation 50) and NOX[009] (Equation 51) was dependent on the concentration of CDH. This finding was emphasized in corresponding experiments described in Chapters 3.6.5.2 and 3.6.6.

$$k_d^{AlDH} = a \cdot c_{CDH} \qquad \text{Equation 50}$$

$$k_d^{NOX009} = a \cdot c_{CDH} \qquad \text{Equation 51}$$

3.4.3 KRED[332]-catalyzed CDH oxidation

The reaction rate r_8 for KRED[332]-catalyzed oxidation of CDH into CDHA (Figure 25) was described by double-substrate Michaelis-Menten kinetics with substrate $NADP^+$ and competitive NADPH inhibitions (Equation 52). Unlike the AlDH-catalyzed CDH oxidation, the KRED[332]-catalyzed CDH oxidation was not a reversible reaction.

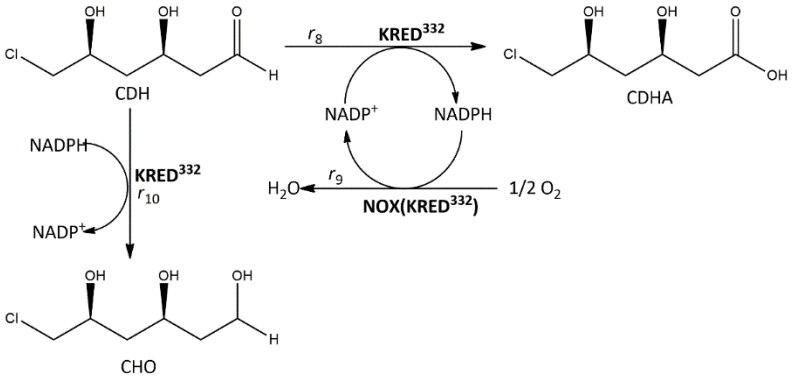

Figure 25 Reaction scheme of KRED[332]-catalyzed CDH oxidation.

$$r_8 = \frac{V_{m,8} \cdot \gamma_{KRED332} \cdot c_{CDH} \cdot c_{NADP^+}}{\left(K_{m,8}^{CDH} + c_{CDH}\right) \cdot \left[K_{m,4}^{NADP^+} \cdot \left(1 + \frac{c_{NADPH}}{K_{i,8}^{NADPH}}\right) + c_{NADP^+} \cdot \left(1 + \frac{c_{NADP^+}}{K_{i,8}^{NADP^+}}\right)\right]} \qquad \text{Equation 52}$$

Due to the application of KRED[332] as a CFE, KRED[332] displayed a certain activity in the reaction of NADPH oxidation, therefore the reaction rate r_9 for the reaction of KRED[332]-

List of reactant and product abbreviations: acetaldehyde (**AA**), chloroacetaldehyde (**CAA**), 4-chloro-3-hydroxybutanal (**CHB**), 6-chloro-3,5-dihydroxyhexanal (**CDH**), 6-chloro-3,5-dihydroxyhexanoic acid (**CDHA**), 3-hydroxy-4(-oxiran-2-yl)butanoic acid (**HOBA**), 6-cyano-3,5-dihydroxyhexanoic acid (**CYDHA**), 3-hydroxybutanal (**HB**), 3,5-dihydroxyhexanal (**DHH**).

catalyzed NADPH oxidation, NOX(KRED^{332}), was described by Michaelis-Menten kinetics with competitive $NADP^+$ and uncompetitive NADPH inhibition (Equation 53).

$$r_9 = \frac{V_{m,9} \cdot \gamma_{NOX(KRED332)} \cdot c_{NADPH}}{K_{m,9}^{NADPH} \cdot \left(1 + \frac{c_{NADP^+}}{K_{i,9}^{NADP^+}}\right) + c_{NADPH} \cdot \left(1 + \frac{c_{NADPH}}{K_{i,9}^{NADPH}}\right)} \qquad \text{Equation 53}$$

Based on the experimental data, it was noted that the KRED^{332} enzyme catalyzed the reaction of CDH reduction into CHO. The reaction rate r_{10} of the CDH reduction was not experimentally determined but was described by second-order kinetics (Equation 54).

$$r_{10} = k_{10} \cdot \gamma_{KRED332} \cdot c_{CDH} \cdot c_{NADPH} \qquad \text{Equation 54}$$

The mass balance equations for substrates CDH and $NADP^+$ and products CDHA and NADPH participating in the KRED^{332}-catalyzed reaction of CDH oxidation into CDHA in a batch reactor are given in Equations 55 – 58.

$$\frac{\mathrm{d}c_{CDH}}{\mathrm{d}t} = -r_8 - r_{10} \qquad \text{Equation 55}$$

$$\frac{\mathrm{d}c_{CDHA}}{\mathrm{d}t} = r_8 \qquad \text{Equation 56}$$

$$\frac{\mathrm{d}c_{NADP^+}}{\mathrm{d}t} = -r_8 + r_9 + r_{10} \qquad \text{Equation 57}$$

$$\frac{\mathrm{d}c_{NADPH}}{\mathrm{d}t} = r_8 - r_9 - r_{10} \qquad \text{Equation 58}$$

The enzyme operational stability decay in the batch reactor was described by second-order kinetics (Equation 59).

$$\frac{\mathrm{d}\gamma_{KRED332}}{\mathrm{d}t} = -k_d^{KRED332} \cdot \gamma_{KRED332}^2 \qquad \text{Equation 59}$$

3.4.4 HHDH^{001}-catalyzed CDHA dehalogenation and epoxide ring-opening with KCN

The reaction rate r_{11} for HHDH^{001}-catalyzed CDHA dehalogenation (Figure 26) was described by modified double-substrate Michaelis-Menten kinetics (Equation 60) that includes KCN activation (K_A^{KCN}) and inhibition (K_i^{KCN}) [181].

List of reactant and product abbreviations: acetaldehyde (**AA**), chloroacetaldehyde (**CAA**), 4-chloro-3-hydroxybutanal (**CHB**), 6-chloro-3,5-dihydroxyhexanal (**CDH**), 6-chloro-3,5-dihydroxyhexanoic acid (**CDHA**), 3-hydroxy-4(-oxiran-2-yl)butanoic acid (**HOBA**), 6-cyano-3,5-dihydroxyhexanoic acid (**CYDHA**), 3-hydroxybutanal (**HB**), 3,5-dihydroxyhexanal (**DHH**).

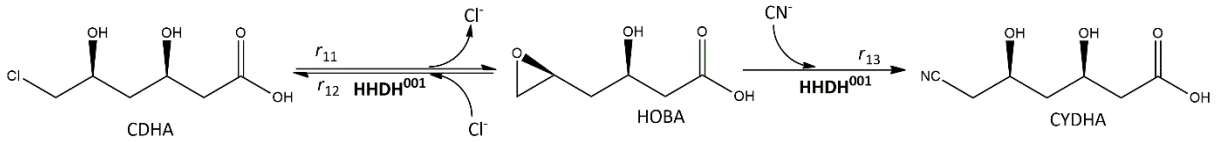

Figure 26 Reaction scheme of HHDH-catalyzed dehalogenation and epoxide ring-opening with KCN.

$$r_{11} = \frac{V_{m,11} \cdot \left(1 + K_{A,11}^{KCN}\right)^{c_{KCN}} \cdot \gamma_{HHDH001} \cdot c_{CDHA}}{\left(K_{m,11}^{CDHA} + c_{CDHA}\right) \cdot \left(1 + \frac{c_{KCN}}{K_{i,11}^{KCN}}\right)} \qquad \text{Equation 60}$$

The reaction rate r_{12} HHDH^{001}-catalyzed reverse reaction of epoxide-ring opening with chloride (Figure 26) was described by first-order kinetics (Equation 61).

$$r_{12} = k_{12} \cdot \gamma_{HHDH001} \cdot c_{HOBA} \qquad \text{Equation 61}$$

The HHDH^{001}-catalyzed epoxide ring-opening in presence of KCN (r_{13}, Figure 26) was described by second-order kinetics (Equation 62).

$$r_{13} = k_{13} \cdot \gamma_{HHDH001} \cdot c_{HOBA} \cdot c_{KCN} \qquad \text{Equation 62}$$

The mass balance equations for substrates and products in the HHDH^{001}-catalyzed reaction in batch reactor are presented in Equations 63 – 66.

$$\frac{\mathrm{d}c_{CDHA}}{\mathrm{d}t} = -r_{11} + r_{12} \qquad \text{Equation 63}$$

$$\frac{\mathrm{d}c_{HOBA}}{\mathrm{d}t} = r_{11} - r_{12} - r_{13} \qquad \text{Equation 64}$$

$$\frac{\mathrm{d}c_{KCN}}{\mathrm{d}t} = -r_{13} \qquad \text{Equation 65}$$

$$\frac{\mathrm{d}c_{CYDHA}}{\mathrm{d}t} = r_{13} \qquad \text{Equation 66}$$

The enzyme operational stability decay in the batch reactor was described by second-order kinetics (Equation 67).

$$\frac{\mathrm{d}\gamma_{HHDH001}}{dt} = -k_d^{HHDH001} \cdot \gamma_{HHDH001}^2 \qquad \text{Equation 67}$$

List of reactant and product abbreviations: acetaldehyde (**AA**), chloroacetaldehyde (**CAA**), 4-chloro-3-hydroxybutanal (**CHB**), 6-chloro-3,5-dihydroxyhexanal (**CDH**), 6-chloro-3,5-dihydroxyhexanoic acid (**CDHA**), 3-hydroxy-4(-oxiran-2-yl)butanoic acid (**HOBA**), 6-cyano-3,5-dihydroxyhexanoic acid (**CYDHA**), 3-hydroxybutanal (**HB**), 3,5-dihydroxyhexanal (**DHH**).

3.5 Data processing

The kinetic parameters of the Michaelis-Menten kinetic models (V_m, K_m, K_i) were estimated from the independent initial reaction rate data by non-linear regression analysis using the simplex or least squares method implemented in the MicroMath *Scientist* software [182]. The same methods were used for the estimation of operational stability decay rate constants (k_d) and parameters (a, b, d) of the polynomial enzyme deactivation model. The operational stability decay rate constants were estimated from the data set enzyme activity *vs* time, while the polynomial parameters were estimated from the data set operational stability decay rate constant *vs* compound concentration. The parameter estimation was done by fitting the model to the experimental data. The calculated data were compared with the experimental data, recalculated in the optimization routine and fitted again until a minimal error between experimental and calculated values was achieved. The residual was defined as the sum of squares of the differences between the experimental and calculated data.

The set of optimum parameters were used for the simulation according to the proposed models. For the simulations, the built-in Episode algorithm for a stiff system of differential equations was used. Coefficients of determination (R^2) and standard deviations (σ), used as measures of goodness-of-fit, were calculated by *Scientist* built-in statistical functions.

3.6 Results and discussion

3.6.1 Influence of buffers on enzyme activity and stability

3.6.1.1 Influence of pH on DERA^{Tm} and DERA^{024} activity and stability

To find the optimal conditions for the DERA-catalyzed reaction of AA addition onto CAA (Figure 1), the activity and stability of DERA^{Tm} and DERA^{024} in different buffers (pH 5.4 – 10) was investigated. Following the DERA assay procedures, the activity and stability results were collected (Figure 27).

DERA^{Tm} showed the highest activity in 0.1 M TEA-HCl buffer pH 7 (Figure 27a), which was in agreement with the previously published codon-optimized DERA [101]. It was found that the residual DERA^{Tm} activity after 24 h of incubation was practically constant (> 80 %) within the pH range from 5.4 to 8 (Figure 27b), which is in accordance with previous

List of reactant and product abbreviations: acetaldehyde (**AA**), chloroacetaldehyde (**CAA**), 4-chloro-3-hydroxybutanal (**CHB**), 6-chloro-3,5-dihydroxyhexanal (**CDH**), 6-chloro-3,5-dihydroxyhexanoic acid (**CDHA**), 3-hydroxy-4(-oxiran-2-yl)butanoic acid (**HOBA**), 6-cyano-3,5-dihydroxyhexanoic acid (**CYDHA**), 3-hydroxybutanal (**HB**), 3,5-dihydroxyhexanal (**DHH**).

investigations for a similar DERA [104]. The highest residual activity of 96 % was noticed in 0.1 M TEA-HCl buffer pH 7.

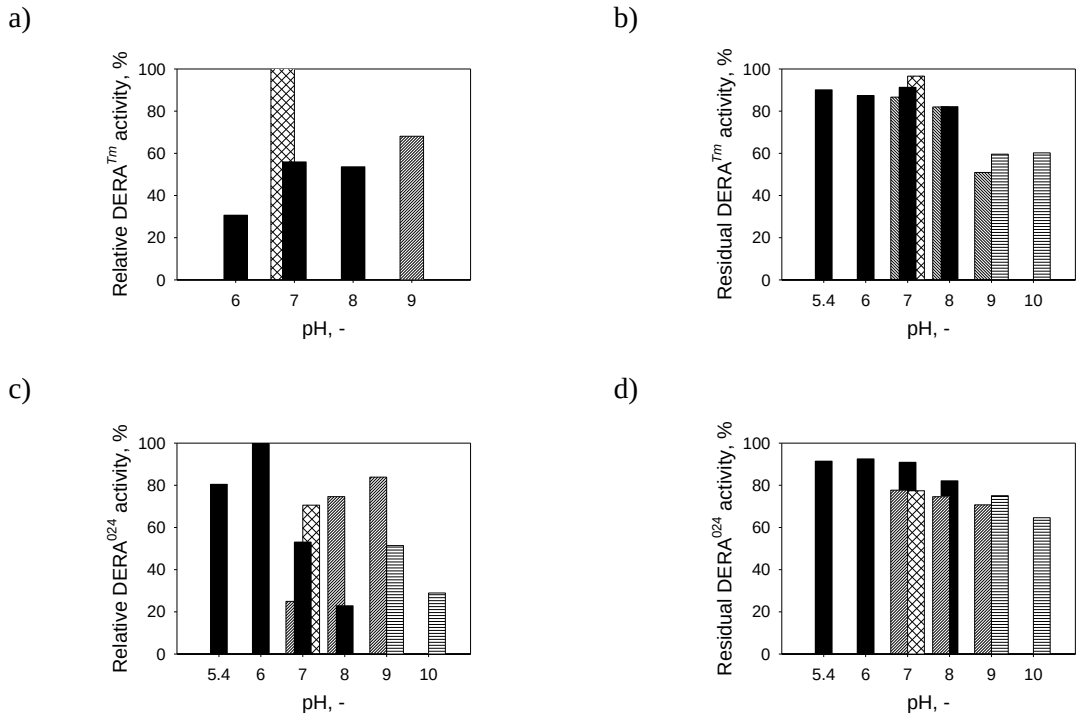

Figure 27 Influence of pH on a) DERA^{Tm} activity, b) DERA^{Tm} stability, c) DERA^{024} activity and d) DERA^{024} stability at different pH (5.4 – 10.0; activity measurements: DERA HPLC Assay; stability measurements: DRP Assay). The stability results regarding the residual activity of both enzymes were collected after 24 hours of incubation. Pattern legend: 0.1 M phosphate buffer (black), 0.1 M TEA-HCl buffer (intercrossing diagonal lines), 0.1 M Tris-HCl buffer (diagonal lines), 0.1 M Glycine-NaOH buffer (horizontal lines).

DERA^{024} showed the highest activity in 0.1 M phosphate buffer pH 6. It was also noted that the enzyme showed a quite high relative activity (> 80 %) in 0.1 M phosphate buffer pH 5.4 and in 0.1 M Tris-HCl buffer pH 9 (Figure 27c). After 24 h of incubation in various buffers, DERA^{024} showed high stability (> 80 %) in 0.1 M phosphate buffer in all examined pH values and relatively good stability (> 70 %) in a wide range of buffers and pH (Figure 27d), which is in accordance with previous findings [96, 131]. The highest measured residual activity after 24 hours of incubation was 93 % in 0.1 M phosphate buffer pH 6.

Based on this, further investigations of DERA^{Tm} and DERA^{024} were performed in 0.1 M TEA-HCl buffer pH 7 and 0.1 M phosphate buffer pH 6, respectively.

List of reactant and product abbreviations: acetaldehyde (**AA**), chloroacetaldehyde (**CAA**), 4-chloro-3-hydroxybutanal (**CHB**), 6-chloro-3,5-dihydroxyhexanal (**CDH**), 6-chloro-3,5-dihydroxyhexanoic acid (**CDHA**), 3-hydroxy-4(-oxiran-2-yl)butanoic acid (**HOBA**), 6-cyano-3,5-dihydroxyhexanoic acid (**CYDHA**), 3-hydroxybutanal (**HB**), 3,5-dihydroxyhexanal (**DHH**).

3.6.1.2 Influence of pH on AlDH and NOX^{009} activity and stability

Since it was found that the optimal buffer for the reaction mediated by the DERA^{024} enzyme was 0.1 M phosphate buffer, and because the AlDH-catalyzed reaction is a consecutive reaction of the DERA-catalyzed reaction, the same buffer with different pH (7.0, 7.4, 7.6, 7.8, and 8.0) was chosen for assessing the influence of pH on the AlDH and NOX^{009} activity and stability. Results of enzyme's activity and stability at different pHs are shown in Figure 28.

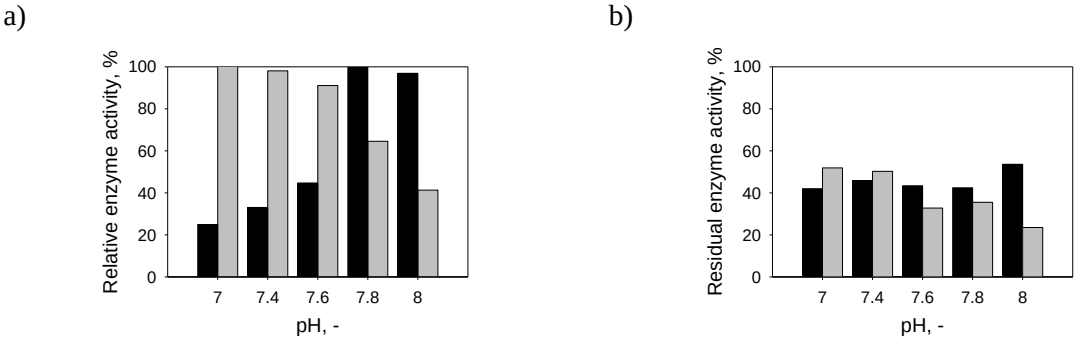

Figure 28 Influence of pH on AlDH and NOX^{009} a) activity and b) stability (0.1 M phosphate buffer, 7 – 8). The stability results were collected after 24 (AlDH) or 5 (NOX^{009}) hours of incubation. Legend: AlDH (black), NOX^{009} (grey).

The relative activity of AlDH increased with the increase of pH, opposite to the activity of NOX^{009} that decreased with the increase of pH (Figure 28a). AlDH showed higher activities (> 97 %) at pH above 7.8, while low activities (< 45 %) were measured at pH 7.6 and below. NOX^{009} showed the high activities at pH below 7.6 (> 91 %), whilst its lowest activity (41 %) was measured at pH 8.0.

Both enzymes showed poor stability (Figure 28b), which was measured after 24 hours and five hours of incubation for AlDH and NOX^{009}, respectively. The highest residual activity for AlDH was noted at pH 8.0 (54 %), while for NOX^{009} at pH 7.0 (52 %) and pH 7.4 (50 %). Due to the obvious instability of the enzymes regardless of pH, the optimum pH for the AlDH-catalyzed CDH oxidation was chosen to be pH 8.0, despite the obtained NOX^{009} stability results. Similar results for AlDH were reported in previously published literature, in spite of enzyme origin, suggesting the pH optimum at 8.0 [183 - 187].

List of reactant and product abbreviations: acetaldehyde (**AA**), chloroacetaldehyde (**CAA**), 4-chloro-3-hydroxybutanal (**CHB**), 6-chloro-3,5-dihydroxyhexanal (**CDH**), 6-chloro-3,5-dihydroxyhexanoic acid (**CDHA**), 3-hydroxy-4(-oxiran-2-yl)butanoic acid (**HOBA**), 6-cyano-3,5-dihydroxyhexanoic acid (**CYDHA**), 3-hydroxybutanal (**HB**), 3,5-dihydroxyhexanal (**DHH**).

3.6.2 Influence of temperature on DERA^{Tm} activity and stability

To find the optimal temperature for the DERA-catalyzed reaction (Figure 1), the activity and stability of DERA^{Tm} at different temperatures (20 – 50 °C, Figure 29) were investigated. While measuring the impact of temperature on the relative activity of DERA^{Tm}, its activity increased with temperature in accordance with the Arrhenius equation given below (Equation 68).

$$A_S = A_{S,0} \cdot e^{-\frac{E_A}{R \cdot T}}$$ Equation 68

The parameters of the Arrhenius equation were estimated from the experimental data shown in Figure 29a. The pre-exponential factor, which was the specific enzyme activity $A_{S,0}$, equaled (7.61 ± 3.83) · 10^5 U/mg, while the activation energy E_A was found to be (3.86 ± 0.13) · 10^4 J/mol.

DERA^{Tm} showed very good thermostability (Figure 29b): more than 80 % of its initial activity was retained after three days of incubation at temperatures in the range between 20 and 40 °C, with the highest residual activity at 20 – 25 °C (approx. 87 %) [96], showing that DERA^{Tm} is more thermostable than the corresponding DERA from *Lactobacillus brevis* [131].

a) b)

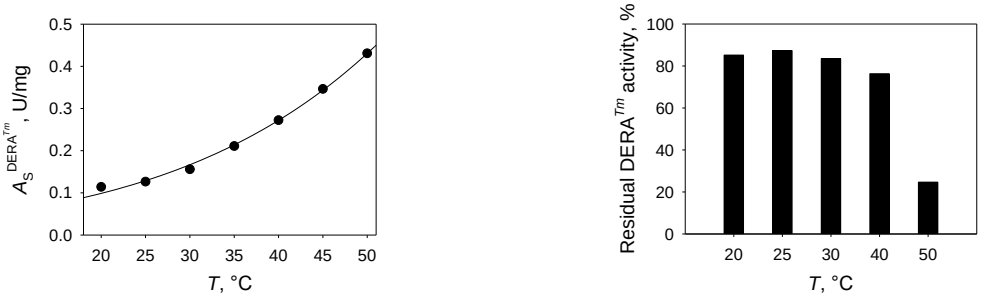

Figure 29 DERA^{Tm} a) activity and b) stability at different temperatures (20 – 50 °C, 0.1 M TEA-HCl buffer; DRP Assay). The stability results regarding the residual DERA^{Tm} activity were collected after three days of incubation. Legend: experiment (dots), model (line).

Due to the low boiling point of AA (22.2 °C) and the presented results (Figure 29), the chosen temperature for all reactions was 25 °C.

List of reactant and product abbreviations: acetaldehyde (**AA**), chloroacetaldehyde (**CAA**), 4-chloro-3-hydroxybutanal (**CHB**), 6-chloro-3,5-dihydroxyhexanal (**CDH**), 6-chloro-3,5-dihydroxyhexanoic acid (**CDHA**), 3-hydroxy-4(-oxiran-2-yl)butanoic acid (**HOBA**), 6-cyano-3,5-dihydroxyhexanoic acid (**CYDHA**), 3-hydroxybutanal (**HB**), 3,5-dihydroxyhexanal (**DHH**).

3.6.3 Influence of organic compounds on enzyme stability

3.6.3.1 Influence of aldehydes on DERA^{Tm} and DERA^{024} stability

According of previous observations reported in the literature [12, 96, 104, 131, 141], it was necessary to investigate individual influences of AA, CAA, CHB, and CDH on DERA^{Tm} and DERA^{024} stability. The purpose of those measurements was to obtain the insight of the operational stability of both enzymes in order to predict the enzyme behavior during the reaction. Within those measurements, the mechanism of deactivation, which has not yet been fully clarified [141], was not investigated. It was found that AA, CA and CHB had a negative effect on the enzyme stability, whereas CDH had practically no effect (Figure 30).

a) b)

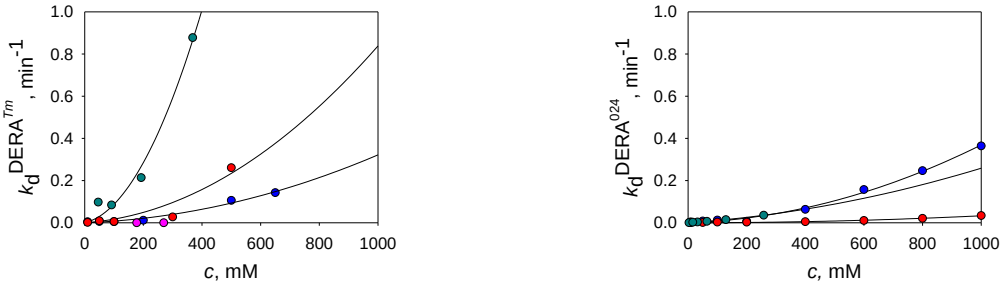

Figure 30 Influence of AA, CAA, CHB and CDH concentration on the deactivation rate constant of a) DERA^{Tm} (γ_{DERA} = 10 mg/mL, 0.1 M TEA-HCl buffer pH 7, 25 °C, 3 h) and b) DERA^{024} (γ_{DERA} = 10 mg/mL, 0.1 M phosphate buffer pH 6, 25 °C, 3 h). Legend: experiment (dots), model (line); AA (blue), CAA (red), CHB (teal), CDH (pink).

Three models were tested for describing the enzyme deactivation: the first- and the second-order decay kinetics model and the parallel model that is based on the three-parameter bi-exponential equation [188]. The second-order decay kinetics and the parallel model resulted with almost the same goodness-of-fit to the experimental data. Due to a smaller number of parameters, the decrease of DERA activity during incubation with AA, CAA and CHB was described by second-order kinetics. The deactivation rate constant was estimated from the experimental results of relative activity *vs* time for each individual aldehyde concentration. The presented results show the dependence of the deactivation rate constant on the concentration of AA, CAA and CHB, which were described by a second-order polynomial model (Figure 30). The estimated parameters of the polynomial model (Equation 39) are presented in Table 5.

List of reactant and product abbreviations: acetaldehyde (**AA**), chloroacetaldehyde (**CAA**), 4-chloro-3-hydroxybutanal (**CHB**), 6-chloro-3,5-dihydroxyhexanal (**CDH**), 6-chloro-3,5-dihydroxyhexanoic acid (**CDHA**), 3-hydroxy-4(-oxiran-2-yl)butanoic acid (**HOBA**), 6-cyano-3,5-dihydroxyhexanoic acid (**CYDHA**), 3-hydroxybutanal (**HB**), 3,5-dihydroxyhexanal (**DHH**).

Table 5 Parameters of the polynomial model for the dependency of the deactivation rate constant on the concentration of AA, CAA, CHB and CDH.

Aldehyde	DERA^{Tm}		DERA^{024}	
	***a*, mM^{-2} min^{-1}**	***b*, mM^{-1} min^{-1}**	***a*, mM^{-2} min^{-1}**	***b*, mM^{-1} min^{-1}**
AA	$2.70 \cdot 10^{-7}$	$5.18 \cdot 10^{-5}$	$3.21 \cdot 10^{-7}$	$4.83 \cdot 10^{-5}$
CAA	$7.40 \cdot 10^{-7}$	$9.85 \cdot 10^{-5}$	$3.30 \cdot 10^{-8}$	$1.42 \cdot 10^{-7}$
CHB	$5.49 \cdot 10^{-6}$	$3.27 \cdot 10^{-5}$	$1.63 \cdot 10^{-7}$	$9.59 \cdot 10^{-5}$
CDH	-	-	-	-

It was noted that the concentrations of AA and CAA of up to 100 mM influence the stability of both DERAs considerably, which was in accordance with previous findings for DERA [18]. Substrate CAA was found to be a more potent deactivator of DERA^{Tm} as compared to AA, which was also the case with previous investigations with DERAs from various sources [14, 18, 67, 131], but in contrast to findings regarding results given in Table 5 obtained for DERA^{024}. The deactivation of DERA^{Tm} by AA was consistent with previous research carried out with DERA^{Tm} [104]. More interestingly, the results indicated that CHB had a stronger destabilizing effect on DERA^{Tm}, compared to either AA or CAA, which was not yet reported in literature. Among the studied DERAs, DERA^{024} showed significant improvement in stability against aldehydes compared to DERA^{Tm}, particularly in presence of CAA and CHB. Both AA and CHB had a similar effect on the DERA^{024} stability, in contrast to CAA, which had notably lower impact on its stability among the examined aldehydes. Due to the negative impact of the aldehyde substrates and the reaction intermediate on the stability of both DERAs, it is of crucial importance to select optimal initial substrate concentrations and a suitable reactor configuration, especially in case when the reaction is catalyzed by DERA^{Tm}, to avoid accumulation of CHB in the reactor.

3.6.3.2 Influence of aldehydes on AlDH, NOX^{009} and KRED^{332} stability

Because the substrate for the AlDH- and KRED^{332}-catalyzed reaction was intended to be used in its crude, unpurified form, it was assumed that certain amounts of unreacted AA, CAA and CHB might be present in the reaction mixture obtained from the DERA-catalyzed reaction. Therefore, the stability of AlDH, NOX^{009} and KRED^{332} in the presence of organic compounds was evaluated. From the collected results of relative activity *vs* time for each individual compound concentration, the deactivation rate constants were estimated and described by second-order kinetics. The dependence of the deactivation rate constant on the concentration of each of the examined compounds is presented in Figure 31.

List of reactant and product abbreviations: acetaldehyde (**AA**), chloroacetaldehyde (**CAA**), 4-chloro-3-hydroxybutanal (**CHB**), 6-chloro-3,5-dihydroxyhexanal (**CDH**), 6-chloro-3,5-dihydroxyhexanoic acid (**CDHA**), 3-hydroxy-4(-oxiran-2-yl)butanoic acid (**HOBA**), 6-cyano-3,5-dihydroxyhexanoic acid (**CYDHA**), 3-hydroxybutanal (**HB**), 3,5-dihydroxyhexanal (**DHH**).

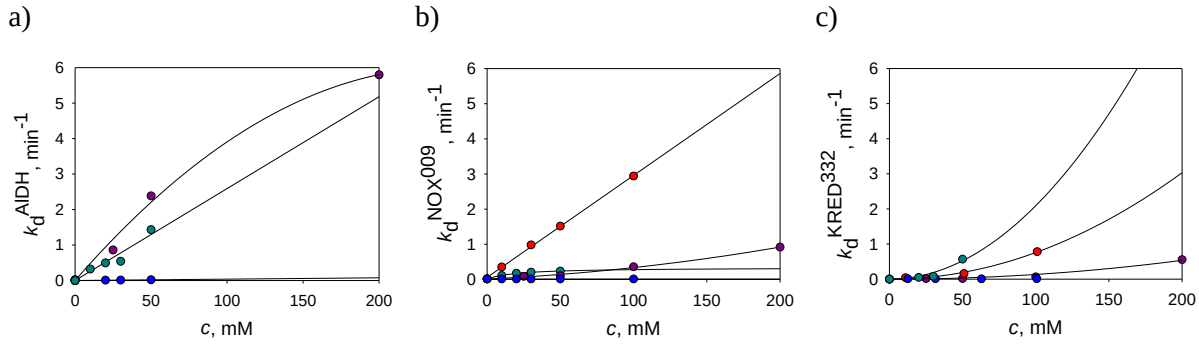

Figure 31 Influence of aldehydes on the deactivation rate constant of a) AlDH, b) NOX^{009}, and c) KRED^{332} (γ_{enzyme} = 10 mg/mL, 0.1 M phosphate buffer pH 8, 25 °C, 3 h). Legend: experiment (dots), model (line); AA (blue), CAA (red), CHB (teal), CDH (purple).

The dependence of the deactivation rate constants on the concentration of organic compounds of all three enzymes were described by either zero-, first- or second-order polynomial model or hyperbolic model, i.e. of AlDH by Equation 69, of NOX^{009} by Equation 70 and of KRED^{332} by Equation 71.

$$k_d^{AlDH} = \sum_i \left(a_i \cdot c_i^2 + b_i \cdot c_i\right) \qquad \text{Equation 69}$$

$$k_d^{NOX009} = \sum_i \left(a_i \cdot c_i^2 + b_i \cdot c_i\right) + \frac{a_{CHB} \cdot c_{CHB}}{b_{CHB} + c_{CHB}} + d \qquad \text{Equation 70}$$

$$k_d^{KRED332} = \sum_i \left(a_i \cdot c_i^2 + d_i\right) \qquad \text{Equation 71}$$

During the measurements, it was found that the presence of AA caused slight deactivation of KRED^{332} and NOX^{009}, but the deactivation rate did not depend on the AA concentration. The estimated parameters of the developed polynomial models (Equations 69 - 71) are given in Table 6. Based on the obtained results (Figure 31), it could be concluded that AA had negligible effects on the AlDH stability, while CAA had a severe impact on the stability of this enzyme. Additionally, it was noted that CDHA does not affect the stability of AlDH (data not shown). Regarding the stability of NOX^{009}, CAA proved to be the strongest inactivator among the examined aldehydes, even at low concentrations (< 1 mM), while AA displayed the lowest impact on the enzyme's stability, followed by CDH and CHB. KRED^{332} proved to be the most stable enzyme, compared to AlDH and NOX^{009}, its stability being the most affected by the presence of higher quantities (> 50 mM) of CAA in the reaction system.

List of reactant and product abbreviations: acetaldehyde (**AA**), chloroacetaldehyde (**CAA**), 4-chloro-3-hydroxybutanal (**CHB**), 6-chloro-3,5-dihydroxyhexanal (**CDH**), 6-chloro-3,5-dihydroxyhexanoic acid (**CDHA**), 3-hydroxy-4(-oxiran-2-yl)butanoic acid (**HOBA**), 6-cyano-3,5-dihydroxyhexanoic acid (**CYDHA**), 3-hydroxybutanal (**HB**), 3,5-dihydroxyhexanal (**DHH**).

Table 6 Estimated parameters of the polynomial models for the dependency of the deactivation rate constant of AlDH, NOX[009] and KRED[332] on the concentration of each of the examined aldehyde compound.

Parameter	AA	CAA	CHB	CDH
AlDH				
***a*, mM^{-2} min^{-1}**	-	-	-	-0.0001
***b*, mM^{-1} min^{-1}**	0.00038	239.64	0.026	0.049
NOX[009]				
***a*, mM^{-2} min^{-1}** or ***a*, min^{-1}** [a]	-	-	0.32 [a]	$1.28 \cdot 10^{-5}$
***b*, mM^{-1} min^{-1}**	-	0.029	20.95	0.002
***d*, min^{-1}**	0.013	0.059	0.013	0.012
KRED[332]				
***a*, mM^{-2} min^{-1}**	-	$7.58 \cdot 10^{-5}$	0.00021	$1.34 \cdot 10^{-5}$
***b*, mM^{-1} min^{-1}**	-	-	-	-
***d*, min^{-1}**	0.0096	-	-	-

[a] hyperbolic dependency

Therefore, if the enzyme-catalyzed CDH oxidation would be carried out as a sequential one-pot reaction, the reaction mixture obtained from the DERA-catalyzed reaction should be purified from CAA, especially in case when the CDH oxidation should be done using the AlDH/NOX[009] system. If the DERA reaction mixture should contain unreacted CAA and CHB, an additional amount of AA should be added into the reactor in order to minimize the presence of CHB and to fully convert CAA into the final product CDH by the action of DERA.

3.6.3.3 Influence of CDHA and KCN on HHDH[001] stability

While measuring the residual activity of HHDH[001], it was observed that CDHA and KCN inactivate the enzyme and that deactivation constant increased with the increase of CDHA and KCN concentration. CDHA and KCN have a similar destabilizing effect on HHDH[001] at concentrations below 75 mM, while at higher concentrations, KCN impacts the enzyme activity much more significantly (Figure 32).

The dependency of the deactivation rate constant on CDHA and KCN concentration was described using the Equation 72 and the estimated values of its parameters are given in Table 7.

$$k_d^{HHDH001} = \sum_i \left(a + b \cdot c_i + d \cdot c_i^2\right) \qquad \text{Equation 72}$$

List of reactant and product abbreviations: acetaldehyde (**AA**), chloroacetaldehyde (**CAA**), 4-chloro-3-hydroxybutanal (**CHB**), 6-chloro-3,5-dihydroxyhexanal (**CDH**), 6-chloro-3,5-dihydroxyhexanoic acid (**CDHA**), 3-hydroxy-4(-oxiran-2-yl)butanoic acid (**HOBA**), 6-cyano-3,5-dihydroxyhexanoic acid (**CYDHA**), 3-hydroxybutanal (**HB**), 3,5-dihydroxyhexanal (**DHH**).

a) b)

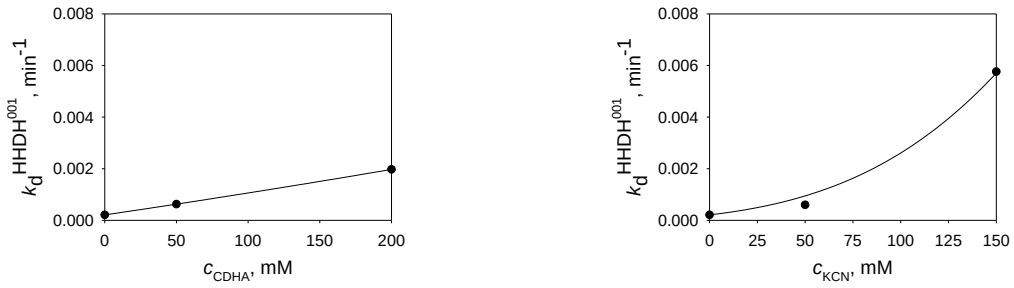

Figure 32 Influence of a) CDHA and b) KCN on the deactivation rate constant of $HHDH^{001}$ ($\gamma_{HHDH001}$ = 10 mg/mL, 0.1 M phosphate buffer pH 8). Legend: experiment (dots), model (line).

Table 7 Parameters of the polynomial models for the dependency of the deactivation rate constant of HHDH on the concentration of each of CDHA and KCN.

Compound	*a*, mM^{-2} min^{-1}	*b*, mM^{-1} min^{-1}	*d*, min^{-1}
CDHA	$1.99 \cdot 10^{-4}$	$8.85 \cdot 10^{-6}$	-
KCN	$2.10 \cdot 10^{-4}$	$-6.84 \cdot 10^{-6}$	$2.92 \cdot 10^{-7}$

3.6.4 Enzyme kinetics

The kinetic investigations for each of the applied enzymes were carried out to develop mathematical models that would be applicable to different reactor configurations. Since the examined statin side-chain productions are considered as a very complex reaction system, the formal kinetic model was applied. During the reaction, many compounds are being produced and consumed resulting in a system of many possible interactions [14]. Applying the mechanistic model for its description would result in a high number of parameters [14] making it hard to get an intrinsic control of correctness in its estimation. The formal kinetic model includes the data-driven or the empirical model which has less kinetic constants [153]. Those constants can be independently evaluated and have a defined physical meaning. Therefore, to describe the kinetics in the explored process, single- or double-substrate Michaelis-Menten equations were used.

The kinetic measurements for the enzymes involved in this reaction route were conducted based on the reaction scheme (Figures 23 – 26) by using the initial reaction rate method. The influences of relevant substrates and products on the specific enzyme activity in the observed reaction were determined.

List of reactant and product abbreviations: acetaldehyde (**AA**), chloroacetaldehyde (**CAA**), 4-chloro-3-hydroxybutanal (**CHB**), 6-chloro-3,5-dihydroxyhexanal (**CDH**), 6-chloro-3,5-dihydroxyhexanoic acid (**CDHA**), 3-hydroxy-4(-oxiran-2-yl)butanoic acid (**HOBA**), 6-cyano-3,5-dihydroxyhexanoic acid (**CYDHA**), 3-hydroxybutanal (**HB**), 3,5-dihydroxyhexanal (**DHH**).

3.6.4.1 DERA^{Tm} and DERA^{024} kinetics in the aldol addition

The DERA^{Tm} and DERA^{024} kinetic measurements were carried out in a batch reactor by adding different amounts of reactants AA, CAA and CHB. By using the initial reaction rate method, the influence of different concentrations of AA and CAA (Figure 23a) or AA and CHB (Figure 23b) on the initial reaction rate of DERA^{Tm} and DERA^{024} are shown in Figure 33 and Figure 34, respectively, were determined.

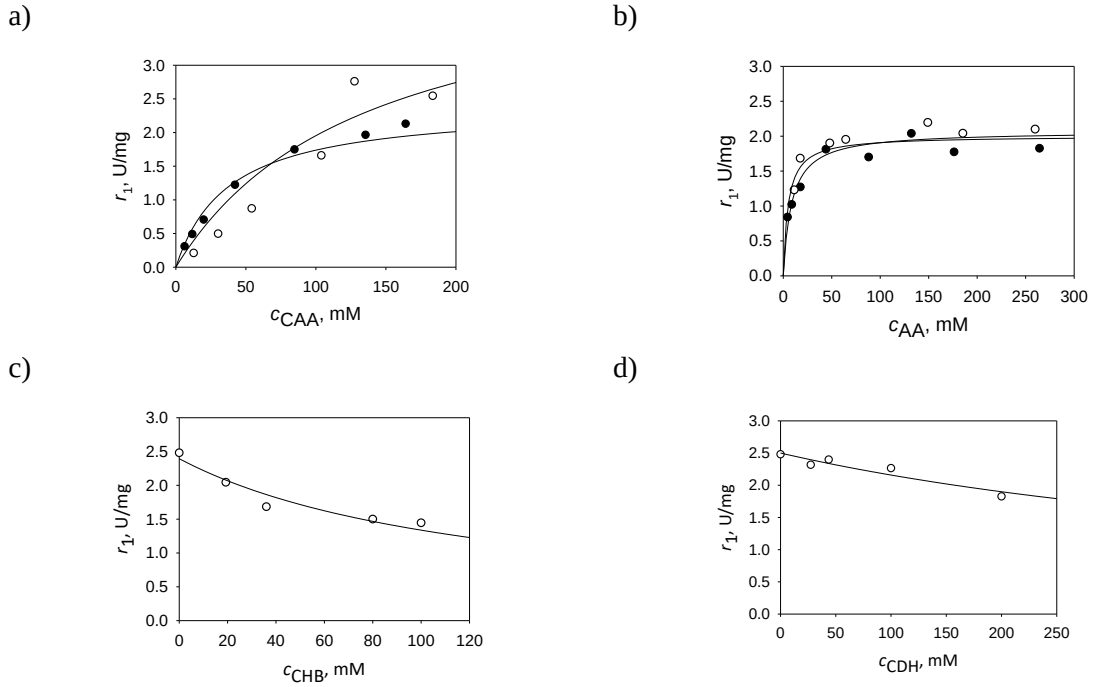

Figure 33 Comparison kinetics of the first aldol addition of AA onto CAA catalyzed by DERA^{Tm} (0.1 M TEA-HCl buffer pH 7) and DERA^{024} (0.1 M phosphate buffer pH 6) (γ_{DERA} = 1 mg/mL, 1 000 rpm, 25 °C). The dependence of the initial reaction rate on a) CAA (c_{AA} = 200 mM), b) AA (c_{CAA} = 200 mM), c) CHB (c_{AA} = 200 mM, c_{CAA} = 200 mM), and d) CDH (c_{AA} = 200 mM, c_{CAA} = 200 mM). Legend: experiment (dots), model (line); DERA^{Tm} (black), DERA^{024} (white).

Since DERA can also utilize AA as an electrophilic aldol component, and thus can catalyze a direct AA self-aldol addition to produce CHH over two steps (Figure 23c), the kinetics of this side reaction was examined as well (Figure 35 and Figure 36). The kinetic parameters of mathematical models for DERA^{Tm} and DERA^{024} of the first and second aldol addition, as well as of the AA self-aldol addition were estimated and are given in Table 8 (Equation 21 – Equation 25). The kinetic measurements revealed that the DERA^{024}-catalyzed first aldol reaction was inhibited by products CHB (Figure 33c) and CDH (Figure 33d), while the second aldol reaction was inhibited by its substrate CHB (Figure 34a). It was found that the

List of reactant and product abbreviations: acetaldehyde (**AA**), chloroacetaldehyde (**CAA**), 4-chloro-3-hydroxybutanal (**CHB**), 6-chloro-3,5-dihydroxyhexanal (**CDH**), 6-chloro-3,5-dihydroxyhexanoic acid (**CDHA**), 3-hydroxy-4(-oxiran-2-yl)butanoic acid (**HOBA**), 6-cyano-3,5-dihydroxyhexanoic acid (**CYDHA**), 3-hydroxybutanal (**HB**), 3,5-dihydroxyhexanal (**DHH**).

reaction of AA self-aldol addition catalyzed by either DERA^{Tm} or DERA^{024} was inhibited by substrate CAA (Figures 35b and 36b) and by the intermediate CHB (Figures 35c and 36c). The possibility of the existence of a retro-aldol reaction catalyzed by DERA^{Tm}- and DERA^{024} was examined, but none was detected (data not shown).

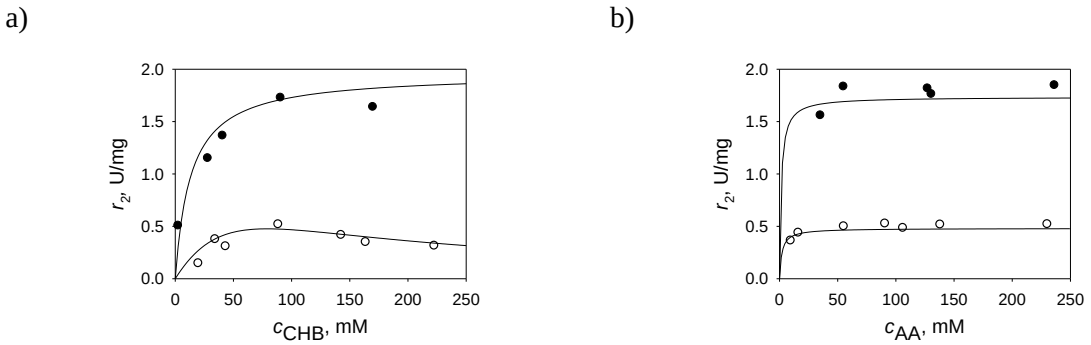

Figure 34 Comparison kinetics of the second aldol addition of AA onto CHB catalyzed by DERA^{Tm} (0.1 M TEA-HCl buffer pH 7) and DERA^{024} (0.1 M phosphate buffer pH 6) (γ_{DERA} = 1 mg/mL, 1 000 rpm, 25 °C). The dependence of the initial reaction rate on a) CHB (c_{AA} = 200 mM) and b) AA (DERA^{Tm}: c_{CHB} = 95 mM; DERA^{024}: c_{CHB} = 80 mM). Legend: experiment (dots), model (line); DERA^{Tm} (black), DERA^{024} (white).

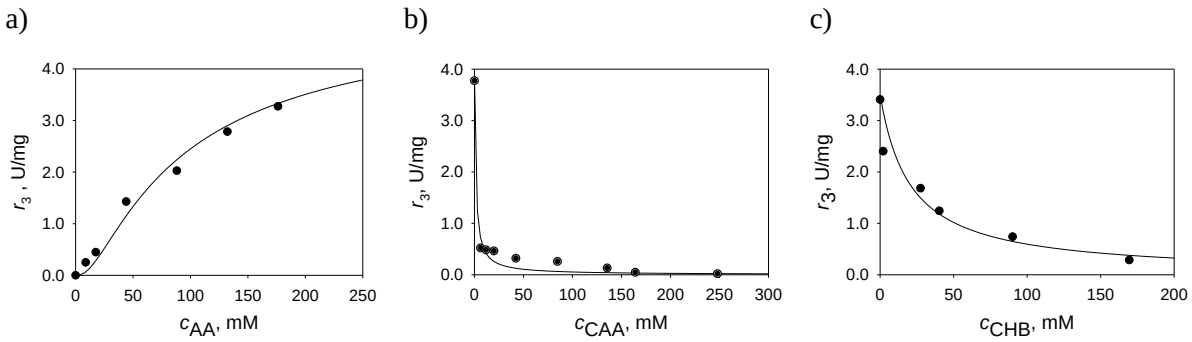

Figure 35 Kinetics of the DERA^{Tm}-catalyzed AA self-aldol addition (0.1 M TEA-HCl, pH 7, $\gamma_{DERA^{Tm}}$ = 1 mg/mL, 1 000 rpm, 25 °C). The dependence of the initial reaction rate on a) AA, b) CAA (c_{AA} = 200 mM) and c) CHB (c_{AA} = 200 mM). Legend: experiment (dots), model (line).

The maximum reaction rate of DERA^{Tm} and DERA^{024} of the first AA addition reaction was 6- and 3-fold higher, respectively, than the maximum reaction rate of the second AA addition step (Table 8). Because of that, accumulation of CHB is to be expected [12], but in lower amounts if the reaction is catalyzed by DERA^{024}. The DERA^{024}-catalyzed first AA addition on CAA was inhibited by its product CHB, which was not observed when the reaction was catalyzed by DERA^{Tm}. Additionally, the second reaction step was inhibited by its substrate CHB.

List of reactant and product abbreviations: acetaldehyde (**AA**), chloroacetaldehyde (**CAA**), 4-chloro-3-hydroxybutanal (**CHB**), 6-chloro-3,5-dihydroxyhexanal (**CDH**), 6-chloro-3,5-dihydroxyhexanoic acid (**CDHA**), 3-hydroxy-4(-oxiran-2-yl)butanoic acid (**HOBA**), 6-cyano-3,5-dihydroxyhexanoic acid (**CYDHA**), 3-hydroxybutanal (**HB**), 3,5-dihydroxyhexanal (**DHH**).

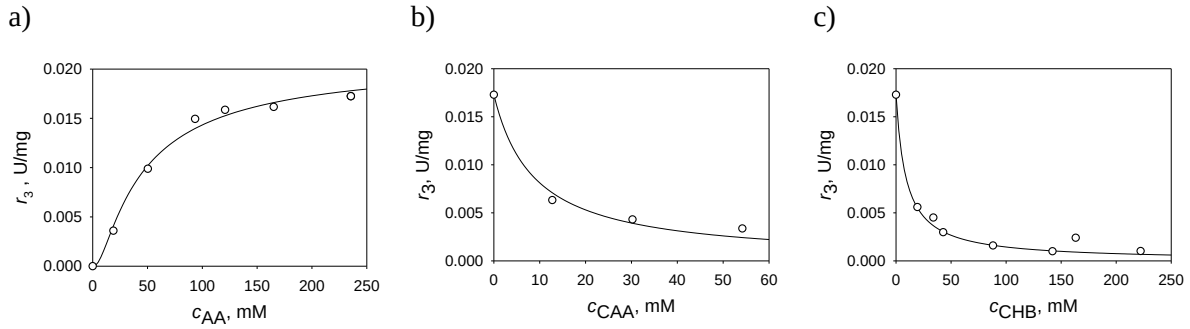

Figure 36 Kinetics of the DERA^{024}-catalyzed AA self-aldol addition (0.1 M phosphate buffer pH 6, γ_{DERA} = 1 mg/mL, 1 000 rpm, 25 °C). The dependence of the initial reaction rate on a) AA, b) CAA (c_{AA} = 200 mM) and c) CHB (c_{AA} = 200 mM). Legend: experiment (dots), model (line).

Table 8 Estimated kinetic parameters for the double aldol addition of AA onto CAA and for the AA self-aldol addition catalyzed by DERA^{Tm} and DERA^{024}.

Parameter	Unit	Value	
		DERA^{Tm}	**DERA^{024}**
First addition of AA to CAA			
$V_{m,1}$	U/mg	1.92 ± 0.15	4.72 ± 0.63
$K_{m,1}^{AA}$	mM	8.67 ± 1.85	5.04 ± 0.54
$K_{m,1}^{CAA}$	mM	37.63 ± 5.55	135.59 ± 12.11
$K_{i,1}^{CHB}$	mM	-	126.55 ± 16.31
$K_{i,1}^{CDH}$	mM	-	632.31 ± 70.21
Second addition of AA to CHB			
$V_{m,2}$	U/mg	0.35 ± 0.04	1.53 ± 0.26
$K_{m,2}^{AA}$	mM	1.43 ± 0.91	2.03 ± 0.28
$K_{m,2}^{CHB}$	mM	13.31 ± 2.18	86.26 ± 7.62
$K_{iS,2}^{CHB}$	mM	-	72.44 ± 7.54
AA self-aldol addition			
$V_{m,3}$	U/mg	2.51 ± 0.51	0.02 ± 0.00
$K_{m,3}^{AA}$	mM	29.04 ± 3.82	13.80 ± 1.68
$K_{i,3}^{CAA}$	mM	0.14 ± 0.02	0.57 ± 0.08
$K_{i,3}^{CHB}$	mM	20.44 ± 5.50	9.11 ± 2.85

The maximum reaction rate of DERA^{Tm}-catalyzed self-aldol addition of AA was somewhat higher than the rates of the aldol additions of CAA with AA ($V_{m,1}$ and $V_{m,2}$), but due to severe inhibition by CAA ($K_{i,3}^{CAA}$) this reaction would not be the preferred one [101]. In case of DERA^{024}-catalyzed AA self-addition, the maximum reaction rate ($V_{m,3}$) was 235-fold lower than the maximum reaction rate of the first aldol addition ($V_{m,1}$) and 77-fold lower than the maximum reaction rate of the second aldol addition ($V_{m,2}$), meaning the reaction occurs slowly. As in case of DERA^{Tm}, high inhibition by CAA as well as by CHB was noted, suggesting that the preferred reaction would be the addition of AA to CAA. The DERA^{024}-catalyzed aldol

List of reactant and product abbreviations: acetaldehyde (**AA**), chloroacetaldehyde (**CAA**), 4-chloro-3-hydroxybutanal (**CHB**), 6-chloro-3,5-dihydroxyhexanal (**CDH**), 6-chloro-3,5-dihydroxyhexanoic acid (**CDHA**), 3-hydroxy-4(-oxiran-2-yl)butanoic acid (**HOBA**), 6-cyano-3,5-dihydroxyhexanoic acid (**CYDHA**), 3-hydroxybutanal (**HB**), 3,5-dihydroxyhexanal (**DHH**).

addition of AA onto CAA should result in insignificant amounts of side-products, opposed to the same reaction catalyzed by DERA^{Tm}.

3.6.4.2 AlDH kinetics in the CDH oxidation

The kinetic measurements for AlDH were conducted by examining the influence of different concentrations of substrates CDH and NAD^+ and products CDHA and NADH on the initial reaction rate of CDH oxidation catalyzed by AlDH (Figure 24). The obtained results are shown in Figure 37, while the estimated kinetic parameters (Equation 40) are presented in Table 9.

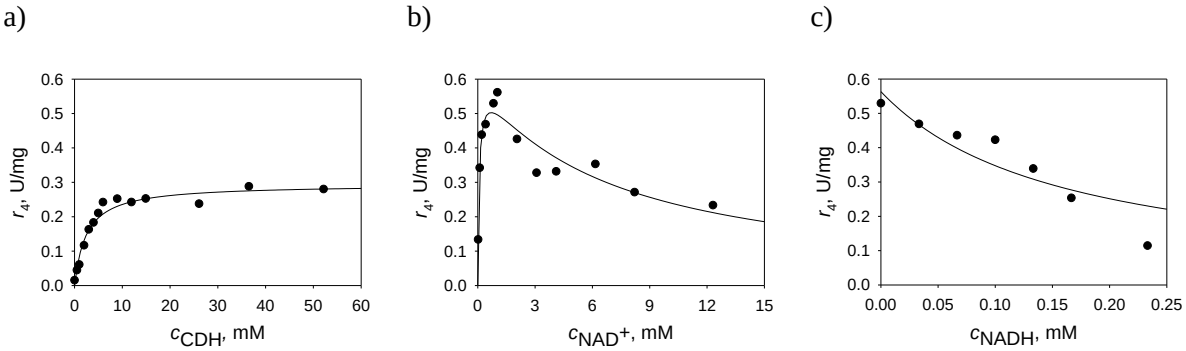

Figure 37 Kinetics of the AlDH-catalyzed oxidation of CDH into CDHA (0.1 M phosphate buffer pH 8, γ_{AlDH} = 0.1 mg/mL, 25 °C). The dependence of the initial reaction rate on substrates a) CDH (c_{NAD} = 10.26 mM) and b) NAD^+ (c_{CDH} = 10.43 mM), as well as on product c) NADH (c_{CDH} = 10.43 mM, c_{NAD} = 10.26 mM). Legend: experiment (dots), model (line).

Table 9 Estimated kinetic parameters for the oxidation of CDH catalyzed by AlDH.

Parameter	Unit	Value
$V_{m,4}$	U/mg	0.754 ± 0.054
$K_{m,4}^{CDH}$	mM	2.470 ± 0.654
$K_{m,4}^{NAD+}$	mM	0.074 ± 0.016
$K_{i,4}^{NAD+}$	mM	6.579 ± 0.756
$K_{i,4}^{NADH}$	mM	0.012 ± 0.004

The results regarding the dependence of the initial reaction rate on the NAD^+ concentration showed inhibition by substrate NAD^+ ($K_{i,4}^{NAD+}$) at higher concentrations (> 1 mM), since the reaction rate decreased with further concentration increase of substrate NAD^+. The influences of products NADH and CDHA, that are formed during the reaction, on the reaction rate of the CDH oxidation were examined as well. The results (Table 9) indicated inhibition by NADH and revealed that CDHA does not inhibit the CDH oxidation (c_{CDH} = 10.43 mM, c_{NAD} = 10.26 mM, γ_{AlDH} = 0.1 mg/mL; data not shown).

List of reactant and product abbreviations: acetaldehyde (**AA**), chloroacetaldehyde (**CAA**), 4-chloro-3-hydroxybutanal (**CHB**), 6-chloro-3,5-dihydroxyhexanal (**CDH**), 6-chloro-3,5-dihydroxyhexanoic acid (**CDHA**), 3-hydroxy-4(-oxiran-2-yl)butanoic acid (**HOBA**), 6-cyano-3,5-dihydroxyhexanoic acid (**CYDHA**), 3-hydroxybutanal (**HB**), 3,5-dihydroxyhexanal (**DHH**).

From the estimated values of the kinetic constants (Table 9), it could be concluded that the enzyme was severely inhibited by NADH, which was formed during the CDH oxidation, while the inhibitory effects of NAD^+ on the AlDH enzyme were not severe.

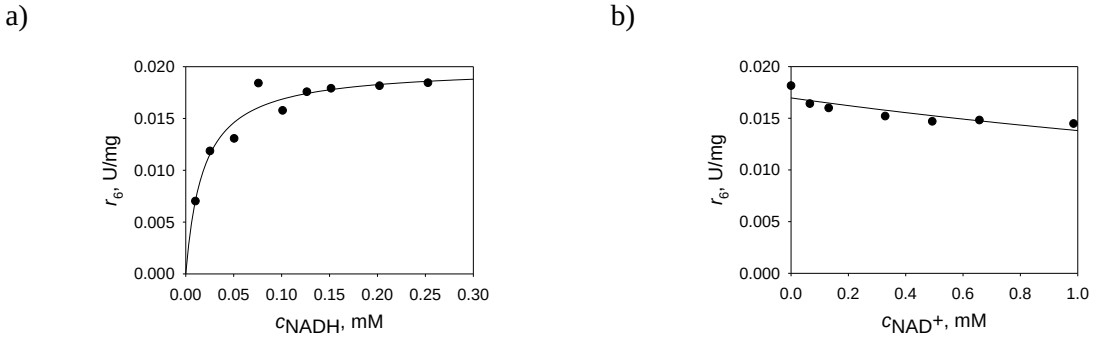

Figure 38 Kinetics of the NOX(AlDH)-catalyzed oxidation of NADH into NAD^+ (0.1 M phosphate buffer pH 8, γ_{AlDH} = 0.25 mg/mL, 25 °C). The dependence of the initial reaction rate on a) substrate NADH and b) product NAD^+ (c_{NADH} = 0.2 mM). Legend: experiment (dots), model (line).

Since it was found that the AlDH CFE contains traces of NOX enzymes, the kinetics of the NADH oxidation catalyzed by NOX(AlDH) was examined as well. By using the initial reaction rate method, the influence of different concentrations of NADH and NAD^+ on the initial reaction rate of NADH oxidation catalyzed by NOX(AlDH) were determined (Figure 38). The estimated kinetic parameters of single-substrate Michaelis-Menten kinetics, expressed as Equation 42, are given Table 10.

Table 2 Estimated kinetic parameters of the NOX(AlDH)-catalyzed NADH oxidation.

Parameter	Unit	Value
$V_{m,6}$	U/mg	0.020 ± 0,001
$K_{m,6}^{NADH}$	mM	0.018 ± 0.003
$K_{i,6}^{NAD+}$	mM	0.367 ± 0.011

Based on the values of estimated kinetic parameters (Tables 9 and 10), the maximum reaction rate of the CDH oxidation ($V_{m,4}$) was 5-fold higher than the maximum reaction rate of the NAD^+ reduction ($V_{m,6}$), which would cause NADH accumulation during the reaction and make the NAD^+ the limiting reactant of the reaction. Because of that and the NADH inhibitory effects on AlDH, the coenzyme regeneration is necessary for carrying out an economically feasible CDH oxidation catalyzed by AlDH.

List of reactant and product abbreviations: acetaldehyde (**AA**), chloroacetaldehyde (**CAA**), 4-chloro-3-hydroxybutanal (**CHB**), 6-chloro-3,5-dihydroxyhexanal (**CDH**), 6-chloro-3,5-dihydroxyhexanoic acid (**CDHA**), 3-hydroxy-4(-oxiran-2-yl)butanoic acid (**HOBA**), 6-cyano-3,5-dihydroxyhexanoic acid (**CYDHA**), 3-hydroxybutanal (**HB**), 3,5-dihydroxyhexanal (**DHH**).

3.6.4.3 NOX[009] kinetics in the NADH oxidation

The NOX[009] kinetic investigations were carried out by examining the impact of different concentrations of NADH, NAD^+ and CDH on the initial reaction rate of NADH oxidation (Figure 24b). The results obtained based on the initial reaction rate are shown in Figure 39, while the kinetic parameters of the single-substrate Michaelis-Menten kinetics (Equation 43) were estimated (Table 11) based on the gathered experimental data.

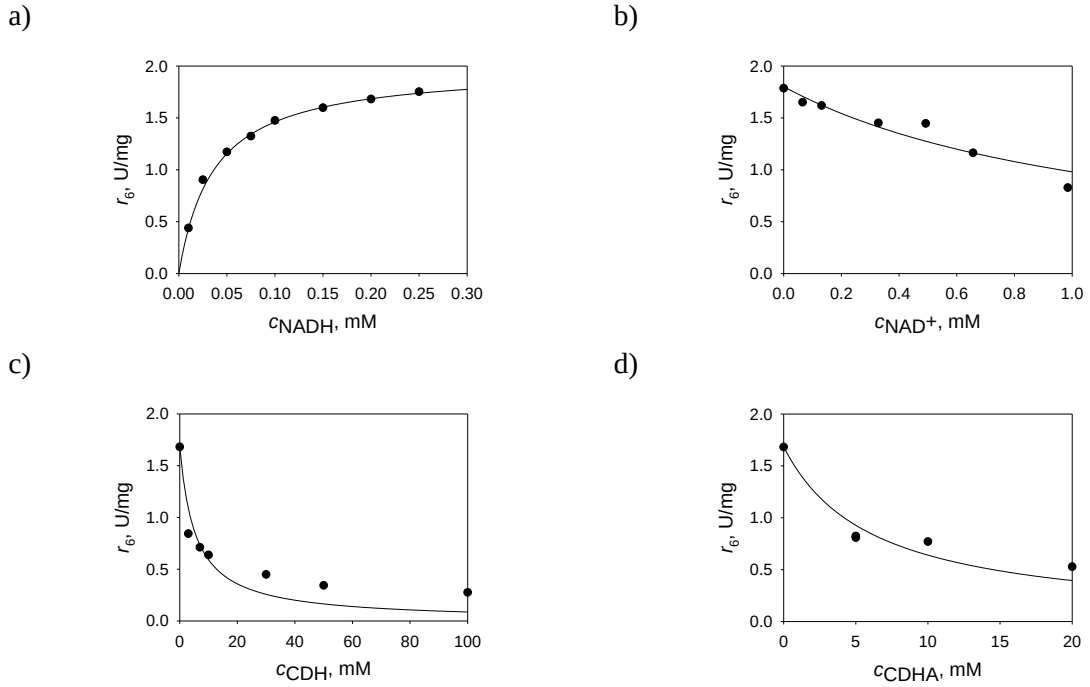

Figure 39 Kinetics of the NOX[009]-catalyzed oxidation of NADH into NAD^+ (0.1 M phosphate buffer pH 8, γ_{NOX009} = 0.01 mg/mL, 25 °C). The dependence of the initial reaction rate on a) substrate NADH, b) product NAD^+ (c_{NADH} = 0.2 mM), and c) co-substrate CDH (c_{NADH} = 0.2 mM). Legend: experiment (dots), model (line).

The results (Table 11, Figure 39) regarding the dependence of the initial reaction rate on the NAD^+ concentration indicated substrate NAD^+ inhibition. The impact of substrate and product of the main reaction (Figure 39c and d) on the NADH oxidation was investigated as well and the results suggested reaction inhibition by both compounds, since with the increase of CDH and CDHA concentration the initial reaction rate decreased.

From the values of estimated kinetic parameters (Table 11), it could be concluded that NOX[009] should successfully serve as an NAD^+ regenerating enzyme. The maximum reaction rate ($V_{m,7}$) was 2.6-fold higher than the maximum reaction rate of the AlDH-catalyzed main

List of reactant and product abbreviations: acetaldehyde (**AA**), chloroacetaldehyde (**CAA**), 4-chloro-3-hydroxybutanal (**CHB**), 6-chloro-3,5-dihydroxyhexanal (**CDH**), 6-chloro-3,5-dihydroxyhexanoic acid (**CDHA**), 3-hydroxy-4(-oxiran-2-yl)butanoic acid (**HOBA**), 6-cyano-3,5-dihydroxyhexanoic acid (**CYDHA**), 3-hydroxybutanal (**HB**), 3,5-dihydroxyhexanal (**DHH**).

reaction (Table 9: $V_{m,4}$), making the AlDH-catalyzed CDH oxidation the rate limiting reaction of the AlDH/NOX^{009} reaction system. Although the value of the inhibition constant for NAD^+ ($K_{i,7}^{NAD+}$) was about 5-fold higher than the Michaelis constant for NADH ($K_{m,7}^{NADH}$), NAD^+ should not affect significantly the NOX^{009} activity during the NADH oxidation since NAD^+ would be consumed in the main reaction (AlDH-catalyzed CDH oxidation). Since the values of the inhibition constants for CDH ($K_{i,7}^{CDH}$) and CDHA ($K_{i,7}^{CDHA}$) were 150- and 170-fold higher, respectively, than the Michaelis constant for NADH ($K_{m,7}$), CDH and CDHA should not have a substantial impact on the NOX^{009}-catalyzed reaction and therefore should enable a successful regeneration of NAD^+.

Table 11 Estimated kinetic parameters of the NOX^{009}-catalyzed NADH oxidation.

Parameter	Unit	Value
$V_{m,7}$	U/mg	1.989 ± 0.024
$K_{m,7}^{NADH}$	mM	0.036 ± 0.002
$K_{i,7}^{NAD+}$	mM	0.183 ± 0.036
$K_{i,7}^{CDH}$	mM	5.409 ± 0.618
$K_{i,7}^{CDHA}$	mM	6.124 ± 0.970

3.6.4.4 KRED^{332} kinetics in the CDH oxidation

The kinetic measurements for KRED^{332} were conducted by examining the effects of the initial concentration of substrates CDH and $NADP^+$ on the initial rate of the reaction of CDH oxidation (Figure 25). Using the obtained experimental data (Figure 40), the kinetic parameters of the double-substrate Michaelis-Menten kinetics (Equation 52) were estimated (Table 12).

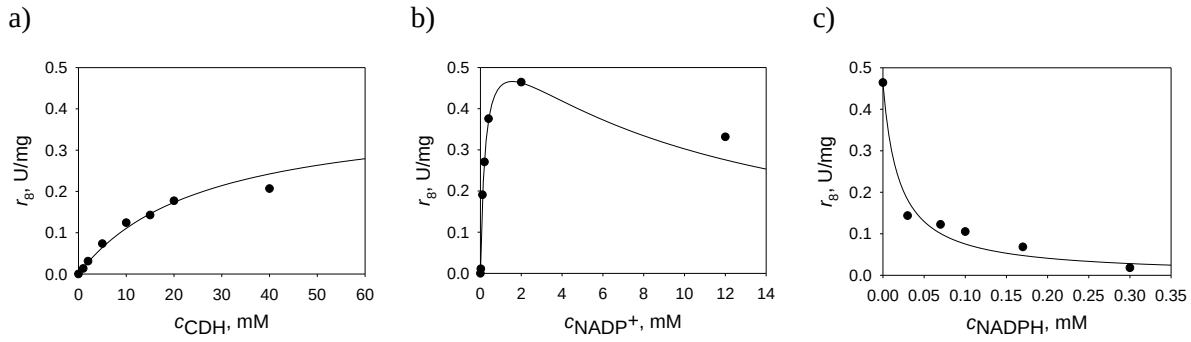

Figure 40 Kinetics of the KRED^{332}-catalyzed oxidation of CDH into CDHA (0.1 M phosphate buffer pH 8, $\gamma_{KRED332}$ = 1.0 mg/mL, 25 °C). The dependence of the initial reaction rate on substrates a) CDH (c_{NADP} = 10 mM) and b) $NADP^+$ (c_{CDH} = 80 mM) and c) product NADH (c_{CDH} = 80 mM, c_{NADP} = 10 mM). Legend: experiment (dots), model (line).

List of reactant and product abbreviations: acetaldehyde (**AA**), chloroacetaldehyde (**CAA**), 4-chloro-3-hydroxybutanal (**CHB**), 6-chloro-3,5-dihydroxyhexanal (**CDH**), 6-chloro-3,5-dihydroxyhexanoic acid (**CDHA**), 3-hydroxy-4(-oxiran-2-yl)butanoic acid (**HOBA**), 6-cyano-3,5-dihydroxyhexanoic acid (**CYDHA**), 3-hydroxybutanal (**HB**), 3,5-dihydroxyhexanal (**DHH**).

Table 12 Estimated kinetic parameters of the KRED^{332}-catalyzed CDH oxidation.

Parameter	Unit	Value
$V_{m,8}$	U/mg	0.812 ± 0.093
$K_{m,8}^{CDH}$	mM	26.35 ± 2.36
$K_{m,8}^{NADP+}$	mM	0.241 ±0.036
$K_{i,8}^{NADP+}$	mM	10.05 ± 1.460
$K_{i,8}^{NADPH}$	mM	$(1.78 \pm 0.293) \cdot 10^{-3}$

Based on the results of the dependence of the initial reaction rate on the NADP$^+$ concentration, it was evident that the reaction rate decreased with further increase of substrate NADP$^+$ concentration (> 1.8 mM), meaning the KRED^{332} enzyme was substrate-inhibited by NADP$^+$. The experimental results regarding the impact of the NADPH product on the initial reaction rate suggested severe inhibition by NADPH (Table 12, Figure 40).

From the estimated kinetic parameters for AlDH (Table 9) and KRED^{332} (Table 12), it could be noted that both enzymes show a similar maximum reaction rate (V_m) of around 0.8 U/mg, but the AlDH enzyme showed about 11-fold higher CDH affinity and 3-fold higher NAD(P)$^+$ affinity than KRED^{332}, which means less CDH and NAD$^+$ substrate was needed to reach ½·V_m. The AlDH-catalyzed reaction would result in faster substrate consumption and thus an overall faster CDH oxidation.

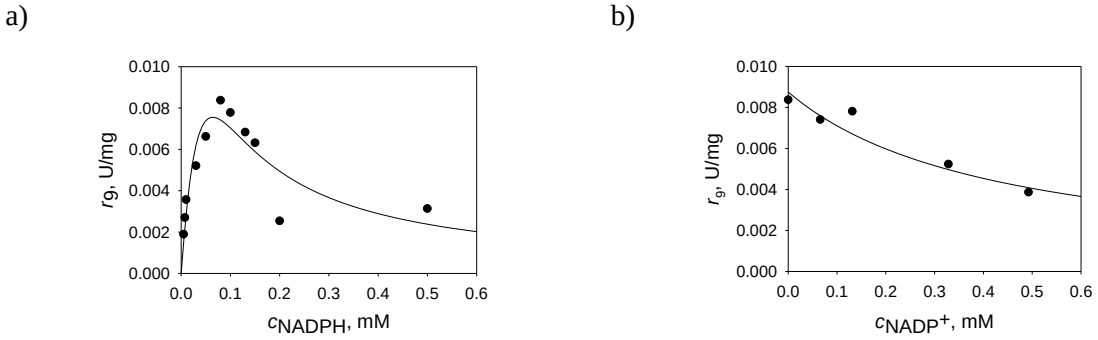

Figure 41 Kinetics of the NOX(KRED^{332})-catalyzed oxidation of NADPH into NADP$^+$ (0.1 M phosphate buffer pH 8, $\gamma_{KRED332}$ = 1.0 mg/mL, 25 °C). The dependence of the initial reaction rate on a) substrate NADPH and b) product NADP$^+$ (c_{NADPH} = 0.08 mM). Legend: experiment (dots), model (line).

During the research it was found that the KRED^{332} enzyme, used as lyophilized CFE, contained NADPH-acting oxidases that participated in the NADP$^+$ coenzyme regeneration. Therefore, the impact of NADPH and NADP$^+$ on the initial reaction rate of the reaction of NADPH oxidation catalyzed by KRED^{332} was examined as well (Figure 41). From the collected data it was evident that the NOX(KRED^{332})-catalyzed reaction of NADPH oxidation was

List of reactant and product abbreviations: acetaldehyde (**AA**), chloroacetaldehyde (**CAA**), 4-chloro-3-hydroxybutanal (**CHB**), 6-chloro-3,5-dihydroxyhexanal (**CDH**), 6-chloro-3,5-dihydroxyhexanoic acid (**CDHA**), 3-hydroxy-4(-oxiran-2-yl)butanoic acid (**HOBA**), 6-cyano-3,5-dihydroxyhexanoic acid (**CYDHA**), 3-hydroxybutanal (**HB**), 3,5-dihydroxyhexanal (**DHH**).

inhibited by both the substrate NADPH and the product $NADP^+$. Using this data, combined with the developed single-substrate Michaelis-Menten kinetics (Equation 53), the kinetic parameters for the NOX($KRED^{332}$) enzyme were estimated and are presented in Table 13.

Table 13 Estimated kinetic parameters of the NOX($KRED^{332}$)-catalyzed NADPH oxidation.

Parameter	Unit	Value
$V_{m,9}$	U/mg	0.028 ± 0.031
$K_{m,9}^{NADPH}$	mM	0.087 ± 0.124
$K_{i,9}^{NADPH}$	mM	0.047 ± 0.068
$K_{i,9}^{NADP+}$	mM	0.124 ± 0.042

By observing the results for $KRED^{332}$ (Table 12) and NOX($KRED^{332}$) (Table 13) it could be concluded that the inhibitory effects of NADPH on $KRED^{332}$ would be circumvented by some degree due to the NADPH being consumed in the NOX($KRED^{332}$)-catalyzed reaction.

From the estimated kinetic parameters for NOX(AlDH) (Table 10) and for NOX($KRED^{332}$) (Table 13), it could be observed that NOXs that were present in AlDH and $KRED^{332}$ CFEs had similar activities, i.e. the maximum reaction rate (V_m) of about 0.02 U/mg. From the Michaelis constants it was evident that NOX($KRED^{332}$) had a lower specificity towards NADPH than NOX(AlDH) towards NADH, the $K_m^{NAD(P)H}$ value of NOX($KRED^{332}$) being 5-fold higher than of NOX(AlDH). In both cases, the enzymes manifested product $NAD(P)^+$ inhibition, whereby the inhibition constant of NOX($KRED^{332}$) was 3-fold higher than of NOX(AlDH). The enzyme NOX($KRED^{332}$) also showed substrate NADPH inhibition. By comparing those results in the results obtained for NOX^{009} (Table 11), it could be noted that the NOX^{009} enzyme showed 100-times higher activity (V_m) than NOXs present in AlDH and $KRED^{332}$ CFEs. The affinity of NOX^{009} towards NAD(P)H ($K_m^{NAD(P)H}$) was 2-fold lower than of NOX(AlDH) and 2.5-fold higher than of NOX($KRED^{332}$), while the estimated value of the inhibition constant for $NAD(P)^+$ was similar to the one estimated for NOX($KRED^{332}$), but 2-times lower than for NOX(AlDH). Therefore, based on those findings, it could be concluded that the $KRED^{332}$-catalyzed reaction would be somewhat slower than the AlDH-catalyzed reaction, due to the rate limiting step being the NOX($KRED^{332}$)-catalyzed coenzyme regeneration. In the AlDH-catalyzed CDH oxidation, the NOX^{009} enzyme would be added and hence would result with a faster coenzyme regeneration process. Since it was found that $KRED^{332}$ catalyzes both CDH oxidation and reduction, reducing the CDHA yield, the $KRED^{332}$-catalyzed CDH oxidation was not further explored with a $NADP^+$ regeneration system.

List of reactant and product abbreviations: acetaldehyde (**AA**), chloroacetaldehyde (**CAA**), 4-chloro-3-hydroxybutanal (**CHB**), 6-chloro-3,5-dihydroxyhexanal (**CDH**), 6-chloro-3,5-dihydroxyhexanoic acid (**CDHA**), 3-hydroxy-4(-oxiran-2-yl)butanoic acid (**HOBA**), 6-cyano-3,5-dihydroxyhexanoic acid (**CYDHA**), 3-hydroxybutanal (**HB**), 3,5-dihydroxyhexanal (**DHH**).

3.6.4.5 HHDH^{001} kinetics in the dehalogenation and epoxide ring-opening with KCN

The kinetic measurements for HHDH^{001} were conducted using the initial reaction rate method by examining the effects of the initial concentration of substrates CDH and KCN on the initial reaction rate of the HHDH^{001}-catalyzed reaction of CDHA dehalogenation into HOBA and epoxide ring-opening with cyanide to produce the CYDHA molecule (Figures 26 and 40). The kinetic parameters for the HHDH^{001}-catalyzed dehalogenation reaction (Equation 60, c_{KNC} = 0 mM) and epoxide ring-opening (Equation 60) were estimated and are presented in Table 14.

a) b)

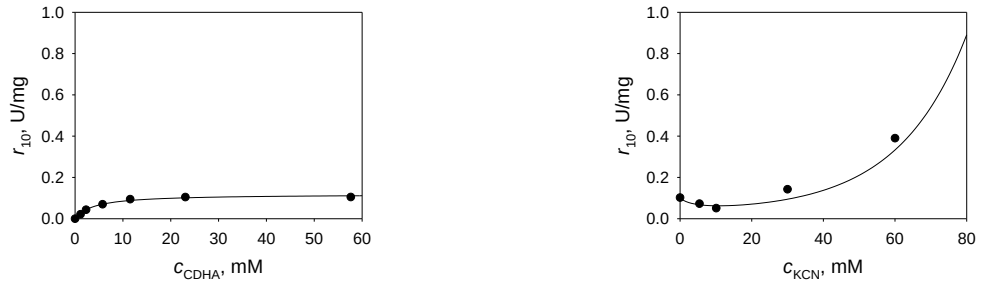

Figure 42 Kinetics of the HHDH^{001}-catalyzed CDHA a) dehalogenation and b) dehalogenation and epoxide ring-opening with cyanide (0.1 M phosphate buffer pH 8, $\gamma_{HHDH001}$ = 1.0 mg/mL, 25 °C). The dependence of the initial reaction rate on substrate a) CDHA (c_{KCN} = 0 mM), and b) KCN (c_{CDHA} = 20 mM). Legend: experiment (dots), model (line).

Table 14 Estimated kinetic parameters of the HHDH^{001}-catalyzed CDHA dehalogenation.

Parameter	Unit	Value
$V_{m,11}$	U/mg	0.119 ± 0.005
$K_{m,11}^{CDHA}$	mM	3.931 ± 0.575
K_A^{KCN}	-	0.065 ± 0.001
K_i^{KCN}	mM	5.118 ± 0.003

From the presented results (Figure 42b), it could be concluded that at lower KCN concentrations (< 18 mM) the cyanide acts as an inhibitor, while at higher concentrations (> 18 mM) it acts as an activator. This suggests that the cyanide shows an inhibitory effect that is outcompeted by its activation effect. Additionally, this could be explained by the fact that the dehalogenation reaction is a reverse reaction. With the addition of KCN, the HOBA epoxide is rapidly consumed in the forward reaction to yield CYDHA during which the reverse reaction does not take place. This was also confirmed by conducting a batch experiment with and without the addition of KCN. Namely, when the reaction was conducted with the addition KCN,

List of reactant and product abbreviations: acetaldehyde (**AA**), chloroacetaldehyde (**CAA**), 4-chloro-3-hydroxybutanal (**CHB**), 6-chloro-3,5-dihydroxyhexanal (**CDH**), 6-chloro-3,5-dihydroxyhexanoic acid (**CDHA**), 3-hydroxy-4(-oxiran-2-yl)butanoic acid (**HOBA**), 6-cyano-3,5-dihydroxyhexanoic acid (**CYDHA**), 3-hydroxybutanal (**HB**), 3,5-dihydroxyhexanal (**DHH**).

the HHDH's substrate CDHA was more rapidly consumed and full conversion was attained, in contrast to the reaction conducted without the KCN addition (Figure 58).

3.6.4.6 Concluding remarks

The kinetics of all enzymes involved in the first reaction route (Figures 1 and 3) were determined.

Based on the DERA kinetic results (Figures 33 – 35; Table 8), the optimal enzyme for the DERA-catalyzed aldol reaction of AA and CAA was $DERA^{024}$ because of its kinetics.

During the AlDH kinetic measurements, it was observed that the enzyme catalyzed NADH oxidation due to present NOXs in the CFE. Taking the collected kinetic data into account (Figures 37 and 38; Tables 9 and 10), it was concluded that the coenzyme regeneration would be necessary for carrying out an economically feasible AlDH-catalyzed CDH oxidation. For that purpose, NOX^{009}, as an auxiliary enzyme, was considered. The kinetic measurements (Figure 39, Table 11) confirmed that NOX^{009} should successfully serve for the regeneration of NAD^+ in the AlDH-catalyzed CDH oxidation.

The kinetic analysis for $KRED^{332}$ (Figure 40, Table 12) confirmed the existence of an internal $NADP^+$ regeneration system, which was due to the usage of unpurified enzymes, i.e. CFEs.

By observing the values of estimated kinetic parameters for AlDH and $KRED^{332}$ it could be concluded that AlDH showed higher affinities towards both substrates (CDH, NAD^+) and lower NAD^+ and NADH inhibition than $KRED^{332}$. Additionally, $KRED^{332}$ was severely inhibited by NADPH. Based on these kinetic results, and that $KRED^{332}$ catalyzes both CDH oxidation and reduction, AlDH shows a better fit for the oxidation of CDH. Because of the CDH reduction catalyzed by $KRED^{332}$, an $NADP^+$ regeneration system was not explored for the $KRED^{332}$-catalyzed CDH oxidation. Based on the NOX^{009} kinetics, it could be concluded that the oxidation of CDH should be faster if the reaction would be catalyzed by the AlDH/NOX^{009} system than by solely AlDH.

If the oxidation would be conducted using the crude (unrefined) CDH, the starting CDH reaction mixture should be free of AA and CAA, especially in case of AlDH, since that enzyme is significantly affected by their presence, even at very low concentrations (Figure 31).

List of reactant and product abbreviations: acetaldehyde (**AA**), chloroacetaldehyde (**CAA**), 4-chloro-3-hydroxybutanal (**CHB**), 6-chloro-3,5-dihydroxyhexanal (**CDH**), 6-chloro-3,5-dihydroxyhexanoic acid (**CDHA**), 3-hydroxy-4(-oxiran-2-yl)butanoic acid (**HOBA**), 6-cyano-3,5-dihydroxyhexanoic acid (**CYDHA**), 3-hydroxybutanal (**HB**), 3,5-dihydroxyhexanal (**DHH**).

The estimated kinetic parameters for $HHDH^{001}$ (Figure 40, Table 14) suggested that KCN acts as both an activator (> 18 mM) and as an inhibitor (< 18 mM) and that the enzyme shows good affinity towards the CDHA substrate.

3.6.5 Validation of developed mathematical models: one-step biocatalysis

The reactions related to the first reaction route (Figure 1) that were conducted as one-step reactions were:

1. $DERA^{Tm}$-catalyzed aldol reaction of AA with CAA,
2. $DERA^{024}$-catalyzed aldol reaction of AA with CAA,
3. AlDH-catalyzed CDH oxidation,
4. AlDH-catalyzed CDH oxidation with NOX^{009}-catalyzed NAD^+ regeneration,
5. $KRED^{332}$-catalyzed CDH oxidation,
6. $HHDH^{001}$-catalyzed CDHA dehalogenation, and
7. $HHDH^{001}$-catalyzed CDHA dehalogenation and epoxide ring-opening with KCN.

All reactions were conducted with either commercially available substrates (AA, CAA) or with substrates enzymatically produced in the lab (CDH, CDHA; procedures described in Chapter 3.3.4).

The developed mathematical models (Chapter 3.4) were validated against obtained experimental data. The models were used to estimate the operational stability rate constants of AlDH (k_d^{AlDH}), NOX^{009} (k_d^{NOX009}), $KRED^{332}$ ($k_d^{KRED332}$) and $HHDH^{001}$ ($k_d^{HHDH001}$) and to estimate the reaction rate constants of AlDH-catalyzed CDHA reduction (k_5), $KRED^{332}$-catalyzed CDH reduction (k_{10}), $HHDH^{001}$-catalyzed epoxide-ring opening with chloride (k_{12}) and $HHDH^{001}$-catalyzed epoxide ring-opening in presence of KCN (r_{13}). To estimate the operational stability rate constants and reaction rate constants, the reactions were conducted in batch reactors.

Because the DH enzymes were dependent upon the $NAD(P)^+$ coenzyme to be catalytically active, $NAD(P)^+$ was added into the reactor prior to the addition of AlDH or $KRED^{332}$.

The enzymatic activity was given as a relative value (maximum activity of 100 %). In case when the reaction was conducted in repetitive batch reactor mode, after each addition of

List of reactant and product abbreviations: acetaldehyde (**AA**), chloroacetaldehyde (**CAA**), 4-chloro-3-hydroxybutanal (**CHB**), 6-chloro-3,5-dihydroxyhexanal (**CDH**), 6-chloro-3,5-dihydroxyhexanoic acid (**CDHA**), 3-hydroxy-4(-oxiran-2-yl)butanoic acid (**HOBA**), 6-cyano-3,5-dihydroxyhexanoic acid (**CYDHA**), 3-hydroxybutanal (**HB**), 3,5-dihydroxyhexanal (**DHH**).

the enzyme into the reactor, its value was regarded as its maximum, defined as 100 %. The substrate conversion (*X*, %) was calculated using the Equation 73, the product yield (*Y*, %) using the Equation 74, the biocatalyst yield (BY, $g_{product}/g_{enzyme}$) using the Equation 75, while the space-time yield (STY, g/(L·day)) using the Equation 76. Regarding DERA-catalyzed reactions, selectivities were calculated at the end of the experiment: using the Equation 77 the CDH-to-CHB ratio was calculated, whereas the CDH-to-CHH ratio was determined using the Equation 78.

$$X = \frac{\left(c_{substrate,t=0} - c_{substrate,t=n}\right)}{c_{substrate,t=0}} \cdot 100\ \% \qquad \text{Equation 73}$$

$$Y = \frac{c_{actual\ product,t=n}}{c_{theoretical\ product,t=0}} \cdot 100\ \% \qquad \text{Equation 74}$$

$$BY = \frac{m_{produced\ product}}{m_{spent\ enzyme}} \qquad \text{Equation 75}$$

$$STY = \frac{\gamma_{product,final}}{t} \qquad \text{Equation 76}$$

$$S_{\frac{CDH}{CHB}} = \frac{c_{CDH}}{c_{CHB}} \qquad \text{Equation 77}$$

$$S_{\frac{CDH}{CHH}} = \frac{c_{CDH}}{c_{CHH}} \qquad \text{Equation 78}$$

3.6.5.1 DERA-catalyzed aldol additions

3.6.5.1.1 Preliminary experiments in batch reactor with different concentrations of DERA^{Tm}

It was reported that lower quantities of DERA would decrease the quantity of product CDH arising from the second aldol reaction [18, 105]. Therefore, to find the optimal DERA concentration for obtaining the highest concentration of CDH, and to minimize the enzyme operational stability decay, several reactions were performed in a batch reactor using the same initial substrate concentrations but different initial DERA^{Tm} concentrations.

The results (Figure 43) show that enzyme concentrations above 5 mg/mL resulted in high product concentration, whilst the enzyme operational stability decay was less prominent. These results implicated that DERA^{Tm} stability was significantly affected by the presence of substrates [12, 14, 18, 67, 104]. Lower DERA^{Tm} concentration caused a lower consumption rate of AA and CAA and, as a consequence, the enzyme was longer exposed to the negative influence of

List of reactant and product abbreviations: acetaldehyde (**AA**), chloroacetaldehyde (**CAA**), 4-chloro-3-hydroxybutanal (**CHB**), 6-chloro-3,5-dihydroxyhexanal (**CDH**), 6-chloro-3,5-dihydroxyhexanoic acid (**CDHA**), 3-hydroxy-4(-oxiran-2-yl)butanoic acid (**HOBA**), 6-cyano-3,5-dihydroxyhexanoic acid (**CYDHA**), 3-hydroxybutanal (**HB**), 3,5-dihydroxyhexanal (**DHH**).

substrates [15, 18]. Based on this preliminary experiment, future DERA^{Tm} and DERA^{024} experiments were conducted taking the presented results (Figure 43) into account.

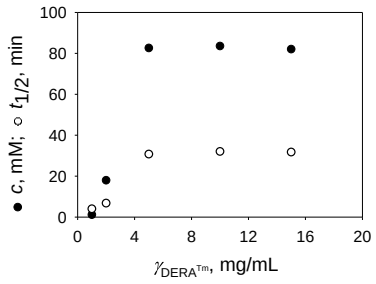

Figure 43 Enzyme half-life and concentration of CDH at different enzyme concentrations in the batch reactor (c_{AA} = 200 mM, c_{CAA} = 100 mM, 0.1 M TEA-HCl buffer pH 7, 25 °C, $\gamma_{DERA^{Tm}}$ = 1; 2; 5; 10; 15 mg/mL). Legend: CDH (black circles), $t_{1/2}$ (white circles).

3.6.5.1.2 DERA-catalyzed aldol additions in batch reactor

The developed model (Equations 21, 23, and 25 – 31) of the DERA^{Tm}-catalyzed aldol reaction was validated in the batch reactor. The obtained experimental and simulation data are shown in Figure 44.

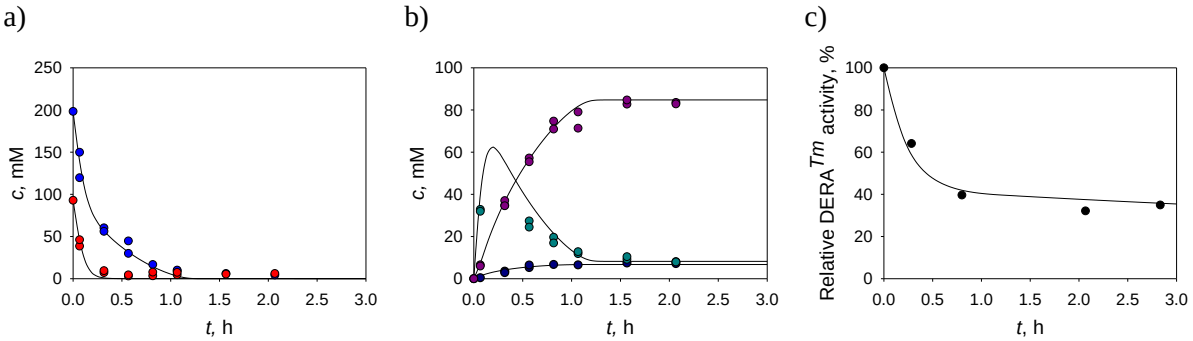

Figure 44 Experimental and simulation data of the double aldol addition of AA to CAA in a batch reactor catalyzed by DERA^{Tm} (0.1 M TEA-HCl buffer pH 7, c_{AA} = 198 mM, c_{CAA} = 93 mM, $\gamma_{DERA^{Tm}}$ = 10 mg/mL). Change of a) substrate concentration, b) product concentration, c) relative enzyme activity during the experiment. Legend: experiment (dots), model (line); AA (blue), CAA (red), CHB (teal), CDH (purple), CHH (dark blue).

Complete conversion of AA and CAA was achieved after 0.5 h and 1.2 h, respectively (Figure 44). The intermediate CHB was not completely transformed into CDH due to a lack of AA, which was also consumed in the side reaction. The yield of the desired product CDH with respect to substrate CAA was 83 % (γ_{CDH} = 14.2 mg/mL). The reaction solution composition for each product at the end of the experiment (1.2 h) are presented in Table 15. The obtained

List of reactant and product abbreviations: acetaldehyde (**AA**), chloroacetaldehyde (**CAA**), 4-chloro-3-hydroxybutanal (**CHB**), 6-chloro-3,5-dihydroxyhexanal (**CDH**), 6-chloro-3,5-dihydroxyhexanoic acid (**CDHA**), 3-hydroxy-4(-oxiran-2-yl)butanoic acid (**HOBA**), 6-cyano-3,5-dihydroxyhexanoic acid (**CYDHA**), 3-hydroxybutanal (**HB**), 3,5-dihydroxyhexanal (**DHH**).

$S_{CDH/CHB}$ and $S_{CDH/CHH}$ were 12.5 and 14.0, respectively. These values suggest the quantity (mol) of CDH that was formed in ratio to the undesired product (CDH or CHH, in mol). Based on them, it can be concluded that the formation of side products cannot be circumvented and that for every 13th and 14th mol of CDH 1 mol of CHB and CHH are formed, respectively. The calculated BY and STY were 2.4 $g_{CDH}/g_{DERA\,Tm}$ and 283.2 g/(L·day), respectively. Based on the statistic goodness-of-fit (R^2 = 0.98, σ = 5.31) and data shown in Figure 44, it could be concluded that the model described the experimental data well.

The model validation of the DERA^{024}-catalyzed aldol reaction in the batch reactor (Equations 22 and 24 – Equation 31) is shown in Figure 45. After one hour from the start of the reaction, complete AA (>> 99.9 %) and 97.2 % of CAA conversion was achieved, due to a lack of AA (AA and CAA were introduced in a ratio of 1.9:1), also spent in the side reaction. The yield on the desired product CDH with respect to substrate CAA was 80 % (γ_{CDH} = 12.9 g/L), while $S_{CDH/CHB}$ and $S_{CDH/CHH}$ were 4.8 and 26.2, respectively. The mass percent product composition for each product at the end of the experiment (1.0 h) are presented in Table 15. The BY of 9.7 $g_{CDH}/g_{DERA024}$ and STY of 309.6 g/(L·day) were calculated. Based on the statistic goodness-of-fit (R^2 = 0.98, σ = 5.67) and data presented in Figure 45, it can be concluded that the model described the experimental data well.

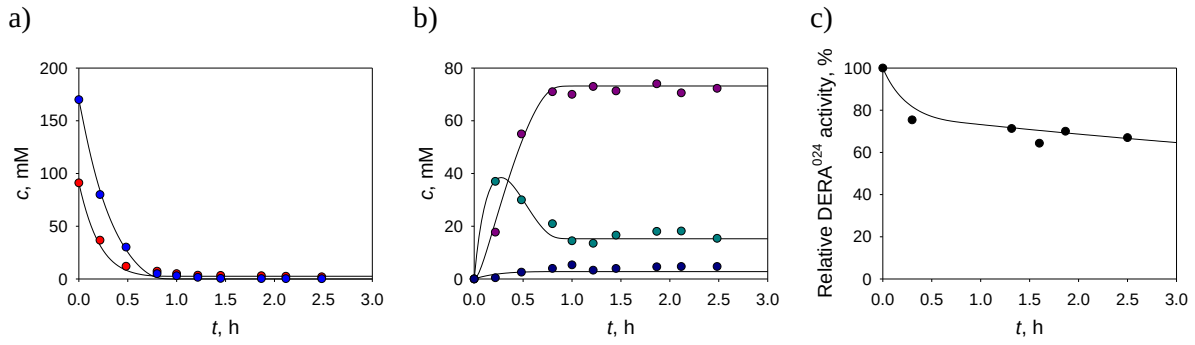

Figure 45 Experimental and simulation data of the double aldol addition of AA to CAA in a batch reactor catalyzed by DERA^{024} (0.1 M phosphate buffer pH 6, c_{AA} = 170 mM, c_{CAA} = 91 mM, $\gamma_{DERA024}$ = 5 mg/mL). Changes of a) substrate concentration, b) product concentration, c) enzyme activity during the experiment. Legend: experiment (dots), model (line); AA (blue), CAA (red), CHB (teal), CDH (purple), CHH (dark blue).

The reaction time until full AA conversion was achieved in the DERA^{Tm}-catalyzed reaction was 1.2 h, whereas the respective reaction time of the DERA^{024}-catalyzed reaction was 1.0 h, which suggested fast aldol reactions. DERA^{024} showed higher operational stability in

List of reactant and product abbreviations: acetaldehyde (**AA**), chloroacetaldehyde (**CAA**), 4-chloro-3-hydroxybutanal (**CHB**), 6-chloro-3,5-dihydroxyhexanal (**CDH**), 6-chloro-3,5-dihydroxyhexanoic acid (**CDHA**), 3-hydroxy-4(-oxiran-2-yl)butanoic acid (**HOBA**), 6-cyano-3,5-dihydroxyhexanoic acid (**CYDHA**), 3-hydroxybutanal (**HB**), 3,5-dihydroxyhexanal (**DHH**).

comparison to DERA^{Tm}. The reaction mixture composition was improved in case when the reaction was catalyzed by DERA^{Tm}, resulting in side product percentage below 10 % (DERA^{Tm} 9.5 % *vs* DERA^{024} 15.1 %), which was due to a lack of AA in the experiment catalyzed by DERA^{024} that caused CHB accumulation. By comparing the BY and STY, higher BYs and STYs were obtained in the experiment catalyzed by DERA^{024} than in the experiment catalyzed by DERA^{Tm}: 4-fold higher BY and 1.1-fold higher STY (Table 18).

Table 15 The final mass percent product composition and the final mass product concentration: results obtained after 24 h of the aldol reaction of AA with CAA catalyzed by DERA^{Tm} and DERA^{024} in repetitive batch reactor mode.

Enzyme	*w/w*, %			*γ*, g/L		
	CHB	**CDH**	**CHH**	**CHB**	**CDH**	**CHH**
DERA^{Tm}	3.8	90.5	5.7	0.6	14.2	0.9
DERA^{024}	12.5	84.9	2.6	1.9	12.9	0.4

Based on the results for both DERA^{Tm} and DERA^{024}, it could be concluded that the developed mathematical models could be used for reaction simulations and thus predictions of the DERA^{Tm}- and DERA^{024}-catalyzed aldol reaction of AA and CAA.

3.6.5.1.3 DERA-catalyzed aldol additions in repetitive batch reactor

Because DERA is deactivated by substrates AA and CAA, as well as by the intermediate CHB, it is very hard to obtain a high final concentration of CDH in a single batch reactor. Therefore, the aldol reaction was further performed in a repetitive batch [189] and fed-batch reactor configurations. Supplying the substrates into the reactor allows their concentration to be maintained at a lower level, by which the enzyme operational stability decay can be lowered, or even minimized. The enzyme should also be freshly added into the reactor to maintain its activity and to prevent operational stability decay. The repetitive technique has been shown to be very effective and easy to handle [170, 175]. Additionally, this type of reactor is a promising alternative to a batch reactor for producing higher concentrations of CDH [175] by having not only additions of substrates, but also fresh enzyme. Therefore, the DERA^{Tm}- and DERA^{024}-catalyzed reactions were carried out in a repetitive batch reactor configuration with three additions of fresh substrates and enzyme, without the removal of the synthesized product (Figures 46 and 47), because CDH does not have a negative impact on the enzyme. Based on the currently available literature, until recently [175], this type of reactor was not used for the

List of reactant and product abbreviations: acetaldehyde (**AA**), chloroacetaldehyde (**CAA**), 4-chloro-3-hydroxybutanal (**CHB**), 6-chloro-3,5-dihydroxyhexanal (**CDH**), 6-chloro-3,5-dihydroxyhexanoic acid (**CDHA**), 3-hydroxy-4(-oxiran-2-yl)butanoic acid (**HOBA**), 6-cyano-3,5-dihydroxyhexanoic acid (**CYDHA**), 3-hydroxybutanal (**HB**), 3,5-dihydroxyhexanal (**DHH**).

DERA-catalyzed aldol reaction. The usual reactor employed for the aldol reaction of AA with CAA catalyzed by DERA, either as an isolated enzyme or as a whole-cell catalyst, were the batch reactor [12, 14, 87, 96, 101, 105, 131] and, rarely, the fed-batch reactor [12, 15, 88].

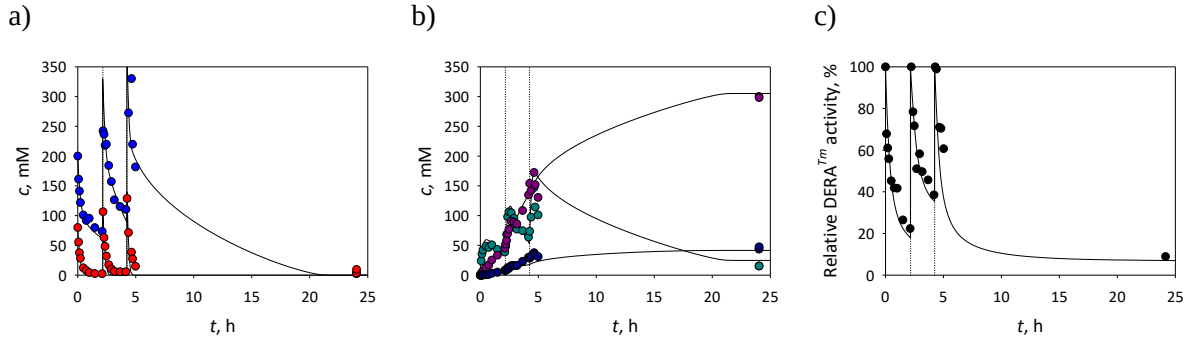

Figure 46 Experimental and simulation data of the double aldol addition of AA to CAA in the repetitive batch reactor catalyzed by DERA^{Tm} (0.1 M TEA-HCl buffer pH 7, c_{AA} = 200 mM, c_{CAA} = 100 mM, γ_{DERATm} = 5 mg/mL per addition). Changes of a) substrate concentration, b) product concentration, and c) relative enzyme activity during the experiment. Legend: experiment (dots), model (line); AA (blue), CAA (red), CHB (teal), CDH (purple), CHH (dark blue).

The concentration of AA was added in surplus considering its consumption in the side reaction [14]. At 2 and 4 h from the start of the reaction, the second and the third fresh feed of substrates and enzyme (of same concentrations as the initial) were added into the reactor (Figurea 46 and 47). It was observed that the concentration of AA was higher in second and third substrate addition, because AA was not fully consumed prior to its addition into the reactor. Also, the concentration of the intermediate CHB increased with the second and third addition of substrates. With both DERA^{Tm} (t = 21.8 h) and DERA^{024} (t = 9.5 h) full conversion of AA and CAA was obtained, and in both cases around 50 g/L of product CDH was obtained (Table 16). Based on the obtained experimental data (Table 16), DERA^{024} gave better results regarding the composition of the reaction solution, containing mainly the final product and fewer side products, and resulted in 2.3-fold higher STY of 56.0 *vs* 126.6 g/(L·day), while a similar BY of 3.7 g_{CDH}/g_{DERATm} for DERA^{Tm} and 4.3 $g_{CDH}/g_{DERA024}$ for DERA^{024} was obtained. The high STY in the reaction conducted with DERA^{024} could be attributed to better DERA^{024} stability and its higher relative activity (Figure 46c *vs* Figure 47c). The yield of the product CDH with respect to substrate CAA was similar: 96 % for DERA^{Tm} and 97 % for DERA^{024}. The selectivity CDH/CHB were 20.1 for DERA^{Tm} or 27.7 for DERA^{024}, while CDH/CHH were 7.2 for DERA^{Tm} or 7.3 for DERA^{024}, which showed that the DERA^{024} had slightly higher selectivity towards CDH than DERA^{Tm}. Complete composition of both aldol reactions

List of reactant and product abbreviations: acetaldehyde (**AA**), chloroacetaldehyde (**CAA**), 4-chloro-3-hydroxybutanal (**CHB**), 6-chloro-3,5-dihydroxyhexanal (**CDH**), 6-chloro-3,5-dihydroxyhexanoic acid (**CDHA**), 3-hydroxy-4(-oxiran-2-yl)butanoic acid (**HOBA**), 6-cyano-3,5-dihydroxyhexanoic acid (**CYDHA**), 3-hydroxybutanal (**HB**), 3,5-dihydroxyhexanal (**DHH**).

(DERA^{Tm}- and DERA^{024}-catalyzed) as well as the calculated mass concentrations of products obtained at the end of the experiment are given in Table 16.

The DERA^{Tm} and DERA^{024} operational stability decay occurred in all three batches and the deactivation rate in this type of reactor was slightly higher than in the batch experiments (Figures 44 and 45).

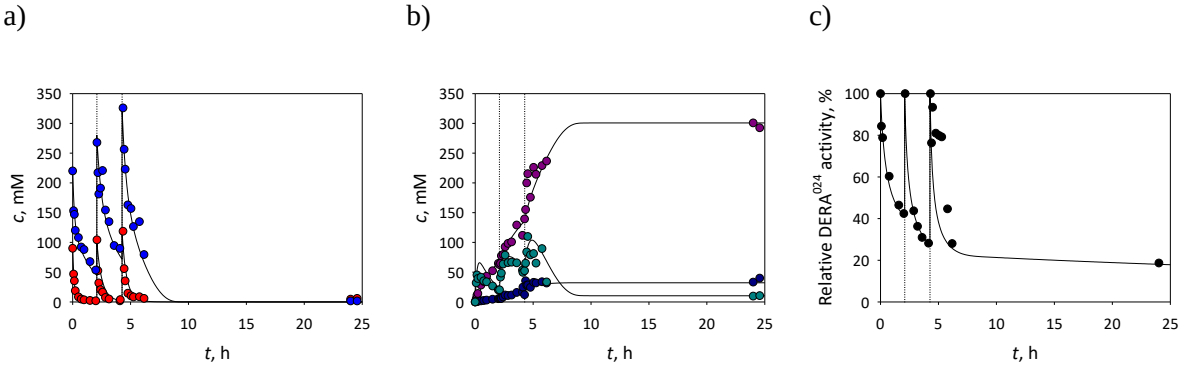

Figure 47 Experimental and simulation data of the double aldol addition of AA to CAA in the repetitive batch reactor catalyzed by DERA^{024} (0.1 M phosphate buffer pH 6, c_{AA} = 220 mM, c_{CAA} = 90 mM, $\gamma_{DERA024}$ = 5 mg/mL per addition). Changes of a) substrate concentration, b) product concentration, and c) relative enzyme activity during the experiment. Legend: experiment (dots), model (line); AA (blue), CAA (red), CHB (teal), CDH (purple), CHH (dark blue).

Table 16 Final mass percent product composition and final mass product concentration: results obtained after 24 h of the aldol reaction of AA with CAA catalyzed by DERA^{Tm} and DERA^{024} in repetitive batch reactor mode.

Enzyme	*w/w*, %			*γ*, g/L		
	CHB	**CDH**	**CHH**	**CHB**	**CDH**	**CHH**
DERA^{Tm}	2.3	87.0	9.7	1.3	50.9	5.7
DERA^{024}	2.1	90.0	7.7	1.2	50.1	4.2

3.6.5.1.4 Optimization of the DERA^{Tm}-catalyzed aldol addition

After carrying out DERA^{Tm}-catalyzed aldol additions in batch (Chapter 3.6.5.1.2) and repetitive batch reactor (Chapter 3.6.5.1.3), the reaction was conducted in a fed-batch reactor to validate the developed mathematical model for the DERA^{Tm}-catalyzed aldol addition in fed-batch reactor (Equation 21, 23, 25, and 32 – 39).

The aldol addition of AA onto CAA catalyzed by DERA^{Tm} in the fed-batch reactor was conducted in 0.1 M TEA-HCl buffer pH 7 at 25 °C. The starting volume of the reaction solution

List of reactant and product abbreviations: acetaldehyde (**AA**), chloroacetaldehyde (**CAA**), 4-chloro-3-hydroxybutanal (**CHB**), 6-chloro-3,5-dihydroxyhexanal (**CDH**), 6-chloro-3,5-dihydroxyhexanoic acid (**CDHA**), 3-hydroxy-4(-oxiran-2-yl)butanoic acid (**HOBA**), 6-cyano-3,5-dihydroxyhexanoic acid (**CYDHA**), 3-hydroxybutanal (**HB**), 3,5-dihydroxyhexanal (**DHH**).

was 6 mL. The reaction was carried out with a constant substrate (q_1) and enzyme supply (q_2) (Figure 48). At the end of the experiment (25 h), the final concentration of CDH was 70 g/L. The final product composition (% *w*/*w*) of the reaction mixture was 6.42% of CHB, 77.12% of CDH and 16.46% of DHH. The statistical output (R^2 = 24.27, σ = 0.93) was weaker than in the previous two types of investigated reactors. This could be attributed to the relatively the high concentration of aldehydes present in the reaction mixture for which the samples had to be diluted before analysis. Additionally, due to high concentration of added crude enzyme (total enzyme addition of 20 mg/mL), the solution became viscous, possibly causing a sampling error. Despite the difficulties, from the data shown in Figure 48, it can be concluded that the model described the experimental data acceptably.

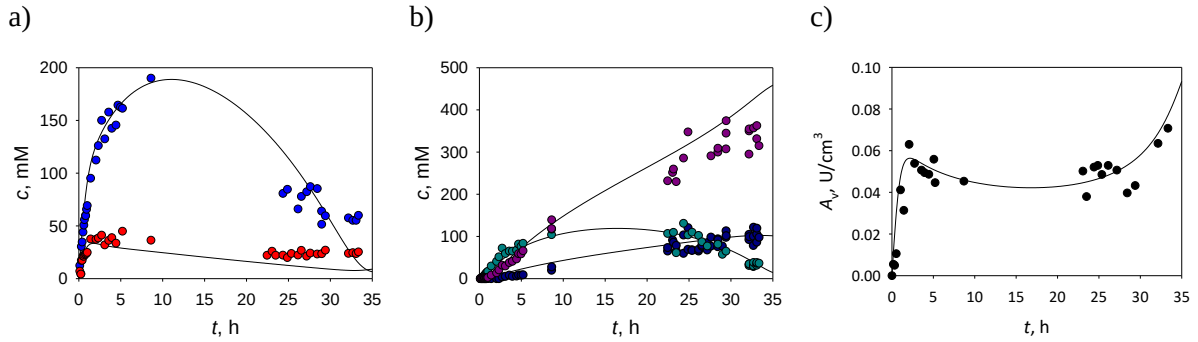

Figure 48 Experimental and simulation data of the double aldol addition of AA to CAA in the fed-batch reactor catalyzed by DERA^{Tm} (0.1 M TEA-HCl buffer pH 7, V_0 = 6 mL; feed 1: q_1 = 5 µL/min, $c_{AA,0}$ = 2450 mM, $c_{CAA,0}$ = 950 mM; feed 2: q_2 = 2 µL/min, $\gamma_{DERATm,0}$ = 100 mg/mL; 33.33 h). Change of a) substrate AA and CAA concentration, b) product CHB, CDH and CHH concentration, and c) enzyme volume activity during the experiment. Legend: experiment (dots), model (line); AA (blue), CAA (red), CHB (teal), CDH (purple), CHH (dark blue).

Based on the carried-out experiments, it could be concluded that the main drawback of DERA^{Tm}-catalyzed aldol reaction is the enzyme operational stability decay caused by aldehydes present in the reaction mixture. Therefore, the choice of effective process design is of crucial importance to minimize the enzyme decay, which should lead to significant process improvement. To accomplish this, it is necessary to find the most effective reactor mode.

Since the statistic output of the proposed model (Chapter 3.4.1), together with the estimated kinetic parameters (Chapter 3.6.4.1: Table 8), was satisfactory for all types of investigated reactors (reactor experiments described in Chapter 3.3.9.1), the validated model was used for reaction optimization in different reactor modes. The model simulations were performed by changing the initial conditions in the batch and fed-batch reactor.

List of reactant and product abbreviations: acetaldehyde (**AA**), chloroacetaldehyde (**CAA**), 4-chloro-3-hydroxybutanal (**CHB**), 6-chloro-3,5-dihydroxyhexanal (**CDH**), 6-chloro-3,5-dihydroxyhexanoic acid (**CDHA**), 3-hydroxy-4(-oxiran-2-yl)butanoic acid (**HOBA**), 6-cyano-3,5-dihydroxyhexanoic acid (**CYDHA**), 3-hydroxybutanal (**HB**), 3,5-dihydroxyhexanal (**DHH**).

The concentration of CDH, Y_{CDH}, STY and BY were taken as the measures of process relevant outputs [190]. Since the bottleneck of this process is the enzyme stability [12, 104], to optimize this process would be finding the minimal enzyme concentration at which the optimal product yield and productivity would be obtained. Therefore, the simulations were performed by varying the enzyme concentration and its supply into the reactor. To minimize enzyme operational stability decay in the batch reactor caused by aldehyde substrates, fresh substrate additions were considered as well. Thus, three different batch reactor modes were investigated:

1. BR1 – batch reactor in which the total amount of substrates and enzyme were added at the beginning of the process,
2. BR2 – repetitive batch reactor in which the total amount of enzyme was added at the beginning of the process combined with three sequential substrate additions, and
3. BR3 – repetitive batch reactor with three sequential additions of substrates and enzyme.

In the last two modes (BR2 and BR3), extra substrates and enzyme additions were simulated when the yield CDH was 80%. The simulations were stopped either when the final CDH yield was 99% or after 24 hours. The results of those simulations are shown in Figure 49.

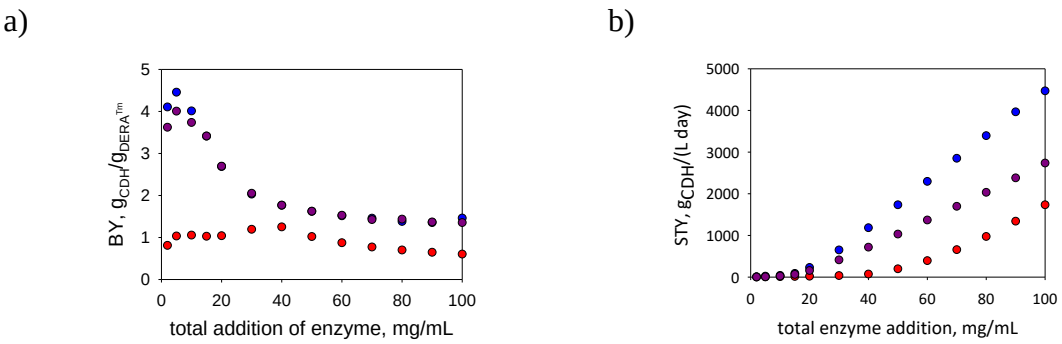

Figure 49 Model simulations of the double aldol addition of AA to CAA catalyzed by DERA^{Tm} in different batch reactor modes (BR1: c_{AA} = 740 mM, c_{CAA} = 300 mM; BR2 and BR3: c_{AA} = 230 x 3 mM, c_{CAA} = 100 x 3 mM). a) Biocatalyst yield and b) productivity change with total enzyme addition. Legend: BR1 (red), BR2 (blue), BR3 (purple).

CDH belongs to the category of pharmaceutical compound [14]. According to the industrial requirements for this kind of compounds, the minimum biocatalyst yield must be 10 g/g and the final product concentration must be at least 50 g/L to become economically feasible (Table 1) Also, the total product yield should be at least 80%. Regarding the final CDH concentration and yield, all three reactor modes satisfied these demands, however, the concentration of enzyme is crucial. BR1 required enzyme addition of at least 40 mg/mL, while

List of reactant and product abbreviations: acetaldehyde (**AA**), chloroacetaldehyde (**CAA**), 4-chloro-3-hydroxybutanal (**CHB**), 6-chloro-3,5-dihydroxyhexanal (**CDH**), 6-chloro-3,5-dihydroxyhexanoic acid (**CDHA**), 3-hydroxy-4(-oxiran-2-yl)butanoic acid (**HOBA**), 6-cyano-3,5-dihydroxyhexanoic acid (**CYDHA**), 3-hydroxybutanal (**HB**), 3,5-dihydroxyhexanal (**DHH**).

in BR2 and BR3 the beforementioned requirements were reached at enzyme concentrations of 15 mg/mL. The highest BY was achieved as in BR2, but at an enzyme concentration of 5 mg/mL at which the required concentration of CDH was not achieved. Taking into account the STY, CDH concentration and BY, BR2 ended being the optimal reactor mode at the total enzyme addition of 15 mg/mL. At that DERA^{Tm} concentration, the same BY was achieved in BR3, but with lower STY. Nevertheless, in all tested batch reactor modes, the industrial requirement for the BY was not achieved.

a) b)

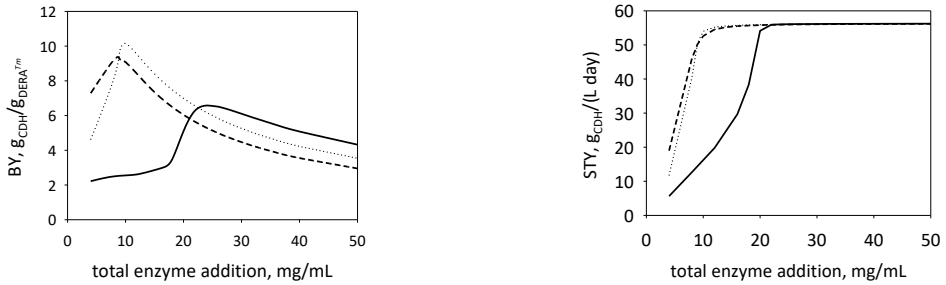

Figure 50 Model simulations of the double aldol addition of AA to CAA catalyzed by DERA^{Tm} in different fed-batch reactor modes (feed 1: q_1 = 5 μL/min; $c_{AA,0}$ = 2300 mM, $c_{CAA,0}$ = 950 mM, FBR1 and FBR2: V_0 = 6 mL; feed 2: q_2 = 2 μL/min; FBR3: V_0 = 10 mL). a) Biocatalyst yield and b) productivity change with total enzyme addition. Legend: FBR1 (solid line), FBR2 (dotted line), FBR3 (dashed line).

For the fed-batch reactor simulation, different conditions of enzyme supply were examined. In all tested fed-batch reactor modes, the substrates were continuously fed into the reactor.

Three different ways of enzyme additions were investigated:

1. FBR1 – fed-batch reactor with enzyme addition only through feed,
2. FBR2 – fed-batch reactor with the addition of half of the amount of the enzyme at the beginning of the reaction and half of the amount through feed, and
3. FBR3 – fed-batch reactor with the addition of the total amount of the enzyme at the beginning of the reactions.

The simulations were stopped at 33.33 h (2000 min) and at that moment the BYs and STYs were calculated (Figure 50).

List of reactant and product abbreviations: acetaldehyde (**AA**), chloroacetaldehyde (**CAA**), 4-chloro-3-hydroxybutanal (**CHB**), 6-chloro-3,5-dihydroxyhexanal (**CDH**), 6-chloro-3,5-dihydroxyhexanoic acid (**CDHA**), 3-hydroxy-4(-oxiran-2-yl)butanoic acid (**HOBA**), 6-cyano-3,5-dihydroxyhexanoic acid (**CYDHA**), 3-hydroxybutanal (**HB**), 3,5-dihydroxyhexanal (**DHH**).

The yield of at least 80% was achieved at total DERA^{Tm} additions of 20, 9 and 8 mg/mL for FBR1, FBR2, and FBR3, respectively. The highest BY was observed at 9 mg/mL of total DERA^{Tm} addition for FBR1 (6.57 $g_{CDH}/g_{DERA Tm}$), 10.2 mg/mL for FBR2 (10.16 $g_{CDH}/g_{DERA Tm}$) and 9 mg/mL for FBR3 (9.25 $g_{CDH}/g_{DERA Tm}$). At these points, the final concentration of CDH was above 70 g/L. The FBR2 (total enzyme addition of 10.2 mg/mL) was chosen as the optimal reactor mode for the aldol reaction based on the highest BY since all other indicators (Y_{CDH}, c_{CDH}, and STY) were similar under all studied conditions (FBR1, FBR2, FBR3).

Based on the conducted simulations, it was concluded that the requirements for CDH concentration and yield were achieved in both types of studied reactors (BRs and FBRs). The desire BY was not achieved in the batch modes. Therefore, this type of reactor proved not to be a good choice. The FBR2 simulation was experimentally validated since this type of studied reactor satisfied all considered requirements. The collected data and results are shown in Figure 53 and Table 17 (Chapter 3.6.5.1.6).

3.6.5.1.5 Optimization of the DERA^{024}-catalyzed aldol addition

To find the optimal reaction conditions for carrying out the DERA^{024}-catalyzed aldol reaction in the fed-batch reactor (Equations 22, 24, 32 – 39), model simulations were carried out. They were done based on the information obtained from the experimental data collected from the DERA^{024}-catalyzed aldol additions in the batch (Chapter 3.6.5.1.2) and repetitive batch reactor (Chapter 3.6.5.1.3) combined with the information based on the results obtained from the DERA^{Tm}-catalyzed aldol addition in the fed-batch reactor (prior optimization: Figure 48, after optimization: Figure 53).

The model simulations were done by changing the initial conditions in different reactor modes. The final CDH concentration, Y_{CDH}, STY and BY were taken as goal functions. Since it was experimentally confirmed that AA and CAA have a negative effect on the DERA^{024} stability (Figure 30) and its operational stability (Figure 50 and Figure 52), the concentration of DERA^{024} and its supply into reactor were varied. Since AA and CHB have a negative impact on the DERA^{024} stability even at lower concentrations (Figure 30, Table 5), the possibility to supply AA and CAA was considered as well.

List of reactant and product abbreviations: acetaldehyde (**AA**), chloroacetaldehyde (**CAA**), 4-chloro-3-hydroxybutanal (**CHB**), 6-chloro-3,5-dihydroxyhexanal (**CDH**), 6-chloro-3,5-dihydroxyhexanoic acid (**CDHA**), 3-hydroxy-4(-oxiran-2-yl)butanoic acid (**HOBA**), 6-cyano-3,5-dihydroxyhexanoic acid (**CYDHA**), 3-hydroxybutanal (**HB**), 3,5-dihydroxyhexanal (**DHH**).

Three different modes of batch reactor were investigated:

1. BR1 – batch reactor with the addition of total amount of substrates and enzyme at the beginning of the process,
2. BR2 – repetitive batch reactor with the addition of total amount of enzyme at the beginning of the process and three sequential additions of substrates, and
3. BR3 – repetitive batch reactor with three sequential additions of substrates and enzyme.

In the last two modes (BR2 and BR3) extra substrates and enzyme additions were simulated when the CDH yield of 99 % was reached. The simulations were stopped when the final CDH yield was 99% or after 24 hours. The simulation results are shown in Figure 51.

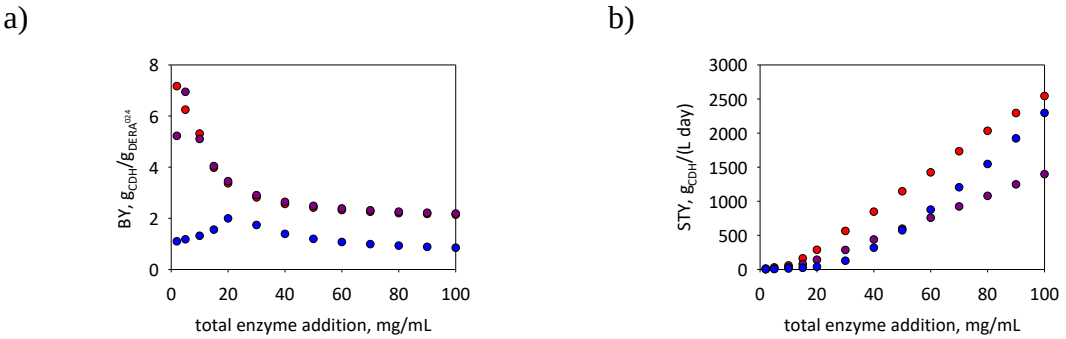

Figure 51 Model simulations of double aldol addition of AA to CAA catalyzed by DERA^{024} in different batch reactor modes (BR1: c_{AA} = 750 mM, c_{CAA} = 300 mM; BR2 and BR3: c_{AA} = 250 x 3 mM, c_{CAA} = 100 x 3 mM). a) Biocatalyst yield and b) productivity change with total enzyme addition. Legend: BR1 (red), BR2 (blue), BR3 (purple).

All three reactor modes (BR1 – BR3, Figure 51) satisfied the industrial requirements (Table 1) for final CDH concentration and CDH yield, but not for the minimum enzyme concentration. In the BR1 the required enzyme addition of at least 30 mg/mL, while in the BR2 and BR3 the minimum required final CDH concentration and Y_{CDH} were achieved at enzyme concentrations of 10 and 15 mg/mL, respectively. The highest BY was achieved in the BR2 but at the enzyme concentration of 5 mg/mL at which the required final CDH concentration was not obtained. Considering STY, final CDH concentration and BY, the optimal reactor mode was the BR2 with total enzyme addition of 10 mg/mL, although in none of the tested batch reactors the industrial requirement for the BY was achieved.

In fed-batch reactor different setups of enzyme supply were considered, while AA and CAA were continuously feed into the reactor. The investigated fed-batch modes were:

List of reactant and product abbreviations: acetaldehyde (**AA**), chloroacetaldehyde (**CAA**), 4-chloro-3-hydroxybutanal (**CHB**), 6-chloro-3,5-dihydroxyhexanal (**CDH**), 6-chloro-3,5-dihydroxyhexanoic acid (**CDHA**), 3-hydroxy-4(-oxiran-2-yl)butanoic acid (**HOBA**), 6-cyano-3,5-dihydroxyhexanoic acid (**CYDHA**), 3-hydroxybutanal (**HB**), 3,5-dihydroxyhexanal (**DHH**).

1. FBR1 – fed-batch reactor with the addition of total amount of enzyme at the beginning of the process,
2. FBR2 – fed-batch reactor with the addition of half of the amount of enzyme at the beginning of the process and half of the amount in the feed,
3. FBR3 – fed-batch reactor with the enzyme addition only in the feed.

Simulations were stopped at 33.33 h (2000 min) and for that moment BYs and STYs were calculated (Figure 52).

a) b)

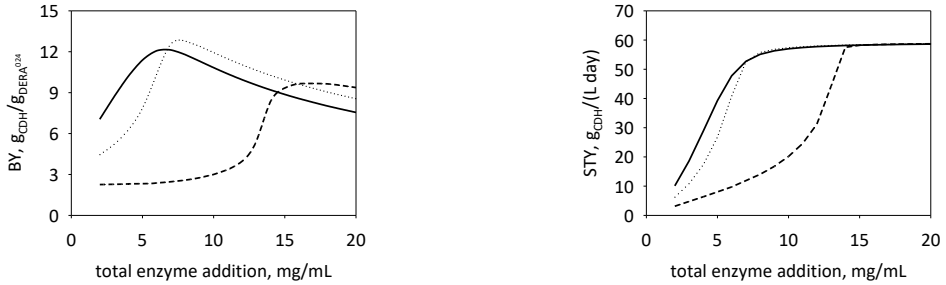

Figure 52 Model simulations of double aldol addition of AA to CAA catalyzed by DERA^{024} in different fed-batch reactor modes (feed 1: q_1 = 5 μL/min; $c_{AA,0}$ = 2200 mM, $c_{CAA,0}$ = 1000 mM, FBR1 and FBR2: V_0 = 6 mL; feed 2: q_2 = 2 μL/min; FBR3: V_0 = 10 mL). a) Biocatalyst yield and b) productivity change with total enzyme addition. Legend: FBR1 (solid line), FBR2 (dotted line), FBR3 (dashed line).

In the FBR1 and FBR2 the CDH yield of at least 80 % was achieved at the total DERA^{024} addition of 7.0 mg/mL, while in the FBR3 at 14.7 mg/mL. The highest BY in the FBs were observed at 7.0 mg/mL of total enzyme addition for FB1 (12.13 $g_{CDH}/g_{DERA024}$), 8.8 mg/mL for FBR2 (12.78 $g_{CDH}/g_{DERA024}$) and 18.4 g for FBR3 (9.68 $g_{CDH}/g_{DERA024}$). At these data points, the final CDH concentration was at least 70 g/L.

The FBR2 was chosen as the optimal reactor mode with a total enzyme addition of 8.8 mg/mL. This reactor mode was chosen based on the highest BY since the remaining indicators (Y_{CDH}, c_{CDH}, and STY) were of similar values in all studied FBR reactor modes. The results of the aldol reaction of AA with CAA catalyzed by DERA^{024} in the fed-batch reactor at these FBR2 conditions are shown in Figure 54.

List of reactant and product abbreviations: acetaldehyde (**AA**), chloroacetaldehyde (**CAA**), 4-chloro-3-hydroxybutanal (**CHB**), 6-chloro-3,5-dihydroxyhexanal (**CDH**), 6-chloro-3,5-dihydroxyhexanoic acid (**CDHA**), 3-hydroxy-4(-oxiran-2-yl)butanoic acid (**HOBA**), 6-cyano-3,5-dihydroxyhexanoic acid (**CYDHA**), 3-hydroxybutanal (**HB**), 3,5-dihydroxyhexanal (**DHH**).

3.6.5.1.6 DERA-catalyzed aldol additions in fed-batch reactor

To validate the developed mathematical model in the fed-batch reactor (Equations 21, 23, 25 and 32 – 39) the DERA^{Tm}-catalyzed aldol addition was conducted in a fed-batch reactor shown in Figure 48 (Chapter 3.6.5.1.4). The reaction resulted in a certain quantity of side products (approx. 23 % *w*/*w*). The statistical output (R^2 = 24.27, σ = 0.93) was weaker than in the previous two types of investigated reactors (Chapters 3.6.5.1.2 and 3.6.5.1.3). This was attributed to (1) increased serial dilution, due to high concentration of aldehydes present in the reaction solution, and to (2) high amount of DERA^{Tm} that caused the reaction mixture to become viscous thus causing a possible sampling error. Since the developed mathematical model described the experimental data well (Figure 48), several model simulations were done to find the optimal reactor mode. The results of carried simulations are described in Chapter 3.6.5.1.4. Based on the carried out simulations (Chapter 3.6.5.1.4: Figures 49 and 50) and taking the predicted final CDH concentration, CDH yield, BY and STY into account, the optimal reactor mode was chosen to be the fed-batch reactor with two feeds: one being the substrate supply and the other enzyme supply. The starting volume was 6.0 mL of 0.1 M TEA-HCl buffer pH 7. At the beginning of the experiment, the concentration of AA and CAA was zero, while half of the total enzyme amount was added into the reactor prior to the start of the reaction (16.67 mg/mL in 6 mL at 0 min). The experimental conditions are given in the description of Figure 53.

At the end of the experiment with DERA^{Tm} (33.33 h, Figure 53), the final concentration of CDH was 76.7 g/L (Table 17) and the yield of the product CDH with respect to the substrate CAA was 96.9 %. The CDH/CHB selectivity was 28.1, which was the highest obtained for this enzyme by comparing the examined reactor configurations: 2.3-fold higher than in batch experiment and 1.4-fold higher than in the repetitive batch experiment. The CDH/CHH selectivity was 7.1 and was 2-fold lower than in the batch experiment and the same as in the repetitive batch experiment (1.01-fold lower). The STY was calculated to be 55.2 g/(L·day), which was 5.1-fold lower than in the batch experiment, and the same as in the repetitive batch experiment (1.01-fold higher).

The final product composition of the reaction mixture and the mass concentrations of obtained products at the end of the experiment are given in Table 17. The statistical output (R^2 = 0.99, σ = 6.95) proved that the experimental data are in good agreement with the model simulations predicted data, which can be seen from Figure 53.

List of reactant and product abbreviations: acetaldehyde (**AA**), chloroacetaldehyde (**CAA**), 4-chloro-3-hydroxybutanal (**CHB**), 6-chloro-3,5-dihydroxyhexanal (**CDH**), 6-chloro-3,5-dihydroxyhexanoic acid (**CDHA**), 3-hydroxy-4(-oxiran-2-yl)butanoic acid (**HOBA**), 6-cyano-3,5-dihydroxyhexanoic acid (**CYDHA**), 3-hydroxybutanal (**HB**), 3,5-dihydroxyhexanal (**DHH**).

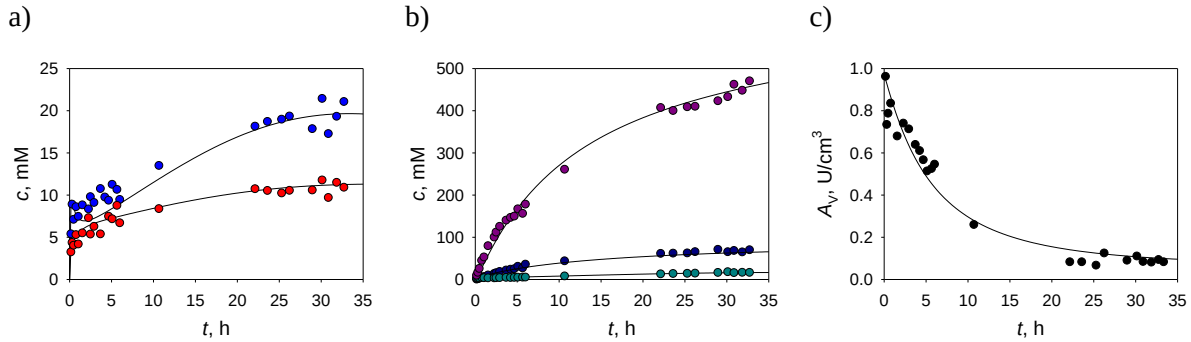

Figure 53 Experimental and simulation data of the double aldol addition of AA to CAA in the fed-batch reactor catalyzed by DERA^{Tm} (0.1 M TEA-HCl buffer pH 7, V_0 = 6 mL, γ_{DERATm} = 16.67 mg/mL; feed 1: q_1 = 5 µL/min, $c_{AA,0}$ = 2300 mM, $c_{CAA,0}$ = 950 mM; feed 2: q_2 = 2 µL/min, $\gamma_{DERATm,0}$ = 25 mg/mL; 33.33 h). Change of a) substrate AA and CAA concentration, b) product CHB, CDH and CHH concentration, and c) enzyme volume activity during the experiment. Legend: experiment (dots), model (line); AA (blue), CAA (red), CHB (teal), CDH (purple), CHH (dark blue).

Model (Equations 22 and 32 – 39) simulations were done for the DERA^{024}-catalyzed aldol reaction as well. The simulations were done by changing the initial conditions in different reactor modes based on the experimental data obtained in the previous two experimental setups for the DERA^{024} aldol reaction (batch reactor: Figure 45, repetitive batch reactor: Figure 47). Based on the simulation results (Figures 51 and 52) the optimum reaction conditions for carrying out the reaction were found to be in the fed-batch reactor with the substrate (AA, CAA) and enzyme supply (Chapter 3.6.5.1.5: Figure 52). The proposed initial reaction volume was 6 mL containing only 0.1 M phosphate buffer pH 6. At the beginning of the experiment, the concentrations of AA, CAA, and DERA^{024} were zero. The reaction conditions are given in detail in the description of Figure 54.

At the end of the experiment with DERA^{024} (33.33 h), the final concentration of CDH was 81 g/L (Table 17). The yield of the product CDH with respect to substrate CAA was 97.9 %. The $S_{CDH/CHB}$ at the end of the experiment was 67.7, which was the highest obtained among both DERAs and reactor types, while the $S_{CDH/CHH}$ equaled 13.6. The calculated STY was 58.6 g/(L·day). The final product composition of the reaction mixture and the mass concentration of each of the product at the end of the experiment are presented in Table 17. According to that data, the DERA^{024}-catalyzed aldol reaction produced higher quantities of the desired CDH product, with less side-products and better selectivity towards CDH, which is in accordance with the estimated kinetic data for the studied DERA enzymes (Table 8).

List of reactant and product abbreviations: acetaldehyde (**AA**), chloroacetaldehyde (**CAA**), 4-chloro-3-hydroxybutanal (**CHB**), 6-chloro-3,5-dihydroxyhexanal (**CDH**), 6-chloro-3,5-dihydroxyhexanoic acid (**CDHA**), 3-hydroxy-4(-oxiran-2-yl)butanoic acid (**HOBA**), 6-cyano-3,5-dihydroxyhexanoic acid (**CYDHA**), 3-hydroxybutanal (**HB**), 3,5-dihydroxyhexanal (**DHH**).

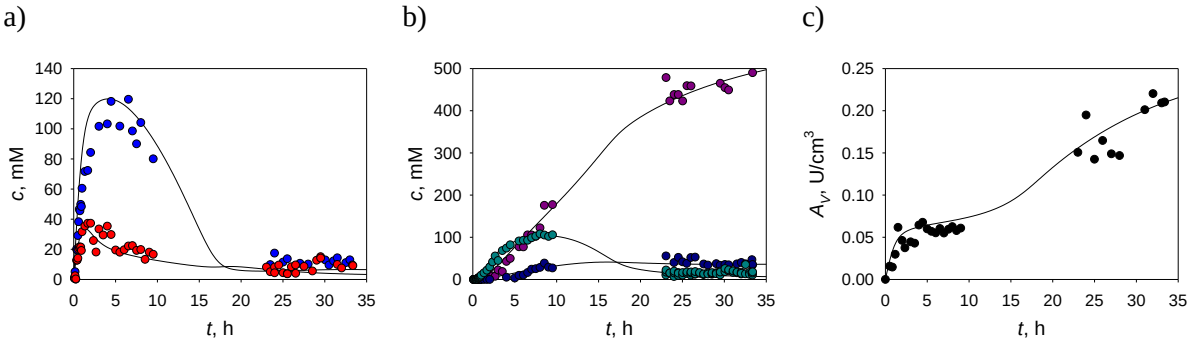

Figure 54 Experimental and simulation data of the double aldol addition of AA to CAA in the fed-batch reactor catalyzed by DERA^{024} (0.1 M phosphate buffer pH 6, V_0 = 6 mL; feed 1: q_1 = 5 µL/min, $c_{AA,0}$ = 2200 mM, $c_{CAA,0}$ = 1000 mM; feed 2: q_2 = 2 µL/min, $\gamma_{DERA024,0}$ = 100 mg/mL; 33.33 h). Change of a) substrate AA and CAA concentration, b) product CHB, CDH and CHH concentration, and c) enzyme volume activity during the experiment. Legend: experiment (dots), model (line); AA (blue), CAA (red), CHB (teal), CDH (purple), CHH (dark blue).

Based on the statistical output (R^2 = 0.98, σ = 11.88) and by comparing the experimental data with the model simulation (Figure 54), it can be concluded that the model described the experimental data well.

Table 17 Final mass percent product composition and final mass product concentration: results obtained after 33.33 h (2000 min) of the aldol reaction of AA with CAA catalyzed by DERA^{Tm} and DERA^{024} in the fed-batch reactor.

Enzyme	*w/w*, %			*γ*, g/L		
	CHB	**CDH**	**CHH**	**CHB**	**CDH**	**CHH**
DERA^{Tm}	2.3	87.8	9.9	2.0	76.7	8.6
DERA^{024}	3.8	90.6	5.6	1.0	81.6	4.3

3.6.5.1.6.1 Concluding remarks: DERA-catalyzed aldol addition

In order to obtain higher amounts of CDH, the aldol reaction had to be conducted either in the repetitive batch reactor or fed-batch reactor mode, since the reaction carried out in the batch reactor resulted in a low amount of CDH.

The developed mathematical models for the DERA-catalyzed aldol reaction were validated in different reactors (Equations 21 – 39). Reaction optimization was done based on the collected experimental data using the validated models. Based on the simulations, optimal reactor setup was found. The DERA^{Tm}- and DERA^{024}-catalyzed aldol reactions were conducted

List of reactant and product abbreviations: acetaldehyde (**AA**), chloroacetaldehyde (**CAA**), 4-chloro-3-hydroxybutanal (**CHB**), 6-chloro-3,5-dihydroxyhexanal (**CDH**), 6-chloro-3,5-dihydroxyhexanoic acid (**CDHA**), 3-hydroxy-4(-oxiran-2-yl)butanoic acid (**HOBA**), 6-cyano-3,5-dihydroxyhexanoic acid (**CYDHA**), 3-hydroxybutanal (**HB**), 3,5-dihydroxyhexanal (**DHH**).

at optimum initial conditions. The obtained experimental data was in accordance with simulation data.

From the results given in Table 18 and presented data (Figures 44 – 54), it was evident that the DERA^{024}-catalyzed aldol reaction produced less side-product (≤ 10 %). The calculated STYs, BYs and product yield suggested a similar reaction outcome, but their values were slightly higher when the reaction was catalyzed by DERA^{024}. By comparing those results to the industrial requirements (Table 1) it could be noted that experiments conducted in a repetitive batch reactor and a fed-batch reactor mode fulfilled some notable requirements, such as the final product concentration (> 50 g/L) or the substrate conversion (> 95 % after 24 hours). Thus, the DERA^{024} enzyme was used for future multi-step one-pot experiments.

Table 18 Results for the DERA^{Tm}- and DERA^{024}-catalyzed aldol reactions in three different reactor modes.

Reactor	DERA type	*t*, h [a]	w_{CDH}/w, %	γ_{CDH}, g/L	*Y*, %	STY	BY
BR	**DERA^{Tm}**	1.2	91	14.2	83	283.2	2.4
	DERA^{024}	1.0	85	12.9	80	309.6	9.7
RBR	**DERA^{Tm}**	21.8	87	50.9	96	56.0	3.7
	DERA^{024}	9.5	90	50.1	97	126.6	4.3
FBR [b]	**DERA^{Tm}**	33.33	88	76.7	97	55.2	9.3
	DERA^{024}	33.33	91	81.6	98	58.6	7.4

[a] end of the reaction; $X_{AA} = X_{CAA} > 99.0$ %
[b] full substrate conversion was not obtained
Abbreviations: batch reactor (BR), repetitive batch reactor mode (RBR), fed-batch reactor (FBR)
Notes: Y represents CDH yield with respect to CAA, while STY is expressed as g/(L·day) and BY as g_{CHD}/g_{DERA}.

The highest obtained CDH mass concentration were obtained in the fed-batch reactor (approx. 6-fold higher than in the batch reactor), the highest CDH yields (≥ 96 %) were obtained in repetitive batch reactor and in fed-batch reactor, the highest STY was calculated for the batch reactor (approx. 5-fold higher than in the fed-batch reactor), while the highest BYs (≥ 7.4 g_{CHD}/g_{DERA}) were obtained in the batch reactor (for DERA^{Tm}) and the fed-batch reactor (for both DERAs). The calculated metrics, such as w_{CDH}/w, γ_{CDH}, Y_{CDH}, BY, were in favor of the reactions catalyzed in the fed-batch reactor, suggesting the fed-batch reactor as the optimal reactor. If taking the calculated STYs into account, the optimal reactor would be the repetitive reactor because it resulted with high STY (DERA^{024}: 2-fold higher than obtained in fed-batch reactor), CDH yield (DERA^{024}: almost identical to the one obtained in fed-batch reactor, ≥ 96 %) and

List of reactant and product abbreviations: acetaldehyde (**AA**), chloroacetaldehyde (**CAA**), 4-chloro-3-hydroxybutanal (**CHB**), 6-chloro-3,5-dihydroxyhexanal (**CDH**), 6-chloro-3,5-dihydroxyhexanoic acid (**CDHA**), 3-hydroxy-4(-oxiran-2-yl)butanoic acid (**HOBA**), 6-cyano-3,5-dihydroxyhexanoic acid (**CYDHA**), 3-hydroxybutanal (**HB**), 3,5-dihydroxyhexanal (**DHH**).

high final CDH concentration (> 50 g/L; DERA^{024}: 0.6-fold lower than obtained in fed-batch reactor).

3.6.5.2 DH-catalyzed CDH oxidation

The CDH oxidation was accomplished in following three ways:

1. AlDH-catalyzed oxidation without NAD^+ regeneration
2. AlDH-catalyzed oxidation with NAD^+ regeneration by NOX^{009}
3. KRED^{354}-catalyzed oxidation without $NADP^+$ regeneration

Each reaction was conducted using purified CDH substrate obtained following the procedure described in Chapter 3.3.4.1. All reactions were carried out in batch reactor.

3.6.5.2.1 AlDH-catalyzed CDH oxidation without NAD^+ regeneration

To validate the mathematical model developed for the AlDH-catalyzed CDH oxidation without coenzyme regeneration (Equations 40 – 42 and 44 – 48), the reaction was carried out in a batch reactor with equimolar concentrations of CDH and NAD^+ (Figure 55).

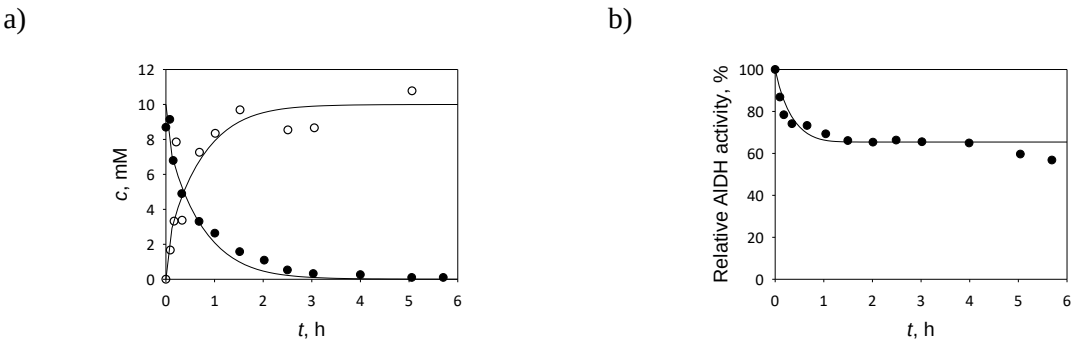

Figure 55 Experimental and simulation data of the oxidation of purified CDH into CDHA catalyzed by AlDH (0.1 M phosphate buffer pH 8, c_{CDH} = 10 mM, c_{NAD} = 10 mM, 1 000 rpm, γ_{AlDH} = 5 mg/mL). Change of a) substrate CDH and product CDHA concentration, b) relative enzyme activity during the experiment. Legend: experiment (dots), model (line); change of concentration with time: CDH (black), CDHA (white).

Although the reaction was originally described without the presence of the reverse reaction (the reaction of CDH oxidation, Equation 41, $r_5 = 0$; data not shown), it was noted that the mathematical model described the results better if it contained the above-mentioned

List of reactant and product abbreviations: acetaldehyde (**AA**), chloroacetaldehyde (**CAA**), 4-chloro-3-hydroxybutanal (**CHB**), 6-chloro-3,5-dihydroxyhexanal (**CDH**), 6-chloro-3,5-dihydroxyhexanoic acid (**CDHA**), 3-hydroxy-4(-oxiran-2-yl)butanoic acid (**HOBA**), 6-cyano-3,5-dihydroxyhexanoic acid (**CYDHA**), 3-hydroxybutanal (**HB**), 3,5-dihydroxyhexanal (**DHH**).

equation (Figure 55). Therefore, using the collected experimental data (Figure 55a), the value of the maximum reaction rate of the AlDH-catalyzed CDHA reduction was estimated to be k_5 = 0.044 mL/(mg·mM·min). The operational stability decay constant was estimated using the experimental data (Figure 55b) and Equation 48 (k_d^{AlDH} = 0.0035 min^{-1}). After just four hours of the reaction, the CDH conversion was 99.9 %. Such conversion would not be possible if the enzyme was used in its purified form. Due to the presence of NOX(AlDH) (Figure 38, Table 10), the reaction ran to its completion. The developed mathematical model contained the Equation 42 as well and thus described the experimental data well (R^2 = 0.97, σ = 1.20, Figure 55).

3.6.5.2.2 AlDH-catalyzed CDH oxidation with NAD^+ regeneration catalyzed by NOX^{009}

To validate the mathematical model that describes the reaction of AlDH-catalyzed oxidation of purified CDH with NOX^{009}-catalyzed NAD^+ regeneration (Equations 40 – 51), three experiments in batch reactor were conducted with the same initial CDH and enzyme concentrations and different NAD^+ concentrations, since the kinetic measurements revealed that the coenzyme NAD^+ inhibits the AlDH-catalyzed reaction (Figure 37b). The reaction rate for the AlDH-catalyzed CDHA reduction (the CDH oxidation reverse reaction, Figure 24a) was estimated from the batch experiment (k_5 = 0.044 mL/(mg·mM·min), Equation 41). Because the enzymes lost their activity during the experiments, fresh amounts of enzymes of the same concentration as the initial were added into the reactor. The results of those three experiments are shown in Figure 56.

From the results (Figure 56) it could be concluded that with an increase of NAD^+ concentration the conversion of CDH increased: in the experiment with 1 mM NAD^+ the CDH conversion was 40 %, with 5 mM NAD^+ 77 %, while with 10 mM NAD^+ the substrate conversion was 82 %.

The values of enzyme operational stability decay rate constants (k_d^{AlDH}, k_d^{NOX009}) were estimated using the second-order deactivation kinetics (Equation 48 for AlDH, Equation 49 for NOX^{009}) and experimental data shown in Figure 56.

List of reactant and product abbreviations: acetaldehyde (**AA**), chloroacetaldehyde (**CAA**), 4-chloro-3-hydroxybutanal (**CHB**), 6-chloro-3,5-dihydroxyhexanal (**CDH**), 6-chloro-3,5-dihydroxyhexanoic acid (**CDHA**), 3-hydroxy-4(-oxiran-2-yl)butanoic acid (**HOBA**), 6-cyano-3,5-dihydroxyhexanoic acid (**CYDHA**), 3-hydroxybutanal (**HB**), 3,5-dihydroxyhexanal (**DHH**).

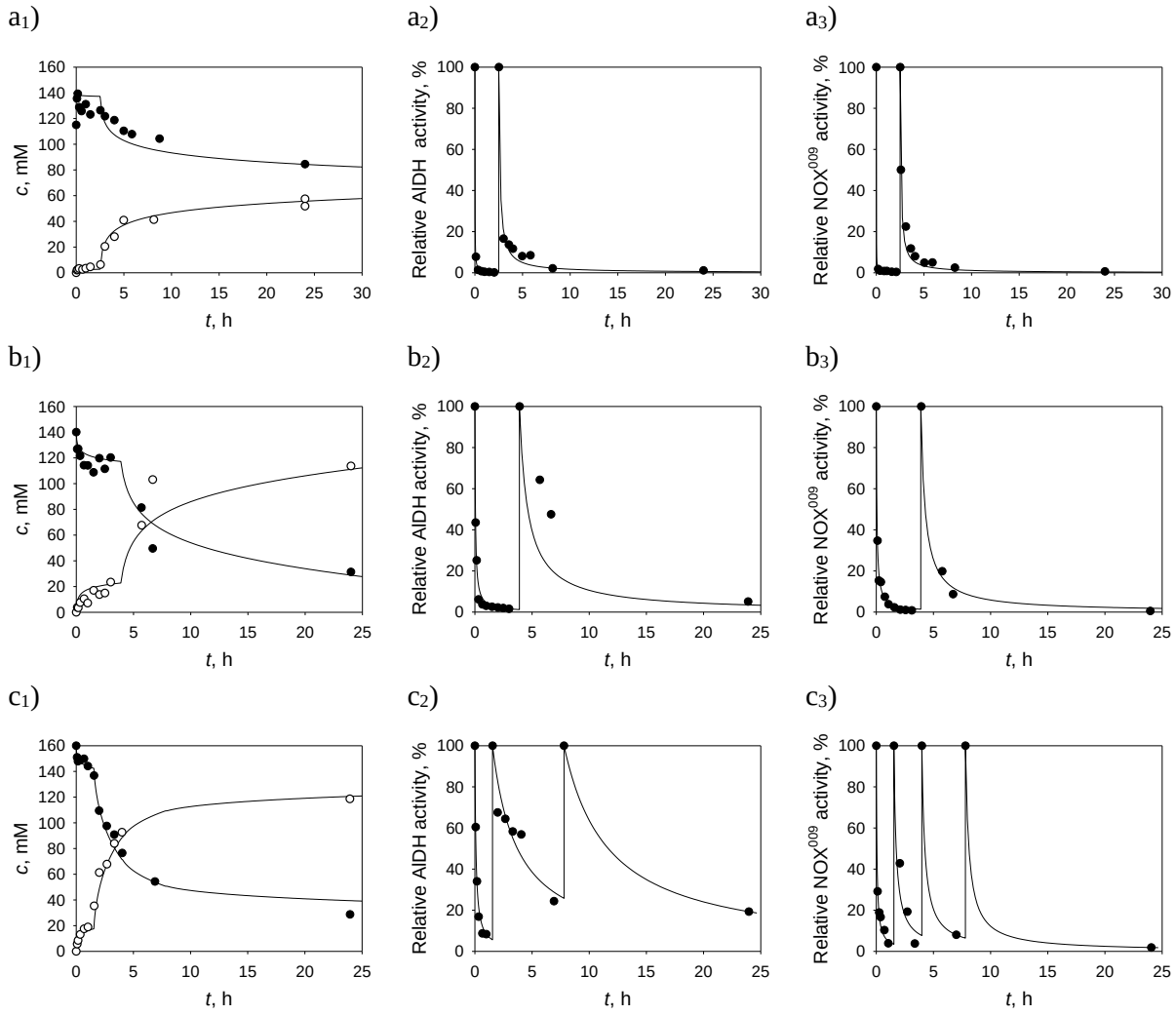

Figure 56 Experimental and simulation data of the AlDH-catalyzed oxidation of purified CDH into CDHA with NOX^{009}-catalyzed NAD^+ regeneration system (0.1 M phosphate buffer pH 8, 1 000 rpm, 25 °C, c_{CDH} = 140 mM, c_{NAD} = 1 - 10 mM, γ_{AlDH} = 5 mg/mL per addition, γ_{NOX009} = 5 mg/mL per addition). Results for the experiments with a) 1 mM NAD^+, b) 5 mM NAD^+ and c) 10 mM NAD^+. Legend: experiment (dots), model (line); change of concentration with time: CDH (black), CDHA (white).

From the estimated operational stability rate constants (Table 19) it can be observed that with the increase of the initial concentration of NAD^+, the value of the estimated constant significantly decreased (k_d for 1st addition, Table 19). With each further enzyme addition, the value of the operational stability rate constants decreased, which suggested that both enzymes were more stable with each fresh enzyme addition, which could be attributed to (1) increased protein concentration in the system that usually contributes to enhanced operational enzyme stability [190] and (2) less CDH was present in the system.

List of reactant and product abbreviations: acetaldehyde (**AA**), chloroacetaldehyde (**CAA**), 4-chloro-3-hydroxybutanal (**CHB**), 6-chloro-3,5-dihydroxyhexanal (**CDH**), 6-chloro-3,5-dihydroxyhexanoic acid (**CDHA**), 3-hydroxy-4(-oxiran-2-yl)butanoic acid (**HOBA**), 6-cyano-3,5-dihydroxyhexanoic acid (**CYDHA**), 3-hydroxybutanal (**HB**), 3,5-dihydroxyhexanal (**DHH**).

Based on the independent measurements of influence of CDH on the AlDH stability, it was concluded that CDH has a negative influence on AlDH stability (Figure 31). Additionally, the data given in Figure 56c suggest that the 3rd AlDH addition and (even 3rd and) 4th NOX^{009} addition were not necessary. This can be also observed based on the corresponding values of k_d for AlDH and NOX^{009} presented in Table 19. Therefore, it should be noted that with the increase of the initial NAD^+ concentration in the reactor the number of necessary AlDH and NOX^{009} additions did not increase.

After 15 hours of the reaction, the AlDH/NOX^{009}-catalyzed CDH oxidation in presence of 10 mM NAD^+ (Figure 56c) resulted in a CDH conversion of 82 % and CDHA yield of 90 %. The calculated BY and STY were 2.4 g_{CDHA}/g_{AlDH} and 38.2 g/(L·day), respectively, while the final CDHA concentration that was obtained was 23.9 g/L.

The goodness-of-fit statistics of the experimental and model simulation data (Figure 56) suggested a very good fit ($R^2 \geq 0.97$).

Table 19 Deactivation rate constant estimated from the experimental data shown in Figure 56.

NAD^+ concentration, mM	**Enzyme addition**	**k_d^{AlDH}, min^{-1}**	**k_d^{NOX009}, min^{-1}**
1	1st	1.94	4.08
	2nd	0.13	0.19
5	1st	0.36	0.31
	2nd	0.006	0.044
10	1st	0.182	0.30
	2nd	0.008	0.08
	3rd	0.004	0.06
	4th	-	0.05

3.6.5.2.3 $KRED^{332}$-catalyzed CDH oxidation

The developed mathematical model for the $KRED^{332}$-catalyzed CDH oxidation in batch reactor (Equations 52 – 59) was validated with the experimental data presented in Figure 57. The obtained experimental data was used to estimate the operational stability rate constant ($k_d^{KRED332}$, Equation 59) and the reaction rate of the CDH reduction (r_{10}, Equation 54). By carrying out the $KRED^{332}$-catalyzed CDH reduction in presence of NADPH, the decrease of NADPH concentration at 340 nm was spectrophotometrically observed (data not shown).

List of reactant and product abbreviations: acetaldehyde (**AA**), chloroacetaldehyde (**CAA**), 4-chloro-3-hydroxybutanal (**CHB**), 6-chloro-3,5-dihydroxyhexanal (**CDH**), 6-chloro-3,5-dihydroxyhexanoic acid (**CDHA**), 3-hydroxy-4(-oxiran-2-yl)butanoic acid (**HOBA**), 6-cyano-3,5-dihydroxyhexanoic acid (**CYDHA**), 3-hydroxybutanal (**HB**), 3,5-dihydroxyhexanal (**DHH**).

The experimental and model simulation data for the oxidation of the purified CDH catalyzed by KRED^{332} in the batch reactor are shown in Figure 57. In this experiment, full conversion (> 99.8 % CDH) was achieved after six hours, but due to a side reaction, a possible CDH reduction (Figure 25), the reaction resulted with a CDHA yield of only 53 %. The reaction rate constant of CDH reduction into CHO (k_{10}) was estimated from the experimental data to be 0.0011 mL/(mg·mM·min).

During the experiment, KRED^{332} was added two-fold (at 0.0 h and 2.1 h; Figure 57). Despite the fact that the coenzyme regeneration was slow, the main reaction was fast (Table 12 and 13), the reason being the potential CDH reduction in which NADPH was oxidized and thus served as an indirect $NADP^+$ regeneration system combined with the action of the NOX(KRED^{332}) enzyme.

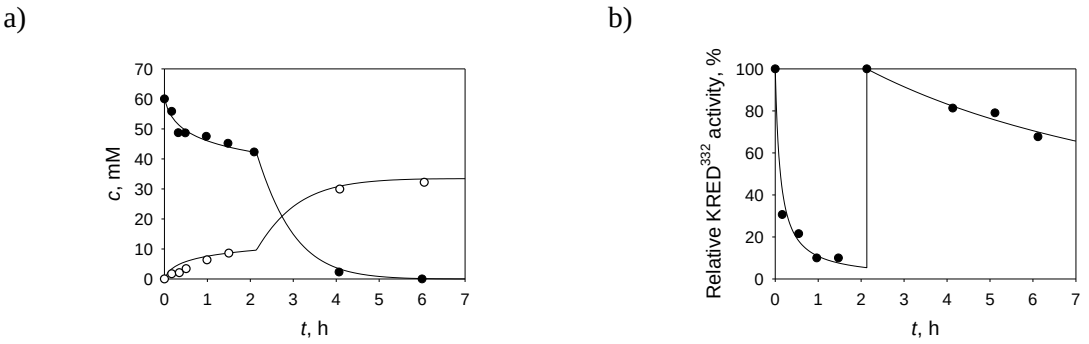

Figure 57 Experimental and simulation data of the oxidation of purified CDH into CDHA catalyzed by KRED^{332} (0.1 M phosphate buffer pH 8, c_{CDH} = 60 mM, c_{NADP} = 10 mM, 1 000 rpm, $\gamma_{KRED332}$ = 10 mg/mL per addition). Change of a) substrate CDH and product CDHA concentration, b) relative enzyme activity during the experiment. Legend: experiment (dots), model (line); change of concentration with time: CDH (black), CDHA (white).

Table 3 Deactivation rate constant estimated from the experimental data shown in Figure 57**.**

Enzyme addition	$k_d^{KRED332}$, 1/min
1st	0.1377
2nd	0.0018

The operational stability rate constants for each KRED^{332} addition ($k_d^{KRED332}$) were estimated based on the experimental data (Figure 57b). Based on them it could be concluded that the enzyme deactivation was almost 80-time lower in the second than in the first addition, which could be attributed to (1) the increased protein content [191] and (2) lowered CDH concentration in the reactor. After six hours, the final CDHA concentration was 6.0 g/L.The calculated BY and STY were 2.0 g_{CDHA}/g_{AlDH} and 24.0 g/(L·day), respectively.

List of reactant and product abbreviations: acetaldehyde (**AA**), chloroacetaldehyde (**CAA**), 4-chloro-3-hydroxybutanal (**CHB**), 6-chloro-3,5-dihydroxyhexanal (**CDH**), 6-chloro-3,5-dihydroxyhexanoic acid (**CDHA**), 3-hydroxy-4(-oxiran-2-yl)butanoic acid (**HOBA**), 6-cyano-3,5-dihydroxyhexanoic acid (**CYDHA**), 3-hydroxybutanal (**HB**), 3,5-dihydroxyhexanal (**DHH**).

3.6.5.2.4 Concluding remarks: DH-catalyzed CDH oxidation

Both AlDH and KRED^{332} could be used as enzymes that catalyze the CDH oxidation. The AlDH-catalyzed CDH oxidation should be coupled with NOX^{009}-catalyzed NAD^+ regeneration to create a feasible reaction system. The optimum coenzyme concentration for the reaction found to be 10 mM (Figure 56), despite obvious deactivation of both enzymes (Table 19). At the reaction conditions described in Figure 56c (for AlDH) and Figure 57 (for KRED^{332}), the AlDH-catalyzed reaction did not result in full CDH conversion, unlike in the experiment catalyzed by KRED^{332}. The obtained full CDH conversion in the KRED^{332}-catalyzed CDH oxidation can be attributed to the noted side reaction of CDH reduction (Figure 25): the CDH being spent in two parallel reactions (in the CDH oxidation and CDH reduction). Due to the existence of that side reaction in the KRED^{332}-catalyzed system, the reaction was not further investigated with an $NADP^+$ regeneration system, which may have improved the CDHA yield. During the KRED^{332} experiments, the side reaction reflected in the CDHA yield which was only 53 %, despite the 99.8 % CDH conversion.

From the estimated operational stability rate constants for each enzyme addition (k_d) in all of the conducted experiments of CDH oxidation, it could be concluded that the enzyme deactivation was less prominent with each enzyme addition, which could be explained by increased protein content [191] and lowered concentration of the CDH substrate in the reactor.

3.6.5.3 HHDH^{001}-catalyzed dehalogenation and epoxide ring-opening with KCN

The HHDH^{001}-catalyzed reaction was conducted with purified CDHA without and with the addition of KCN. The developed mathematical model was validated in a batch reactor (Equations 60 – 67). Since HOBA and CYDHA are not commercially available, they were not quantified.

The operational stability rate constant ($k_d^{HHDH001}$) was estimated using the Equation 67 and the obtained experimental data from relative enzyme activity *vs* time. The discrepancy between the deactivation rate constants estimated using Equation 67 and 72 (independent measurements) could be explained by unknown effects of HOBA and CYDHA on the enzyme activity.

List of reactant and product abbreviations: acetaldehyde (**AA**), chloroacetaldehyde (**CAA**), 4-chloro-3-hydroxybutanal (**CHB**), 6-chloro-3,5-dihydroxyhexanal (**CDH**), 6-chloro-3,5-dihydroxyhexanoic acid (**CDHA**), 3-hydroxy-4(-oxiran-2-yl)butanoic acid (**HOBA**), 6-cyano-3,5-dihydroxyhexanoic acid (**CYDHA**), 3-hydroxybutanal (**HB**), 3,5-dihydroxyhexanal (**DHH**).

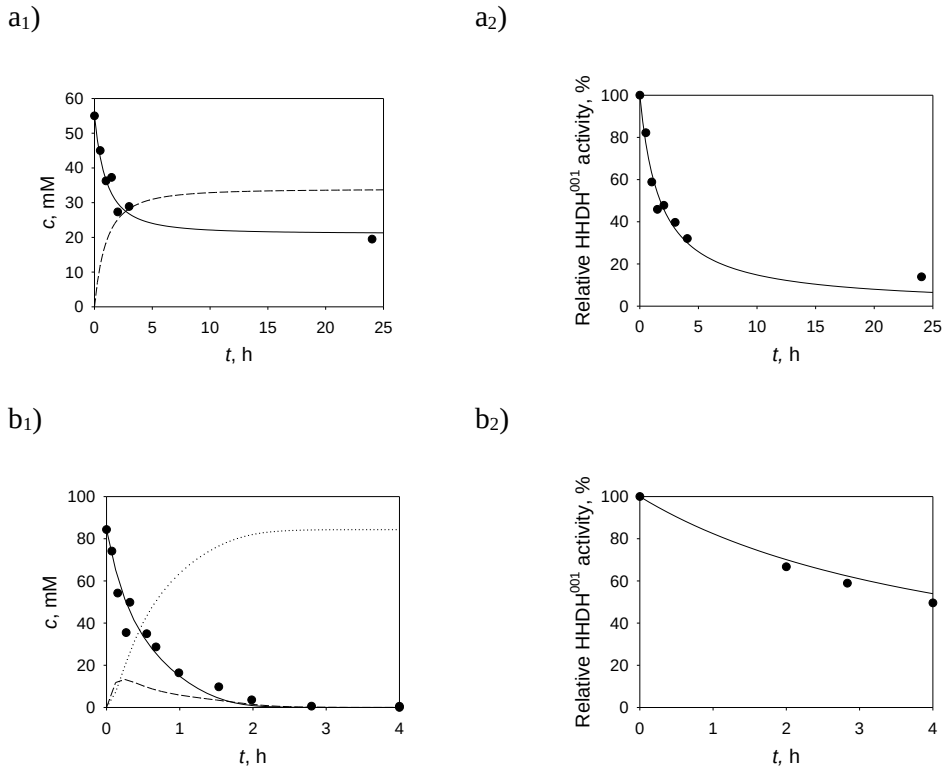

Figure 58 Experimental and simulation data of the HHDH^{001}-catalyzed reaction of a) CDHA dehalogenation (c_{CDHA} = 55 mM) and b) CDHA dehalogenation and epoxide-ring opening with KCN (c_{CDHA} = 85 mM, c_{KCN} = 200 mM) ($\gamma_{HHDH001}$ = 10 mg/mL, 0.1 M phosphate buffer pH 8, 1 000 rpm, 25 °C). Legend: experiment (dots), model (line: CDHA, solid line; HOBA, dashed, CYDHA, dotted), change of concentration with time: CDHA (black).

Using the data shown for the HHDH^{001}-catalyzed reaction of CDHA dehalogenation (reaction conducted without the presence of KCN, Figure 58a), the reaction rate constant of the HHDH^{001}-catalyzed halogenation of HOBA into CDHA (the reverse reaction of HHDH^{001}-catalyzed CDHA dehalogenation, k_{12}, Equation 61) was estimated to be 0.0029 mL/(mg·min). The enzyme deactivation rate constant ($k_d^{HHDH001}$, Equation 67) was estimated using the experimental data and equaled 0.01 min^{-1}. After approximately seven hours from the beginning of the experiment the substrate conversion was 58.4 %, while the relative residual enzyme activity was 20 %. Such conversion outcome was expected, due to the dehalogenation being an equilibrium reaction. Only after the KCN addition, full conversion would be possible as the epoxide ring-opening with CN^- is not reversible and hence, shifts the equilibrium of the dehalogenation reaction towards the product CYDHA formation.

The same reaction was conducted with the addition of KCN (Figure 58b) to estimate the reaction rate parameter of epoxide ring-opening (k_{13}, Equation 62). From the collected data, the

List of reactant and product abbreviations: acetaldehyde (**AA**), chloroacetaldehyde (**CAA**), 4-chloro-3-hydroxybutanal (**CHB**), 6-chloro-3,5-dihydroxyhexanal (**CDH**), 6-chloro-3,5-dihydroxyhexanoic acid (**CDHA**), 3-hydroxy-4(-oxiran-2-yl)butanoic acid (**HOBA**), 6-cyano-3,5-dihydroxyhexanoic acid (**CYDHA**), 3-hydroxybutanal (**HB**), 3,5-dihydroxyhexanal (**DHH**).

value of the reaction rate parameter was estimated to be 0.0006 mL/(mg·mM·min). Due to enzyme deactivation, the value of the deactivation rate constant ($k_d^{HHDH001}$, Equation 67) was estimated using the collected experimental data to be 0.003 min^{-1}. After three hours, ≥ 99.9 % CDHA conversion was obtained, whilst the relative residual $HHDH^{001}$ activity was 61 %.

From the experimental results of reactions conducted without and with the addition of KCN (Figure 58), it could be observed that the reaction with KCN resulted in almost full substrate conversion (>> 99.9 %), as expected, after just three hours, as opposed to the reaction without the KCN addition when less than half of the substrate was converted (3 h: X_{CDHA} = 53 %). Based on the model simulation prediction (Figure 58), it could be also noted that HOBA was virtually immediately consumed in the subsequent reaction. Interestingly enough, the enzyme retained 3-fold higher activity in the experiment with KCN addition than without, which could be due to HOBA being rapidly consumed during the reaction, because of the possible negative effects of HOBA on the $HHDH^{001}$ enzyme. This was, however, also expected based on the results obtained in the kinetic measurements (the KCN being a potent activator,) and the nature of the reaction (epoxide ring-opening with CN^- being an irreversible reaction thus shifting the reaction in the desired direction).

3.6.5.4 Concluding remarks: one-step biocatalysis

Based on all the experimental and simulation data for the DERA-catalyzed aldol reaction, DH-catalyzed oxidation and $HHDH^{001}$-catalyzed dehalogenation and epoxide ring-opening with KCN, the following could be concluded.

$DERA^{024}$ yielded better results, such as product yield, final product concentration, STY or BY, than $DERA^{Tm}$ in the aldol reaction of AA with CAA, while the repetitive batch reactor proved to be the optimal reactor mode for the observed reaction system.

Both AlDH and $KRED^{332}$ can be used as enzymes that catalyze the reaction of CDH oxidation. In the reaction catalyzed by $KRED^{332}$, a side reaction of CDH reduction into CHO occurred, causing low CDHA yields, which was experimentally proven. Therefore, an $NADP^+$ regeneration system was not further explored for the $KRED^{332}$-catalyzed CDH oxidation. The AlDH proved to be a better reaction system for the examined CDH oxidation than $KRED^{332}$. The AlDH-catalyzed CDH oxidation was carried out with NOX^{009}-catalyzed NAD^+ regeneration. The AlDH/NOX^{009} reaction system conducted in batch reactor resulted with

List of reactant and product abbreviations: acetaldehyde (**AA**), chloroacetaldehyde (**CAA**), 4-chloro-3-hydroxybutanal (**CHB**), 6-chloro-3,5-dihydroxyhexanal (**CDH**), 6-chloro-3,5-dihydroxyhexanoic acid (**CDHA**), 3-hydroxy-4(-oxiran-2-yl)butanoic acid (**HOBA**), 6-cyano-3,5-dihydroxyhexanoic acid (**CYDHA**), 3-hydroxybutanal (**HB**), 3,5-dihydroxyhexanal (**DHH**).

better values of the calculated metrics, such as final product concentration, product yield, BY and STY.

The results of the HHDH^{001}-catalyzed CDHA dehalogenation and epoxide ring-opening with KCN revealed that the presence of KCN shifts the reaction in the desired direction, yielding full substrate CDHA conversion (t = 3 h, ≥ 99.9 %), as opposed to the reaction without the presence of KCN (t = 8 h, 59 %).

Based on the statistic parameters provided by *Scientist* and goodness-of-fit of experimental results with the model, it was concluded that the developed mathematical models could be utilized for future optimization of this system.

3.6.6 Validation of developed mathematical models: multi-step one-pot biocatalysis

To simplify the reaction system of the first reaction route (Figure 1), different multi-step one-pot setups were examined:

1. DERA^{024}-catalyzed CDH production → AlDH-catalyzed CDH oxidation with NOX^{009}-catalyzed NAD^+ regeneration,
2. DERA^{024}-catalyzed CDH production → KRED^{332}-catalyzed CDH oxidation, and
3. DERA^{024}-catalyzed CDH production → AlDH -catalyzed CDH oxidation with NOX^{009}-catalyzed NAD^+ regeneration → HHDH^{001}-catalyzed dehalogenation and epoxide ring-opening with KCN.

A simultaneous one-step one-pot reaction containing the DERA and DH enzymes was not possible, since the DHs (AlDH, KRED^{332}) do not oxidize the aldehydes selectively and therefore would oxidize the DERA substrates (AA, CAA) into their corresponding acids (acetic acid, chloroacetic acid).

All multi-enzyme reactions were conducted with crude substrates without the removal of enzymes from the previous reaction step. The crude CDH substrate was obtained by carrying out the DERA^{024}-catalyzed reaction (Figure 47). Depending on the required crude CDH concentration, the reaction mixture was diluted using 0.1 M phosphate buffer pH 8 to obtain the desired CDH concentration.

List of reactant and product abbreviations: acetaldehyde (**AA**), chloroacetaldehyde (**CAA**), 4-chloro-3-hydroxybutanal (**CHB**), 6-chloro-3,5-dihydroxyhexanal (**CDH**), 6-chloro-3,5-dihydroxyhexanoic acid (**CDHA**), 3-hydroxy-4(-oxiran-2-yl)butanoic acid (**HOBA**), 6-cyano-3,5-dihydroxyhexanoic acid (**CYDHA**), 3-hydroxybutanal (**HB**), 3,5-dihydroxyhexanal (**DHH**).

The only condition to start the following consecutive reaction was that the substrates from the previous reaction step had fully reacted into the designated product. When needed, the pH of the reaction mixture was adjusted to pH 8 using 5 M KOH solution or 9.2 M sulfuric acid solution, due to changes of pH during the reaction.

Due to the occurrence of the cyanohydrin reaction[6] when carrying out the experiment consisting of (1) a DERA^{024}-catalyzed CDH production followed by (2) a simultaneous AlDH/NOX^{009}-catalyzed CDH oxidation combined with HHDH^{001}-catalyzed dehalogenation and epoxide ring-opening with KCN, the obtained experimental data are not presented, but are described under *Concluding remarks* within this Chapter.

3.6.6.1 Sequential one-pot CDH synthesis with AlDH/NOX^{009}

The sequential one-pot CDH synthesis consisted of two reactions conducted in sequential manner:

1. DERA^{024}-catalyzed aldol reaction
2. AlDH-catalyzed CDH oxidation with NOX^{009}-catalyzed NAD^+ regeneration.

The oxidation was conducted with 10 mM of NAD^+, since in the experiment with pure CDH (Figure 56) it was observed that under those conditions higher substrate conversions were obtained, while the values for the operational stability rate constants of both AlDH and NOX^{009} were lower (Table 19). In order to further reduce the enzyme deactivation during the reaction, the experiment was performed with a two-fold higher initial concentration of both enzymes than in the experiments with purified CDH (5 *vs* 10 mg/mL; Figure 56). Fresh additions of enzymes were added into the reactor once their residual activity was less than 20 %.

The experimental data of the AlDH-catalyzed oxidation of 80 mM and 335 mM CDH with NOX^{009}-catalyzed NAD^+ regeneration as well as the data obtained by model simulation are presented in Figure 59.

From the experimental data shown in Figure 59a, it was concluded that during the observed time-course AlDH and NOX^{009} became completely stable after one hour from the

[6] A chemical reaction of CDH with KCN that resulted with the formation of a cyanohydrin.

List of reactant and product abbreviations: acetaldehyde (**AA**), chloroacetaldehyde (**CAA**), 4-chloro-3-hydroxybutanal (**CHB**), 6-chloro-3,5-dihydroxyhexanal (**CDH**), 6-chloro-3,5-dihydroxyhexanoic acid (**CDHA**), 3-hydroxy-4(-oxiran-2-yl)butanoic acid (**HOBA**), 6-cyano-3,5-dihydroxyhexanoic acid (**CYDHA**), 3-hydroxybutanal (**HB**), 3,5-dihydroxyhexanal (**DHH**).

beginning of the experiment, which was most likely caused by high protein content in the reaction mixture, since DERA^{024} was present in the mixture as well [191]. Therefore, a linear dependence of the operational stability decay rate constant on the concentration of CDH (Equations 50 and 51) was introduced into the model. If the operational stability rate constant was calculated using independent measurements at given conditions (Figure 59a), the a^{AlDH} (Equation 50) and a^{NOX009} (Equation 51) values would be 0.045 and 0.0033 1/(mM·min), respectively. Using the experimental data and the beforementioned equations, the value of the *a* parameter for both AlDH and NOX^{009} were estimated and their values are presented in Table 21. Based on the estimated values (Table 21), it could be concluded that the enzyme operational stabilities, especially of AlDH, significantly improved in the experiment with crude CDH (Figure 59a): the observed stability was 115-fold higher in the experiment with crude CDH than the one calculated using the equation developed for independent measurements (Equation 69). The enzyme even showed improved stability as compared to the experiment conducted with purified CDH (Chapter 3.6.5.1). Additionally, NOX^{009} demonstrated improved stability in comparison to the experiment conducted with purified CDH (Table 19) and in case if the equation of independent measurement (Equation 70) was used for calculating the NOX^{009} operational stability (approx. 8-fold).

A similar positive outcome regarding improved enzyme (operational) stabilities were noted in the experiment shown in Figure 59b, although the enzymes demonstrated deactivation during the CDH oxidation and had to be added two (AlDH) and four (NOX^{009}) times during 24 hours of the experiment. The operational stability rate constants (k_d) were estimated using the collected data (Figure 59b) and second-order kinetics (Equations 48 and 49), and the values are given in Table 27. It can be observed that with the second AlDH addition into the reactor, the enzyme exhibited improved operational stability.

The experimental data in Figure 59a show that almost full conversion of substrate CDH was achieved after 2.5 hours of the reaction, which was not obtained in the experiments with purified CDH, even after 24 hours of reaction (Figure 56c). Accordingly, in the experiment with purified CDH (140 mM, Figure 56c), the final CDH conversion was 82 % (23.9 g/L of produced CDHA; CDHA yield of 90 %), whereas in the experiment with 80 mM of crude CDH (Figure 59a) 98.9 % CDH conversion was accomplished after just 2.5 hours (14.4 g/L CDHA; yield of 98.9 %), and in the experiment with 335 mM of crude CDH (Figure 59b) 95.3 % CDH

List of reactant and product abbreviations: acetaldehyde (**AA**), chloroacetaldehyde (**CAA**), 4-chloro-3-hydroxybutanal (**CHB**), 6-chloro-3,5-dihydroxyhexanal (**CDH**), 6-chloro-3,5-dihydroxyhexanoic acid (**CDHA**), 3-hydroxy-4(-oxiran-2-yl)butanoic acid (**HOBA**), 6-cyano-3,5-dihydroxyhexanoic acid (**CYDHA**), 3-hydroxybutanal (**HB**), 3,5-dihydroxyhexanal (**DHH**).

conversion was achieved after 24 hours (58.3 g/L CDHA; yield of 95.4 %). It could be concluded that in case when the reaction was conducted with crude CDH, higher yields were achieved (≥ 95 %). Additionally, the experiment with 335 mM of CDH met the industrial requirements (Table 1).

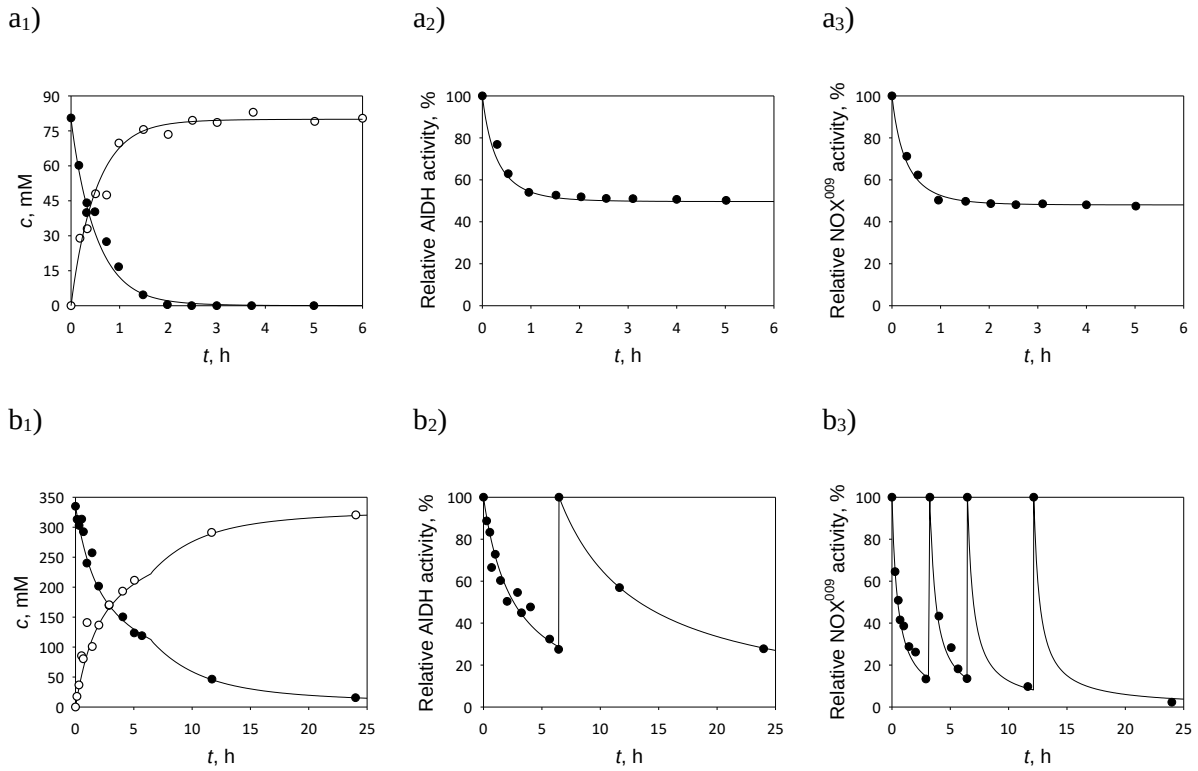

Figure 59 Experimental and simulation data of the AlDH-catalyzed oxidation of crude CDH into CDHA with NOX-catalyzed NAD^+ regeneration (0.1 M phosphate buffer pH 8, 1 000 rpm,, c_{NAD} = 10 mM, γ_{AlDH} = 10 mg/mL per addition, γ_{NOX009} = 10 mg/mL per addition, 25 °C). Experiment with a) 80 mM of CDH and b) 335 mM of CDH. Legend: experiment (dots), model (line); change of concentration with time: CDH (black), CDHA (white).

Table 21 Parameter estimated for the experiment shown Figure 59a for AlDH (Equation 50) and NOX^{009} (Equation 51).

Enzyme	*a*, 1/(mM·min)
AlDH	0.00039
NOX^{009}	0.00042

The results presented in Table 21 and Table 27 implicate that higher protein content, since the $DERA^{024}$ enzyme was present in the reaction mixture as well, positively affect the operational stabilities of AlDH and NOX^{009} [191].

List of reactant and product abbreviations: acetaldehyde (**AA**), chloroacetaldehyde (**CAA**), 4-chloro-3-hydroxybutanal (**CHB**), 6-chloro-3,5-dihydroxyhexanal (**CDH**), 6-chloro-3,5-dihydroxyhexanoic acid (**CDHA**), 3-hydroxy-4(-oxiran-2-yl)butanoic acid (**HOBA**), 6-cyano-3,5-dihydroxyhexanoic acid (**CYDHA**), 3-hydroxybutanal (**HB**), 3,5-dihydroxyhexanal (**DHH**).

Table 22 Deactivation rate constant estimated form the experimental data shown in Figure 59b.

Enzyme addition	k_d^{AlDH}, min^{-1}	k_d^{NOX009}, min^{-1}
1st	0.007	0.033
2nd	0.002	
3rd	-	
4th	-	

Comparing the deactivation rate constants estimated in experiments conducted with purified (Table 19, 5 mg/mL per enzyme) and crude CDH (Table 27, 10 mg/mL per enzyme), it is evident that higher initial enzyme concentration (5 *vs* 10 mg/mL per enzyme) contributed to the increase of the operational stability of NOX^{009}. The deactivation of AlDH was higher after its first than after its second addition into the reactor. This could be attributed to the presence of aldehydes in the reaction mixture, such as CHB and CHH, which had a negative effect on the AlDH activity, causing its deactivation. The second addition of AlDH resulted with a lower k_d value, which can be attributed to two facts. The first being relatively high protein concentration present in the reactor. The second, the diminished negative effects of CHB and CHH, which were oxidized into corresponding acids, because AlDH does not selectively oxidize aldehydes.

Table 23 BYs and STYs calculated for the experiments shown in Figure 59a and Figure 60.

Metric	80 mM of crude CDH	335 mM of crude CHD
BY, g_{CDH}/g_{AlDH}	2.9	3.7
STY, g/(L·day)	138.2	53.8

For both experiments shown in Figure 59 BYs and STYs were calculated and their values are given in Table 23. The developed mathematical model described the experimental results well (Figure 59a: R^2 = 0.99, σ = 4.10; Figure 59b: R^2 = 0.98, σ = 1.37).

3.6.6.2 Sequential one-pot CDH synthesis with KRED^{332}

The sequential one-pot CDH synthesis consisted of two reactions conducted in sequential manner:

3. DERA^{024}-catalyzed aldol reaction
4. KRED^{332}-catalyzed CDH oxidation without NADP$^+$ regeneration

List of reactant and product abbreviations: acetaldehyde (**AA**), chloroacetaldehyde (**CAA**), 4-chloro-3-hydroxybutanal (**CHB**), 6-chloro-3,5-dihydroxyhexanal (**CDH**), 6-chloro-3,5-dihydroxyhexanoic acid (**CDHA**), 3-hydroxy-4(-oxiran-2-yl)butanoic acid (**HOBA**), 6-cyano-3,5-dihydroxyhexanoic acid (**CYDHA**), 3-hydroxybutanal (**HB**), 3,5-dihydroxyhexanal (**DHH**).

The crude CDH substrate was obtained by carrying out the DERA^{024}-catalyzed reaction (Figure 47). Depending on the required crude CDH concentration, the reaction mixture was diluted using 0.1 M phosphate buffer pH 8 to obtain the desired CDH concentration.

The enzyme KRED^{332} was examined as an alternative catalyst in the reaction of crude CDH oxidation. The reaction was conducted with same substrate and enzyme concentration as the experiments catalyzed by the AlDH/NOX^{009} system (Figure 59). During the experiment, if the relative enzyme activity dropped below 20 %, a fresh amount of enzyme (same amount as the initial) was added into the reactor.

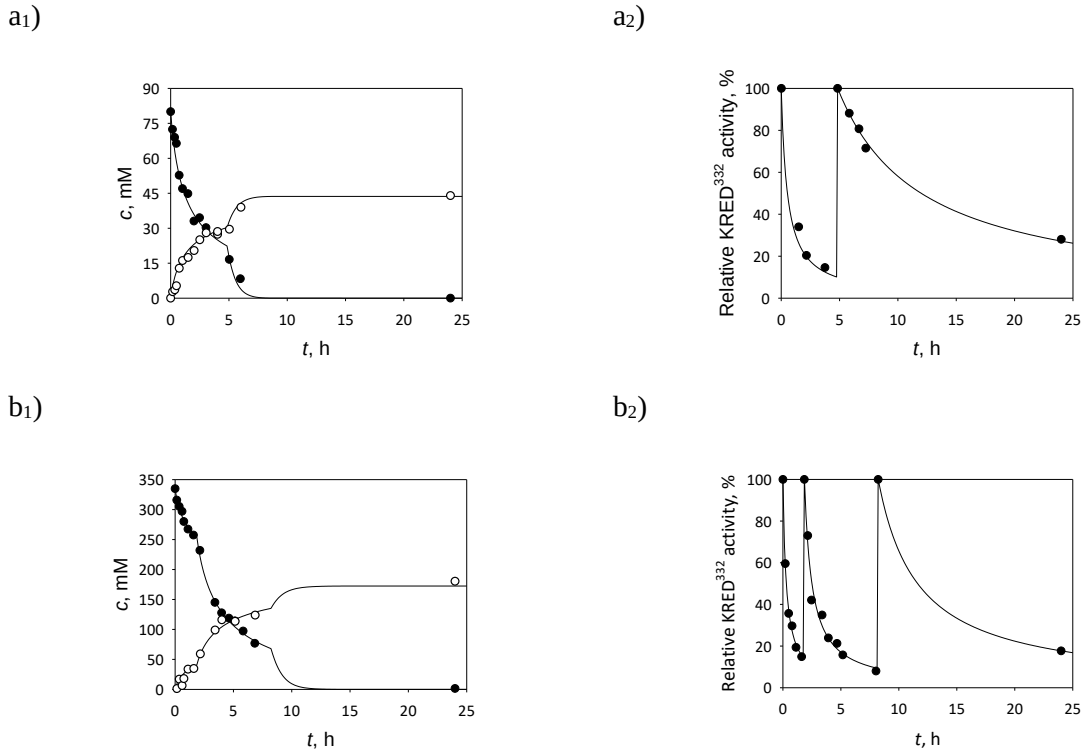

Figure 60 Experimental and simulation data of the KRED^{332}-catalyzed oxidation of crude CDH into CDHA (0.1 M phosphate buffer pH 8, c_{NADP} = 10 mM, $\gamma_{KRED332}$ = 10 mg/mL per addition, 1 000 rpm, 25 °C). Experiment with a) 80 mM of CDH and b) 335 mM of CDH. Legend: experiment (dots), model (line); change of concentration with time: CDH (black), CDHA (white).

The experimental and simulation data are shown in Figure 60, while the estimated deactivation constants ($k_d^{KRED332}$, Equation 59) are given in Table 24. Due to the increased protein content (presence of DERA^{024}) [191], KRED^{332} manifested higher operational stability than the stability expected by independent measurements when using Equation 71 (data not shown).

List of reactant and product abbreviations: acetaldehyde (**AA**), chloroacetaldehyde (**CAA**), 4-chloro-3-hydroxybutanal (**CHB**), 6-chloro-3,5-dihydroxyhexanal (**CDH**), 6-chloro-3,5-dihydroxyhexanoic acid (**CDHA**), 3-hydroxy-4(-oxiran-2-yl)butanoic acid (**HOBA**), 6-cyano-3,5-dihydroxyhexanoic acid (**CYDHA**), 3-hydroxybutanal (**HB**), 3,5-dihydroxyhexanal (**DHH**).

The reaction rate constant (r_{10}, Equation 54) for the KRED^{332}-catalyzed CDH reduction was previously estimated in the batch experiment (Chapter 3.6.5.2.3, 0.0011 mL/(mg·mM·min)).

The experimental data collected from the experiment conducted with 80 mM of CDH (Figure 60a) showed that full CDH conversion (> 99.9%) was accomplished after nine hours of reaction, while the CDHA yield was 54.6 % (7.9 g/L final CDHA concentration). In the experiment with 335 mM of CDHA (Figure 60b), almost full conversion was achieved (99.7%) after twelve hours of reaction, while the CDHA yield was 54 % and 31.3 g/L of CDHA concentration. By comparing those results with the results using pure CDH (60 mM, Figure 57), in which almost full conversion was obtained after six hours (99.8 %) and a CDHA yield of 53 % (6.0 g/L CDHA), it could be concluded that the yields were of similar value, regardless of the CDH concentration or form (purified or crude/unrefined).

Table 24 Deactivation rate constant estimated from the experimental data shown in Figure 60.

Enzyme addition	$k_d^{KRED332}$, min^{-1}
Oxidation of 80 mM CDH	
1st	0.0312
2nd	0.0065
Oxidation of 335 mM CDH	
1st	0.0560
2nd	0.0258
3rd	0.0049

Since KRED^{332} was inactivated during the reaction, the enzyme was added two (Figure 60a) or three (Figure 60b) times during the experiment. The experimental data for the time-dependence of KRED^{332} activity show that the enzyme deactivation decreases with each fresh enzyme addition as a result of CDH concentration reduction and protein content increase (Table 24). Comparing those results with the results of the experiment using purified CDH (Table 20), the experiments with crude CDH resulted in lower values of deactivation rate constants, because the reaction mixture had higher protein content due to the presence of the protein from the DERA^{024} reaction.

Table 25 BYs and STYs calculated for the experiments shown in Figure 60.

Metric	80 mM of crude CDH	335 mM of crude CHD
BY, $g_{CDH}/g_{KRED332}$	1.0	2.0
STY, g/(L·day)	21.1	62.6

List of reactant and product abbreviations: acetaldehyde (**AA**), chloroacetaldehyde (**CAA**), 4-chloro-3-hydroxybutanal (**CHB**), 6-chloro-3,5-dihydroxyhexanal (**CDH**), 6-chloro-3,5-dihydroxyhexanoic acid (**CDHA**), 3-hydroxy-4(-oxiran-2-yl)butanoic acid (**HOBA**), 6-cyano-3,5-dihydroxyhexanoic acid (**CYDHA**), 3-hydroxybutanal (**HB**), 3,5-dihydroxyhexanal (**DHH**).

The BYs and STYs were calculated for both conducted experiments (Figure 60) and are presented in Table 25. The goodness-of-fit statistics of the experimental and model simulation data (Figure 60) suggested a very good fit ($R^2 \geq 0.98$).

3.6.6.3 Sequential one-pot CYDH synthesis

The sequential one-pot CYDH synthesis consisted of four reactions conducted in a sequential manner:

1. DERA^{024}-catalyzed aldol reaction,
2. AlDH-catalyzed CDH oxidation with $NADP^+$ regeneration catalyzed by NOX^{009}, and
3. HHDH^{001}-catalyzed CDH dehalogenation, followed by
4. HHDH^{001}-catalyzed HOBA ring-opening with KCN.

The HHDH^{001}-catalyzed dehalogenation and epoxide ring-opening was conducted using the crude CDHA substrate obtained in the experiment of AlDH/NOX^{009}-catalyzed CDH oxidation shown in Figure 59b.

The value of the operational stability rate constant ($k_d^{HHDH001}$) was estimated to be 0.006 min^{-1}. It was estimated using the Equation 67 and the obtained experimental results from relative enzyme activity *vs* time (Figure 61b). It could be concluded that the value of the estimated deactivation constant was 2-fold higher than in the experiment with purified CDHA (Chapter 3.6.5.1), which could be due to the high initial substrate CDHA and KCN concentrations in the reactor.

The HHDH^{001}-catalyzed reaction was conducted with high concentration of substrates CDHA and KCN. HOBA and CYDHA were not quantified, since they are not commercially available. After 24 hours of the reaction, almost full CDHA conversion was obtained (99.99 %), while the enzyme residual activity was 25 %. From the HOBA simulation (Figure 61a) it could be observed that the epoxide is practically immediately consumed in the reaction of epoxide-ring opening with KCN. Using the simulation data, substrate CDHA conversion, product CYDHA yield, final CYDHA concentration, BY and STY were calculated. At the 18-hour mark, the CDHA conversion was 99.7 %, while the simulated CYDHA yield, with respect to CDHA, was 99.6 %. The simulated final product CYDHA concentration was 62.7 g/L, the simulated BY was 14.2 $g_{CYDHA}/g_{HHDH001}$ and the simulated STY was 83.6 g/(L·day).

List of reactant and product abbreviations: acetaldehyde (**AA**), chloroacetaldehyde (**CAA**), 4-chloro-3-hydroxybutanal (**CHB**), 6-chloro-3,5-dihydroxyhexanal (**CDH**), 6-chloro-3,5-dihydroxyhexanoic acid (**CDHA**), 3-hydroxy-4(-oxiran-2-yl)butanoic acid (**HOBA**), 6-cyano-3,5-dihydroxyhexanoic acid (**CYDHA**), 3-hydroxybutanal (**HB**), 3,5-dihydroxyhexanal (**DHH**).

a) b)

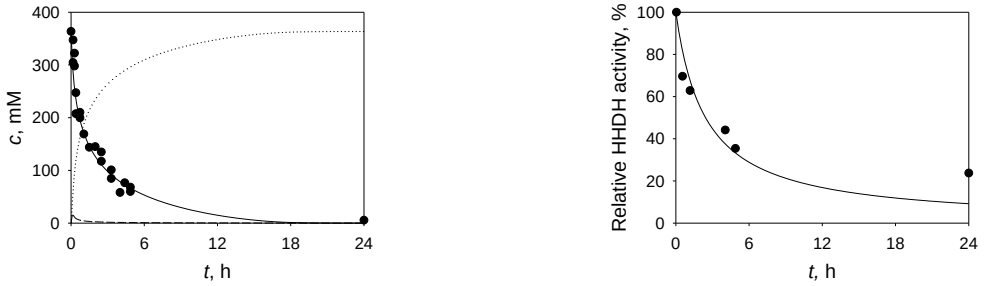

Figure 61 Experimental and simulation data of the HHDH^{001}-catalyzed dehalogenation and epoxide ring-opening of crude CDHA into CYDHA (0.1 M phosphate buffer pH 8, c_{CDHA} = 364 mM, c_{KCN} = 600 mM, $\gamma_{HHDH001}$ = 5 mg/mL, 1 000 rpm, 25 °C). Change of a) substrate CDHA, and b) relative enzyme activity during the experiment. Legend: experiment (dots), model (line); change of concentration over time: CDHA (dots), modeled concentration expressed as lines: CDHA (solid), HOBA (dashed), CYDHA (dotted).

Based on the goodness-of-fit statistics (R^2 = 0.97, σ = 2.8) and Figure 61, it could be concluded that the developed mathematical model described the experimental results well.

3.6.6.4 Concluding remarks: multi-step one-pot biocatalysis

Considering the estimated kinetic parameters for AlDH (Table 9), AlDH proved to be a more suitable enzyme for the reaction of CDH oxidation than KRED^{332} (Table 12). When considering the enzyme stability in presence of aldehydes, the KRED^{332} enzyme showed to be more aldehyde-resistant and, therefore, stable in presence of higher concentrations of CAA and CDH (Figure 31). It was observed that high protein content in the reactor had a significant stabilization effect on all three applied enzymes (AlDH, NOX, KRED^{332}). Both AlDH and KRED^{332} were stable during the reaction of pure CDH oxidation (Figures 56 and 57). When the oxidation was carried out with purified CDH, both enzymes (AlDH, KRED^{332}) manifested similar operational stability (k_d), for KRED^{332} being slightly lower (0.75-fold lower; Tables 19 and 20). When crude (unrefined) substrate CDH was applied, when the CDH reaction mixture contained a considerable amount of proteins (due to the use of the DERA^{024} CFE), the AlDH enzyme proved to be very stable and its operational stability rate constant was more than 10-times lower than the KRED^{332} operational stability rate constant under same reaction conditions. The AlDH stability in the reaction mixture increased 100 – 1500-fold, depending on the crude substrate concentration, i.e. protein content (Tables 22 and 24).

List of reactant and product abbreviations: acetaldehyde (**AA**), chloroacetaldehyde (**CAA**), 4-chloro-3-hydroxybutanal (**CHB**), 6-chloro-3,5-dihydroxyhexanal (**CDH**), 6-chloro-3,5-dihydroxyhexanoic acid (**CDHA**), 3-hydroxy-4(-oxiran-2-yl)butanoic acid (**HOBA**), 6-cyano-3,5-dihydroxyhexanoic acid (**CYDHA**), 3-hydroxybutanal (**HB**), 3,5-dihydroxyhexanal (**DHH**).

To obtain industrially relevant metrics, the reaction was conducted with 335 mM of CDH. The comparative results of the oxidation conducted by AlDH/NOX^{009} and KRED^{332} are presented in Table 26. The presented summary results show that AlDH/NOX^{009} is a better catalyst than KRED^{332}, although the reaction catalyzed by KRED^{332} was without $NADP^+$ regeneration. The KRED^{332}-catalyzed CDH oxidation was not further explored due to the obvious impact of the side reaction (the CDH reduction into CHO, Figure 1), which occurred in the KRED^{332}-catalyzed reaction resulting in lower CDHA yields.

Table 26 Results between AlDH/NOX^{009}- and KRED^{332}-catalyzed oxidation of 335 mM of crude CDH in batch reactor.

Catalyst	t, h [a]	X_{CDH}, %	Y_{CDHA}, %	γ_{CDH}, g/L	STY	BY
AlDH/NOX^{009}	24	95.3	95.4	53.8	53.8	2.9
KRED^{332}	12	99.7	54	31.3	62.6	2.0

[a] end of the reaction
Notes: STY is expressed as g/(L·day) and BY as g_{CHDA}/g_{AlDH} or $g_{CHDA}/g_{kRED332}$

The AlDH/NOX^{009} catalyst system thus fulfilled some important industrial requirements, such as substrate conversion (> 95 %) or final product concentration (> 50 g/L). Hence, it could be concluded that the AlDH was a more appropriate enzyme for the observed reaction than the KRED^{332} enzyme (Y_{CDHA}) and that it would be better to conduct the reaction with crude substrate than with a purified one (Chapter 3.6.5.1), due to the stabilization effects of the proteins present in the crude reaction solution. Additionally, the multi-enzyme (cascade) reaction setup represents an advantageous system, due to no need for a mid-step CDH isolation, making the process economically and environmentally more acceptable (circumvented mid-downstream processes). This way, the loss of product CDH is minimized and, consequently, the yield of product CDHA is maximized.

The HHDH^{001}-catalyzed reactions could only be examined as sequential one-pot reactions consisting of three stages: (1) DERA^{024}-, (2) AlDH/NOX^{009}-, and (3) HHDH^{001}-catalyzed reactions. A simultaneous one-pot reaction consisting of (1) DERA^{024}-catalyzed CDH synthesis and (2) simultaneous AlDH/NOX^{009}- and HHDH^{001}-catalyzed reactions could not be carried out due to the occurrence of the cyanohydrin reaction between the aldehyde CDH and KCN. This was tested by adding 1 M of KCN into the reaction solution obtained at the end of the DERA^{024} reaction (Figure 47). The HPLC analysis (Method 1, aldehyde derivatization) revealed that 300 mM CDH immediately reacted with KCN to yield corresponding α-

List of reactant and product abbreviations: acetaldehyde (**AA**), chloroacetaldehyde (**CAA**), 4-chloro-3-hydroxybutanal (**CHB**), 6-chloro-3,5-dihydroxyhexanal (**CDH**), 6-chloro-3,5-dihydroxyhexanoic acid (**CDHA**), 3-hydroxy-4(-oxiran-2-yl)butanoic acid (**HOBA**), 6-cyano-3,5-dihydroxyhexanoic acid (**CYDHA**), 3-hydroxybutanal (**HB**), 3,5-dihydroxyhexanal (**DHH**).

cyanohydrin, since no CDH could be detected in the analysis of the sample taken right after the addition of the cyanide. Thus, the reaction indeed cannot be carried out in a simultaneous mode.

Nevertheless, the HHDH^{001}-catalyzed dehalogenation and epoxide ring-opening with KCN was conducted using a purified (Chapter 3.6.5.1) and crude CDHA (Chapter 3.6.6.3) substrate. Due to commercial unavailability of HOBA and CYDHA, they were not quantified, but simulation data was used for calculating product yield, final product concentration, BY and STY (Table 27). This was done to obtain insight, but the model should be validated with the experimental data. Based on those results of the HHDH^{001}-catalyzed reaction with purified and crude CDHA, presented in Table 27, it could be concluded that the reaction could be simplified and thus carried out as a sequential one-pot system using the crude substrate as starting material. By observing the presented values for the experiment conducted with crude CDHA, it could be noted that all met the industrial requirements (Table 1).

Table 27 HHDH^{001}-catalyzed reaction with purified and crude CDHA substrate in batch reactor.

CDHA	c_{CDHA}, mM	t, h [a]	X_{CDHA}, %	Y_{CYDHA}, % [b]	γ_{CYDHA}, g/L [b]	STY [b]	BY [b]
Purified	85	3	99.9	99.9	14.6	116.8	7.5
Crude	364	18	99.7	99.6	62.7	83.6	14.2

[a] end of the reaction
[b] results calculated based on model simulation data
Notes: STY is expressed as g/(L·day) and BY as $g_{CYHDA}/g_{HHDH001}$.

List of reactant and product abbreviations: acetaldehyde (**AA**), chloroacetaldehyde (**CAA**), 4-chloro-3-hydroxybutanal (**CHB**), 6-chloro-3,5-dihydroxyhexanal (**CDH**), 6-chloro-3,5-dihydroxyhexanoic acid (**CDHA**), 3-hydroxy-4(-oxiran-2-yl)butanoic acid (**HOBA**), 6-cyano-3,5-dihydroxyhexanoic acid (**CYDHA**), 3-hydroxybutanal (**HB**), 3,5-dihydroxyhexanal (**DHH**).

4 SYNTHESIS OF THE SECOND STATIN SIDE-CHAIN PRECURSOR

4.2 Introduction

The second reaction route consisted of two enzyme-catalyzed reactions in the following order (Figure 2):

1. DERA^{062}-catalyzed double-aldol reaction, and
2. KRED^{354}-catalyzed oxidation with NADP+ regeneration catalyzed by NADPH-dependent auxiliary enzyme

The starting materials of the aldol reaction were *N*-(3-oxopropyl)-2-phenylacetamide (OPA) and AA. The aldol reaction resulted in the formation of *N*-(2-((2*R*,4*R*)-4,6-dihydroxytetrahydro-2*H*-pyran-2-yl)ethyl)-2-phenylacetamide (DHP) which was subsequently oxidized into *N*-(2-((2*R*,4*R*)-4-hydroxy-6-oxotetrahydro-2*H*-pyran-2-yl)ethyl)-2-phenylacetamide (HOP). The oxidation was paired with an $NADP^+$ regeneration system. Two different enzymes were examined for that purpose: the H_2O-forming NOX (NOX^{001}) and NADPH-dependent DH (KRED^{011}), in which case co-substrate acetone (ACE) was added.

The DERA^{062}-catalyzed side reaction of self-aldol addition of AA is a two-step reaction (Figure 3) that results with the production of DHH.

The substrate and product abbreviation list are presented in Table 28.

Table 28 Abbreviation list of compounds of the first statin side-chain reaction route.

Abbreviation	Full name of the compound
AA	Acetaldehyde
OPA	*N*-(3-oxopropyl)-2-phenylacetamide
DHP	*N*-(2-((2*R*,4*R*)-4,6-dihydroxytetrahydro-2*H*-pyran-2-yl)ethyl)-2-phenylacetamide
HOP	*N*-(2-((2*R*,4*R*)-4-hydroxy-6-oxotetrahydro-2*H*-pyran-2-yl)ethyl)-2-phenylacetamide
DHH	3,5-dihidroxyhexanal

List of reactant and product abbreviations: acetaldehyde (**AA**), *N*-(3-oxopropyl)-2-phenylacetamide (**OPA**), *N*-(2-((2*R*,4*R*)-4,6-dihydroxytetrahydro-2*H*-pyran-2-yl)ethyl)-2-phenylacetamide (**DHP**), *N*-(2-((2*R*,4*R*)-4-hydroxy-6-oxotetrahydro-2*H*-pyran-2-yl)ethyl)-2-phenylacetamide (**HOP**), 3,5-dihidroxyhexanal (**DHH**).

4.3 Experimental part

4.3.1 Materials

In this thesis, following chemicals were used: acetone (ACE), dichloromethane (DCM), ethyl acetate (EtOAc), hydrochloric acid, $NADP^+$, nitric acid, sulfuric acid (BDH Prolabo Chemicals, UK), 2-deoxyribose 5-phosphate sodium salt (DRP), 3-hydroxybutanal (aldol, CHB), acetaldehyde (AA), magnesium sulfate anhydrous, triosephosphate isomerase from rabbit muscle (TPI), α-glycerophosphate dehydrogenase from rabbit muscle (GDH), σ-benzylhydroxylamine hydrochloride (Merck, Germany); dipotassium phosphate, methanol (MetOH), monopotassium phosphate, NAD^+, NADH, $NADP^+$, potassium hydroxide, propionaldehyde (PA), pyridine, silica gel (0.035-0.070 mm, 60 Å, for chromatography), triethanolamine hydrochloride (TEA-HCl), tris(hydroxymethyl)aminomethane (Tris), *O*-benzylhydroksylamine hydrochloride (Acros Organics, USA); acetic acid (T.T.T., Croatia); acetonitrile (ACN), ethanol absolute (EtOH), magnesium sulfate anhydrous, trifluoroacetic acid (TFA) (Fisher Scientific, UK); albumin from bovine serum (BSA) (Fluka Chemie, Germany); isopropyl alcohol (IPA), potassium hydroxide (Kemika, Croatia), Coomassie brilliant blue G-250, sodium chloride, sodium sulfate anhydrous (Lach-Ner, Czech Republic); NADPH (AppliChem, Germany); sodium hydroxide (Gram-mol, Croatia).

Large quantities of purified *N*-(3-oxopropyl)-2-phenylacetamide (OPA) were provided by Enzymicals (Germany).

The 2-deoxyribose-5-phosphate aldolases ($DERA^{062}$) and NAD(P)(H)-dependent dehydrogenases (NOX^{001}, $KRED^{011}$, $KRED^{354}$) were expressed and supplied by Prozomix (UK), while the halohydrin dehalogenase ($HHDH^{001}$) was expressed and provided by Enzymicals (Germany). The enzymes were supplied as cell-free extracts (CFEs).

4.3.2 Apparatus

Same apparatus were used as in Chapter 3.3.2.

List of reactant and product abbreviations: acetaldehyde (**AA**), *N*-(3-oxopropyl)-2-phenylacetamide (**OPA**), *N*-(2-((2*R*,4*R*)-4,6-dihydroxytetrahydro-2*H*-pyran-2-yl)ethyl)-2-phenylacetamide (**DHP**), *N*-(2-((2*R*,4*R*)-4-hydroxy-6-oxotetrahydro-2*H*-pyran-2-yl)ethyl)-2-phenylacetamide (**HOP**), 3,5-dihidroxyhexanal (**DHH**).

4.3.3 Analytical methods

4.3.3.1 HPLC analysis

The HPLC analysis was done on the Phenomenex Kinetex RP-HPLC column (C18, 5 μm, 250 x 4.6 mm, 100 Å).

The samples were analyzed with and without the application of a aldehyde derivatization procedure. The derivatization procedures are described in Chapter 3.3.3.1. If the samples were analyzed without prior compound derivatization, the non-derivatized samples were diluted in ACN, vortexed and centrifuged (14 000 rpm, 4 °C, 5 min) to remove any solid and analyzed by HPLC.

To analyze derivatized aldehyde and carboxylic acid samples Method 2 was used. The mobile phase consisted of solvent A (mixture of ACN, water and TFA in the ratio 80:20:0.1) and solvent B (0.1 % v/v TFA in water) with gradient elution from 90 to 30 % B for the first 12 minutes and from 30 to 90 % B from minute 16 to 18. The flow rate was 1.5 mL/min, the column temperature was set at 30 °C and the UV detection at 215 nm. Examples of calibration curves are presented in the Appendix. Calibration curve for OPA is shown in Appendix figure 10, DHP in Appendix figure 11, AA shown in Appendix figure 12, while for DHH in Appendix figure 13. The retention time of AA, OPA, DHP, HB and DHH were 12.6, 13.0, 11.2, 10.2 and 9.2 minutes, respectively, while the retention time of the HOP was 6.2 minutes. Respective examples HPLC chromatograms for the DERA^{062}-catalyzed aldol addition are shown in Figure 105, while for the KRED^{354}-catalyzed DHP oxidation in Figure 106.

To analyze non-derivatized analytes OPA, DHP and acetic acid Method 3 was used. The mobile phase consisted of solvent A (mixture of ACN, water and TFA in the ratio 80:20:0.1) and solvent B (0.1 % v/v TFA in water) with gradient elution from 100 to 80 % B for the first 13 minutes and from 80 to 100 % B from minute 15 to 16. The flow rate was 1.5 mL/min, the column temperature was set at 30 °C and the UV detection at 215 nm. Examples of calibration curves are presented in the Appendix: in Appendix figure 14 for OPA, Appendix figure 15 for DHP and Appendix figure 16 for acetic acid. The retention time of OPA, DHP and acetic acid were 19.5, 21.0 and 1.9 minutes, respectively. Respective example HPLC chromatograms are shown in Appendix figure 21 for OPA and DHP, while for the acetic acid is shown in Appendix figure 22.

List of reactant and product abbreviations: acetaldehyde (**AA**), *N*-(3-oxopropyl)-2-phenylacetamide (**OPA**), *N*-(2-((2*R*,4*R*)-4,6-dihydroxytetrahydro-2*H*-pyran-2-yl)ethyl)-2-phenylacetamide (**DHP**), *N*-(2-((2*R*,4*R*)-4-hydroxy-6-oxotetrahydro-2*H*-pyran-2-yl)ethyl)-2-phenylacetamide (**HOP**), 3,5-dihidroxyhexanal (**DHH**).

4.3.3.2 Spectrophotometric measurements

4.3.3.2.1 Quantitative determination of protein content

The procedure is described in Chapter 3.3.3.2.1.

4.3.3.3 Enzyme assays

All enzymes used in this work were provided as CFEs and were used without further purification unless stated otherwise. All measurements were carried out in quartz cuvettes (10 mm path, 1 mL) at 25 °C.

The specific enzyme activity was calculated following the procedure described in Chapter 3.3.3.3 and using the Equation 19.

4.3.3.3.1 DERA^{062} activity assay

To measure the activity of DERA^{062}, DRP Assay was used. The procedure is described in Chapter 3.3.3.3.1.

4.3.3.3.2 Activity assays for oxidoreductases

The KRED^{354} activity mixture contained 600 mM PA, 0.1 mM NADPH and diluted KRED^{354} enzyme (0.1 mg/mL) in 0.1 M phosphate buffer pH 7. The reaction was initiated by the addition of KRED^{354}, and the subsequent decrease of NADPH concentration was monitored at 340 nm. 1 U of KRED^{354} activity was defined as the amount of enzyme required for oxidation of 1 μmol of NADPH per minute 0.1 M phosphate buffer pH 7 at 25 °C.

The NOX^{001} activity mixture contained 0.1 mM NADPH and diluted NOX^{001} enzyme (0.04 mg/mL) in 0.1 M phosphate buffer pH 7. The reaction was initiated by the addition of NOX^{001}, and the subsequent decrease of NADPH concentration was monitored at 340 nm. 1 U of NOX^{001} activity was defined as the amount of enzyme required for oxidation of 1 μmol of NAPDH per minute 0.1 M phosphate buffer pH 7 at 25 °C.

The KRED^{011} activity mixture contained 30 mM ACE, 0.1 mM NADPH and diluted KRED^{11} enzyme (0.01 mg/mL) in 0.1 M phosphate buffer pH 7. The reaction was initiated by the addition of KRED^{11}, and the subsequent decrease of NADPH concentration was monitored

List of reactant and product abbreviations: acetaldehyde (**AA**), *N*-(3-oxopropyl)-2-phenylacetamide (**OPA**), *N*-(2-((2*R*,4*R*)-4,6-dihydroxytetrahydro-2*H*-pyran-2-yl)ethyl)-2-phenylacetamide (**DHP**), *N*-(2-((2*R*,4*R*)-4-hydroxy-6-oxotetrahydro-2*H*-pyran-2-yl)ethyl)-2-phenylacetamide (**HOP**), 3,5-dihidroxyhexanal (**DHH**).

at 340 nm. 1 U of KRED[11] activity was defined as the amount of enzyme required for oxidation of 1 μmol of NADPH per minute 0.1 M phosphate buffer pH 7 at 25 °C.

4.2.4. Synthesis and purification of chemicals

4.2.4.1. Enzymatic synthesis and purification of DHP

The DHP was obtained by carrying the reaction in a repetitive batch mode (glass bottle, 50 mL). The reaction of total reaction volume of 100 mL was conducted with 100 mM of OPA and 400 mM AA and catalyzed by DERA^{062} (30 mg/mL) in 0.1 M phosphate buffer pH 7 placed on a shaker (200 rpm, 25 °C). After 2.5 and 5.2 hours from the beginning of the reaction, an additional quantity of fresh substrates of the same concentration as the initial were added into the reactor, while the additional amount of DERA^{062} of 15 mg/mL was added after 6.5 hours. After 24 hours from the beginning of the reaction, the reaction solution was transferred into two CFUs (15 mL) and centrifuged (4 °C, 5 000 rpm, 60 min) to remove the enzyme. The filtrate was equally divided into four conical centrifuge tubes (15 mL) and frozen at -80 °C overnight. The frozen samples were lyophilized for 48 hours using the freeze dryer and then purificatied *via* preparative column chromatography (CC).

Figure 2 Column chromatography (CC).

The DHP sample (0.6 g) was purified using a glass column (21 x 1.5 cm) with silica gel (14 g) as the stationary phase (Figure 62). DCM was used as mobile phase A, while a mixture of solvents (DCM, ACE and acetic acid in ratio 60:30:1) was used as mobile phase B. The sample was placed into the column and the column was washed with 38 mL of mobile phase A. After that, the solvent was switched to mobile phase B. The fractions of 10 to 15 mL were

List of reactant and product abbreviations: acetaldehyde (**AA**), *N*-(3-oxopropyl)-2-phenylacetamide (**OPA**), *N*-(2-((2*R*,4*R*)-4,6-dihydroxytetrahydro-2*H*-pyran-2-yl)ethyl)-2-phenylacetamide (**DHP**), *N*-(2-((2*R*,4*R*)-4-hydroxy-6-oxotetrahydro-2*H*-pyran-2-yl)ethyl)-2-phenylacetamide (**HOP**), 3,5-dihidroxyhexanal (**DHH**).

collected and analyzed using the HPLC Method 3. Those fractions which contained the aldol product were pooled and the solvent was removed under reduced pressure (40 °C). Since the presence of low quantities of acetic acid were noted in the obtained DHP sample, to remove the acetic acid, the sample was diluted in 2 mL of ultrapure water, disseminated in 1.5 mL-locking centrifuges, frozen at -80 °C and lyophilized for 24 hours (Figure 63).

Figure 63 Removal of acetic acid from the CDHA sample by diluting the CDHA sample obtained after evaporation. CDHA lyophilization in 1.5 mL-locking microcentrifuges.

4.2.4.2. Enzymatic synthesis of HOP

Due to unavailability of purified HOP, it was biocatalytically produced by carrying the KRED^{354}-catalyzed DHP oxidation. The reaction (1 mL) was conducted in a batch reactor (locking microcentrifuge tube, 1.5 mL) placed on a shaker (1 000 rpm, 25 °C) in 0.1 phosphate buffer pH 8 at 25 °C with 50 mM of DHP, 10 mM $NADP^+$, 10 mg/mL NOX^{001} and 10 mg/mL KRED^{354}. The addition of KRED^{354} was the start of the reaction. After 2.5 hours from the beginning of the reaction, full DHP conversion into HOP was obtained. The reaction was stopped by transferring the reaction mixture into two CFUs (0.50 mL) to precipitate the proteins by centrifugation (60 min, 14 000 rpm, 4 °C). The supernatant was transferred into a locking microcentrifuge tube (1.5 mL) that was placed on a shaker (1 000 rpm, 25 °C) to assess the HOP stability. The change of HOP concentration was monitored using the HPLC Method 3.

4.2.5 Influence of buffers on DERA^{062} stability

The DERA^{062} stability was assest in the following buffers: 0.1 M phosphate buffer (pH 6 – 8), 0.1 M TEA-HCl buffer pH 7 and 0.1 M Tris-HCl buffer (pH 7 and 8). The stability was determined by dissolving 10 mg/mL DERA^{062} in the chosen buffer in a 1.5 mL-locking microcentrifuge tube by incubating it using a thermomixer (1 000 rpm, 25 °C) for three days. The residual DERA^{062} activity was measured by applying the DRP Assay.

List of reactant and product abbreviations: acetaldehyde (**AA**), *N*-(3-oxopropyl)-2-phenylacetamide (**OPA**), *N*-(2-((2*R*,4*R*)-4,6-dihydroxytetrahydro-2*H*-pyran-2-yl)ethyl)-2-phenylacetamide (**DHP**), *N*-(2-((2*R*,4*R*)-4-hydroxy-6-oxotetrahydro-2*H*-pyran-2-yl)ethyl)-2-phenylacetamide (**HOP**), 3,5-dihidroxyhexanal (**DHH**).

4.2.6 Influence of OPA and AA on DERA^{062} stability

The influence of OPA and AA on the stability of DERA^{062} was examined by placing the enzyme in a single-aldehyde solution. The experiments were carried out in 1.5 mL-locking microcentrifuge tubes with a total reaction volume of 1 mL by placing the tube containing the enzyme dissolved in the solution on a shaker at 1 000 rpm and 25 °C for 3 h. During incubation, the samples were taken at regular time intervals to measure the residual activity using the DRP Assay. Prior to carrying out the activity measurements, the compound was removed using 0.5 mL-CFUs and the DERA^{062} residue was washed with 0.1 M TEA-HCl pH 7, respecting the enzyme concentration in the DRP Assay. To determine the enzyme's operational stability decay rate constant the activity was measured using the same procedure.

4.2.7 Enzyme kinetics

The kinetic measurements were carried following the description given in Chapter 3.3.8. All kinetic measurements concerning DERA^{062} were following using the HPLC Method 2, while kinetic measurements concerning oxidoreductases were measured spectrophotometrically at 340 nm in 1 mL-quartz cuvettes (10 mm path).

4.2.8 Reactor experiments: one-step biocatalysis

The reactions for the synthesis of the second statin side-chain precursor were carried out following the procedure described in Chapter 3.3.9. To determine the concentration of substrates and products *via* HPLC, Method 2 and Method 3 were used.

Since KRED^{354} requires the presence of the $NADP^+$ coenzyme to be catalytically active, the coenzyme was added into the reactor prior to the addition of KRED^{354}. When needed, the pH of the reaction solution was adjusted using the 5 M KOH solution, since the pH decreased during the DHP oxidation.

4.2.8.1 DERA^{062}-catalyzed aldol addition

The DERA^{062}-catalyzed tandem aldol addition of AA onto OPA was conducted in batch, repetitive-batch and fed-batch reactor modes in 0.1 M phosphate buffer pH 6. During all reactions, the samples were taken at regular time-intervals to evaluate the substrate and product concentration *via* HPLC and the residual DERA^{062} activity using the DRP assay.

List of reactant and product abbreviations: acetaldehyde (**AA**), *N*-(3-oxopropyl)-2-phenylacetamide (**OPA**), *N*-(2-((2*R*,4*R*)-4,6-dihydroxytetrahydro-2*H*-pyran-2-yl)ethyl)-2-phenylacetamide (**DHP**), *N*-(2-((2*R*,4*R*)-4-hydroxy-6-oxotetrahydro-2*H*-pyran-2-yl)ethyl)-2-phenylacetamide (**HOP**), 3,5-dihidroxyhexanal (**DHH**).

The batch reaction was conducted in a 2 mL-locking microcentrifuge tube placed on a shaker at 1 000 rpm. Reaction conditions are given in detail in Figure 75. The repetitive-batch reaction of reaction volume of 4 mL was conducted in a 5 mL-glass bottle used as a batch reactor placed on a shaker at 400 rpm. The reaction was performed with several substrates and/or enzyme additions. New amounts of OPA and AA were added once their full conversion was attained, while fresh amounts of DERA^{062} were added once the enzyme showed low residual relative activity of below 20 %. Full reaction conditions are given in Figure 76. The reaction in fed-batch reactor was conducted in a 5 mL-glass bottle. The reaction setup consisted of AA supply using a syringe pump, while OPA and DERA^{062} were added into the reactor prior the beginning of the reaction. Full reaction conditions and details are given in Figure 77.

3.9.1.2 KRED^{354}-catalyzed DHP oxidation

All KRED^{354}-catalyzed DHP oxidations were conducted in a 2 mL-locking microcentrifuge tube used as a batch reactor placed on a shaker at 1 000 rpm in 0.1 M phosphate buffer pH 8 with purified DHP. In case when the coenzyme regeneration was required, *in situ* NADP$^+$ regeneration system was used. Two different auxiliary enzymes were investigated: NOX^{001} and KRED^{011}. When the NADP$^+$ regeneration was performed by KRED^{011}, ACE was added into the reactor as a co-substrate.

4.2.9 Reactor experiments: multi-step one-pot biocatalysis

The cascade reactions in the second reaction route for the synthesis of statin intermediate were carried following the procedure described in Chapter 3.3.10. To determine the concentration of substrates and products *via* HPLC, Method 2 and Method 3 were used.

Because KRED^{354} requires the presence of the NADP$^+$, the coenzyme was added into the reactor prior to the addition of KRED^{354}. When needed, the pH of the reaction solution was adjusted using the 5 M KOH solution, since the pH decreased during the DHP oxidation.

4.3.3.4 Cascade synthesis of HOP without and with NADP$^+$ regeneration

The sequential multi-step one-pot reaction of HOP production consisted of two consecutive reactions:

1. DERA^{062}-catalyzed aldol addition, and

List of reactant and product abbreviations: acetaldehyde (**AA**), *N*-(3-oxopropyl)-2-phenylacetamide (**OPA**), *N*-(2-((2*R*,4*R*)-4,6-dihydroxytetrahydro-2*H*-pyran-2-yl)ethyl)-2-phenylacetamide (**DHP**), *N*-(2-((2*R*,4*R*)-4-hydroxy-6-oxotetrahydro-2*H*-pyran-2-yl)ethyl)-2-phenylacetamide (**HOP**), 3,5-dihidroxyhexanal (**DHH**).

2. KRED^{354}-catalyzed DHP oxidation without and with coenzyme regeneration.

The reactions were conducted in 2 mL-locking microcentrifuge tubes used as batch reactors. The first reaction was the DERA^{062}-catalyzed aldol reaction of AA and OPA in a batch reactor (0.1 M phosphate buffer pH 7). Once total AA and OPA conversion were obtained, if needed, the obtained reaction solution was diluted to desired DHP concentration using 0.1 M phosphate buffer pH 8 and the pH of that reaction solution was further adjusted using 5 M KOH. The second reaction was the KRED^{354}-catalyzed DHP oxidation with and without coenzyme NADP$^+$ regeneration. The coenzyme regeneration was accomplished by the action of NOX^{001} or KRED^{011} as an auxiliary enzyme. In case when the coenzyme regeneration was conducted by KRED^{011}, ACE was added into the reactor as a co-substrate. Full reaction conditions are given in detail in Figure 75 (DERA^{062}-catalyzed aldol reaction), Figure 84 (KRED^{354}-catalyzed DHP oxidation without NADP$^+$ regeneration), Figure 85 (KRED^{354}-catalyzed DHP oxidation with NADP$^+$ regeneration catalyzed by NOX^{001}) and Figure 86 (KRED^{354}-catalyzed DHP oxidation with NADP$^+$ regeneration catalyzed by KRED^{011}).

4.4 Mathematical modeling

The kinetic parameters were estimated from the dependence of the initial reaction rate on the concentrations of compounds in single- and multi-enzyme reactions. The mathematical models for all enzyme-catalyzed reactions. The mathematical model consisted of kinetic equations, mass balance equations in an appropriate reactor and operational stability decay equations. The model was developed using the estimated kinetic parameters and relevant reaction scheme.

4.4.1 DERA^{062}-catalyzed aldol additions

The reaction rate r_1 for DERA^{062}-catalyzed double addition of AA to OPA (Figure 64a) was described by the double-substrate Michaelis-Menten kinetics (Equation 79). The reaction rate r_2 for the DERA^{062}-catalyzed AA self-aldol addition (Figure 64b) was described by three-substrate Michaelis-Menten kinetics (Equation 80), while the reaction rate r_3 of its reverse reaction was described using the first-order kinetic model (Equation 81).

List of reactant and product abbreviations: acetaldehyde (**AA**), *N*-(3-oxopropyl)-2-phenylacetamide (**OPA**), *N*-(2-((2*R*,4*R*)-4,6-dihydroxytetrahydro-2*H*-pyran-2-yl)ethyl)-2-phenylacetamide (**DHP**), *N*-(2-((2*R*,4*R*)-4-hydroxy-6-oxotetrahydro-2*H*-pyran-2-yl)ethyl)-2-phenylacetamide (**HOP**), 3,5-dihidroxyhexanal (**DHH**).

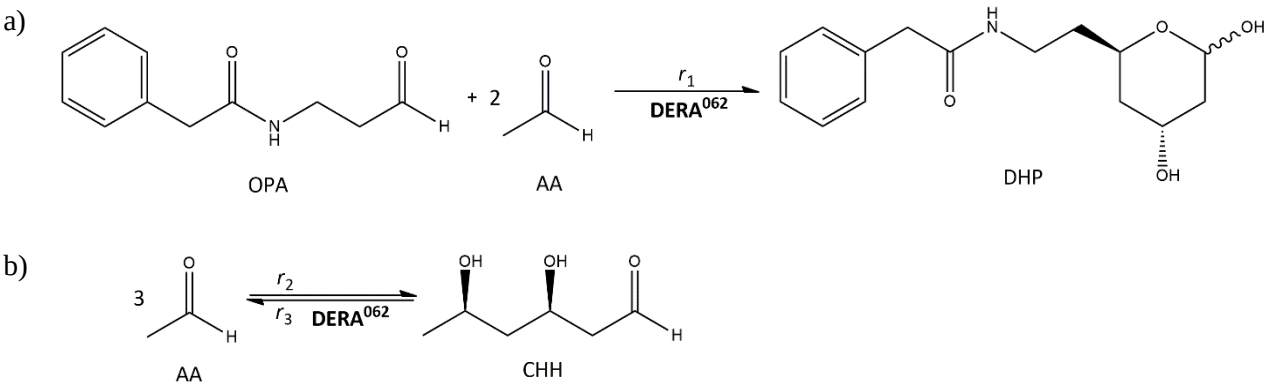

Figure 64 Reaction scheme of DERA^{062}-catalyzed a) tandem AA addition onto OPA and b) AA self-aldol addition.

$$r_1 = \frac{V_{m,1} \cdot \gamma_{\mathrm{DERA062}} \cdot c_{AA} \cdot c_{OPA}}{\left(K_{m,1}{}^{AA} + c_{AA}\right) \cdot \left(K_{m,1}{}^{OPA} + c_{OPA}\right)} \qquad \text{Equation 79}$$

$$r_2 = \frac{V_{m,2} \cdot \gamma_{\mathrm{DERA062}} \cdot c_{AA}^3}{\left(K_{m,2}{}^{AA} + c_{AA}\right)^3} \qquad \text{Equation 80}$$

$$r_3 = k_3 \cdot \gamma_{\mathrm{DERA062}} \cdot c_{DHH} \qquad \text{Equation 81}$$

The mass balances for substrates AA and OPA and products DHP and DHH in the batch and repetitive batch reactor are presented by Equations 82 – 85, respectively. The operational stability decay in batch and in repetitive batch reactor was described using the second-order kinetic (Equation 86).

$$\frac{\mathrm{d}c_{\mathrm{AA}}}{\mathrm{d}t} = -r_1 - 3 \cdot r_2 + 3 \cdot r_3 \qquad \text{Equation 82}$$

$$\frac{\mathrm{d}c_{OPA}}{\mathrm{d}t} = -r_1 \qquad \text{Equation 83}$$

$$\frac{\mathrm{d}c_{DHP}}{\mathrm{d}t} = r_1 \qquad \text{Equation 84}$$

$$\frac{\mathrm{d}c_{\mathrm{DHH}}}{\mathrm{d}t} = -r_3 + r_2 \qquad \text{Equation 85}$$

$$\frac{\mathrm{d}\gamma_{\mathrm{DERA062}}}{\mathrm{d}t} = -k_d^{DERA062} \cdot \gamma_{\mathrm{DERA062}}^2 \qquad \text{Equation 86}$$

List of reactant and product abbreviations: acetaldehyde (**AA**), *N*-(3-oxopropyl)-2-phenylacetamide (**OPA**), *N*-(2-((2*R*,4*R*)-4,6-dihydroxytetrahydro-2*H*-pyran-2-yl)ethyl)-2-phenylacetamide (**DHP**), *N*-(2-((2*R*,4*R*)-4-hydroxy-6-oxotetrahydro-2*H*-pyran-2-yl)ethyl)-2-phenylacetamide (**HOP**), 3,5-dihidroxyhexanal (**DHH**).

The mass balance equations for reactants AA and OPA and products DHP and DHH in the fed-batch reactor are presented by Equation 87 – 90. Equation 91 represents the change in reactor volume during the aldol reaction. The DERA^{062} operational stability decay in the fed-batch reactor was described by Equation 92.

$$\frac{\mathrm{d}c_{AA}}{\mathrm{d}t} = \frac{1}{V} \cdot \left(-c_{AA} \cdot \frac{\mathrm{d}V}{\mathrm{d}t} + c_{AA,0} \cdot q_1\right) - 2 \cdot r_1 - 3 \cdot r_2 + 3 \cdot r_3 \qquad \text{Equation 87}$$

$$\frac{\mathrm{d}c_{OPA}}{\mathrm{d}t} = \frac{1}{V} \cdot \left(-c_{OPA} \cdot \frac{\mathrm{d}V}{\mathrm{d}t}\right) - r_1 \qquad \text{Equation 88}$$

$$\frac{\mathrm{d}c_{DHP}}{\mathrm{d}t} = \frac{1}{V} \cdot \left(-c_{DHP} \cdot \frac{\mathrm{d}V}{\mathrm{d}t}\right) + r_1 \qquad \text{Equation 89}$$

$$\frac{\mathrm{d}c_{DHH}}{\mathrm{d}t} = \frac{1}{V} \cdot \left(-c_{DHH} \cdot \frac{\mathrm{d}V}{\mathrm{d}t}\right) + r_2 - r_3 \qquad \text{Equation 90}$$

$$\frac{\mathrm{d}V}{\mathrm{d}t} = q \qquad \text{Equation 91}$$

$$\frac{\mathrm{d}\gamma_{DERA062}}{\mathrm{d}t} = \frac{1}{V} \cdot \left(-\gamma_{DERA062} \cdot \frac{\mathrm{d}V}{\mathrm{d}t}\right) - k_d^{DERA062} \cdot \gamma_{DERA062}^2 \qquad \text{Equation 92}$$

The operational stability decay rate constants in all types of reactors were calculated from the second-order model that includes its dependency on the AA and OPA concentration (Equation 93).

$$k_d^{DERA062} = \sum_i a \cdot c_i^2 + b \cdot c_i \qquad \text{Equation 93}$$

4.4.2 KRED^{354}-catalyzed DHP oxidation with NADP$^+$ regeneration catalyzed by NOX^{001} or KRED^{011}

The reaction rate r_4 for KRED^{354}-catalyzed oxidation of DHP into HOP (Figure 65a) was described by double-substrate Michaelis-Menten kinetics with substrate DHP and product NADPH inhibition (Equation 94). Since this enzyme is coenzyme-dependent, two possible enzymes for the regeneration of NADP$^+$ coenzyme were considered: NOX^{001} (Figure 65b) and KRED^{011} (Figure 65c). If the regeneration was carried out using the KRED^{011} as the auxiliary enzyme, which requires ACE as a substrate, the Equation 94 was extended with corresponding terms, since it was noted that both ACE and IPA, which are co-substrate and co-product of the regeneration reaction, inhibit the man reaction of DHP oxidation.

List of reactant and product abbreviations: acetaldehyde (**AA**), *N*-(3-oxopropyl)-2-phenylacetamide (**OPA**), *N*-(2-((2*R*,4*R*)-4,6-dihydroxytetrahydro-2*H*-pyran-2-yl)ethyl)-2-phenylacetamide (**DHP**), *N*-(2-((2*R*,4*R*)-4-hydroxy-6-oxotetrahydro-2*H*-pyran-2-yl)ethyl)-2-phenylacetamide (**HOP**), 3,5-dihidroxyhexanal (**DHH**).

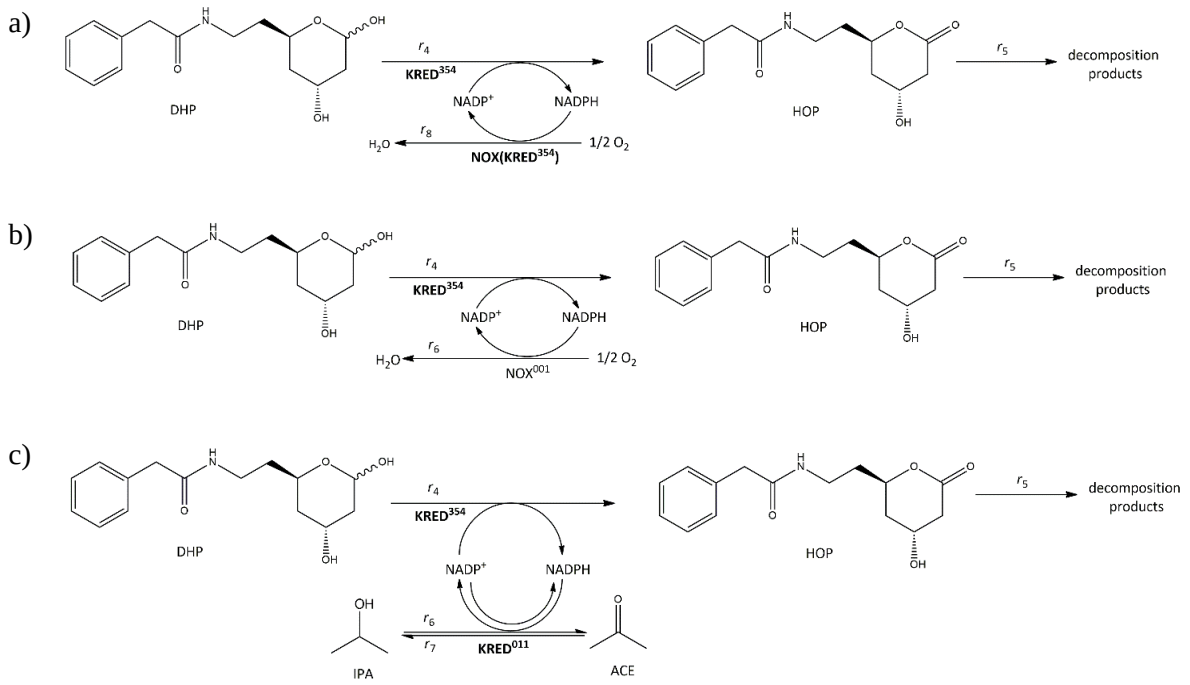

Figure 65 Reaction scheme of KRED^{354}-catalyzed DHP oxidation: a) without coenzyme regeneration, b) combined with NOX^{001}-catalyzed NADP$^+$ regeneration and c) combined with KRED^{011}-catalyzed NADP$^+$ regeneration.

$$r_4 = \frac{V_{m,4} \cdot \gamma_{KRED354} \cdot c_{DHP} \cdot c_{NADP^+}}{\left[K_{m,4}^{DHP} \cdot \left(1 + \frac{c_{ACE}}{K_{i,4}^{ACE}} + \frac{c_{IPA}}{K_{i,4}^{IPA}}\right) + c_{DHP} \cdot \left(1 + \frac{c_{DHP}}{K_{iS,4}^{DHP}}\right)\right] \cdot \left[K_{m,4}^{NADP^+} \cdot \left(1 + \frac{c_{NADPH}}{K_{i,4}^{NADPH}}\right) + c_{NADP^+}\right]}$$

Equation 94

While carrying out the batch experiments, the drop in HOP concentration was observed due to its decomposition, which was also confirmed by independent measurements (Figure 83). The reaction rate r_5 for HOP decomposition side reaction was described by first-order kinetics (Equation 95).

$$r_5 = k_5 \cdot c_{HOP}$$ Equation 95

During the batch experiments it was noted that the enzyme demonstrates certain activity on the NADPH coenzyme, since the KRED^{354} enzyme was used as CFE, the reaction rate r_8 of the NOX(KRED^{354})-catalyzed NADPH oxidation was described by Equation 96.

List of reactant and product abbreviations: acetaldehyde (**AA**), *N*-(3-oxopropyl)-2-phenylacetamide (**OPA**), *N*-(2-((2*R*,4*R*)-4,6-dihydroxytetrahydro-2*H*-pyran-2-yl)ethyl)-2-phenylacetamide (**DHP**), *N*-(2-((2*R*,4*R*)-4-hydroxy-6-oxotetrahydro-2*H*-pyran-2-yl)ethyl)-2-phenylacetamide (**HOP**), 3,5-dihidroxyhexanal (**DHH**).

$$r_8 = \frac{V_{m,8} \cdot \gamma_{NOX(KRED354)} \cdot c_{NADPH}}{K_{m,8}^{NADPH} \cdot \left(1 + \frac{c_{NADP^+}}{K_{i,8}^{NADP^+}}\right) + c_{NADPH} \cdot \left(1 + \frac{c_{NADPH}}{K_{i,8}^{NADPH}}\right)}$$ Equation 96

The reaction rate r_6 for NOX^{001}-catalyzed NADP$^+$ regeneration was described by single-substrate Michaelis-Menten kinetics with competitive product NADP$^+$ and co-substrate DHP inhibitions (Equation 97).

$$r_6 = \frac{V_{m,6} \cdot \gamma_{NOX001} \cdot c_{NADPH}}{K_{m.6}^{NADPH} \cdot \left(1 + \frac{c_{NADP^+}}{K_{i,6}^{NADP^+}} + \frac{c_{DHP}}{K_{i,6}^{DHP}}\right) + c_{NADPH}}$$ Equation 97

The reaction rate r_6 for KRED^{011}-catalyzed NADP$^+$ regeneration was described by double-substrate Michaelis-Menten kinetics with substrate ACE, product IPA and NADP$^+$, and co-substrate DHP inhibition (Equation 98).

$$r_6 = \frac{V_{m,6} \cdot \gamma_{\mathrm{KRED011}} \cdot c_{ACE} \cdot c_{NADPH}}{\left[K_{m,6}^{ACE} \cdot \left(1 + \frac{c_{IPA}}{K_{i,6}^{IPA}} + \frac{c_{DHP}}{K_{i,6}^{DHP}}\right) + c_{ACE} \cdot \left(1 + \frac{c_{ACE}}{K_{iS,6}^{ACE}}\right)\right] \cdot \left[K_{m,6}^{NADPH} + c_{NADPH} \cdot \left(1 + \frac{c_{NADP}}{K_{i,6}^{NADP}}\right)\right]}$$

Equation 98

The KRED^{011}-catalyzed reverse reaction of IPA oxidation into ACE was noted and was described by double-substrate Michelis-Menten kinetics with substrate NADP$^+$ and competitive product ACE inhibition (Equation 99).

$$r_7 = \frac{V_{m,7} \cdot \gamma_{KRED001} \cdot c_{IPA} \cdot c_{NADP^+}}{\left[K_{m,7}^{IPA} \cdot \left(1 + \frac{c_{ACE}}{K_{i,7}^{ACE}}\right) + c_{IPA}\right] \cdot \left[K_{m,7}^{NADP^+} + c_{NADP^+} \cdot \left(1 + \frac{c_{NADP^+}}{K_{iS,7}^{NADP^+}}\right)\right]}$$ Equation 99

The mass balances for DHP, HOP, NADP$^+$, NADPH, ACE and IPA in the batch reactor are presented by Equation 100 – 105.

$$\frac{\mathrm{d}c_{DHP}}{\mathrm{d}t} = -r_4$$ Equation 100

$$\frac{\mathrm{d}c_{HOP}}{\mathrm{d}t} = r_4 - r_5$$ Equation 101

List of reactant and product abbreviations: acetaldehyde (**AA**), *N*-(3-oxopropyl)-2-phenylacetamide (**OPA**), *N*-(2-((2*R*,4*R*)-4,6-dihydroxytetrahydro-2*H*-pyran-2-yl)ethyl)-2-phenylacetamide (**DHP**), *N*-(2-((2*R*,4*R*)-4-hydroxy-6-oxotetrahydro-2*H*-pyran-2-yl)ethyl)-2-phenylacetamide (**HOP**), 3,5-dihidroxyhexanal (**DHH**).

$$\frac{\mathrm{d}c_{NADP^+}}{\mathrm{d}t} = -r_4 + r_6 - r_7 + r_8 \quad \text{Equation 102}$$

$$\frac{\mathrm{d}c_{NADPH}}{\mathrm{d}t} = r_4 - r_6 + r_7 - r_8 \quad \text{Equation 103}$$

$$\frac{\mathrm{d}c_{ACE}}{\mathrm{d}t} = -r_6 + r_7 \quad \text{Equation 104}$$

$$\frac{\mathrm{d}c_{IPA}}{\mathrm{d}t} = r_6 - r_7 \quad \text{Equation 105}$$

The operational stability decay of enzymes KRED^{354}, NOX^{001} and KRED^{011} in the batch reactor were described by second-order kinetics (Equation 106 – 108).

$$\frac{\mathrm{d}\gamma_{KRED354}}{\mathrm{d}t} = -k_d^{KRED354} \cdot \gamma_{KRED354}^2 \quad \text{Equation 106}$$

$$\frac{\mathrm{d}\gamma_{NOX001}}{\mathrm{d}t} = -k_d^{NOX011} \cdot \gamma_{NOX001}^2 \quad \text{Equation 107}$$

$$\frac{\mathrm{d}\gamma_{KRED011}}{\mathrm{d}t} = -k_d^{KRED011} \cdot \gamma_{KRED011}^2 \quad \text{Equation 108}$$

4.5 Data processing

Data processing was done as previously described in Chapter 3.5.

4.6 Results and discussion

4.6.1 Influence of pH on DERA^{062} stability

To find the optimal buffer conditions for the DERA^{062}-catalyzed reaction of AA addition onto OPA (Figure 2), the stability of DERA^{062} in different buffers of various pH (pH 6 – 8) was investigated. Applying the DRP Assay, the residual activity results were collected (Figure 66).

The DERA^{062} enzyme showed good stability in the examined pH range, the enzyme retaining its activity for three days (72 hours), which was in accordance with previously published data for a similar DERA [104]. The highest residual activity was measured in the 0.1 M phosphate buffer (74 – 90 %), while the lowest was measured in 0.1 Tris-HCl buffer pH 7 (65 %). Thus, further investigations of DERA^{062} were performed in 0.1 M phosphate buffer pH 7.

List of reactant and product abbreviations: acetaldehyde (**AA**), *N*-(3-oxopropyl)-2-phenylacetamide (**OPA**), *N*-(2-((2*R*,4*R*)-4,6-dihydroxytetrahydro-2*H*-pyran-2-yl)ethyl)-2-phenylacetamide (**DHP**), *N*-(2-((2*R*,4*R*)-4-hydroxy-6-oxotetrahydro-2*H*-pyran-2-yl)ethyl)-2-phenylacetamide (**HOP**), 3,5-dihidroxyhexanal (**DHH**).

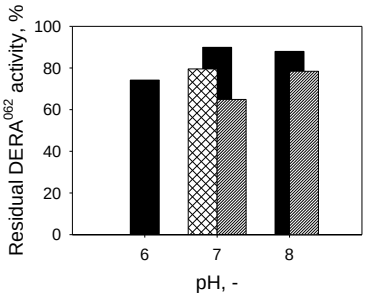

Figure 66 Influence of pH on DERA^{062} stability at different pH (6 – 8; DRP Assay). The stability results were collected after three days of incubation. Pattern legend: 0.1 M phosphate buffer (black), 0.1 M TEA-HCl buffer (intercrossing diagonal lines), 0.1 M Tris-HCl buffer (diagonal lines).

4.6.2 Influence of aldehydes on DERA^{062} stability

The measurements of the individual influence of AA, OPA and DHP on the stability of DERA^{062} revealed that AA (Figure 67a) and OPA (Figure 67b) have a negative impact on the enzyme, the latter having a higher impact, while HOP does not affect its activity (data not shown). The parameters of the deactivation rate constant for AA and OPA were estimated using the given polynomial model (Equation 93; Table 29).

a) b)

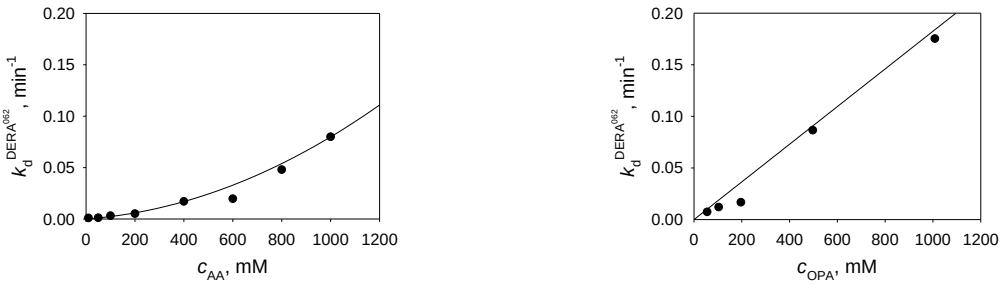

Figure 67 Influence of AA and OPA concentration on the deactivation rate constant of DERA^{062} ($\gamma_{DERA062}$ = 10 mg/mL, 0.1 M phosphate buffer pH 7, 25 °C, 3 h). Legend: experiment (dots), model (line).

Table 29 Parameters of the polynomial model for the dependency of the deactivation rate constant on the concentration of AA, OPA and HOP.

Aldehyde	*a*, mM^{-2} min^{-1}	*b*, mM^{-1} min^{-1}
AA	$6.26 \cdot 10^{-8}$	$1.73 \cdot 10^{-5}$
OPA	$1.80 \cdot 10^{-4}$	-
HOP	-	-

4.6.3 Enzyme kinetics

Kinetic investigations were conducted as described in Chapter 3.6.4.

List of reactant and product abbreviations: acetaldehyde (**AA**), *N*-(3-oxopropyl)-2-phenylacetamide (**OPA**), *N*-(2-((2*R*,4*R*)-4,6-dihydroxytetrahydro-2*H*-pyran-2-yl)ethyl)-2-phenylacetamide (**DHP**), *N*-(2-((2*R*,4*R*)-4-hydroxy-6-oxotetrahydro-2*H*-pyran-2-yl)ethyl)-2-phenylacetamide (**HOP**), 3,5-dihidroxyhexanal (**DHH**).

The kinetic measurements for each of the enzymes involved in this reaction route were done based on the reaction scheme (Figure 64 and 65) by using the initial reaction rate method. The effects of the concentration of substrates and products on the initial reaction rate of the reaction were evaluated.

4.6.3.1 DERA^{062} kinetics in the aldol addition

The kinetic measurements for DERA^{062} were carried out in a batch reactor by varying the concentration of substrates and product (Figure 64a). The obtained results are shown in Figure 68, while the estimated kinetic parameters of the double-substrate Michaelis-Menten equation (Equation 79) are given in Table 30.

The influence of product DHP on the DERA^{062}-catalyzed aldol reaction was measured as well (c_{AA} = 200 mM, c_{OPA} = 200 mM, $\gamma_{DERA062}$ = 5 mg/mL). It was found that DHP does not inhibit DERA^{062} in the aldol reaction up to 350 mM (data not shown).

Since the enzyme catalyzes the side reaction of AA self-aldol addition, the kinetics of the side reaction was investigated as well (Figure 64b). The influence of AA on the initial reaction rate was studied (Figure 69) and the estimated kinetic parameters are presented in Table 30. A retro-aldol reaction of formed DHH was observed. Because DHH is not commercially available, the maximum reaction rate of the retro-aldol reaction was estimated from a batch experiment (Chapter 4.2.8.1: Figure 75).

a) b)

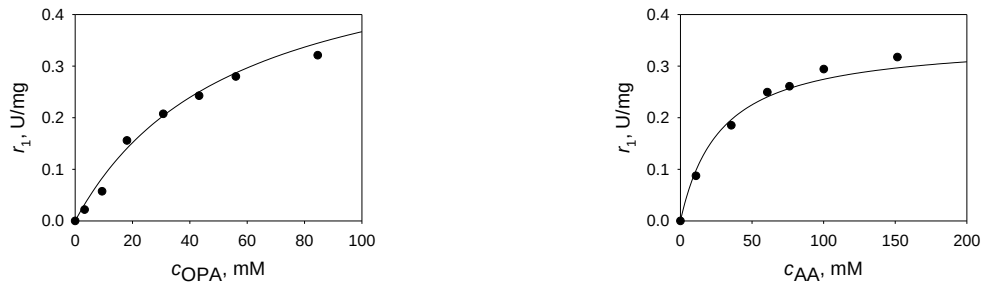

Figure 68 Kinetics of the DERA^{062}-catalyzed aldol addition of AA onto OPA (0.1 M phosphate buffer pH 7, $\gamma_{DERA062}$ = 5.0 mg/mL, 1 000 rpm, 25 °C). The dependence of the initial reaction rate on substrates a) OPA (c_{AA} = 200 mM) and b) AA (c_{OPA} = 200 mM). Legend: experiment (dots), model (line).

List of reactant and product abbreviations: acetaldehyde (**AA**), *N*-(3-oxopropyl)-2-phenylacetamide (**OPA**), *N*-(2-((2*R*,4*R*)-4,6-dihydroxytetrahydro-2*H*-pyran-2-yl)ethyl)-2-phenylacetamide (**DHP**), *N*-(2-((2*R*,4*R*)-4-hydroxy-6-oxotetrahydro-2*H*-pyran-2-yl)ethyl)-2-phenylacetamide (**HOP**), 3,5-dihidroxyhexanal (**DHH**).

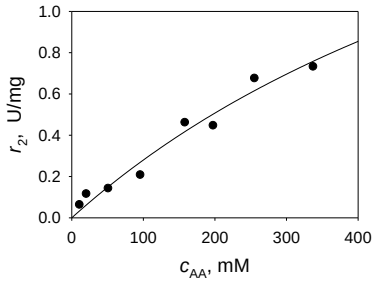

Figure 69 Kinetics of the DERA^{062}-catalyzed AA self-aldol addition (0.1 M phosphate buffer pH 7, $\gamma_{DERA062}$ = 2.0 mg/mL, 1 000 rpm, 25 °C). The dependence of the initial reaction rate on substrate AA. Legend: experiment (dots), model (line).

Table 30 Estimated kinetic parameters of the DERA^{062}-catalyzed aldol addition of AA onto OPA.

Parameter	Unit	Value
Addition of AA to OPA		
$V_{m,1}$	U/mg	0.55 ± 0.05
$K_{m,1}^{AA}$	mM	24.06 ± 2.85
$K_{m,1}^{OPA}$	mM	42.81 ± 5.55
AA self-aldol addition		
$V_{m,2}$	U/mg	2.71 ± 0.36
$K_{m,2}^{AA}$	mM	868.47 ± 66.05

From the estimated kinetic parameters (Table 30), it could be noted that the reaction rate of the side reaction ($V_{m,2}$) was 38-fold higher than the one of the main reaction ($V_{m,1}$), meaning the enzyme displayed higher activity in the side reaction. Despite, the enzyme showed higher affinity towards both substrates of the main reaction. Therefore, the addition of AA onto OPA should be the predominant DERA^{062}-catalyzed reaction at lower AA concentrations. During the batch experiments (Figure 75), the retro-aldol reaction of DHH was observed with an estimated maximum reaction rate (k_3 = 0.0063 mL/(mg·min)).

4.6.3.2 KRED^{354} kinetics in the DHP oxidation

The kinetic measurements for KRED^{354} were carried out by varying the concentration of substrates DHP and NADP and of product NADP$^+$ (Figure 65a). Since the regeneration of NADP$^+$ was conducted *via* KRED^{011}-catalyzed reduction of ACE to IPA (Figure 65c), the influence of ACE and IPA on the initial reaction rate of KRED^{354}-catalyzed DHP oxidation was examined. Using the obtained results (Figure 70), the kinetic parameters of the double-substrate Michaelis-Menten kinetics (Equation 94) were estimated (Table 31).

List of reactant and product abbreviations: acetaldehyde (**AA**), *N*-(3-oxopropyl)-2-phenylacetamide (**OPA**), *N*-(2-((2*R*,4*R*)-4,6-dihydroxytetrahydro-2*H*-pyran-2-yl)ethyl)-2-phenylacetamide (**DHP**), *N*-(2-((2*R*,4*R*)-4-hydroxy-6-oxotetrahydro-2*H*-pyran-2-yl)ethyl)-2-phenylacetamide (**HOP**), 3,5-dihidroxyhexanal (**DHH**).

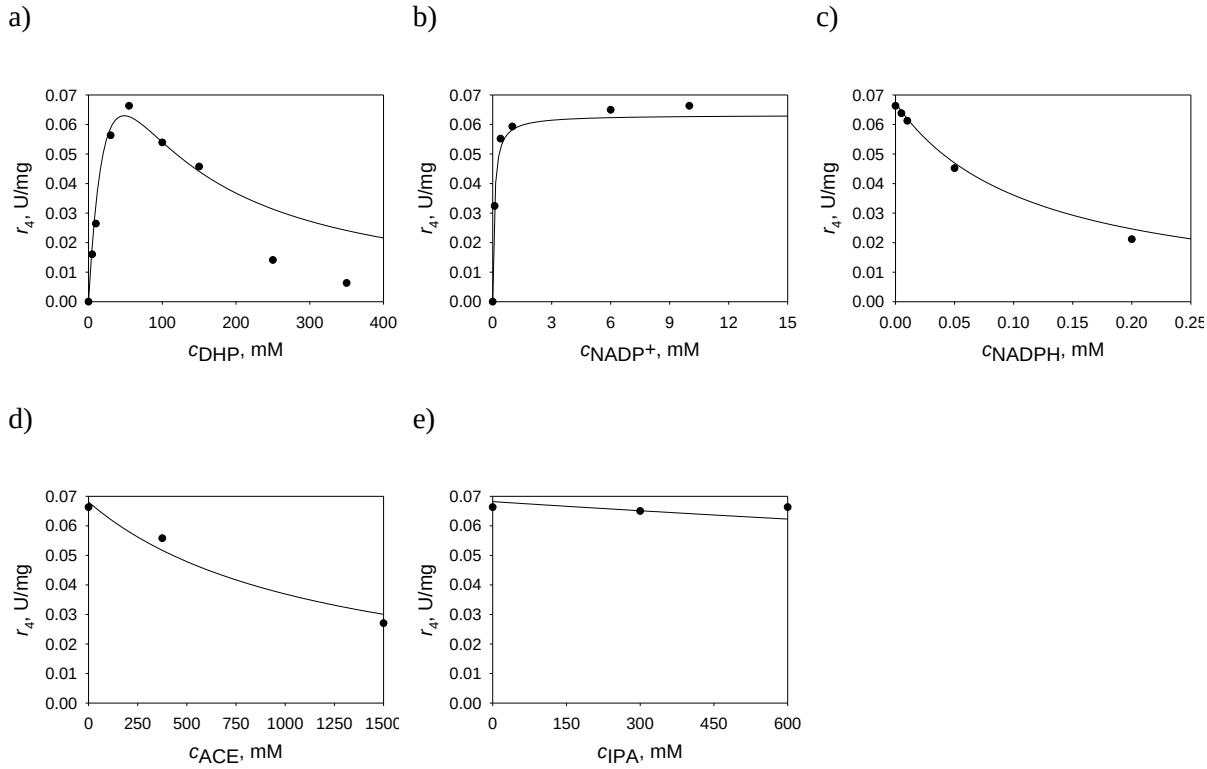

Figure 70 Kinetics of the KRED^{354}-catalyzed DHP oxidation into HOP (0.1 M phosphate buffer pH 8, $\gamma_{KRED354}$ = 0.5 mg/mL, 25 °C). The dependence of the initial reaction rate on substrates a) DHP (c_{NADP} = 10 mM) and b) NADP$^+$ (c_{DHP} = 55 mM), c) product NADPH (c_{DHP} = 55 mM, c_{NADP} = 10 mM), d) co-substrate ACE (c_{DHP} = 55 mM, c_{NADP} = 10 mM) and e) co-product IPA (c_{DHP} = 55 mM, c_{NADP} = 10 mM). Legend: experiment (dots), model (line).

Table 31 Estimated kinetic parameters of the KRED^{354}-catalyzed DHP oxidation into HOP.

Parameter	Unit	Value
$V_{m,4}$	U/mg	0.158 ± 0.083
$K_{m,4}^{DPH}$	mM	36.201 ± 30.911
$K_{m,4}^{NADP+}$	mM	0.086 ± 0.048
$K_{i,4}^{DPH}$	mM	64.418 ± 0.519
$K_{i,4}^{NADPH}$	mM	$(2.430 \pm 0.325) \cdot 10^{-3}$
$K_{i,4}^{ACE}$	mM	310.789 ± 100.72
$K_{i,4}^{IPA}$	mM	357.250 ± 399.72

Since it was noted that the KRED^{354} CFE contains a certain quantity of NADPH-acting oxidases, the influence of NADPH and NADP$^+$ on the initial reaction rate of the reaction of NADPH oxidation catalyzed by NOX(KRED^{354}) was investigated. The enzyme demonstrated inhibitions by both NADPH ($K_{iS,8}^{NADPH}$) and NADP$^+$ ($K_{i,8}^{NADP+}$) (Figure 71). Using the collected experimental data, combined with the developed single-substrate Michaelis-Menten

List of reactant and product abbreviations: acetaldehyde (**AA**), *N*-(3-oxopropyl)-2-phenylacetamide (**OPA**), *N*-(2-((2*R*,4*R*)-4,6-dihydroxytetrahydro-2*H*-pyran-2-yl)ethyl)-2-phenylacetamide (**DHP**), *N*-(2-((2*R*,4*R*)-4-hydroxy-6-oxotetrahydro-2*H*-pyran-2-yl)ethyl)-2-phenylacetamide (**HOP**), 3,5-dihidroxyhexanal (**DHH**).

kinetics (Equation 96), the kinetic parameters for the NOX(KRED^{354}) enzyme were estimated and are presented in Table 32.

a) b)

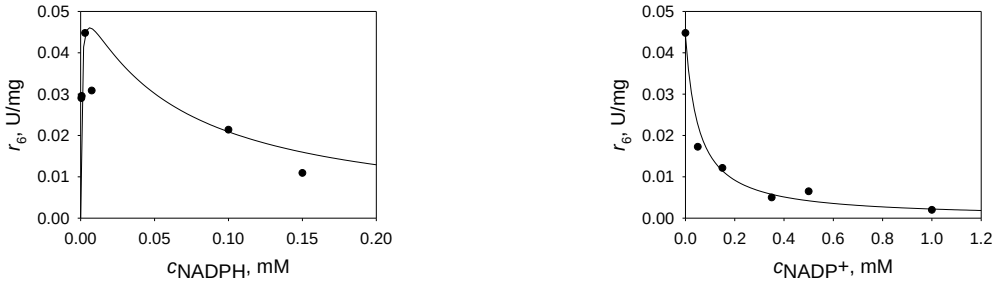

Figure 71 Kinetics of the NOX(KRED^{354})-catalyzed oxidation of NADPH into NADP$^+$ (0.1 M phosphate buffer pH 8, $\gamma_{KRED354}$ = 1.0 mg/mL, 25 °C). The dependence of the initial reaction rate on a) substrate NADPH and b) product NADP$^+$ (c_{NADPH} = 0.003 mM). Legend: experiment (dots), model (line).

Table 32 Estimated kinetic parameters of the NOX(KRED^{354})-catalyzed NADPH oxidation.

Parameter	Unit	Value
$V_{m,8}$	U/mg	0.055 ± 0.011
$K_{m,8}^{NADPH}$	mM	0.0006 ± 0.0003
$K_{iS,8}^{NADPH}$	mM	0.0612 ± 0.047
$K_{i,8}^{NADP+}$	mM	0.008 ± 0.002

From the values presented in Table 31, it could be concluded that the enzyme showed 420-fold higher affinity towards the NADPH than DHP, which is reasonable considering the aldehyde not being its natural substrate. Based on the value of the Michaelis constant of the DPH substrate ($K_{m,4}^{DPH}$), the enzyme showed quite high affinity towards DHP. The kinetic measurements revealed that the enzyme was inhibited by DHP, NADPH, ACE and IPA. From the values of the inhibition constants (Table 31) it could be concluded that the inhibitory effects of ACE ($K_{i,4}^{ACE}$) and IPA ($K_{i,4}^{IPA}$) were quite weak, while that of NADPH ($K_{i,4}^{NADPH}$) was very strong.

From the results presented in Table 32, it could be concluded that a satisfactory regeneration system would be needed to circumvent the negative effect of NADPH which is formed during the DHP oxidation and accumulated due to relatively low maximum reaction rate of the reaction of NOX(KRED^{354})-catalyzed NADPH oxidation (Table 32: $V_{m,8}$).

List of reactant and product abbreviations: acetaldehyde (**AA**), *N*-(3-oxopropyl)-2-phenylacetamide (**OPA**), *N*-(2-((2*R*,4*R*)-4,6-dihydroxytetrahydro-2*H*-pyran-2-yl)ethyl)-2-phenylacetamide (**DHP**), *N*-(2-((2*R*,4*R*)-4-hydroxy-6-oxotetrahydro-2*H*-pyran-2-yl)ethyl)-2-phenylacetamide (**HOP**), 3,5-dihidroxyhexanal (**DHH**).

4.6.3.3 NOX[001] kinetics in the NADPH oxidation

The kinetic measurements for NOX[001] were done by varying the concentration of substrate NADPH and of product $NADP^+$ (Figure 65b). The kinetic parameters of Michaelis-Menten kinetics (Equation 97) were estimated based on the obtained kinetic measurements (Figure 72). The estimated values are given in Table 33.

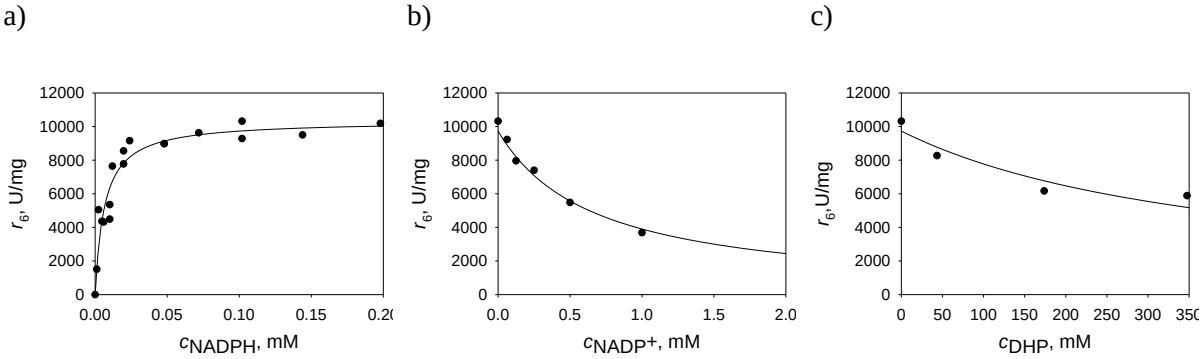

Figure 72 Kinetics of the NOX[001]-catalyzed NADPH oxidation into $NADP^+$ (0.1 M phosphate buffer pH 8, $\gamma_{NOX001} = 10^{-6}$ mg/mL, 25 °C). The dependence of the initial reaction rate on a) substrate a) NADPH, b) product $NADP^+$ (c_{NADPH} = 0.1 mM), c) co-substrate DHP (c_{NADPH} = 0.1 mM). Legend: experiment (dots), model (line).

Table 33 Estimated kinetic parameters of the NOX[001]-catalyzed NADPH oxidation into $NADP^+$.

Parameter	Unit	Value
$V_{m,6}$	U/mg	10350.704 ± 4.372
$K_{m,6}^{NADPH}$	mM	0.006 ± 0.001
$K_{i,6}^{NADP+}$	mM	0.040 ± 0.003
$K_{i,6}^{DHP}$	mM	23.795 ± 0.503

The enzyme displayed very high maximum reaction rate ($V_{m,6}$), high affinity towards the substrate NADPH ($K_{m,6}^{NADPH}$), strong inhibition in presence of high concentrations of $NADP^+$ ($K_{i,6}^{NADP+}$) and slight inhibition in presence of high concentrations of DHP ($K_{i,6}^{DHP}$). Despite the manifested inhibitions, the enzyme should serve as a good auxiliary enzyme for the regeneration of coenzyme $NADP^+$, mainly due to the high reaction rate.

4.6.3.4 KRED[011] kinetics in the DHP oxidation

The kinetic measurements for KRED[011] were carried out by varying the concentration of substrates ACE and NADP and of products IPA and $NADP^+$ (Figure 65c). The kinetic parameters of Michaelis-Menten kinetics (Equation 98) were estimated based on the obtained kinetic measurements (Figure 73). The estimated values are given in Table 34.

List of reactant and product abbreviations: acetaldehyde (**AA**), *N*-(3-oxopropyl)-2-phenylacetamide (**OPA**), *N*-(2-((2*R*,4*R*)-4,6-dihydroxytetrahydro-2*H*-pyran-2-yl)ethyl)-2-phenylacetamide (**DHP**), *N*-(2-((2*R*,4*R*)-4-hydroxy-6-oxotetrahydro-2*H*-pyran-2-yl)ethyl)-2-phenylacetamide (**HOP**), 3,5-dihidroxyhexanal (**DHH**).

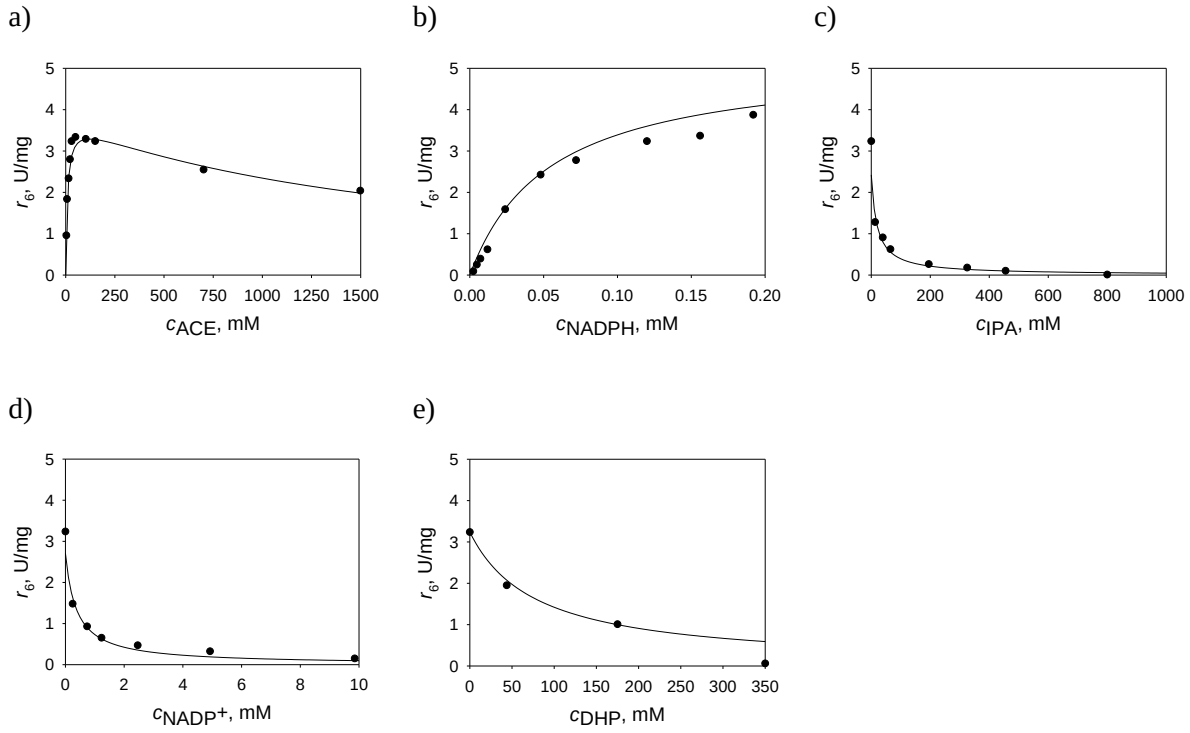

Figure 73 Kinetics of the KRED^{011}-catalyzed ACE reduction into IPA (0.1 M phosphate buffer pH 8, $\gamma_{KRED011}$ = 0.01 mg/mL, 25 °C). The dependence of the initial reaction rate on substrates a) ACE (c_{NADPH} = 0.1 mM) and b) NADPH (c_{ACE} = 30 mM), product c) IPA (c_{ACE} = 30 mM, c_{NADPH} = 0.1 mM) and d) NADP (c_{ACE} = 30 mM, c_{NADPH} = 0.1 mM) and co-substrate e) DHP (c_{ACE} = 30 mM, c_{NADPH} = 0.1 mM). Legend: experiment (dots), model (line).

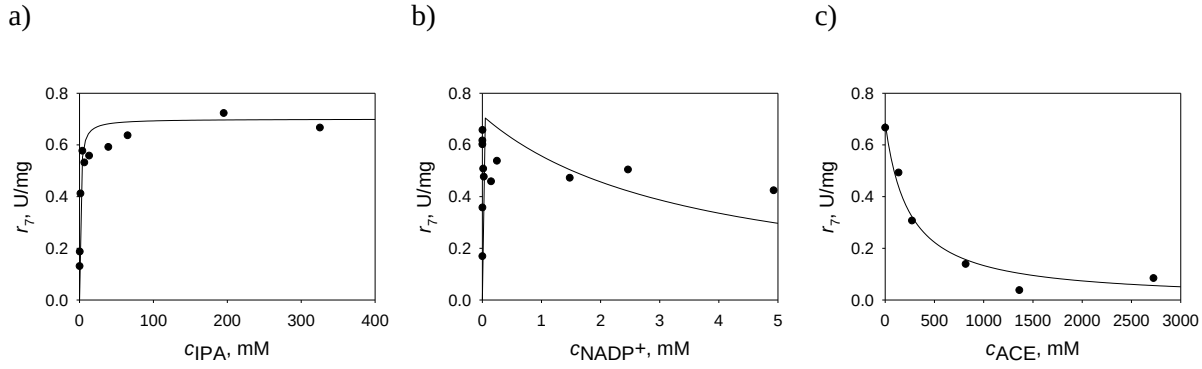

Figure 74 Kinetics of the KRED^{011}-catalyzed IPA oxidation into ACE (0.1 M phosphate buffer pH 8, $\gamma_{KRED011}$ = 0.03 mg/mL, 25 °C). The dependence of the initial reaction rate on substrates a) IPA (c_{NADP} = 4.9 mM) and b) NADP$^+$ (c_{IPA} = 130 mM) and c) product ACE (c_{IPA} = 130 mM, c_{NADP} = 0.246 mM). Legend: experiment (dots), model (line).

Since the enzyme catalyzed the IPA oxidation, the kinetics was measured in the KRED^{011}-catalyzed reaction of IPA oxidation as well. The kinetic parameters of the double-substrate

List of reactant and product abbreviations: acetaldehyde (**AA**), *N*-(3-oxopropyl)-2-phenylacetamide (**OPA**), *N*-(2-((2*R*,4*R*)-4,6-dihydroxytetrahydro-2*H*-pyran-2-yl)ethyl)-2-phenylacetamide (**DHP**), *N*-(2-((2*R*,4*R*)-4-hydroxy-6-oxotetrahydro-2*H*-pyran-2-yl)ethyl)-2-phenylacetamide (**HOP**), 3,5-dihidroxyhexanal (**DHH**).

Michaelis-Menten kinetics (Equation 99) were estimated using the obtained results are shown in Figure 74 (Table 34).

Table 4 Estimated kinetic parameters of the KRED^{011}-catalyzed ACE reduction into IPA.

Parameter	Unit	Value
Reduction of ACE to IPA		
$V_{m,6}$	U/mg	5.80 ± 0.56
$K_{m,6}^{ACE}$	mM	10.98 ± 2.39
$K_{m,6}^{NADPH}$	mM	0.068 ± 0.016
$K_{i,6}^{ACE}$	mM	2121.26 ± 546.77
$K_{i,6}^{IPA}$	mM	4.57 ± 1.47
$K_{i,6}^{NADP+}$	mM	0.29 ± 0.05
$K_{i,6}^{DHP}$	mM	17.33 ± 1.20
Oxidation of IPA to ACE		
$V_{m,7}$	U/mg	1.67 ± 0.11
$K_{m,7}^{IPA}$	mM	2.51 ±3.46
$K_{m,7}^{NADP+}$	mM	$(1.44 \pm 1.91) \cdot 10^{-6}$
$K_{iS,7}^{NADP+}$	mM	8.29 ± 2.86
$K_{i,7}^{ACE}$	mM	0.73 ± 0.04

The KRED^{011} enzyme showed 160-fold higher affinity towards the coenzyme than ACE and did display some notable inhibitions caused by ACE, IPA, NADP$^+$ and DHP. The inhibition caused by the ACE substrate can almost be neglected due to high value of the inhibition constant ($K_{i,6}^{ACE}$), whereas the strongest inhibitions were caused by products IPA ($K_{i,6}^{IPA}$) and NADP$^+$ ($K_{i,6}^{NADP+}$). In the reaction of IPA oxidation, based on the inhibition constants, it could be observed that the enzyme was severely inhibited by both NADP$^+$ and ACE. Regardless, comparing the maximum reaction rates of the ACE reduction and IPA oxidation, it could be noted that the main reaction (ACE reduction) was 3.5 times higher than in the reverse reaction (IPA oxidation). Therefore, KRED^{011} should offer a good NADP$^+$ regeneration system, especially considering that NADP$^+$ is consumed during the DHP oxidation and, to some extent, in the IPA oxidation as well. Hence, NADP$^+$ should not accumulate in high amounts during the KRED^{354}-catalyzed DHP oxidation. Regarding the inhibition caused by NADPH in the reaction of NADPH oxidation, from the estimated value of the maximum reaction rates for KRED^{354} (Table 31: $V_{m,4}$) and KRED^{011} (Table 34: $V_{m,6}$) it could be concluded that the predominant reaction would be the KRED^{011}-catalyzed NADPH oxidation, since the value of the maximum reaction rate of DHP oxidation was 37-fold lower than the value of the maximum reaction rate of NADPH oxidation. Hence should not cause NADPH accumulation. This would prevent severe NADPH inhibitory effects on KRED^{354}.

List of reactant and product abbreviations: acetaldehyde (**AA**), *N*-(3-oxopropyl)-2-phenylacetamide (**OPA**), *N*-(2-((2*R*,4*R*)-4,6-dihydroxytetrahydro-2*H*-pyran-2-yl)ethyl)-2-phenylacetamide (**DHP**), *N*-(2-((2*R*,4*R*)-4-hydroxy-6-oxotetrahydro-2*H*-pyran-2-yl)ethyl)-2-phenylacetamide (**HOP**), 3,5-dihidroxyhexanal (**DHH**).

By comparing the estimated kinetic parameters for the reactions involved in the $NADP^+$ regeneration, i.e. NOX^{001}- or $KRED^{011}$-catalyzed NADPH oxidation (Table 33, Table 34), it could be noted that NOX^{001} displayed a high maximum reaction rate of NADPH oxidation: almost 1800-fold higher than the one estimated for the $KRED^{011}$-catalyzed reaction.

4.6.3.5 Concluding remarks

By observing the estimated values of $DERA^{062}$ kinetic parameters (Figure 69, Table 30), it was concluded that the main reaction would be the aldol reaction of OPA and AA due to the enzyme's high affinity towards both of the substrates in that aldol reaction, despite the $DERA^{062}$-catalyzed AA self-aldol addition reaction manifested a higher maximum reaction rate.

The kinetic measurements for $KRED^{354}$ (Figure 70, Table 31) suggested good affinity towards DHP, but a satisfactory regeneration system should be implemented. Two different enzymes for NADPH oxidation were examined: NOX^{001} and $KRED^{011}$. The kinetic analysis revealed a better fit of the NOX^{001} (Figure 72, Table 33) enzyme over the $KRED^{011}$ enzyme (Figure 73 and 74, Table 34). NOX^{001} manifested higher maximum reaction rate (1784-fold higher) and higher affinity towards the NADPH (11-fold higher), in comparison to $KRED^{011}$. For both enzymes, the inhibitory effects of $NADP^+$ were not prominent, which was concluded by comparing the Michaelis constant for NADPH ($K_{m,6}^{NADPH}$) and the inhibition constant for $NADP^+$ ($K_{i,6}^{NADP+}$).

4.6.4 Validation of developed mathematical models: one-step biocatalysis

The reactions related to the first reaction route (Figure 1) that were conducted as one-step reactions were:

1. $DERA^{062}$-catalyzed aldol reaction of AA with OPA,
2. $KRED^{354}$-catalyzed DHP oxidation without $NADP^+$ regeneration,
3. $KRED^{354}$-catalyzed DHP oxidation with $NADP^+$ regeneration catalyzed by NOX^{001},
4. $KRED^{354}$-catalyzed DHP oxidation with $NADP^+$ regeneration catalyzed by $KRED^{011}$.

All reactions were conducted with either commercially available substrates (AA) or with substrates enzymatically produced in the lab (OPA; procedures described in Chapter 4.2.4: DHP, HOP).

List of reactant and product abbreviations: acetaldehyde (**AA**), *N*-(3-oxopropyl)-2-phenylacetamide (**OPA**), *N*-(2-((2*R*,4*R*)-4,6-dihydroxytetrahydro-2*H*-pyran-2-yl)ethyl)-2-phenylacetamide (**DHP**), *N*-(2-((2*R*,4*R*)-4-hydroxy-6-oxotetrahydro-2*H*-pyran-2-yl)ethyl)-2-phenylacetamide (**HOP**), 3,5-dihidroxyhexanal (**DHH**).

The developed mathematical models (Chapter 4.4) were validated against obtained experimental data. They were used to estimate the operational stability rate constants of all used enzymes ($k_d^{KRED354}$, k_d^{NOX001}, $k_d^{KRED011}$) and to estimate the reaction rate constants of the DERA^{062}-catalyzed reverse reaction of DHH synthesis (k_3, Equation 81) and of the HOP decomposition (k_5, Equation 95).

Since KRED^{354} requires NADP$^+$ for its activity, NADP$^+$ was added into the reaction mixture prior to the addition of the KRED^{354} enzyme. If the NADP$^+$ regeneration reaction was conducted with KRED^{011}, ACE was added into the reactor and served as a co-substrate in the NADP$^+$ regeneration.

The enzymatic activity is given as a relative value (0 – 100 %) with its initial value (at t = 0 min) regarded as its maximum, defined as 100 %. In case of repetitive batch reactor mode, after each addition of the enzyme into the reactor its value was regarded as 100 %.

The substrate conversion was calculated using the Equation 73, the product yield using the Equation 74, the BY using the Equation 75, and the STY using the Equation 76.

4.6.4.1 DERA^{062}-catalyzed aldol additions

4.6.4.1.1 DERA^{062}-catalyzed aldol addition in batch reactor

The developed mathematical model for the DERA^{062}-catalyzed reaction was validated in a batch reactor (Equations 79 – 86). The experimental data of concentration of AA and DHH *vs* time (Figure 75) indicated the existence of a reverse reaction: a retro-aldol reaction of the AA-self aldol addition. The reaction rate constant for that retro-aldol reaction was estimated using the data collected from the reactor experiment (Figure 75: k_3 = 0.0063 mL/(mg·min)).

Full conversion of AA was not reached, even after 24 hours, due to the addition of AA in large excess. After 7.8 h of the experiment, the reaction yielded 27.3 g/L of DHP and 9.2 g/L of DHH. At that time-point, the conversion of AA was 90.1 %, whereas the conversion of OPA was 99.2 % and the $Y_{DHP/OPA}$ was 99.2 %. The reaction mixture contained 20.8 % AA, 0.4 % OPA, 45.8 DHP and 33.0 % DHH. The STY and BY were calculated and equaled 84.1 g/(L·day) and 3.3 $g_{DHP}/g_{DERA062}$, respectively.

List of reactant and product abbreviations: acetaldehyde (**AA**), *N*-(3-oxopropyl)-2-phenylacetamide (**OPA**), *N*-(2-((2*R*,4*R*)-4,6-dihydroxytetrahydro-2*H*-pyran-2-yl)ethyl)-2-phenylacetamide (**DHP**), *N*-(2-((2*R*,4*R*)-4-hydroxy-6-oxotetrahydro-2*H*-pyran-2-yl)ethyl)-2-phenylacetamide (**HOP**), 3,5-dihidroxyhexanal (**DHH**).

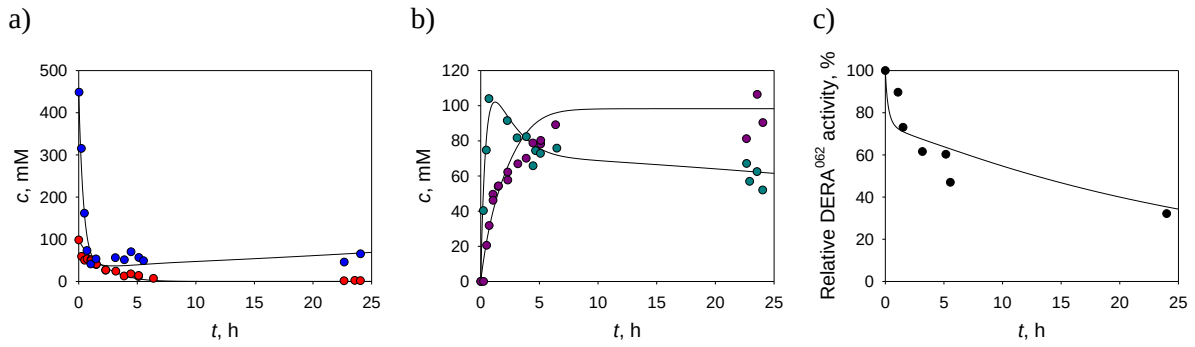

Figure 75 Experimental and simulation data of the double aldol addition of AA to OPA in a batch reactor catalyzed by DERA^{062} (0.1 M TEA-HCl buffer pH 7, c_{AA} = 450 mM, c_{OPA} = 100 mM, $\gamma_{DERA062}$ = 20 mg/mL). Change of a) substrates AA and OPA concentrations, b) products DHP and CHH concentrations, c) relative enzyme activity during the experiment. Legend: experiment (dots), model (line); AA (blue), OPA (red), DHP (purple), CHH (teal).

Based on the goodness-of-fit statistics (R^2 = 0.98, σ = 13.90) and data show in Figure 75, it was concluded that the developed mathematical model with estimated kinetic parameters could serve as a useful basis for future optimization of the examined aldol reaction with DERA^{062}.

4.6.4.1.2 DERA^{062}-catalyzed aldol addition in repetitive batch reactor

To obtain higher concentration of DHP, the reaction was conducted in a repetitive batch reactor mode (Figure 76) thus model (Equations 79 – 86) validation. Fresh substrate was added three times during the experiment: 0.0, 2.5 and 5.2 h. The added substrate concentrations were same as the initial substrate concentration. During the experiment, the enzyme was added two times: into the reactor at the beginning of the reaction (0.0 h; 30 mg/mL) and at the time-point when the enzyme lost 69 % of its initial activity (6.5 h; 15 mg/mL). The reaction rate constant for that retro-aldol reaction was estimated using the data collected from the previous batch reactor experiment (k_3 = 0.0063 mL/(mg·min), Chapter 3.6.5.1).

List of reactant and product abbreviations: acetaldehyde (**AA**), *N*-(3-oxopropyl)-2-phenylacetamide (**OPA**), *N*-(2-((2*R*,4*R*)-4,6-dihydroxytetrahydro-2*H*-pyran-2-yl)ethyl)-2-phenylacetamide (**DHP**), *N*-(2-((2*R*,4*R*)-4-hydroxy-6-oxotetrahydro-2*H*-pyran-2-yl)ethyl)-2-phenylacetamide (**HOP**), 3,5-dihidroxyhexanal (**DHH**).

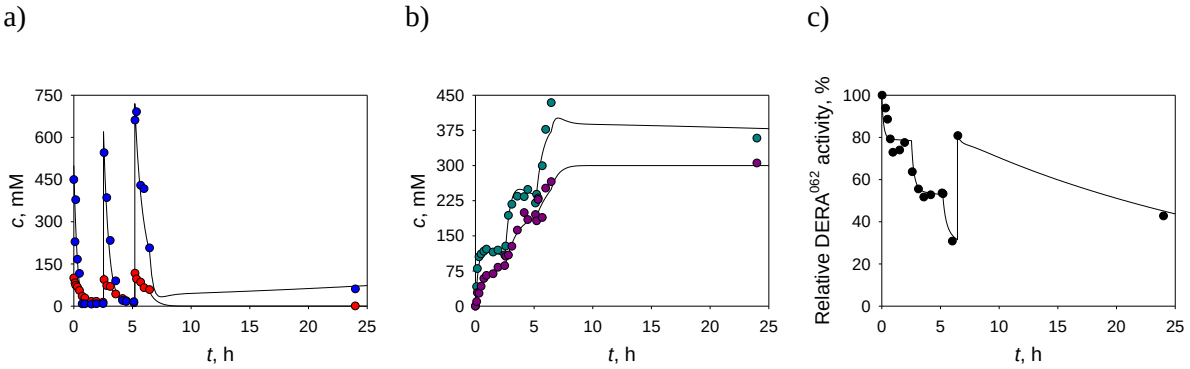

Figure 76 Experimental and simulation data of the double aldol addition of AA to OPA in a repetitive batch reactor catalyzed by DERA^{062} (0.1 M TEA-HCl buffer pH 7, c_{AA} = 450 mM, c_{OPA} = 100 mM, $\gamma_{DERA062}$ = 30 mg/mL + 15 mg/mL). Change of a) substrate AA and OPA concentration, b) product DHP and CHH concentration, c) relative enzyme activity during the experiment. Legend: experiment (dots), model (line); AA (blue), OPA (red), DHP (purple), CHH (teal).

Although the reaction was monitored for 24 hours, almost full OPA conversion (99.8 %) was already reached after 8.8 h of the experiment. The reaction resulted in the production of 94.0 g/L DHP ($Y_{DHP/OPA}$ = 99.8 %), which was 3-fold higher than the amount obtained in the reaction conducted in the batch reactor. The reaction composition at that time point was: 0.1 % OPA, 5.8 % AA, 40.9 % DHP and 53.2 % DHH. The STY and BY were calculated and equaled 229.1 g/(L·day) and 3.8 $g_{DHP}/g_{DERA062}$, respectively. The reaction resulted with a high concentration of side-product DHH (51.4 g/L). To obtain lower amounts of DHH, since the production DHH cannot be avoided, the reaction was conducted in a fed-batch reactor as well.

From the goodness-of-fit statistics (R^2 = 0.95, σ = 27.9) and data shown in Figure 76, the model described the experimental data well.

4.6.4.1.3 DERA^{062}-catalyzed aldol addition in fed-batch reactor

The developed mathematical model for the aldol addition in fed-batch reactor (Equations 79 – 81 and 87 – 92) was validated. The obtained data is shown in Figure 77.

The experimental setup consisted of a single substrate supply containing only AA that was slowly fed into the reactor, while OPA and DERA^{062} were added at the beginning of the experiment (Figure 77). The value of the reaction rate constant for the retro-aldol reaction (k_3) was estimated in the batch reactor experiment (0.0063 mL/(mg·min), Chapter 3.6.5.1).

List of reactant and product abbreviations: acetaldehyde (**AA**), *N*-(3-oxopropyl)-2-phenylacetamide (**OPA**), *N*-(2-((2*R*,4*R*)-4,6-dihydroxytetrahydro-2*H*-pyran-2-yl)ethyl)-2-phenylacetamide (**DHP**), *N*-(2-((2*R*,4*R*)-4-hydroxy-6-oxotetrahydro-2*H*-pyran-2-yl)ethyl)-2-phenylacetamide (**HOP**), 3,5-dihidroxyhexanal (**DHH**).

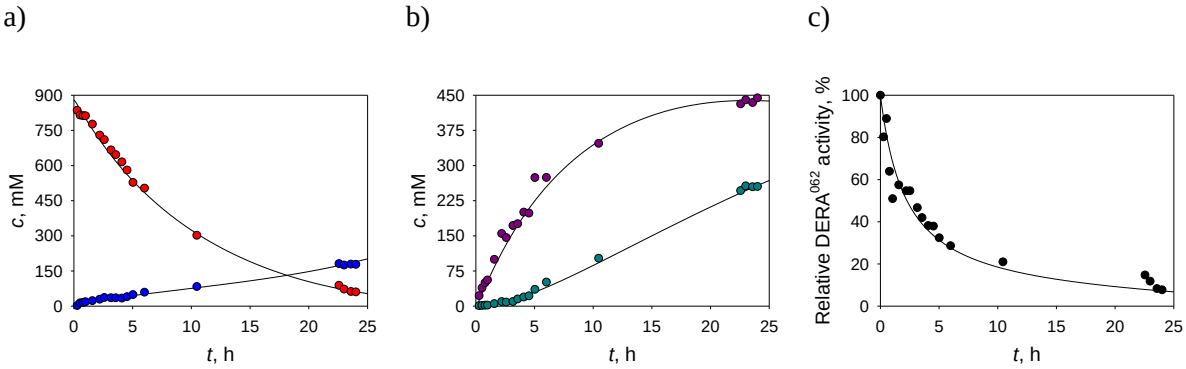

Figure 77 Experimental and simulation data of the double aldol addition of AA to OPA in the fed-batch reactor catalyzed by DERA^{062} (0.1 M phosphate buffer pH 7, V_0 = 2.84 mL, c_{OPA} = 880 mM, $\gamma_{DERA062}$ = 35.21 mg/mL; feed 1: q_1 = 1.5 µL/min, $c_{AA,0}$ = 3472 mM; 24 h). Change of a) substrate AA and OPA concentration, b) product DHP and DHH concentration, and c) relative enzyme activity during the experiment. Legend: experiment (dots), model (line); AA (blue), OPA (red), DHP (purple), CHH (teal).

After 24 hours of the reaction, the reaction mixture had 20 % and 6.4 % of unreacted substrates AA and OPA, respectively, and contained 46.4 % DHP and 27.2 % DHH. The reaction yielded 124.0 g/L of DHP. Although complete conversion of neither substrates was obtained, the DHP yield with respect to substrate OPA was 87.7 %. The STY was 124.0 g/(L·day). The total amount of enzyme added into the reactor was 20 mg/mL at the end of the experiment, when the reaction volume was 5 mL, the calculated BY was 6.7 $g_{DHP}/g_{DERA062}$. The reaction produced 34.0 g/L of DHH, which is slightly less than in the repetitive batch reactor (1.5-fold lower). Despite of impurities, DHP isolation from the reaction mixture containing certain quantities of DHH should not be challenging.

Based on the goodness-of-fit statistics (R^2 = 0.99, σ = 14.14) and data shown in Figure 77, it was concluded that the model simulation predicted the experimental outcome well.

4.6.4.1.4 Optimization of the DERA^{062}-catalyzed aldol addition

Based on the results collected from the kinetic (Figure 68, Table 30) and stability measurements (Figure 67, Table 29), the developed mathematical model (Equations 79 –81; in batch and repetitive batch reactor: Equations 82 – 85, in fed-batch reactor: Equation 87 – 90 and 93) and conducted reactions in batch (Figure 75), repetitive batch (Figure 76) and fed-batch

List of reactant and product abbreviations: acetaldehyde (**AA**), *N*-(3-oxopropyl)-2-phenylacetamide (**OPA**), *N*-(2-((2*R*,4*R*)-4,6-dihydroxytetrahydro-2*H*-pyran-2-yl)ethyl)-2-phenylacetamide (**DHP**), *N*-(2-((2*R*,4*R*)-4-hydroxy-6-oxotetrahydro-2*H*-pyran-2-yl)ethyl)-2-phenylacetamide (**HOP**), 3,5-dihidroxyhexanal (**DHH**).

reactor (Figure 77), model simulations were done by changing the initial conditions in the (repetitive) batch and fed-batch reactor to optimize the DERA^{064}-catalyzed aldol addition.

In addition to investigating the impact of the total enzyme concentration on the DHP production, the effects of initial ratios of AA and OPA on process metrics was investigated as well. Because AA is rapidly consumed in the side reaction of AA self-aldol addition, the optimal ratio of AA and OPA could have a significant effect on the reaction rate and STY.

a)

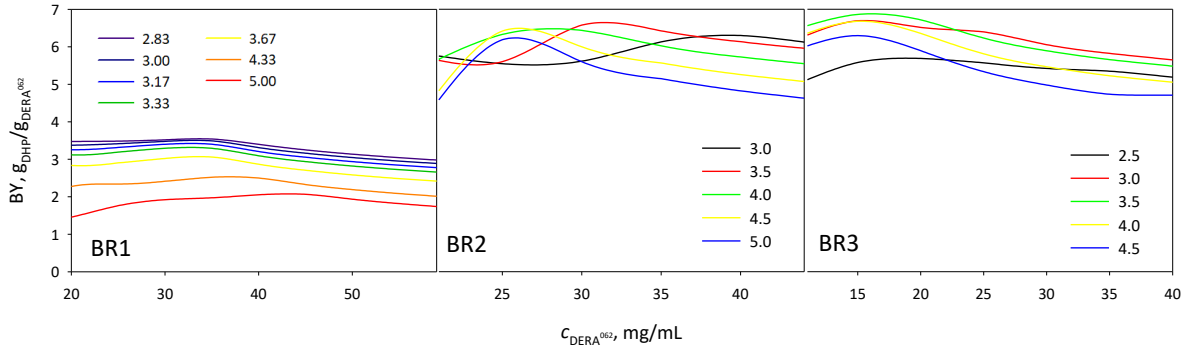

b)

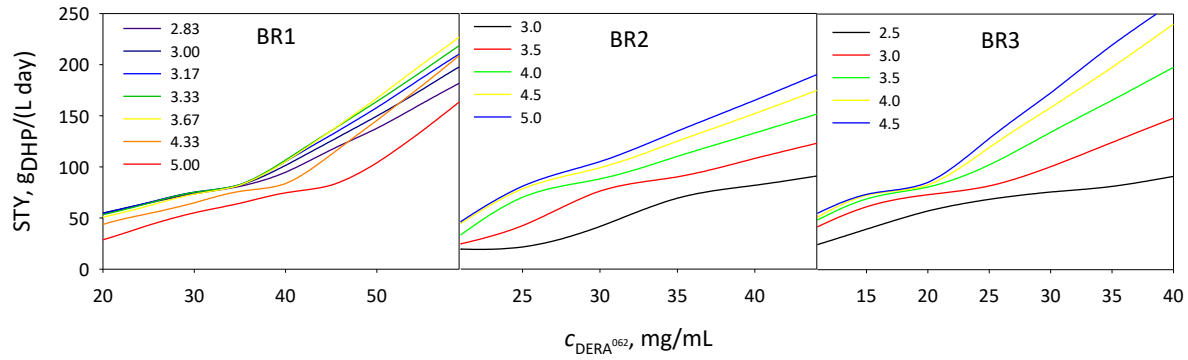

Figure 78 Model simulations of double aldol addition of AA to OPA catalyzed by DERA^{062} in different batch reactor modes (c_{OPA} = 300 mM, repetitive batch: 3 x 100 mM; c_{AA} = (ratio AA:OPA) x c_{OPA} mM). Legend: OPA:AA ratio (colored lines).

Three different batch reactor modes were investigated:

1. BR1 – batch reactor with the addition of total amount of substrates and enzyme at the beginning of the process,
2. BR2 – repetitive batch reactor with three sequential additions of substrates and enzyme,

List of reactant and product abbreviations: acetaldehyde (**AA**), *N*-(3-oxopropyl)-2-phenylacetamide (**OPA**), *N*-(2-((2*R*,4*R*)-4,6-dihydroxytetrahydro-2*H*-pyran-2-yl)ethyl)-2-phenylacetamide (**DHP**), *N*-(2-((2*R*,4*R*)-4-hydroxy-6-oxotetrahydro-2*H*-pyran-2-yl)ethyl)-2-phenylacetamide (**HOP**), 3,5-dihidroxyhexanal (**DHH**).

3. BR3 – repetitive batch reactor with the addition of total amount of enzyme at the beginning of the process and three sequential additions of substrates.

The results of the carried-out simulations are shown in Figure 78.

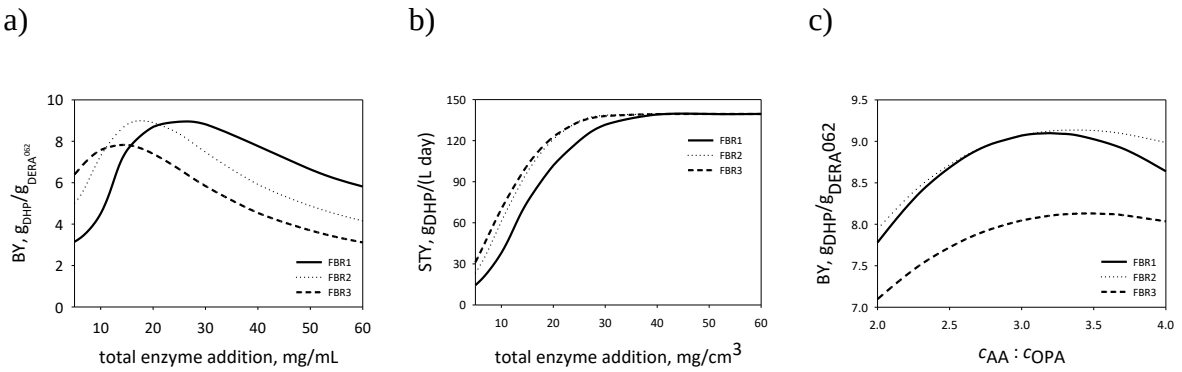

Figure 79 Model simulations of double aldol addition of AA to OPA catalyzed by DERA^{062} in different fed-batch reactor modes (c_{OPA} = 781 mM (FBR1 and FBR2), c_{OPA} = 638 mM (FBR3); V_0 = 6.4 mL (FBR1 and FBR2), V_0 = 7.84 mL (FBR3); feed 1: q_1 = 1.5 µL/min, $c_{AA,0}$ = 6944 mM; feed 2: 1.0 µL/min, $c_{DERA062}$ calculated from the total amount of enzyme addition; all calculations are based on V_{final} = 10 mL, 24 h). a) Biocatalyst yield and b) STY change with total enzyme concentration. C) Impact of AA:OPA ration on BY (c_{OPA} = 702 mM (FBR1 and FBR2), 584 mM (FBR3); V_0 = 7.12 mL (FBR1 and FBR2), 8.56 mL (FBR3); $c_{DERA062,0}$ = 14.0 mg/mL (FBR2), 17.5 mg/mL (FBR3); V_0 = 7.12 mM, feed 1: q_1 = 1 µL/min, feed = (c_{AA}:c_{OPA}) x 500 x 6.94; feed 2: q_2 = 1 µL/min, $c_{DERA062,0}$ = 173.6 mg/mL (FBR1), 69.44 mg/mL (FBR2); all calculations are based on V_{final} = 10 mL, 24 h). Legend: FBR1 (solid line), FBR2 (dotted line), FBR3 (dashed line).

Based on the BY results (Figure 78a), BR2 and BR2 resulted in a similar outcome. BR3 proved to be the best reactor considering productivity (Figure 78b). It was also evident that STY increased with the increase of the AA:OPA ratio. Taking BY into account, the AA:OPA ratio of 3.5 should be the optimal ratio for carrying the aldol addition in either BR2 or BR3. Based on these results (Figure 78) and regarding the process metrics (Table 1) it was concluded that from the tested batch reactors, the BR3 would be the most convenient.

The model simulations were done in the fed-batch reactor as well. In all investigated modes, AA was slowly added into the reactors. The studied modes differed in terms of enzyme supply. Following fed-batch setups were examined:

1. FBR1 – fed-batch reactor with enzyme addition only in the feed,

List of reactant and product abbreviations: acetaldehyde (**AA**), *N*-(3-oxopropyl)-2-phenylacetamide (**OPA**), *N*-(2-((2*R*,4*R*)-4,6-dihydroxytetrahydro-2*H*-pyran-2-yl)ethyl)-2-phenylacetamide (**DHP**), *N*-(2-((2*R*,4*R*)-4-hydroxy-6-oxotetrahydro-2*H*-pyran-2-yl)ethyl)-2-phenylacetamide (**HOP**), 3,5-dihidroxyhexanal (**DHH**).

2. FBR2 – fed-batch reactor with the addition of half of the amount of enzyme at the beginning of the process and half of the amount in the feed,
3. FBR3 – fed-batch reactor with the addition of the total amount of enzyme at the beginning of the process.

The results of FBR simulations are shown in Figure 52.

The highest BY values were obtained for FBR1 and FBR2, while they were the lowest for FBR3 (Figure 52a). Regarding STYs, slightly higher STY values were observed for FBR2 and FBR3 (Figure 52b). The influence of the AA volumetric flow rate on the BY was investigated as well. It was observed that with the increase of flow BY linearly decreases. By studying the effects of AA:OPA ratio on BY (Figure 52c), it was found that the highest BY values were obtained at ratios between 3.0 and 3.5.

Based on the data collected from the conducted model simulations shown in Figure 78 and Figure 52, it was concluded that FBR2 would be the most convenient reactor for the DERA^{062}-catalyzed aldol addition. Despite these findings, the reaction was not carried out at these conditions since the simulated results were not significantly better than the data obtained by the previously conducted aldol reaction shown in Figure 77.

4.6.4.1.5 Concluding remarks: DERA^{062}-catalyzed aldol addition

The developed mathematical model for the DERA^{062}-catalyzed reaction was validated in a batch, repetitive batch and fed-batch reactor (Equations 79 – 92). The obtained data was used for reaction optimization *via* model simulation, but the simulation results did not yield with a significant improvement in the process outputs, such as c_{DHP}, Y_{DHP}, STY or BY (Figure 75, 76 and 77 *vs* Figure 78 and 79). From the obtained results (Table 35), it could be summarized that highest substrate conversions were obtained in both batch and repetitive batch reactors.

In all three types of reactor the reaction mixture at the end of the experiment had similar composition regarding DHP, while in the fed-batch had side product DHH. The highest STY and BY were obtained in the repetitive batch reactor. The calculated STY in the repetitive batch reactor was 2-fold higher than in fed-batch reactor and was 3-fold higher than in batch reactor,

List of reactant and product abbreviations: acetaldehyde (**AA**), *N*-(3-oxopropyl)-2-phenylacetamide (**OPA**), *N*-(2-((2*R*,4*R*)-4,6-dihydroxytetrahydro-2*H*-pyran-2-yl)ethyl)-2-phenylacetamide (**DHP**), *N*-(2-((2*R*,4*R*)-4-hydroxy-6-oxotetrahydro-2*H*-pyran-2-yl)ethyl)-2-phenylacetamide (**HOP**), 3,5-dihidroxyhexanal (**DHH**).

while the calculated BY in the repetitive batch reactor was similar to the one obtained in the in fed-batch reactor, but 2-fold higher than obtained in the batch reactor. By comparing these values with the industrial requirements (Table 1), it could be concluded that the aldol reaction conducted in the repetitive batch reactor mode resulted in industrially relevant metrics, such as STY, substrate conversion or final product concentration within only nine hours of reaction at the given reaction conditions. Although the relevant industrial metrics were satisfied, the examined aldol reaction catalyzed by DERA^{062} may not be industrially viable due to high amount of DHH formed in all three reactor types. Despite, the isolation of DHP from the reaction solution containing DHH as well should not represent a challenge, especially because DHP is an important statin building block.

Table 35 Results for the DERA^{062}-catalyzed aldol reaction in three different reactor modes.

Reactor	*t*, h [a]	γ_{DHP}, g/L	DHP, %[c]	DHH, % [c]	X_{OPA}, %	STY	BY
BR	7.8	27.3	45.8	33.0	99.2	84.1	3.3
RBR	8.8	84.0	40.9	53.2	99.8	229.1	3.8
FBR [b]	24.0	124.0	46.3	27.2	87.7	124.0	6.7

[a] end of the reaction, $X_{AA} \geq 90$ %, $X_{OPA} \geq 99$ %
[b] end of the reaction, $X_{AA} = 87.4$ % $X_{OPA} = 93.0$ %
[c] molar percentage, % *n*/*n*
Abbreviations: batch reactor (BR), repetitive batch reactor mode (RBR), fed-batch reactor (FBR)
Notes: STY is expressed as g/(L·day), while BY as $g_{DHP}/g_{DERA062}$.

4.6.4.2 KRED^{354}-catalyzed DHP oxidations

The DHP oxidation was accomplished in following three ways:

1. KRED^{354}-catalyzed DHP oxidation without $NADP^+$ regeneration,
2. KRED^{354}-catalyzed DHP oxidation with $NADP^+$ regeneration catalyzed by NOX^{001},
3. KRED^{354}-catalyzed DHP oxidation with $NADP^+$ regeneration catalyzed by KRED^{011}.

Each reaction was conducted using purified DHP substrate obtained following the procedure described in Chapter 4.2.4.1. All reactions were conducted in batch rector.

List of reactant and product abbreviations: acetaldehyde (**AA**), *N*-(3-oxopropyl)-2-phenylacetamide (**OPA**), *N*-(2-((2*R*,4*R*)-4,6-dihydroxytetrahydro-2*H*-pyran-2-yl)ethyl)-2-phenylacetamide (**DHP**), *N*-(2-((2*R*,4*R*)-4-hydroxy-6-oxotetrahydro-2*H*-pyran-2-yl)ethyl)-2-phenylacetamide (**HOP**), 3,5-dihidroxyhexanal (**DHH**).

4.6.4.2.1 KRED^{354}-catalyzed DHP oxidation without NADP$^+$ regeneration

The developed mathematical model was validated by carrying out the experiment of DHP oxidation by KRED^{354} without coenzyme regeneration in batch reactor (Equations 94 – 96 and 100 – 106). The experimental and model simulation data are shown in Figure 80.

The reaction rate constant of the HOP decomposition (k_5) was estimated using the Equation 95 and experimental data shown in Figure 80a. The value was estimated to be 0.0025 min^{-1}.

Since the KRED^{354} activity decreased during the reaction (Figure 80b), the operational stability rate constant ($k_d^{KRED354}$) was estimated using the Equation 106 and experimental data shown in Figure 80b. It was estimated to be 0.0069 min^{-1}.

a) b)

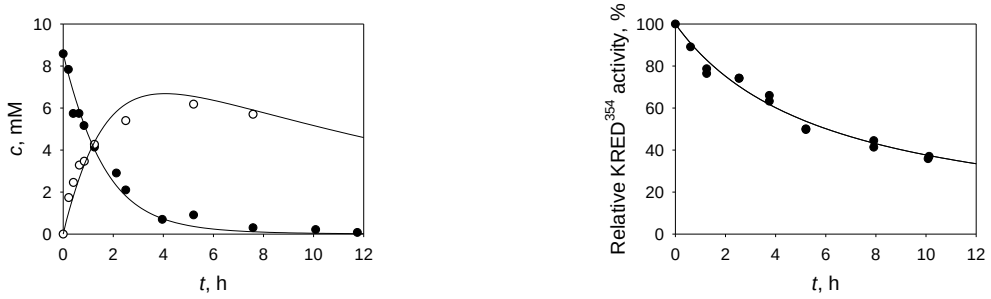

Figure 80 Experimental and simulation data of the oxidation of purified DHP into HOP catalyzed by KRED^{354} (0.1 M phosphate buffer pH 8, c_{DHP} = 8.6 mM, c_{NADP} = 10 mM, 1 000 rpm, $\gamma_{KRED354}$ = 10 mg/mL). Change of a) substrate DHP and product HOP concentration, b) relative enzyme activity during he experiment. Legend: experiment (dots), model (line); change of concentration with time: DHP (black), HOP (white).

Using the collected experimental data (Figure 80a), HOP yield, DHP conversion, STY, and BY were calculated. After three hours of the reaction, 1.8 g/L of HOP was produced, the obtained product yield was 74 %, substrate conversion was 96 %, the STY was 13.9 g/(L·day), while the BY was 0.33 $g_{HOP}/g_{KRED354}$. To obtain higher amounts of HOP, two NADP$^+$ regeneration systems were explored.

According to statistical outputs (R^2 = 0.99, σ = 0.96) and data shown in Figure 80 it could be concluded that the developed mathematical model described the experimental data well.

List of reactant and product abbreviations: acetaldehyde (**AA**), *N*-(3-oxopropyl)-2-phenylacetamide (**OPA**), *N*-(2-((2*R*,4*R*)-4,6-dihydroxytetrahydro-2*H*-pyran-2-yl)ethyl)-2-phenylacetamide (**DHP**), *N*-(2-((2*R*,4*R*)-4-hydroxy-6-oxotetrahydro-2*H*-pyran-2-yl)ethyl)-2-phenylacetamide (**HOP**), 3,5-dihidroxyhexanal (**DHH**).

4.6.4.2.2 KRED^{354}-catalyzed DHP oxidation with NADP$^+$ regeneration catalyzed by NOX^{001}

The developed mathematical model for the DHP oxidation catalyzed by KRED^{354} with NADP$^+$ regeneration catalyzed by NOX^{001} was validated in the batch reactor (Equations 94 – 97 and 100 – 107).

The experimental data for the oxidation of purified DHP catalyzed by KRED^{354} with NOX^{001}-catalyzed coenzyme regeneration system in the batch reactor are shown in Figure 81.

It was observed that the concentration of the HOP started to decrease at one point of the experiment. This side reaction was described as first-order kinetics (Equation 95) and its reaction rate constant was estimated (k_5 = 0.0012 min^{-1}).

During the experiment, both enzymes (Figure 81b and c) showed good operational stability, although they had lost a certain amount of their initial activity during the reaction. The values of the operational stability rate constants for both enzymes were estimated using the experimental data, Equation 106 ($k_d^{KRED354}$ = 0.0031 min^{-1}) and Equation 107 (k_d^{NOX001} = 0.0047 min^{-1}).

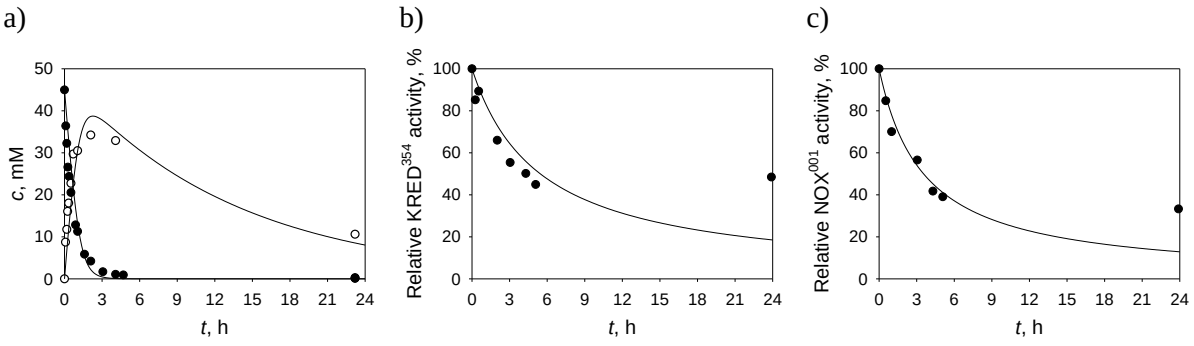

Figure 81 Experimental and simulation data of the KRED^{354}-catalyzed oxidation of purified DHP into HOP with NOX^{001}-catalyzed regeneration system (0.1 M phosphate buffer pH 8, c_{DHP} = 45 mM, c_{NADP} = 10 mM, $\gamma_{KRED354}$ = 10 mg/mL, γ_{NOX001} = 10 mg/mL, 1 000 rpm, 25 °C). Change of a) substrate DHP and product HOP concentration; and relative enzyme activity of b) KRED^{354} and c) NOX^{001} during the experiment. Legend: experiment (dots), model (line); change of concentration with time: DHP (black), HOP (white).

After 24 hours of the experiment, full substrate conversion was achieved (X_{DHP} >> 99.9 %), although the product yield was only 51 %. The HOP yield, due to the obvious side reaction, started to decrease after 2.3 hours from the start of the reaction (t = 2.3 h: $Y_{HOP/DHP}$ = 86 %,

List of reactant and product abbreviations: acetaldehyde (**AA**), *N*-(3-oxopropyl)-2-phenylacetamide (**OPA**), *N*-(2-((2*R*,4*R*)-4,6-dihydroxytetrahydro-2*H*-pyran-2-yl)ethyl)-2-phenylacetamide (**DHP**), *N*-(2-((2*R*,4*R*)-4-hydroxy-6-oxotetrahydro-2*H*-pyran-2-yl)ethyl)-2-phenylacetamide (**HOP**), 3,5-dihidroxyhexanal (**DHH**).

X_{DHP} = 96 %). The STY was calculated after 2.3 h of the experiment (10.7 g/L HOP produced) and equaled 111.7 g/(L·day), while the BY was 3.7 $g_{HOP}/g_{KRED354}$.

Comparing the experimental and simulation data (Figure 81) and taking statistical calculations into account (R^2 = 0.96, σ = 4.4) it can be concluded that the developed models described the experimental results acceptable.

4.6.4.2.3 KRED^{354}-catalyzed DHP oxidation with NADP$^+$ regeneration catalyzed by KRED^{011}

The developed mathematical model of the KRED^{354}-catalyzed DHP oxidation with NADP$^+$ regeneration catalyzed by KRED^{011} was validated in the batch reactor (Equations 94 – 96, 98 – 106 and 108). The experimental data for the KRED^{354}-catalyzed oxidation of purified DHP with KRED^{011}-catalyzed coenzyme regeneration in a batch reactor are shown in Figure 82.

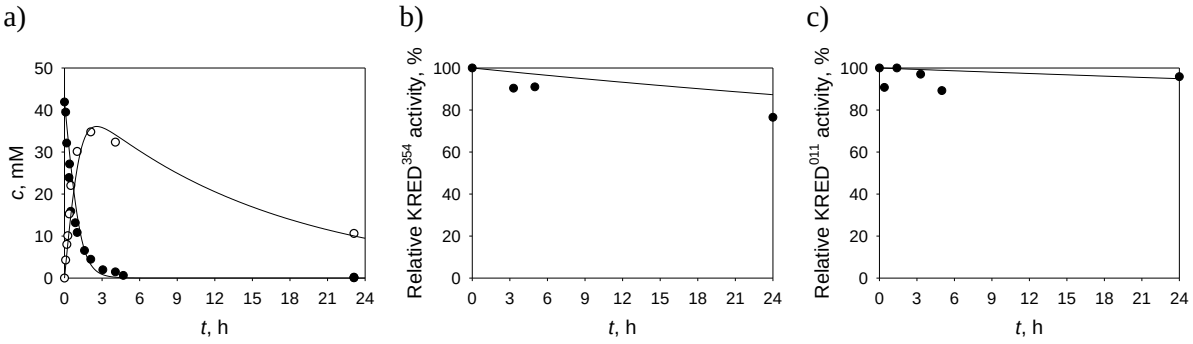

Figure 82 Experimental and simulation data of the KRED^{354}-catalyzed oxidation of purified DHP into HOP with KRED^{011}-catalyzed regeneration system (0.1 M phosphate buffer pH 8, 1 000 rpm, 25 °C, c_{DHP} = 42 mM, c_{NADP} = 10 mM, c_{ACE} = 150 mM, $\gamma_{KRED354}$ = 10 mg/mL, $\gamma_{KRED011}$ = 10 mg/mL). Change of a) substrate DHP and product HOP concentration; and relative enzyme activity of b) KRED^{354} and c) KRED^{011} during the experiment. Legend: experiment (dots), model (line); change of concentration with time: DHP (black), HOP (white).

The reaction rate constant for the observed side reaction of HOP degradation was estimated using the Equation 95 and collected data (Figure 82a). It was estimated to be 0.0011 min^{-1}, which was, as expected, almost of identical value as the one estimated in the experiment with NOX^{001}-catalyzed NADP$^+$ regeneration system.

List of reactant and product abbreviations: acetaldehyde (**AA**), *N*-(3-oxopropyl)-2-phenylacetamide (**OPA**), *N*-(2-((2*R*,4*R*)-4,6-dihydroxytetrahydro-2*H*-pyran-2-yl)ethyl)-2-phenylacetamide (**DHP**), *N*-(2-((2*R*,4*R*)-4-hydroxy-6-oxotetrahydro-2*H*-pyran-2-yl)ethyl)-2-phenylacetamide (**HOP**), 3,5-dihidroxyhexanal (**DHH**).

The enzymes showed higher operational stability during this experiment than in the $KRED^{354}/NOX^{001}$-catalyzed experiment, losing between 10 and 20 % of their initial activity (Figure 82b and c). Using the experimental data (Figure 82b and c) and the second-order enzyme deactivation kinetics (Equation 106 and 108), the deactivation rate constants of both enzymes were estimated ($k_d^{KRED354}$ = 0.00010 min^{-1}, $k_d^{KRED011}$ = 0.00003 min^{-1}). By comparing the estimated $k_d^{KRED354}$s in the experiment with NOX^{001}-catalyzed $NADP^+$ regeneration (0.0031 min^{-1}, Figure 81b) with the value estimated from this experiment (Figure 82b), it can be observed that in this experiment the operational stability rate constant was 31-fold lower than in the previous experiment. This may be caused by different composition of used CFEs, suggesting that the $KRED^{011}$ CFE has an additional stabilizing effect on $KRED^{354}$.

The experiment had a similar outcome as the experiment with NOX^{001}-catalyzed coenzyme regeneration (Figure 81a *vs* Figure 82a). After 24 hours, the final product yield was only 27 % despite full substrate conversion was obtained (X_{DHP} >> 99.9 %). The highest product yield was observed after 2.6 hours (t = 2.6 h: $Y_{HOP/DHP}$ = 86 %, X_{DHP} = 96 %). The final HOP concentration, STY and BY were calculated after 2.6 h and equaled 10.0 g/L HOP, 92.3 g/(L·day) and 57.6 $g_{DHP}/g_{KRED354}$, respectively. The calculated STY was lower in this experiment than in the experiment with NOX^{001}-catalyzed $NADP^+$ regeneration.

Comparing the experimental and simulation data (Figure 82) it can be concluded that the developed models described the experimental results well (R^2 = 0.97, σ = 3.4).

4.6.4.2.4 Concluding remarks: $KRED^{354}$-catalyzed DHP oxidation

To obtain higher amounts of HOP and to make the reaction economically feasible, two $NADP^+$ regeneration systems were explored: NOX^{001}- and $KRED^{011}$-catalyzed NADPH oxidation. Summarized results are presented in Table 36. From the data for the oxidation of purified DHP with and without coenzyme regeneration it could be concluded that higher STYs and BYs were obtained when the reaction was conducted with enzyme-catalyzed $NADP^+$ regeneration. Both $KRED^{354}/NOX^{001}$ and $KRED^{354}/KRED^{011}$ systems revealed similar reaction trend.

List of reactant and product abbreviations: acetaldehyde (**AA**), *N*-(3-oxopropyl)-2-phenylacetamide (**OPA**), *N*-(2-((2*R*,4*R*)-4,6-dihydroxytetrahydro-2*H*-pyran-2-yl)ethyl)-2-phenylacetamide (**DHP**), *N*-(2-((2*R*,4*R*)-4-hydroxy-6-oxotetrahydro-2*H*-pyran-2-yl)ethyl)-2-phenylacetamide (**HOP**), 3,5-dihidroxyhexanal (**DHH**).

During all conducted reactions, HOP decomposition was noted. The reaction rate constant (k_5, Equation 95) for its degradation was estimated in each conducted experiment:

1. KRED^{354}-catalyzed DHP oxidation,
2. KRED^{354}-catalyzed DHP oxidation with NOX^{001}-catalyzed NADP$^+$ regeneration, and
3. KRED^{354}-catalyzed DHP oxidation with KRED^{011}-catalyzed NADP$^+$ regeneration.

As expected, in all three experiments its reaction rate constant was estimated to be of similar value. Additionally, to confirm that the HOP decomposition is not dependent on the presence of enzymes, the stability of HOP in buffer (0.1 M phosphate buffer pH 8) was examined as well. HOP was obtained following the procedure described in Chapter 4.2.4.2. The HOP stability was followed for 2 days since it lost around 80 % of its initial concentration during first 24 hours of incubation (Figure 83). This finding is in accordance with the HOP degradation during all KRED^{354}-catalyzed DHP oxidations (with and without NADP$^+$ regeneration). Based on this, it was concluded that HOP decomposition is a chemical decomposition.

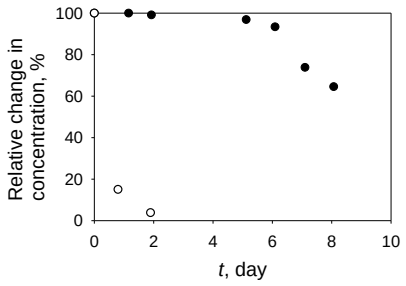

Figure 83 Stability of DHP and HOP in buffer expressed as relative change of their concentration over time. Legend: DHP (black), HOP (white). Reaction conditions: 0.1 M phosphate buffer pH 8, 25 °C.

4.6.4.3 Concluding remarks: one-step biocatalysis

Based on the collected data for the one-step production of the second statin side-chain precursor, following could be concluded.

List of reactant and product abbreviations: acetaldehyde (**AA**), *N*-(3-oxopropyl)-2-phenylacetamide (**OPA**), *N*-(2-((2*R*,4*R*)-4,6-dihydroxytetrahydro-2*H*-pyran-2-yl)ethyl)-2-phenylacetamide (**DHP**), *N*-(2-((2*R*,4*R*)-4-hydroxy-6-oxotetrahydro-2*H*-pyran-2-yl)ethyl)-2-phenylacetamide (**HOP**), 3,5-dihidroxyhexanal (**DHH**).

By carrying out the DERA^{062}-catalyzed aldol reaction in a repetitive batch reactor, the reaction should yield industrially relevant metrics, such as for STY, substrate conversion or final product concentration within nine hours of the reaction (Table 35).

The KRED^{354}-catalyzed DHP oxidation should be paired with a $NADP^+$ regeneration system (Table 36).

Based on the statistic parameters provided by *Scientist* and goodness-of-fit of experimental data with the model, it was concluded that the developed mathematical models could be used for future predictions of the reaction conditions in the studied reactions.

4.6.5 Validation of developed mathematical models: multi-step one-pot biocatalysis

To simplify the reaction system, the production of the second statin side-chain precursor (Figure 2) was examined to be conducted as a multi-step one-pot reaction. Thus, the following multi-step one-pot setups were explored:

1. DERA^{062}-catalyzed DHP production → KRED^{354}-catalyzed DHP oxidation,
2. DERA^{062}-catalyzed DHP production → KRED^{354}-catalyzed DHP oxidation with NOX^{001}-catalyzed $NADP^+$ regeneration, and
3. DERA^{062}-catalyzed DHP production → KRED^{354}-catalyzed DHP oxidation with KRED^{011}- catalyzed $NADP^+$ regeneration.

A simultaneous one-step one-pot reaction containing both DERA^{062} and KRED^{354} enzyme could not be conducted, since the KRED^{354} enzyme does not oxidize the aldehydes selectively and therefore would oxidize the DERA^{062} substrates into their corresponding acids.

The multi-step one-pot reactions were conducted with crude DHP substrate without the removal of the DERA^{062} enzyme. The crude DHP substrate was obtained by carrying the DERA^{062}-catalyzed aldol addition as described in Figure 76. If lower concentrations of crude DHP were needed, the DERA^{062} reaction solution was diluted using 0.1 M phosphate buffer pH 8. Prior to carrying the oxidation, the pH was adjusted to pH 8 using 5 M KOH solution, since the DHP oxidation is conducted at pH 8.

List of reactant and product abbreviations: acetaldehyde (**AA**), *N*-(3-oxopropyl)-2-phenylacetamide (**OPA**), *N*-(2-((2*R*,4*R*)-4,6-dihydroxytetrahydro-2*H*-pyran-2-yl)ethyl)-2-phenylacetamide (**DHP**), *N*-(2-((2*R*,4*R*)-4-hydroxy-6-oxotetrahydro-2*H*-pyran-2-yl)ethyl)-2-phenylacetamide (**HOP**), 3,5-dihidroxyhexanal (**DHH**).

4.6.5.1 Sequential one-pot HOP synthesis with KRED^{354}

The sequential one-pot HOP synthesis was conducted by carrying following two reactions in sequential order:

1. DERA^{062}-catalyzed DHP production, and
2. KRED^{354}-catalyzed DHP oxidation without $NADP^+$ regeneration.

The model simulation and experimental data of the sequential one-pot reaction of KRED^{354}-catalyzed DHP oxidation are shown in Figure 84. Since the reaction was conducted with five times higher concentration of DHP than $NADP^+$, instead of equimolar concentrations, the model predicted expectable results.

The experimental data (Figure 84a) and the developed model were used for estimating the values of the reaction rate constant of the side reaction (HOP decomposition, k_5 = 0.0012 min^{-1}) and the enzyme deactivation rate constant ($k_d^{KRED354}$ = 0.0009 min^{-1}).

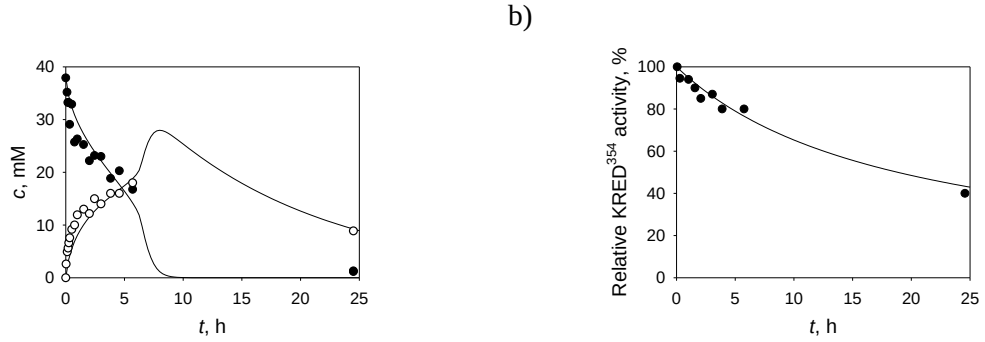

Figure 84 Experimental and simulation data of the KRED^{354}-catalyzed oxidation of crude DHP into HOP (0.1 M phosphate buffer pH 8, c_{DHP} = 38 mM, c_{NADP} = 10 mM, $\gamma_{KRED354}$ = 10 mg/mL, 1 000 rpm, 25 °C). Change of a) substrate DHP and product HOP concentration and b) relative enzyme activity of KRED^{354} during the experiment. Legend: experiment (dots), model (line); change of concentration with time: DHP (black), HOP (white).

By comparing the KRED^{354} operational stability rate constant estimated in this experiment (Figure 84b) with the one estimated in the experiment conducted with purified DHP (Figure 80b), it could be observed that the KRED^{354} operational stability rate constant was approx. 8-fold lower, which could be attributed to higher protein content in the reaction solution [191]. Additionally, it was concluded that HOP had 2-fold higher stability in this reaction (Figure 84b) than in the reaction conducted with purified DHP (Figure 80a), suggesting a

List of reactant and product abbreviations: acetaldehyde (**AA**), *N*-(3-oxopropyl)-2-phenylacetamide (**OPA**), *N*-(2-((2*R*,4*R*)-4,6-dihydroxytetrahydro-2*H*-pyran-2-yl)ethyl)-2-phenylacetamide (**DHP**), *N*-(2-((2*R*,4*R*)-4-hydroxy-6-oxotetrahydro-2*H*-pyran-2-yl)ethyl)-2-phenylacetamide (**HOP**), 3,5-dihidroxyhexanal (**DHH**).

favorable impact of the unrefined (crude) reaction solution on the compounds participating in the examined reaction.

After 3.9 hours of the reaction, when maximal concentration of HOP was observed in the reaction, 4.9 g/L of HOP was produced. The DHP conversion at that point was 50 %, while the HOP yield was 46 %. The calculated STYs and BYs were 30.2 g/(L·day) and 0.49 $g_{HOP}/g_{KRED354}$, respectively.

Based on the goodness-of-fit statistics (R^2 = 0.98, σ = 0.98) and data shown in Figure 84, the developed mathematical model described the experimental results well.

4.6.5.2 Sequential one-pot HOP synthesis with KRED^{354}/NOX^{001}

The KRED^{354}-catalyzed DHP oxidation with NOX^{001}-catalyzed coenzyme regeneration resulted after 24 hours in 99.7 % substrate conversion and 12 % product yield. The experimental and simulation data are shown in Figure 85.

The reaction rate constant for the observed side reaction (k_5) was estimated using the collected experimental data (Figure 85a) and Equation 95. The estimated value was 0.0013 min^{-1} and was of similar value as the one estimated in the same experiment but with purified DHP (k_5 = 0.0012 min^{-1}, Chapter 4.6.4.2.2).

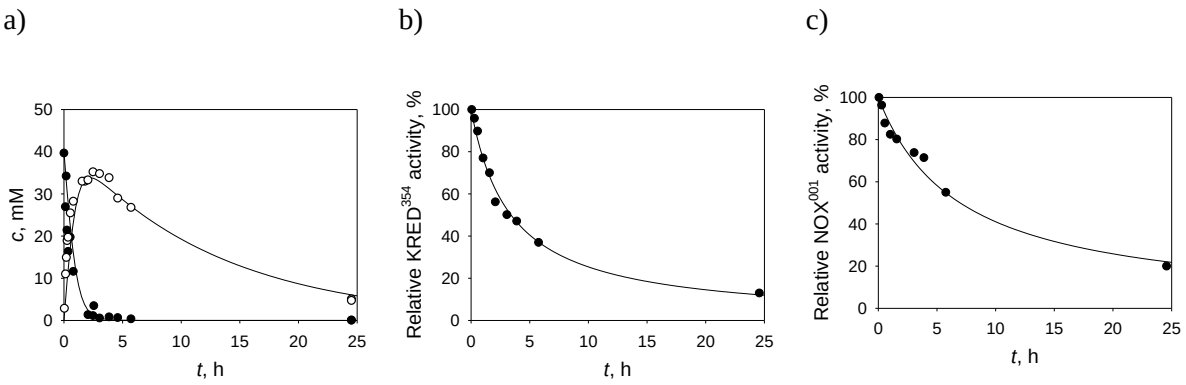

Figure 85 Experimental and simulation data of the KRED^{354}-catalyzed oxidation of crude DHP into HOP with NOX^{001}-catalyzed regeneration system (0.1 M phosphate buffer pH 8, c_{DHP} = 40 mM, c_{NADP} = 10 mM, $\gamma_{KRED354}$ = 10 mg/mL, γ_{NOX001} = 10 mg/mL, 1 000 rpm, 25 °C). Change of a) substrate DHP and product HOP concentration; and relative enzyme activity of b) KRED^{354} and c) NOX^{001} during the experiment. Legend: experiment (dots), model (line); change of concentration with time: DHP (black), HOP (white).

List of reactant and product abbreviations: acetaldehyde (**AA**), *N*-(3-oxopropyl)-2-phenylacetamide (**OPA**), *N*-(2-((2*R*,4*R*)-4,6-dihydroxytetrahydro-2*H*-pyran-2-yl)ethyl)-2-phenylacetamide (**DHP**), *N*-(2-((2*R*,4*R*)-4-hydroxy-6-oxotetrahydro-2*H*-pyran-2-yl)ethyl)-2-phenylacetamide (**HOP**), 3,5-dihidroxyhexanal (**DHH**).

The operational stability rate constant (k_d) for both enzymes were estimated using the experimental data (Figure 85b and c) and second-order deactivation kinetics (Equation 106 and 107). For KRED^{354}, the estimated value of the deactivation rate constant was 0.0049 min^{-1}, while for NOX^{001} it was 0.0024 min^{-1}. The estimated constants were of similar value to the constants estimated in the same experiment but conducted with purified DHP (Figure 85).

The maximum HOP yield of 85 % was obtained after 2.3 hours (9.4 g/L HOP produced), while the conversion of DHP equaled 96 %. The STY and BY were calculated for the 2.3 h time point and were 98.1 g/(L·day) and 2.4 $g_{HOP}/g_{KRED354}$, respectively.

By comparing the simulation and experimental data (Figure 85), it could be concluded that the developed mathematical model described the experimental data well (R^2 = 0.97, σ = 0.84).

4.6.5.3 Sequential one-pot HOP synthesis with KRED^{354}/KRED^{011}

The KRED^{354}-catalyzed DHP oxidation with KRED^{011}-catalyzed coenzyme regeneration resulted after 24 hours in full substrate conversion (X_{DHP} >> 99.9 %) and 16 % yield of product HOP. The experimental and simulation data are shown in Figure 86.

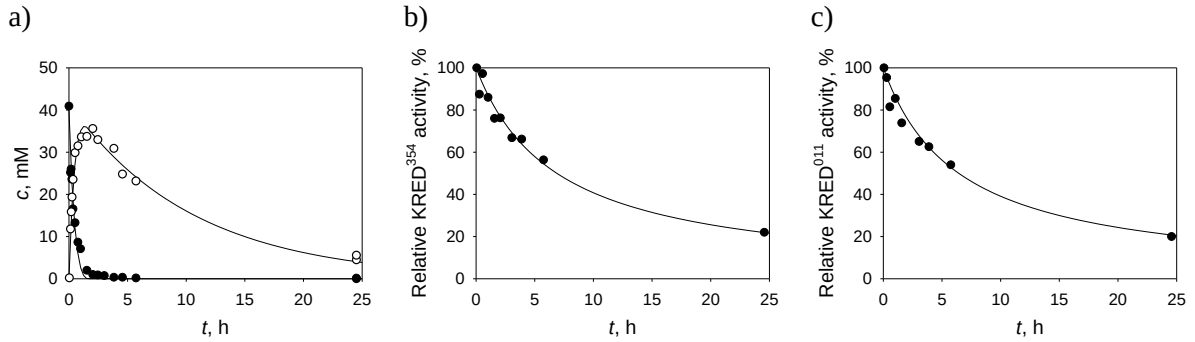

Figure 86 Experimental and simulation data of the KRED^{354}-catalyzed oxidation of crude DHP into HOP with KRED^{011}-catalyzed regeneration system (0.1 M phosphate buffer pH 8, c_{DHP} = 40 mM, c_{NADP} = 10 mM, c_{ACE} = 150 mM, $\gamma_{KRED354}$ = 10 mg/mL, $\gamma_{KRED011}$ = 10 mg/mL, 1 000 rpm, 25 °C). Change of a) substrate DHP and product HOP concentration; and relative enzyme activity of b) KRED^{354} and c) KRED^{011} during the experiment. Legend: experiment (dots), model (line); change of concentration with time: DHP (black), HOP (white).

Using the collected data (Figure 86a) and the first-order kinetics (Equation 95), the reaction rate constant for the HOP decomposition was estimated (k_5 = 0.0016 min^{-1}). As a

List of reactant and product abbreviations: acetaldehyde (**AA**), *N*-(3-oxopropyl)-2-phenylacetamide (**OPA**), *N*-(2-((2*R*,4*R*)-4,6-dihydroxytetrahydro-2*H*-pyran-2-yl)ethyl)-2-phenylacetamide (**DHP**), *N*-(2-((2*R*,4*R*)-4-hydroxy-6-oxotetrahydro-2*H*-pyran-2-yl)ethyl)-2-phenylacetamide (**HOP**), 3,5-dihidroxyhexanal (**DHH**).

comparison, when the same reaction was catalyzed using purified DHP substrate (Figure 85), the estimated value of the reaction rate constant was 0.0011 min^{-1}, predicting a similar value.

During the 24-hour period, the enzymes lost around 60 % of their initial activity, and the deactivation rate constants for $KRED^{354}$ and $KRED^{011}$ were estimated using the second-order kinetics and obtained experimental data. The estimated values of the deactivation rate constants for $KRED^{354}$ and $KRED^{011}$ were 0.0024 and 0.0026 min^{-1}, respectively.

The highest HOP yield was after 2.5 hours and equaled 82 % at which point 9.1 g/L of HOP was produced. The DHP conversion was 92 %. Using this data, STY and BY were calculated and equaled 87.3 g/(L·day) and 3.4 $g_{HOP}/g_{KRED354}$, respectively.

By comparing the experimental data with model simulation data (Figure 86), it could be concluded that the developed model described the experimental results very good (R^2 = 0.99, σ = 0.98).

4.6.5.4 Concluding remarks: multi-step one-pot biocatalysis

The summarized results regarding the multi-enzyme one-pot $KRED^{354}$-catalyzed oxidation of purified and crude DHP are given in Table 36. All described experiments were conducted in a batch reactor at similar reaction conditions: ~ 40 mM DHP, 10 mM $NADP^+$ and 10 mg/mL $KRED^{354}$. In case when the reaction was conducted with a coenzyme regeneration system, 10 mg/mL of the auxiliary enzyme (NOX^{001}, $KRED^{011}$ + 150 mM ACE) was added, except in case of the $KRED^{354}$-catalyzed oxidation of purified DHP without coenzyme regeneration when the DHP concentration was 8.6 mM instead of 40 mM.

From the reactions carried out with *in situ* $NADP^+$ regeneration systems, it could be concluded that both regeneration systems served equally good regardless of substrate type (purified *vs* crude) and that the experimental outcome of all four experiments showed comparable data. Due to an obvious side reaction of product HOP decomposition, the product yield decreased with time, but reached its peak quite fast: after about 2.4 hours from the beginning of the experiment. The HOP decomposition rate constant was estimated in all four experiments separately but ended being of similar value. This could serve as a confirmation that decomposition proceeded at the same rate (k_5) and does not depend on the reaction mixture composition, in addition to HOP stability data shown in Figure 83.

List of reactant and product abbreviations: acetaldehyde (**AA**), *N*-(3-oxopropyl)-2-phenylacetamide (**OPA**), *N*-(2-((2*R*,4*R*)-4,6-dihydroxytetrahydro-2*H*-pyran-2-yl)ethyl)-2-phenylacetamide (**DHP**), *N*-(2-((2*R*,4*R*)-4-hydroxy-6-oxotetrahydro-2*H*-pyran-2-yl)ethyl)-2-phenylacetamide (**HOP**), 3,5-dihidroxyhexanal (**DHH**).

Table 36 The KRED^{354}-catalyzed oxidation of purified and crude CDH. The reactions were conducted with 40 mM DHP, 10 mM NADP$^+$, and 10 mg/mL per enzyme.

Catalyst system	DHP	k_5, min^{-1}	*t*, h [a]	*X*, %	*Y*, %	STY	BY
KRED^{354}	Purified	0.0025	3.1	96	74	13.9	0.18
	Crude	0.0012	3.9	50	46	30.2	0.49
KRED^{354}/NOX^{001}	Purified	0.0012	2.3	96	86	111.7	0.54
	Crude	0.0012	2.3	96	85	98.1	0.47
KRED^{354}/KRED^{011}	Purified	0.0011	2.6	96	86	92.3	0.5
	Crude	0.0016	2.5	92	82	87.3	0.46

[a] end of the reaction
Notes: X represents DHP conversion, *Y* represents HOP yield, while STY is expressed as g/(L·day) and BY as $g_{HOP}/g_{KRED354}$.

During all KRED^{354}-catalyzed DHP oxidations, HOP decomposition was observed (Figure 80 – 86). Independent measurements on HOP stability revealed chemical HOP degradation (Figure 83). HOP decomposition may be circumvented by carrying out a simultaneous one-pot KRED^{354}-catalyzed DHP oxidation (with NOX^{001}- or KRED^{011}-catalyzed NADP$^+$ regeneration) and e.g. lipase-catalyzed acylation with vinyl acetate [192]. This way, DHP is oxidized into HOP and HOP is immediately acylated, thus preventing loss on product yields.

By comparing the KRED^{354}/NOX^{001} to KRED^{354}/KRED^{011}, marginally higher values of DHP conversion, HOP yield, STY and BY were reached slightly earlier. All four enzymes in both experimental setups showed high operational stability.

Based on this, both regeneration systems (NOX^{001}, KRED^{011}/ACE) fulfilled their purpose and resulted with a very similar experimental outcome. Thus, the NOX^{001}-catalyzed coenzyme regeneration should be favorable, due to no need of an additional co-substrate.

List of reactant and product abbreviations: acetaldehyde (**AA**), *N*-(3-oxopropyl)-2-phenylacetamide (**OPA**), *N*-(2-((2*R*,4*R*)-4,6-dihydroxytetrahydro-2*H*-pyran-2-yl)ethyl)-2-phenylacetamide (**DHP**), *N*-(2-((2*R*,4*R*)-4-hydroxy-6-oxotetrahydro-2*H*-pyran-2-yl)ethyl)-2-phenylacetamide (**HOP**), 3,5-dihidroxyhexanal (**DHH**).

5 CONCLUSION

Two statin side-chain precursors were examined using a multi-step approach that combined enzymes from different classes. The first precursor was produced by combining DERA^{Tm}- or DERA^{024}-, AlDH/NOX^{009}- or KRED^{332}-, and HHDH^{001}-catalyzed reactions using AA and CAA as starting materials, whereas the second precursor was obtained by combining DERA^{062}- and KRED^{354}/NOX^{001}- or KRED^{354}/KRED^{011}-catalyzed reactions using OPA and AA as starting compounds.

The optimum buffer and pH for running the examined enzyme-catalyzed reactions were experimentally determined based on the enzyme stability and activity results in the designated buffer. It was experimentally determined that the optimal buffer for the DERA^{Tm}-catalyzed aldol reaction of AA with CAA was 0.1 M TEA-HCl buffer pH 7, while the optimal buffer for the DERA^{024}-catalyzed aldol reaction was 0.1 M phosphate buffer pH 6. For the reaction catalyzed by the AlDH enzyme or by the AlDH/NOX^{009} system, 0.1 M phosphate buffer pH 8 was chosen. The optimal buffer for the DERA^{062}-catalyzed aldol reaction of AA with OPA was found to be 0.1 M phosphate buffer pH 7, while for the consecutive KRED^{354}-catalyzed reaction the same buffer was chosen but at pH 8.

The influence of temperature on the DERA^{Tm} activity and stability was investigated. The results confirmed that the enzyme's activity increases with the increase of temperature, which is in accordance with the Arrhenius equation. Using the collected data, the equations' parameters were estimated. The enzyme displayed good thermostability retaining 87 % of its initial activity after three days of incubation at 20 – 25 °C.

The influence of different compounds (substrates, products) on the enzyme stability was evaluated and was described by a polynomial model. These results confirmed that it was necessary to determine optimal initial substrate concentrations and to select a suitable reactor configuration to avoid accumulation of compounds which have a destabilizing effect on the enzymes.

By applying the initial reaction rate method, the kinetics of each elementary reaction within the observed multi-enzyme (cascade) systems was determined. Each enzyme-catalyzed reaction was described by single- or double-substrate Michaelis-Menten kinetics. When experimentally observed, the kinetic equations were expanded with substrate and/or inhibition terms. Based on

the collected data of enzyme dependence on different concentrations of reaction compounds and developed kinetic models, mathematical models for different types of reactors were proposed. The developed mathematical models were validated in appropriate reactor types by conducting single- and multi-enzyme reactions.

The mathematical models were developed based on the reaction scheme and data collected from kinetic measurements. Using the validated mathematical models, the reaction conditions for the DERA-catalyzed aldol additions were optimized to obtain optimal quantity of key molecules and volume productivity. Final product concentration (> 50 g/L), substrate conversion (> 95 %, 24 h), BY (> 10 $g_{product}/g_{enzyme}$) and STY (> 100 g/(L·day)) served as relevant industrial requirements. The optimum conditions and reactor modes were found and validated in the reactor at experimental conditions proposed by optimum simulation.

To simplify the reaction systems, the examined reactions were carried out as cascade reactions. They were conducted as simultaneous and/or sequential one-pot reactions in batch reactors. The simultaneous one-pot reactions were carried out as DH-catalyzed oxidation with enzyme-catalyzed $NAD(P)^+$ regeneration. The sequential one-pot reactions were carried out with substrates and enzymes added to the rector one at a time. In both one-pot modes, the reactions were done without work-up. According the collected data, it was confirmed that it is possible to simplify the reaction setup by carrying out multi-enzyme multi-step one-pot reactions and thus obtain higher quantities of the desired product. It was not possible to conduct a simultaneous cascade consisting of DERA and DH enzymes, since the DH enzymes do not selectively oxidize aldehydes. Additionally, due to the cyanohydrin reaction, the simultaneous one-pot cascade consisting of AlDH/NOX^{009} and $HHDH^{001}$ could not be performed as well. Despite, it was experimentally proven that these cascades could be conducted in a sequential manner.

In the first cascade, between $DERA^{Tm}$ and $DERA^{024}$, $DERA^{024}$ was chosen as the preferred DERA catalyst in the aldol reaction of AA with CAA, while for the CDH oxidation the suitable enzyme system was the AlDH/NOX^{009} system instead of the $KRED^{332}$ enzyme. The multi-step one-pot cascade involving the $DERA^{024}$ and AlDH/NOX^{009} enzymes met certain industrial requirements, in comparison to the multi-step one-pot $DERA^{024}$ and $KRED^{332}$ cascade. The cascades were conducted in a batch reactor. The aldol reactions were further carried out in a repetitive batch reactor mode, meaning both substrates and $DERA^{024}$ were added again into the batch reactor once full substrate conversion was achieved or the activity of the

enzyme was recorded to be below 20 %. Once the desired quantity of the aldol product was obtained, the following, consecutive oxidation was carried out in the same reactor by adding the necessary $NAD(P)^+$ coenzyme and the DH enzyme(s). The oxidations were conducted in repetitive mode regarding enzyme additions: fresh amounts of enzymes were added into the reactor when their residual activity was measured to be less than 20 %.

By carrying out the second cascade, consisting of the $DERA^{062}$-catalyzed aldol reaction as the first catalytic step and the $KRED^{354}$-catalyzed DHP oxidation with NOX^{001}- or $KRED^{011}$-catalyzed $NADP^+$ regeneration as the second catalytic step, in a sequential, multi-step mode at optimal reaction conditions, the collected data suggested that both enzymes (NOX^{001} and $KRED^{011}$) could be successfully applied for the $NADP^+$ regeneration. Due to simplicity and slightly better results, the recommended regeneration system should be NOX^{001}. It was experimentally found that non-enzymatic HOP decomposition occurs. HOP decomposition may be circumvented by carrying out a simultaneous one-pot $KRED^{354}$-catalyzed DHP oxidation (with $NADP^+$ regeneration) combined with e.g. lipase-catalyzed acylation with vinyl acetate to avoid loss on product yields.

The conducted multi-step multi-enzyme one-pot reactions demonstrated that it is possible to carry out a successful cascade to meet certain industrial relevant metrics to produce fine chemicals, although the examined systems need further improvement due to observed side reactions in both systems.

All the developed mathematical models represent a valuable basis for future optimization of the applied enzyme cascades for the synthesis of statin side-chain precursors in different types of reactors.

6 BIBLIOGRAPHY

[1] M. D. Truppo, "Biocatalysis in the pharmaceutical industry: the need for speed," *ACS Medicinal Chemistry Letters,* vol. 8, no. 5, pp. 476-480, 2017.

[2] G. de Gonzalo and P. D. de Maria, Biocatalysis: an industrial perspective, Croydon: The Royal Society of Chemistry, pp. 44-97, 2018.

[3] D. J. Pollard and J. M. Woodey, "Biocatalysis for pharmaceutical intermediates: the future is now," *Trends in Biotechnology,* vol. 25, no. 2, pp. 66-73, 2007.

[4] J. M. Woodley, "New opportunities for biocatalysis: making pharmaceutical processes greener," *Trends in Biotechnology,* vol. 26, no. 6, pp. 321-327, 2008.

[5] P. J. Dunn, A. S. Wells and M. T. Williams, Eds., Green chemistry in the pharmaceutical industry, Weinheim: Wiley-VCH, pp. 1-48, 127-144, 2010.

[6] D. Maji, S. Shaikh, D. Solanki and K. Gauray, "Safety of statins," *Indian Journal of Endocrinology and Metabolism,* vol. 17, no. 4, pp. 636-646, 2013.

[7] A. Endo, "A historical perspective on the discovery of statins," *Proceedings of the Japan Academy, Series B,* vol. 86, no. 5, p. 484–493, 2010.

[8] A. Liljeblad, A. Kallinen and L. T. Kanerva, "Biocatalysis in the preparation of the statin side chain," *Current Organic Synthesis,* vol. 6, no. 4, pp. 362-379, 2009.

[9] D. De Berardis, S. Marini, M. Piersanti, M. Cavuto, G. Perna, A. Valchera, M. Mazza, M. Fornaro, F. Iasevoli, G. Martinotti and M. Di Giannantonio, "The relationships between cholesterol and suicide: an update," *International Scholarly Research Notices: Psychiatry,* vol. 2012, no. ID 387901, pp. 1-6, 2012.

[10] M. M. Zhang, X. Su, E. L. Ang and H. Zhao, "Recent advances in biocatalyst development in the pharmaceutical industry," *Pharmaceutical Bioprocessing,* vol. 1, no. 2, pp. 179-196, 2013.

[11] J. M. Patel, "Biocatalytic synthesis of atorvastatin intermediates," *Journal of Molecular Catalysis B: Enzymatic,* vol. 61, pp. 123-128, 2009.

[12] M. Ošlaj, J. Cluzeau, D. Orkić, G. Kopitar, P. Mrak and Z. Časar, "A highly productive, whole-cell DERA chemoenzymatic process for production of key lactonized side-chain intermediates in statin synthesis," *PLoS ONE,* vol. 8, no. 5, p. e62250, 2013.

[13] M. Müller, "Chemoenzymatic synthesis of building blocks for statin side chains," *Angewandte Chemie International Edition,* vol. 44, no. 3, pp. 362-365, 2005.

[14] A. Ručigaj and M. Krajnc, "Kinetic modeling of a crude DERA lysate-catalyzed process in synthesis of statin intermediates," *Chemical Engineering Journal,* vol. 259, pp. 11-24, 2015.

[15] A. Ručigaj and M. Krajnc, "Optimization of a crude deoxyribose-5-phosphate aldolase lyzate-catalyzed process in synthesis of statin intermediates," *Organic Process Research & Development (ACS Publications),* vol. 17, no. 5, pp. 854-862, 2013.

[16] J. Tao and J.-H. Xu, "Biocatalysis in development of green pharmaceutical processes," *Current Opinion in Chemical Biology,* vol. 13, no. 1, pp. 43-50, 2009.

[17] S. M. Nasmetova, D. M. Ruzieva, G. A. Rasulova, R. S. Sattarova and T. Gulyamova, "Effect of the principal nutrients on simvastatin production by wild strain *Aspergillus terreus* 20 in submerged fermentation," *International Journal of Current Microbiology and Applied Sciences,* vol. 4, no. 9, pp. 894-898, 2015.

[18] M. Schürmann, M. Wolberg, S. Panke and H. Kierkels, "The development of short, efficient, economic, and sustainable chemoenzymatic processes for statin side chains," in *Green chemistry in the pharmaceutical industry,* P. J. Dunn, A. S. Wells and M. T. Williams, Eds., Weinheim, Wiley-VCH, pp. 127-144, 2010..

[19] L. Hilterhaus, A. Liese, U. Kettling and G. Antranikian, Applied biocatalysis, Weinheim: Wiley-VCH, pp. 13-30, 53-70, 219-251, 367-404, 2016.

[20] M. Majerić Elenkov, L. Tang, B. Hauer and D. B. Janssen, "Sequential kinetic resolution catalyzed by halohydrin dehalogenase," *Organic Letters,* vol. 8, no. 19, pp. 4227-4229, 2006.

[21] Z.-Y. You, Z.-Q. Liu and Y.-G. Zheng, "Chemical and enzymatic approaches to the synthesis of optically pure ethyl (R)-4-cyano-3-hydroxybutanoate," *Applied Microbiology and Biotechnology,* vol. 98, no. 1, pp. 11-21, 2014.

[22] D. B. Janssen, M. Majerić-Elenkov, G. Hasnaoui, B. Hauer and J. H. Lutje Spelberg, "Enantioselective formation and ring-opening of epoxides catalysed by halohydrin dehalogenases," *Biochemical Society Transactions,* vol. 34, no. 2, pp. 291-295, 2006.

[23] N.-W. Wan, Z.-Q. Liu, K. Huang, Z.-Y. Shen, F. Xue, Y.-G. Zheng and Y.-C. Shen, "Synthesis of ethy (*R*)-4-cyano-3-hydroxybutarate in high concentration using novel halohydrin dehalogenase HHDH-PL from *Parvibaculum lavamenticvorans* DS-1," *RSC Advances,* vol. 4, no. 109, pp. 64027-64032, 2014.

[24] A. Schallmey and M. Schallmey, "Recent advances on halohydrin dehalogenases - from enzyme identification to novel biocatalytic applications," *Applied Microbiology and Biotechnology,* vol. 100, no. 18, pp. 7827-7839, 2016.

[25] X.-C. Jiao, Y.-J. Zhang, Q. Chen, J. Pan and J.-H. Xu, "A green-by-design system for efficient bio-oxidation of an unnatural hexapyranose into chiral lactone for building statin side-chains," *Catalysis Science & Technology,* vol. 6, pp. 7094-7100, 2016.

[26] S. Jennewein, M. Schürmann, M. Wolberg, I. Hilker, R. Luiten, M. Wubbolts and D. Mink, "Directed evolution of an industrial biocatalyst: 2-deoxy-D-ribose 5-phosphate aldolase," *Biotechnology Journal,* vol. 1, no. 5, pp. 537-548, 2006.

[27] Y. Luo, Y. Chen, H. Ma, Z. Tian, Y. Zhang and J. Zhang, "Enhancing the biocatalytic manufacture of the key intermediate of atorvastatin by focused directed evolution of halohydrin dehalogenase," *Scientific Reports,* vol. 7, no. 42064, pp. 1-9, 2017.

[28] A. K. Samland and G. A. Sprenger, "Microbial aldolases as C-C bonding enzymes - unknown treasures and new developments," *Applied Microbiology and Biotechnology,* vol. 71, no. 3, pp. 253-264, 2006.

[29] S. Schoffelen and J. C. M. van Hest, "Multi-enzyme systems: bringing enzymes together *in vitro*," *Soft Matter,* vol. 8, no. 6, pp. 1736-1746, 2012.

[30] J. Enoki, J. Meisborn, A. C. Müller and R. Kourist, "A multi-enzymatic cascade reaction for the stereoselective production of γ-oxyfunctionalyzed amino acids," *Frontiers in Microbiology,* vol. 7, no. 425, pp. 1-8, 2016.

[31] D. Vasić-Rački, U. Kragl and A. Liese, "Benefits of enzyme kinetics modelling," *Chemical and Biochemical Engineering Quarterly,* vol. 17, no. 1, pp. 7-18, 2003.

[32] A. Vrsalović Presečki and Đ. Vasić-Rački, "Mathematical modelling of the dehydrogenase catalyzed hexanol oxidation," *Process Biochemistry,* vol. 44, pp. 54-61, 2009.

[33] M. Sudar, Z. Findrik, Đ. Vasić-Rački, P. Clapés and C. Lozano, "Mathematical model for aldol addition catalyzed by two D-fructose-6-phosphate aldolases variants overexpressed in *E. coli*," *Journal of Biotechnology,* vol. 167, no. 3, pp. 191-200, 2013.

[34] T. Suau, G. Álvaro, M. D. Benaiges and J. López-Santín, "Kinetic modelling of aldolase-catalyzed addition between dihydroxyacetone phosphate and (*S*)-alaninal," *Biochemical Engineering Journal,* vol. 4, no. 1, pp. 95-103, 2008.

[35] J. H. Lutje Spelberg, R. Rink, R. M. Kellogg and D. B. Janssen, "Enantioselectivity of a recombinant epoxide hydrolase from *Agrobacterium radiobacter*," *Tetrahedron: Asymmetry,* vol. 9, pp. 459-466, 1998.

[36] G. Hasnaoui-Dijoux, M. Majerić Elenkov, J. H. Lutje Spelberg, B. Hauer and D. B. Janssen, "Catalytic promiscuity of halohydrin dehalogenase and its application in enantioselective epoxide ring opening," *ChemBioChem,* vol. 9, no. 7, pp. 1048-1051, 2008.

[37] J. Wolfe, "The Father of Green Chemistry," Forbes, Feb 2, 2012. [Online]. Available: www.forbes.com/sites/joshwolfe/2012/02/02/the-father-of-green-chemistry/#2d2aa3373a49. [Accessed Apr 10,2016].

[38] D. E. Nathan, "Paul Anastas, father of green chemistry, says world on an unsustainable course," BrandeisNOW, Apr 10, 2013. [Online]. Available: www.brandeis.edu/now/2013/april/cohenlecture.html. [Accessed Apr 10, 2016].

[39] M. Deetlefs and K. R. Seddon, "Assessing the greenness of some typical laboratory ionic liquid preparations," *Green Chemistry,* vol. 12, no. 1, pp. 17-30, 2010.

[40] M. Poliakoff, J. M. Fitzpatrick, T. R. Farren and P. T. Anastas, "Green chemistry: science and politics of change," *Science,* vol. 297, pp. 807-810, 2002.

[41] A. S. Bommarius and B. R. Riebel, Biocatalysis, Weinheim: Wiley-VCH, pp. 1-42, 91-134, 209-242, 373-412, 2004.

[42] M. Jukić, S. Đaković, Ž. Filipović-Kovačević and J. Vorkapić-Furač, "“Zelena” kemija otvara put čistim ekološki prihvatljivim kemijskim procesima," *Kemija u industriji,* vol. 53, no. 5, pp. 217-224, 2004.

[43] R. A. Sheldon, I. Arends and U. Hanefeld, Green Chemistry and Catalysis, Weinheim: Wiley-VCH, pp. 1-48, 223-264, 389-408, 2007.

[44] ACS, "12 Principles of Green Chemistry," American Chemical Society, [Online]. Available: www.acs.org/content/acs/en/greenchemistry/what-is-green-chemistry/principles/12-principles-of-green-chemistry.html. [Accessed Apr10, 2016].

[45] P. Anastas and J. C. Warner, Green Chemistry: Theory and Practice, Oxford: Oxford University Press, pp.1-7,1998.

[46] R. A. Sheldon, "Atom utilisation, *E* factors and the catalytic solution," *Surface chemistry and catalysis,* vol. 3, no. 7, pp. 541-551, 2000.

[47] I. T. Horvath and P. T. Anastas, "Innovations and green chemistry," *Chemical Reviews,* vol. 107, pp. 2169-2173 , 2007.

[48] P. T. Anastas, L. G. Heine and T. C. Williamson, "Green chemical syntheses and processes: introduction," in *Green chemical syntheses and processes*, P. T. Anastas, L. G. Heine and T. C. Williamson, Eds., Washington, DC, American Chemical Society, pp. 1-6, 2000.

[49] P. T. Anastas and J. B. Zimmerman, "The twelve principles of green engineering as a foundation of sustainability," in *Sustainability Science and Engineering Defining Principles*, M. Abraham, Ed., Oxford, Elsevier Science, pp. 11-32, 2006.

[50] M. Lancaster, Green Chemistry : An Introductory Text, Cambridge: Royal Society of Chemistry, pp. 1-20, 2010.

[51] ACS, "Green Chemistry Definition," American Chemical Society, [Online]. Available: www.acs.org/content/acs/en/greenchemistry/what-is-green-chemistry/definition.html. [Accessed Apr 10, 2016].

[52] A. Ivanković, A. Dronjić, A. Martinović Bevanda and S. Talić, "Review of 12 principles of green chemistry in practice," *International Journal of Sustainable and Green Energy,* vol. 6, no. 3, pp. 39-48, 2017.

[53] T. Dropper, T. Eggert, W. Hummel, C. Leggewie, M. Pohl, F. Rosenau, S. Wilhelm and K.-E. Jaeger, "Novel biocatalysis for white biotechnology," *Biotechnology Journal,* vol. 1, no. 7-8, pp. 777-786, 2006.

[54] T. Haas, M. Kircher, T. Köhler, W. Günter, U. Schörken and R. Hagen, "White Biotechnology," in *Sustainable solutions for modern economies*, R. Höfer, Ed., Cambridge, Royal Society of Chemistry, pp. 436-478, 2009.

[55] P. Lorenz and H. Zinke, "White biotechnology: differences in US and EU approaches?," *Trends in Biotechnology,* vol. 23, no. 12, pp. 570-574, 2005.

[56] A. G. Sabale and V. M. Rane, "Enzymes: for today and tomorrow," *Colourage,* vol. 59, no. 5, pp. 33-39, 2012.

[57] M. Moo-Young and Y. Chisti, "Biochemical engineering in biotechnology (Technical Report)," *Pure and Applied Chemistry,* vol. 66, no. 1, pp. 117-136, 1994.

[58] R. C. Simon, F. G. Mutti and W. Kroutil, "Biocatalytic synthesis of enantiopure building blocks for pharmaceuticals," *Drug Discovery Today: Technologies,* vol. 10, no. 1, pp. 37-44, 2013.

[59] G. Frazzetto, "White biotechnology," *European Molecular Biology Organization ,* vol. 4, no. 9, pp. 835-837, 2003.

[60] O. Kirk, T. V. Borchert and C. C. Fuglsang, "Industrial enzyme applications," *Current Opinion in Biotechnology,* vol. 13, no. 4, p. 2002, 345-351.

[61] K. Faber, Biotransformations in organic chemistry: a textbook, Berlin: Springer-Verlag, pp. 1-312, 2011.

[62] H.-P. Meyer, E. Eichhorn, S. Hanlon, S. Lütz, M. Schürmann, R. Wohlgemuth and R. Coppolecchia, "The use of enzymes in organic synthesis and life sciences: perspectives from Swiss Industrial Biocatalysis Consortium (SIBC)," *Catalysis Science & Technology,* vol. 3, no. 29, pp. 29-40, 2013.

[63] B. M. Nestl, B. A. Nebel and B. Hauer, "Recent progress in industrial biocatalysi," *Current Opinion in Chemical Biology,* vol. 15, no. 2, pp. 187-193, 2011.

[64] U. T. Bornscheuer, W. Huisman, R. J. Kazlauskas, S. Lutz, J. C. Moore and K. Robins, "Engineering the thirdwave of biocatalysis," *Nature,* vol. 485, pp. 185-194, 2012.

[65] B. Sarrouh, T. M. Santon, A. Miyoshi, R. Dias and V. Azevedo, "Up-to-date insight on industrial enzymes applications and global market," *Journal of Bioprocessing & Biotechniques,* vol. S4, no. 002, pp. 1-10, 2012.

[66] M. Vellard, "The enzyme as drug: application of enzymes as pharmaceuticals," *Current Opinion in Biotechnology,* vol. 14, no. 4, pp. 444-450, 2003.

[67] S. M. Dean, W. A. Greenberg and C. H. Wonga, "Recent advances in aldolase-catalyzed asymmetric synthesis," *Advanced Synthesis & Catalysis,* vol. 349, no. 8-9, pp. 1308-1320, 2007.

[68] G. W. Huisman, J. Liang and A. Krebber, "Practical chiral alcohol manufacture using ketoreductases," *Current Opinion in Chemical Biology,* vol. 14, no. 2, pp. 122-129, 2010.

[69] F. Hollmann, I. Arends, K. Buehler, A. Schallmey and B. Bühler, "Enzyme-mediated oxidations for the chemist," *Green. Chem.*, vol. 13, no. 2, pp. 226-265, 2011.

[70] S. Panke and M. Wubbolts, "Advances in biocatalytic synthesis of pharmaceutical intermediates," *Current Opinion in Chemical Biology,* vol. 9, no. 2, pp. 188-194, 2005.

[71] T. Johannes, M. R. Simurdiak and H. Zhao, "Biocatalysis," in *Encyclopedia of chemical processing*, S. Lee, Ed., New York, Taylor & Francis, pp. 101-110, 2006.

[72] A. Illanes, Enzyme Biocatalysis, Berlin: Springer, pp. 1-57, 2008.

[73] E. Ricca, B. Brucher and J. H. Schrittwieser, "Multi-enzymatic cascade reactions: overview and perspectives," *Advanced Synthesis & Catalysis,* vol. 353, pp. 2239-2262, 2011.

[74] C. H. Wong and G. M. Whitesides, Enzymes in synthetic organic chemistry, vol. 12, Oxford, UK: Tetrahedron organic chemistry series, Pergamon Press/Elsevier Science Ltd, pp. 131-194, 1994.

[75] P. E. Swanson, "Dehalogenases applied to industrial-scale biocatalysis," *Current Opinion in Biotechnology,* vol. 10, no. 4, pp. 365-369, 1999.

[76] R. A. Shenvi, D. P. O'Malley and P. S. Baran, "Chemoselectivity: the mother of invention in total synthesis," *Accounts of Chemical Research,* vol. 42, no. 4, pp. 530-541, 2009.

[77] G. P. Moss, "Enzyme nomenclature" in *Nomenclature Committee of the International Union of Biochemistry and Molecular Biology* (NC-IUBMB), E. C. Webb, Ed., , pp. 23-533 2014.

[78] W. Hummel and B. Riebel, "Isolation and biochemical characterization of a new NADH oxidase from *Lactobacillus brevis*," *Biotechnology Letters,* vol. 25, no. 1, pp. 51-54, 2003.

[79] L. G. Lee and G. M. Whitesides, "Enzyme-catalyzed organic chemistry: a comparison of strategies for in situ regneration of NAD from NADH," *Journal of American Chemical Society,* vol. 107, no. 24, pp. 6999-7008, 1985.

[80] W. Hummel, "Large-scale applications of NAD(P)-dependent oxidoreductases: recent developments," *Trends in Biotechnology,* vol. 17, no. 12, pp. 487-492, 1999.

[81] C. Nowak, B. Beer, A. Pick, T. Roth, P. Lommes and V. Sieber, "A water-forming NADH oxidase from *Lactobacillus pentosus* suitable for the regeneration of synthetic biomimetic cofactors," *Frontiers in Microbiology,* vol. 16, no. 6, Article 957, 2015.

[82] F. Hollmann, I. W. C. E. Arends and D. Holtmann, "Enzymatic reductions for the chemist," *Green Chemistry,* vol. 13, no. 9, pp. 2285-2313, 2011.

[83] B. R. Riebel, P. R. Gibbs and A. S. Bommarius, "Cofactor regeneration of both NAD^+ from NADH and $NADP^+$ from NADPH: NADH oxidase from *Lactobacillus sanfanciscensis*," *Advanced Synthesis & Catalysis,* vol. 345, no. 6-7, pp. 707-712, 2003.

[84] H.-L. Schmidt, W. Stöcklein, J. Danzer, P. Kirch and B. Limbach, "Isolation and properties of an H_20-forming NADH oxidase from *Streptococcus faecalis*," *European Journal of Biochemistry,* vol. 156, no. 1, pp. 149-155, 1986.

[85] B. R. Riebel, P. R. Gibbs, W. B. Wellborn and A. S. Bommarius, "Cofactor regeneration of NAD^+ from NADH: novel water-forming NADH oxidases," *Advanced Synthesis & Catalysis,* vol. 344, no. 10, pp. 1156-1168, 2002.

[86] T. D. Machajewski and C. H. Wong, "The catalytic asymmetric aldol reaction," *Angewandte Chemie International Edition,* vol. 39, no. 8, pp. 1352-1374, 2000.

[87] H. J. M. Gijsen and W. C. H., "Sequential three- and four-substrate aldol reactions catalyzed by aldolases," *Journal of the American Chemical Society,* vol. 117, no. 29, pp. 7585-7591, 1995.

[88] W. A. Greenberg, A. Varvak, S. R. Hanson, K. Wong, H. Huang, P. Chen and M. J. Burk, "Development of an efficient, scalable, aldolase-catalyzed process for enantioselective synthesis of statin intermediates," *Proceedings of the National Academy of Sciences,* vol. 101, no. 16, pp. 5788-5793, 2004.

[89] K. Fesko and M. Gruber-Khadjawi, "Biocatalytic methods for C-C bond formation," *ChemCatChem,* vol. 5, no. 6, pp. 1248-1272, 2013.

[90] W. D. Fessner, "Aldolases: enzymes for making and breaking C-C bonds," in *Asymmetric organic synthesis with enzymes*, V. Gotor, I. Alfonso and E. Garcia-Urdiales, Eds., Weinheim, Wiley-VCH, pp. 275319, 2008.

[91] J. Sukumaran and U. Hanefeld, "Enantioselective C-C bond synthesis catalysed by enzymes," *Chemical Society Reviews,* vol. 34, no. 6, pp. 530-542, 2005.

[92] P. Clapes, W.-D. Fessner, G. A. Sprenger and S. A. K., "Recent progress in stereoselective synthesis with aldolases," *Current Opinion in Chemical Biology,* vol. 14, no. 2, pp. 154-167, 2010.

[93] M. G. Silvestri, G. DeSantis, M. Mitchell and C.-H. Wong, " Asymmetric aldol reactions using aldolases," in *Topics in stereochemistry*, vol. 23, S. E. Denmark, Ed., New Jersey, John Wiley & Sons, 2003, pp. 267-342.

[94] L. Chen, D. P. Dumas and C. H. Wong, "Deoxyribose-5-phosphate aldolase as a catalyst in asymmetric aldol condensation," *Journal of American Society,* vol. 114, no. 2, pp. 741-748, 1992.

[95] H. Ma, "Aldolase for enzymatic carboligation, PhD," Uppsala University, Uppsala, 2015.

[96] M. H. Woo, M. S. Kim, N. Chung and J. S. Kim, "Expression and characterization of a novel 2-deoxyribose-5-phosphate aldolase from *Haemophilus influenzae* Rd KW20," *Journal of the Korean Society for Applied Biological Chemistry,* vol. 57, no. 5, pp. 655-660, 2014.

[97] V. Andrushko and N. Andrushko, Eds., "Enzyme-catalyzed stereoselective C-C bond fomration reactions in total synthesis," in *Stereoselective synthesis of drugs and natural products*, New Jersey, John Wiley & Sons, pp. 831-908 2013.

[98] L. Salleron, G. Magistrelli, C. Mary, N. Fischer, A. Bairoch and L. Lane, "DERA is the human deoxyribose phosphate aldolase and is involved in stress response," *Biochimica et Biophysica Acta (BBA) - Molecular Cell Research,* vol. 1843, no. 12, pp. 2913-2925, 2014.

[99] J. Liu, C. C. Hsu and C. H. Wong, "Sequential aldol condensation catalyzed by DERA mutant Ser238Asp and a formal total synthesis of atorvastatin," *Tetrahedron Letters,* vol. 45, no. 11, pp. 2439–2441, 2004.

[100] C. L. Windle, M. Müller, A. Nelson and A. Berry, "Engineering aldolases as biocatalysts," *Current Opinion in Chemical Biology,* vol. 19, no. 1, pp. 25-33, 2014.

[101] Z. Y. You, Z. Q. Liu and Y. G. Zheng, "Characterization and application of a newly synthesized 2-deoxyribose-5-phosphate aldolase," *J Ind Microbiol Biotechnol,* vol. 50, pp. 29-39, 2013.

[102] Z. Časar, "Historic overview and recent advances in the synthesis of super-statins," *Current Organic Chemistry,* vol. 14, no. 8, pp. 816-845, 2010.

[103] T. Y. Nara, H. Togashi, S. Ono, M. Egami, C. Sekikawa, Y. Suzuki, I. Masuda, J. Ogawa, N. Horinouchi, S. Shimizu, F. Mizukamia and T. Tsunoda, "Improvement of aldehyde tolerance and sequential aldol condensation activity of deoxyriboaldolase *via* immobilization on interparticle pore type mesoporous silica," *Journal of Molecular Catalysis B: Enzymatic,* vol. 68, no. 2, pp. 181-186, 2011.

[104] H. Sakuraba, K. Yoneda, K. Yoshihara, K. Satoh, R. Kawakami, Y. Uto, H. Tsuge, K. Takahashi, H. Hori and T. Ohshima, "Sequential aldol condensation catalyzed by hyperthermophilic 2-deoxy-D-ribose-5-phosphate aldolase," *Applied and Environmental Microbiology,* vol. 73, no. 22, pp. 7427-7434, 2007.

[105] H. J. M. Gijsen and C. H. Wong, "Unprecedented asymmetric aldol reactions with three aldehyde substrates catalyzed by 2-deoxyribose-5-phosphate aldolase," *Journal of the American Chemical Society,* vol. 116, no. 18, pp. 8422-8423, 1994.

[106] C. F. Barbas, Y. F. Wang and C. H. Wong, "Deoxyribose-5-phosphate aldolase as a synthetic catalyst," *Journal of the American Chemical Society,* vol. 112, no. 5, pp. 2013-2014, 1990.

[107] X. Garrabou, J. A. Castillo, C. Guérard-Hélaine, T. Parella, J. Joglar, M. Lemaire and P. Clapés, "Asymmetric self- and cross-aldol reactions of glycolaldehyde catalyzed D-fructose-6-phosphate aldolase," *Angewandte Chemie International Edition,* vol. 48, no. 30, pp. 5521-5525, 2009.

[108] A. K. Samland and G. A. Sprenger, "Synthetic potential of dihydroxyacetone-utilizing aldolases," in *Industrial biocatalysis*, vol. 1, P. Grunwald, Ed., Florida, Taylor & Francis Grouo, pp. 783-816, 2015.

[109] D. Ager, Ed., Handbook of Chiral Chemicals, second ed., Florida: Taylor & Francis Group, pp. 2-8, 2005.

[110] S. Fetzner and F. Lingens, "Bacterial dehalogenation: biochemistry, genetics, and biotechnological applications," *Microbiological Reviews,* vol. 58, no. 4, pp. 641-685, 1994.

[111] M. Schallmey, J. Koopmeiners, E. Wells, R. Wardenga and R. Schallmey, "Expanding the halohydrin dehalogenase enzyme family: identification of novel enzymes by database mining," *Applied and Environmental Microbiology,* vol. 80, no. 23, pp. 7303-7315, 2014.

[112] J. E. T. van Hylckama Vlieg, L. Tang, J. H. Lutje Spelberg, T. Smilda, G. J. Poelarens, T. Bosma, A. E. J. von Merode, M. W. Fraaije and D. B. Janssen, "Halohydrin dehalogenases are structurally and mechanistically related to short-chain dehydrogenases/reductases," *Journal of Bacteriology,* vol. 183, no. 17, pp. 5058-5066, 2001.

[113] L. Tang, J. H. Lutje Spelberg, M. W. Fraaije and D. B. Janssen, "Kinetic mechanism and enatioselectivity of halohydrin dehalogenase from *Agrobacterium radiobacter*," *Biochemistry* , vol. 42, no. 18, pp. 5378-5386, 2003.

[114] M. Schallmey, R. J. Floor, B. hauer, M. Breuer, P. A. Jekel, H. J. Wijma, B. Dijkstra and D. B. Janssen, "Biocatalytic and structural properties of a highly engineered halohydrin dehalogenase," *ChemBioChem,* vol. 14, no. 7, pp. 870-881, 2013.

[115] D. J. Hardman and J. H. Slater, "Dehalogenases in soil bacteria," *Journal of General Microbiology,* vol. 123, no. 1, pp. 117-128, 1981.

[116] L. Tang, Y. Li and X. Wang, "A high-throughput colorimetric assay for screening halohydrin dehalogenase saturation mutagenesis library," *Journal of Biotechnology,* vol. 147, no. 3-4, pp. 164-168, 2010.

[117] M. Schallmey, P. Jekel, L. Tang, M. Majerić Elenkov, H. W. Höffken, B. Hauer and D. B. Janssen, "A single point mutation enhances hydroxynitrile synthesis by halohydrin dehalogenase," *Enzyme and Microbial Technology,* vol. 70, no. 1, pp. 50-57, 2015.

[118] S.-Z. Wang, Y.-H. Zhang, H. Ren, Y.-L. Wang, W. Jiang and B.-S. Fang, "Strategies and perspectives of assembling multi-enzyme systems," *Critical Reviews in Biotechnology,* vol. 37, no. 8, pp. 1024-1037, 2017.

[119] C. Rodríguez, I. Lavandera and V. Gotor, "Recent advances in cofactor regeneration systems applied to biocatalyzed oxidative processes," *Current Organic Chemistry,* vol. 16, no. 21, pp. 2525-2541, 2012.

[120] M. M. Kayser, "'Designer reagents' recombinant microorganisms: new and powerful tools for organic synthesis," *Tetrahedron,* vol. 65, no. 5, pp. 947-974, 2009.

[121] B. Lin and Y. Tao, "Whole-cell biocatalysts by design," *Microbial Cell Factories,* vol. 16, no. 1, p. 106, 2017.

[122] S. Wenda, S. Illner, A. Mell and U. Kragl, "Industrial biotechnology - the future of green chemistry?," *Green Chemistry,* vol. 13, no. 11, pp. 3007-3047, 2011.

[123] R. Wichmann and Đ. Vasić-Rački, "Cofactor regeneration at the lab scale," *Adv Biochem Eng,* vol. 92, pp. 225-260, 2005.

[124] S. S. Wang and C.-K. King, "The use of coenzymes in biochemical reactors," *Advances in Biomedical Engineering,* vol. 12, no. 1, pp. 119-146, 1979.

[125] A. Vrsalović Presečki, K. Makovšek and Đ. Vasić-Rački, "Coenzyme regeneration in hexanol oxidation catalyzed by alcohol dehydrogenase," *Applied Biochemistry and Biotechnology,* vol. 16, no. 3, pp. 595-611, 2012.

[126] B. Gueke, B. Riebel and W. Hummel, "NADH Oxidase from *Lactobacillus brevis*: a new catalyst for regeneration of NAD," *Enzyme and Microbial Technology,* vol. 32, no. 2, pp. 205-211, 2003.

[127] P. Pollak, Fine chemicals: the industry and the business, New Jersey: John Wiley & Sons, pp. 1-27, 93-155, 176-186, 2011.

[128] A. K. Scott, "Stereoisomers and drug toxicity: the value of single stereoisomer therapy," *Drug Safety,* vol. 8, no. 2, pp. 149-159, 1993.

[129] K. Faber and R. Patel, "Chemical biotechnology. A happy marriage between chemistry and biotechnology: asymmetric synthesis via green chemistry," *Current Opinion in Biotechnology,* vol. 11, no. 6, pp. 517-519, 2000.

[130] T. R. Pedersen, J. Kjekshus, K. Berg, T. Haghfelt, O. Faergeman, K. Pyörälä, T. Miettinen, L. Wilhelmsen, A. G. Olsson and H. Wedel, "Randomised trial of cholesterol lowering in 4444 patients with coronary heart disease: the Scandinavian Simvastatin Survival Study (4S)," *The Lancet,* vol. 344, no. 8934, pp. 1383-1389, 1994.

[131] X.-C. Jiao, J. Pan, G.-C. Xu, X.-D. Kong, Q. Chen, Z.-J. Zhang and J.-H. Xu, "Efficient synthesis of a statin precursor in high space-time yield by a new aldehyde-tolerant aldolase identified from *Lactobacillus brevis*," *Catalysis Science & Technology,* vol. 5, no. 8, pp. 4048-4054, 2015.

[132] A. Čaušević-Ramosevac and S. Semiz, "Drug interactions with statins," *Acta Pharmaceutica,* vol. 63, no. 3, pp. 277-293, 2013.

[133] A. Patel and S. V. Pisklakov, "Statins as potentially neuroprotective agents: a review," *Journal of Anesthesia and Clinical Research,* vol. 3, no. 10, pp. 1-5, 2012.

[134] T. Vajdič, M. Ošlaj, G. Kopitar and P. Mrak, "Engineered, highly productive biosynthesis of artificial, lactonized statin side-chain building blocks: the hidden potential of *Escherichia coli* unleashed," *Metabolic Engineering,* vol. 24, no. 1, pp. 160-172, 2014.

[135] I. Buhaescu and H. Izzedine, "Mevalonate pathway: a review of clinical and therapeutical implications," *Clinical Biochemistry,* vol. 40, no. 9-10, pp. 575-584, 2007.

[136] R. F. da Costa, F. Valder, E. M. Bezerra, B. S. Cavada, E. W. S. Caetano, J. L. de Lima Filho and E. L. Albuquerque, "Explaining statin inhibition effectiveness of HMG-CoA reductase by quantum biochemistry computations," *Physical Chemistry Chemical Physics,* vol. 14, no. 4, pp. 1389-1398, 2012.

[137] R. Floor, "Efficient protein engineering by combining computational design and directed evolution, " Doctoral Thesis, Groningen: University of Groningen, Groningen, Netherlands, 2015.

[138] E. S. Istvan and J. Deisenhofer, "Structural mechanism for statin inhibition of HMG-CoA reductase," *Science,* vol. 292, no. 5519, pp. 1160-1164, 2001.

[139] H. M. Miziorko, "Enzymes of the mevalonate pathway of isoprenoid biosynthesis.," *Archives of Biochemistry and Biophysics,* vol. 505, no. 2, pp. 131-143, 2011.

[140] Z. Casar, "Historic overview and recent advances in the synthesis of super-statins," *Current Organic Chemistry,* vol. 14, no. 8, pp. 816-845, 2010.

[141] H. Fei, C. Zheng, X. Liu and Q. Li, "An industrially applied biocatalyst: 2-deoxy-D-ribose-5-phosphate aldolase," *Process Biochemistry,* vol. 63, no. 1, pp. 55-59, 2017.

[142] Q. Wu and J. Tao, "Biocatalysis," in *Green Techniques for Organic Synthesis and Medicinal Chemistry,* W. Zhang and B. Cue, Eds., Chichester, John Wiley & Sons, pp. 217-240, 2012.

[143] W. Greenberg, K. Wong, A. Varvak and R. V. Swanson, "Chemoenzymatic methods for the synthesis of statins and statin intermediates". International Patent WO 2004/027075 A2, Apr 1, 2004.

[144] F. Subrizi, M. Crucianelli, V. Grossi, M. Passacantando, G. Botta, R. Antiochia and R. Saladino, "Versatile and efficient immobilization of 2-deoxyribose-5-phosphate aldolase (DERA) on multiwalled carbon nanotubes," *ACS Catalysis,* vol. 4, no. 9, pp. 3059-3068, 2014.

[145] J. G. T. Kierkels, D. Mink, S. Panke, F. A. Lommen and D. Heemskerk, "Process for the preparation of 2,4-dideoxyhexoses and 2,4,6-trideoxyhexoses". International Patent WO 03/006656 A2, Jan 23, 2003.

[146] J. H. M. H. Kooistra, H. J. M. Zeegers, D. Mink and J. M. C. A. Mulders, "Process for the preparation of 2-(6-substituted-1,3-dioxane-4-yl)acetic acid derivatives". International Patent WO 02/06266 A1, Jan 24, 2002.

[147] W. Greenberg, M. J. Burk, A. Varvak and K. Wong, "Chemoenzymatic methods for the synthesis of statins and statin intermediates". United States Patent US 8,148,324 B2, Apr 3, 2012.

[148] P. Mrak, T. Zohar, M. Ošlaj and G. Kopitar, "Enzymatic synthesis of active pharmaceutical ingredient and intermediates thereof". United States Patent US 2013/0337485 A1, Dec 19, 2013.

[149] J. Koopmeiners, B. Halmschlag, M. Schallmey and A. Schallmey, "Biochemical and biocatalytic characterization of 17 novel halohydrin dehalogenases," *Applied Microbiology and Biotechnology,* vol. 100, no. 17, pp. 7517-7527, 2016.

[150] L. J. Giver, L. M. Newman, E. Mundorff, G. W. Huisman, S. J. Henne, J. Zhu, B. Behrouzian, J. H. Grete and J. Lalonde, "Ketoreductase enzymes and uses thereof". United States Patent US 2008/0248539 A1, 9 October 2008.

[151] L. J. Giver, L. M. Newman, E. Mundorff, G. W. Huisman, S. J. Jenne, J. Zhu, B. Behrouzian, J. H. Grete and J. Lalonde, "Polynucleotides encoding ketoreductases for producing stereoisomerically pure statins and synthetic intermediates therefor". United States Patent US 2013/0040364 A1, Feb 14, 2013.

[152] D. Mink, J. H. Lutje Spelberg and E. J. De Vries, "Process for the preparation of epoxide intermediates for pharmaceutical compounds such as statins". International Patent WO/2007/137816 A1, Dec 6, 2007.

[153] Đ. Vasić-Rački, Z. Findrik and A. Vrsalović Presečki, "Modelling as a tool of enzyme reaction engineering for enzyme," *Applied Microbiology and Biotechnology*, vol. 91, no. 4, pp. 845-856, 2011.

[154] J. M. Brass, F. W. J. M. M. Hoecks and M. Rohner, "Application of modeling techniques for the improvement of industrial bioprocesses," *Journal of Biotechnology*, vol. 59, no. 1-2, pp. 63-72, 1997.

[155] G. Sin, J. M. Woodley and K. V. Gernaey, "Application of modeling and simulation tools for the evaluation of biocatalytic processes: a future perspective," *Biotechnology Progress,*, vol. 25, no. 6, pp. 1529-1538, 2009.

[156] Đ. Vasić-Rački, "Biokemijsko inženjerstvo," *Kemija u industriji*, vol. 39, no. 10, pp. 459-467, 1990.

[157] E. F. Murphy, S. G. Gilmour and M. J. C. Crabbe, "Effective experimental design: enzyme kinetics in the bioinformatics era," *Drug Discovery Today*, vol. 7, no. 20, pp. s187-s191, 2002.

[158] A. R. Tzafriri, "Michaelis-Menten kinetics at high enzyme concentrations," *Bulletin of Mathematical Biology*, vol. 65, no. 6, pp. 1111-1129, 2003.

[159] P. K. Robinson, "Enzymes: principles and biotechnological applications," *Essays in Biochemistry*, vol. 59, pp. 1-41, 2015.

[160] T. P. Kenakin, "Chapter 6 - Enzymes as Drug Targets," in *Pharmacology in drug discovery: understanding drug response*, London, Academic Press, pp. 105-124, 2012.

[161] L. Michaelis and M. L. Menten, "Die Kinetik der Invertinwirkung," *Biochemische Zeitschrift*, vol. 49, pp. 333-369, 1913.

[162] M. Vijayalakshmi, Michaelis Menten Kinetics, NPTEL – Biotechnology – Systems Biology, Joint Initiative of IITs and IISc, Funded by MHRD , lecture materials, 2004.

[163] "The effect of substrate concentration on enzyme activity," University College London, [Online]. Available: https://www.ucl.ac.uk/~ucbcdab/enzass/substrate.htm. [Accessed Jan 24, 2019].

[164] D. S. Clark and H. W. Blanch, Biochemical Engineering, New York: Marcel Dekker, pp. 1-162, 1993.

[165] A. M. Westley and J. Westley, "Enzyme Inhibition in Open Systems," *Journal of Biological Chemistry*, vol. 271, no. 10, pp. 5347-5352, 1996.

[166] K. J. Laider and P. S. Bunting, The chemical kinetics of enzyme action, Oxford: Claderon Press, pp. 93-97, 1973.

[167] S. Li, F. Xi and L. Li, Reaction engineering, Oxford: Elsiver Inc., pp. 1-161, 2017.

[168] Z. Gomzi, Kemijski reaktori, Zagreb: HINUS, pp. 39, 345-349, 1998.

[169] M. T. Lundemo, "Bioprocess engineering for the application of P450s ," PhD Thesis, Technical University of Denmark, Lyngby, Denmark, 2015.

[170] U. Kragl, A. Gödde and C. Wandrey, "Repetitive batch as an efficient method for preparative scale enzymic synthesis of 5-azido-neuraminic acid and 15*N*-*L*-glutamic acid," *Tetrahedron: Asymmetry*, vol. 4, no. 6, p. 1193-1202, 1993.

[171] U. Saarela, K. Leiviskä and E. Juuso, "Modelling of a fed-batch fermentation process," Report A No. 21, June 2003, Control Engineering Laboratory, University of Oulu.

[172] T. Yamanè and S. Shimizu, "Fed-batch techniques in microbial processes," in *Bioprocess Parameter Control*, vol. 30, A. Fiechter, Ed., Berlin, Springer, pp. 147-194, 1984.

[173] V. Kosar, Reaktori i bioreaktori (1st part), lecturematerials,University of Zagreb, Zagreb, Croatia, 2017.

[174] A. Liese, Biological principles applied to technical asymmetric catalysis, vol. 7, Jülich: Forschungszentrum Jülich GmbH, pp. 1-14, 19-44, 119-134, 2003.

[175] A. Švarc, Z. Findrik Blažević, Đ. Vasić-Rački, A. Szekrenyi, W.-D. Fessner, S. J. Charnock and A. Vrsalović Presečki, "2-Deoxyribose-5-phosphate aldolase from *Thermotoga maritima* in the synthesis of a statin side-chain precursor: characterization, modeling and optimization," *Journal of Chemical Technology & Biotechnology,* vol. 94, no. 6, pp. 1832-1842, 2019.

[176] M. Eggink, M. Wijtmans, A. Kretschmer, J. Kool, H. Lingeman, I. J. P. de Esch, W. M. A. Niessen and H. Irth, "Targeted LC-MS derivatization for aldehydes and carboxylic acids with a new derivatization agent 4-APEBA," *Analytical and Bioanalytical Chemistry,* vol. 397, no. 2, pp. 665-675, 2010.

[177] Z. Chen, Y. Wang, H. Wang, S. Chen, Z. Lie, J. Li, W. Shu, J. Zhou, Z. Fang, Y. Zhang and M. Huang, "Simultaneous determination of valproic acid and 2-propyl-4-pentenoic acid for the prediction of clinical adverse effects in Chinese patients with epilepsy," *Seizure,* vol. 21, no. 2, pp. 110-117, 2012.

[178] S. Shukla, "A Bradford multiplexing method for protein estimation in fermented foods: soy sauces," *Bangladesh Journal of Pharmacology,* vol. 11, no. 1, pp. 24-27, 2016.

[179] Spinreact, "Quantitative determination of chloride ion," [Online]. Available: http://www.spinreact.com/files/Inserts/MD/BIOQUIMICA/MDBSIS10_CLORURO_2017.pdf . [Accessed Feb 12, 2019].

[180] D. Hampel, E. R. York and L. H. Allen, "Ultra-performance liquid chromatography tandem mass-spectrometry (UPLC-MS/MS) for the rapid, simultaneous analysis of thiamin, riboflavin, flavin adenine dinucleotide, nicotinamide and pyridoxal in human milk," *Journal of Chromatography B,* vol. 903, no. 1, pp. 7-13, 2012.

[181] R. Fontes, J. Meireles Ribeiro and A. Sillero, "Inhibition and activation of enzymes. The effect of a modifier on the reaction rate and on kinetic parameters," *Acta Biochemica Polonica,* vol. 47, no. 1, pp. 233-257, 2000.

[182] SCIENTIST handbook, Salt Lake City: Micromath, pp. 110-300, 1896-1995,.

[183] N. Stiti, I. O. Adewale, J. Petersen, D. Bartels and H. H. Kirch, "Engineering the nucleotide coenzyme specificity and sulfhydryl redox sensitivity of two stress-responsive aldehyde dehydrogenase isoenzymes of *Arabidopsis thaliana*," *Biochemical Journal,* vol. 434, no. 3, pp. 459-471, 2011.

[184] J. E. Jo, S. Mohan Raj, C. Rathnasingh, E. Selvakumar, W. C. Jung and S. Park, "Cloning, expression, and characterization of an aldehyde dehydrogenase from *Escherichia coli* K-12 that utilizes 3-hydroxypropionaldehyde as a substrate," *Applied Microbiology and Biotechnology,* vol. 81, no. 1, pp. 51-60, 2008.

[185] X. Li, Y. Li, D. Wei, P. Li, L. Wang and L. Feng, "Characterization of a broad-range aldehyde dehydrogenase involved in alkane degradation in *Geobacillus thermodenitrificans* NG80-2," *Microbiological Research,* vol. 165, no. 8, pp. 706-712, 2010.

[186] A. Takeuchi and I. Uritani, "Partial purification and characterization of aldehyde dehydrogenase from sweet potato roots," *Agricultural and Biological Chemistry,* vol. 45, no. 8, pp. 1753-1759, 1981.

[187] T. Liu, L. Hao, R. Wang and B. Liu, "Molecular characterization of a thermostable aldehyde dehydrogenase (ALDH) from the hyperthermophilic archaeon *Sulfolobus tokodaii* strain 7," *Extremophiles,* vol. 17, no. 1, pp. 181-190, 2013.

[188] A. Vrsalović Presečki, L. Pintarić, A. Švarc and Đ. Vasić-Rački, "Different strategies for multi-enzyme cascade reaction for chiral *vic*-1,2-diol production," *Bioprocess and Biosystems Engineering,* vol. 41, no. 6, pp. 793-802, 2018.

[189] B. Srinivasan and D. Bonvin, "Controllability and stability of repetitive batch processes," *Journal of Process Control,* vol. 17, no. 3, pp. 285-295, 2007.

[190] P. Tufvesson, J. Lima-Ramos, N. Al Haque, K. V. Gernaey and J. M. Woodley, "Advances in the process development of biocatalytic processes," *Organic Process Research & Development,* vol. 17, no. 10, pp. 1233-1238, 2013.

[191] I. M. Kuznetsova, K. K. Turoverov and V. N. Uversky, "What macromolecular lecular crowding can do to a protein," *International Journal of Molecular Sciences,* vol. 15, no. 12, pp. 23090-23140, 2014.

[192] A. C. Carvalho, T. d. S. Fonseca, M. C. de Mattos, M. d. C. de Oliveira, T. L. de Lemos, F. Molinari, D. Romano and I. Serra, "Recent advances in lipase-mediated preparation of pharmaceuticals and their intermediates," *International Journal of Molecular Sciences,* vol. 16, no. 12, pp. 29682-716, 2015.

[193] ACS, "What is Green Chemistry?," American Chemical Society, [Online]. Available: www.acs.org/content/acs/en/greenchemistry/what-is-green-chemistry.html. [Accessed Apr10, 2016].

[194] S. L. Y. Tang, S. R. L. and M. Poliakoff, "Principles of green chemistry: PRODUCTIVELY," *Green Chemistry,* vol. 7, pp. 761-762, 2005.

[195] K. E. Parent, "Cleaning up with atom economy," online materials, *Green Chemistry Institute American Chemical Society, Washington,* [Online]. Available: https://www.acs.org/content/dam/acsorg/greenchemistry/education/resources/cleaning-up-with-atom-economy.pdf. [Accessed Apr 10, 2016].

[196] C.-J. Li and B. M. Trost, "Green chemistry for chemical synthesis," *Proceedings of the National Academy of Sciences of the United States of America,* vol. 105, no. 36, pp. 13197-13202, 2008.

[197] M. Schürmann and G. A. Sprenger, "Fructose-6-phosphate aldolase is a novel class I aldolase from *Eschrichia coli* and is related to a novel group of bacterial transaldolases," *The Journal of Biological Chemistry,* vol. 276, no. 14, pp. 11055-11061, 2001.

[198] K. Faber, W.-D. Fessner and N. J. Turner, Eds., Biocatalysis in Organic Synthesis 2, vol. 2, Stuttgart: Georg Thieme Verlag, pp.1-92, 159-176, 313-334, 507-528, 2015.

[199] I. Sánchez-Moreno, L. Nauton, V. Théry, A. Pinet, J.-L. Petit, V. de Berardinis and A. K. Samland, "FSAB: a new fructose-6-phosphate aldolase from *Escherichia coli*. Cloning, over-expression and comparative kinetic characterization with FSAA," *Journal of Molecular Catalysis B: Enzymatic,* vol. 84, pp. 9-14, 2012.

[200] R. Huang, "Coenzyme engineering of NAD(P)-dependent dehydrogenases," PhD Thesis, Virginia Polytechnic Institute and State University, University in Blacksburg, Blacksburg, Virginia, USA, 2017.

[201] S. Datta, L. R. Christena and Y. R. S. Rajaram, "Enzyme immobilization: an overview on techniques and support materials," *3 Biotech,* vol. 3, no. 1, pp. 1-9, 2013.

[202] M. E. Hassan, T. M. Tamer and A. M. Omer, "Methods of enzyme immobilization," *International Journal of Current Pharmaceutical Review and Research,* vol. 7, no. 6, pp. 385-392, 2016.

[203] M. J. Krantz, J. Martin, B. Stimmel and M. C. P. Haigney, "Concerns about consensus guidelines for QTc interval screening in methadone treatment response," *Annals of Internal Medicine,* vol. 151, no. 3, pp. 218-219, 2009.

[204] M. J. Krantz, J. Martin, B. Stimmel, D. Mehta and M. C. P. Haigney, "QTc interval screening in methadone treatment," *Annals of Internal Medicine,* vol. 150, no. 6, pp. 387-395, 2009.

[205] G. DeSantis, J. Liu, D. P. Clark, A. Heine, I. A. Wilson and C. H. Wong, "Structure-based mutagenesis approaches toward expanding the substrate specificity of D-2-deoxyribose-5-phosphate aldolase," *Bioorganic & Medicinal Chemistry,* vol. 11, no. 1, pp. 43-52, 2003.

[206] J. Almquist, M. Cvijovic, V. Hatzimanikatis and J. Nielsen, "Kinetic models in industrial biotechnology - improving cell factory performance," *Metabolic Engineering,* vol. 24, pp. 38-60, 2014.

[207] W. H. Organisation, "Definition of active pharmaceutical ingredient," 2011. [Online]. Available: http://www.who.int/medicines/areas/quality_safety/quality_assurance/DefinitionAPI-QAS11-426Rev1-08082011.pdf. [Accessed Sept 2, 2018].

[208] Research and Markets (https://www.researchandmarkets.com), "Industrial enzymes - a global market overview," report ID: 4555807, Dublin, 2018.

[209] R. Roldán, I. Sanchez-Moreno, T. Scheid, V. Hélaine, M. Lemaire, T. Parella, P. Clapés, W.-D. Fessner and C. Guérard-Hélaine, "Breaking the dogma of aldolase specificity: simple aliphatic ketones and aldehydes are nucleophiles for fructose-6-phosphate aldolase," *Chemistry,* vol. 23, no. 21, pp. 5005-5009, 2017.

[210] "Wikimedia Commons," 6 Dec 2009. [Online]. Available: https://commons.wikimedia.org/wiki/File:Tlc_sequence.png. [Accessed Jan 24,2019].

[211] "Thin Layer Chromatography (TLC)," University of Colorado at Boulder, Department of Chemistry and Biochemistry, [Online]. Available: http://orgchemboulder.com/Technique/Procedures/TLC/TLC.shtml. [Accessed Jan 24, 2019].

[212] S. Millar, "Tips and Tricks for the Lab: Column Choices," ChemistryViews; Wiley-VCH Verlag GmbH & Co. KGaA, Weinheim, July 3, 2012. [Online]. Available: https://www.chemistryviews.org/details/education/2101817/Tips_and_Tricks_for_the_Lab_Column_Choices.html. [Accessed Dec 3, 2018].

[213] S. Millar, "Tips and Tricks for the Lab: Column Packing," ChemistryViews; Wiley-VCH Verlag GmbH & Co. KGaA, Weinheim, June 5, 2012. [Online]. Available: https://www.chemistryviews.org/details/education/2040151/Tips_and_Tricks_for_the_Lab_Column_Packing.html. [Accessed Dec 3, 2018].

[214] S. Millar, "Tips and Tricks for the Lab: Column Troubleshooting and Alternatives," ChemistryViews; Wiley-VCH Verlag GmbH & Co. KGaA, Weinheim, Aug 7, 2012. [Online]. Available: https://www.chemistryviews.org/details/education/2345141/Tips_and_Tricks_for_the_Lab_Column_Troubleshooting_and_Alternatives.html. [Accessed Dec 3, 2018].

[215] R. Singh, M. Kumar, A. Mittal and P. Kumar Mehta, "Microbial enzymes: industrial progress in 21st century," *3 Biotech,* vol. 6, no. 2, p. 174, pp. 1-15, 2016.

[216] J. M. Woodley, "Biocatalytic Process Development," in *Applied Bioengineering: Innovations and Future Directions*, Weinheim, Wiley-VCH, pp. 81-98, 2017.

7 APPENDIX

7.1 Calibration curves

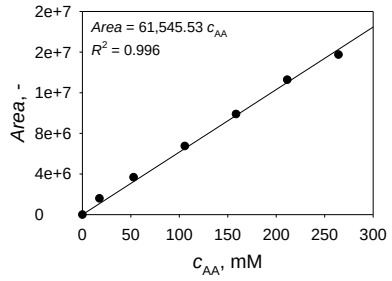

Appendix figure 1 Calibration curve for acetaldehyde (AA). HPLC analysis using Method 1. Retention time: 11.1 minutes. AA is commercially available.

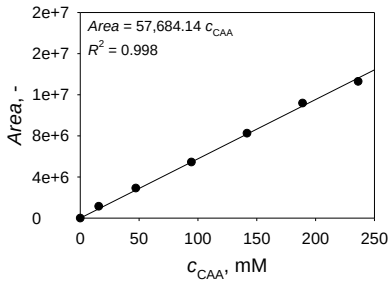

Appendix figure 2 Calibration curve for chloroacetaldehyde (CAA). HPLC analysis using Method 1. Retention time: 12.9 minutes. CAA is commercially available.

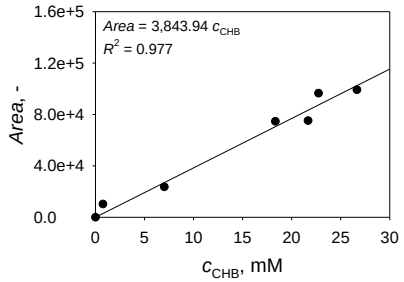

Appendix figure 3 Calibration curve for 4-chloro-3-hidroxybutanal (CHB). HPLC analysis using Method 1. Retention time: 10.4 minutes. The calibration curve was made based on the reaction scheme and mass balance equations. The reaction from which the data was used was the aldol reaction of AA with CAA catalyzed by D-fructose-6-phosphate aldolase (FSA) in 0.1 M TEA-HCl buffer pH 7 at 25 °C. The reaction was catalyzed in 1.5 mL-locking microcentrifuge tube used as a batch reactor placed on a shaker at 1 000 rpm. The total reaction volume was 0.5 mL. The reaction was carried out with 50 mM AA, 50 mM CAA and 3 mg/mL of FSA. The FSA is an enzyme that catalyzes the aldol addition of AA onto CAA to yield CHB. FSA was provided by Prof. P. Clapés, PhD from The Institute of Advanced Chemistry of Catalonia (IQAC-CSIC; Barcelona).

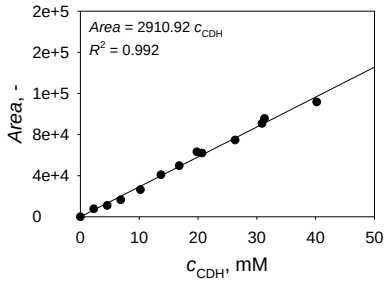

Appendix figure 4 Calibration curve for 6-chloro-3,5-dihidroxyhexanal (CDH). HPLC analysis using Method 1. Retention time: 9.3 minutes. The calibration curve was made based on the reaction scheme and mass balance equations. The reaction from which the data was used was the DERA^{Tm}-catalyzed reaction in 0.1 M TEA-HCl buffer pH 7. The reaction was conducted in 1.5 mL-locking microcentrifuge tube used as batch reactor. The total volume of the reaction was 0.5 mL. The reaction was carried out with 100 mM AA, 50 mM CAA and 2 mg/mL DERA^{Tm} at 25 °C. The reactor was placed on a shaker at 1 000 rpm.

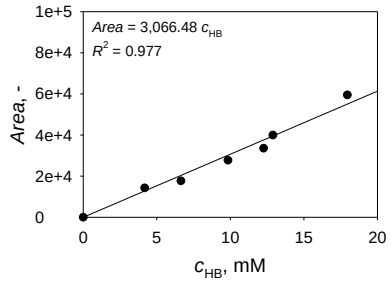

Appendix figure 5 Calibration curve for 3-hidroxybutanal (HB). HPLC analysis using Method 1. Retention time: 9.1 minutes. The calibration curve was made based on the reaction scheme and mass balance equations. The reaction from which the data was used was the aldol reaction of AA catalyzed by D-fructose-6-phosphate aldolase (FSA) in 0.1 M TEA-HCl buffer pH 7 at 25 °C. The reaction was catalyzed in 1.5 mL-locking microcentrifuge tube used as a batch reactor placed on a shaker at 1 000 rpm. The total reaction volume was 0.5 mL. The reaction was carried out with 50 mM AA and 2 mg/mL of FSA. The FSA is an enzyme that catalyzes the aldol addition of two molecules of AA to yield HB. FSA was provided by Prozomix Ltd (UK).

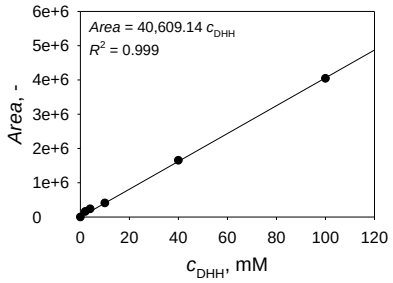

Appendix figure 6 Calibration curve for 3,5-dihidroxyhexanal (DHH). HPLC analysis using Method 1. Retention time: 10.2 minutes. The DHH standard was provided by Prof. W.-D. Fessner, PhD from Technische Universität Darmstadt (Germany).

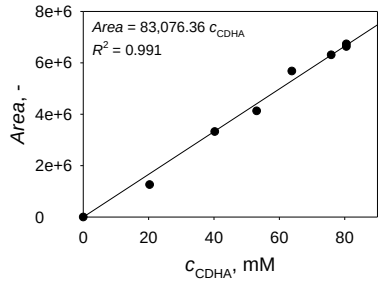

Appendix figure 7 Calibration curve for 6-chloro-3,5-dihidroxyhexanoic acid (CDHA). HPLC analysis using Method 1. Retention time: 9.9 minutes. The calibration curve was made using the experimental data from an experiment of AlDH-catalyzed oxidation of purified CDH. CDH was obtained following the procedure described in Chapter 3.3.4.2.

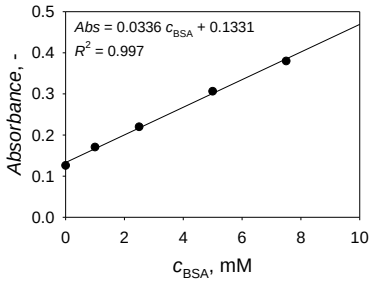

Appendix figure 8 Bovine serum albumin (BSA) calibration curve.

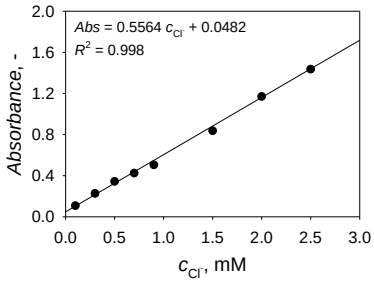

Appendix figure 9 Calibration curve for chloride ions.

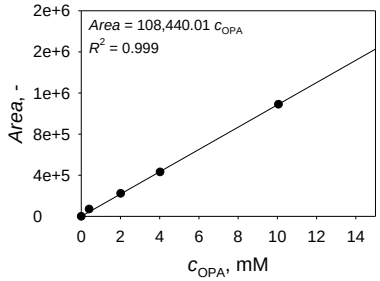

Appendix figure 10 Calibration curve for *N*-(3-oxopropyl)-2-phenylacetamide (OPA). HPLC analysis using Method 2. Retention time: 13.0 minutes. OPA was produced in the lab following a standard operating procedure provided by the CarbaZymes partners. Larger quantities of OPA were provided by M. Fekete, PhD from Enzymicals AG (Germany).

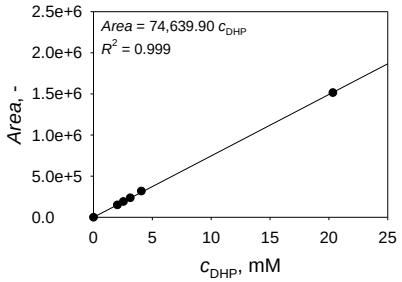

Appendix figure 11 Calibration curve for *N*-(2-((2*R*,4*R*)-4,6-dihydroxytetrahydro-2*H*-pyran-2-yl)ethyl)-2-phenylacetamide (DHP). HPLC analysis using Method 2. Retention time: 11.2 minutes. DHP was produced in lab following the procedure described in Chapter 4.2.4.1.

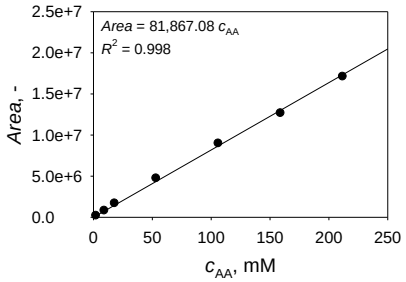

Appendix figure 12 Calibration curve for acetaldehyde (AA). HPLC analysis using Method 2. Retention time: 12.6 minutes. AA is commercially available.

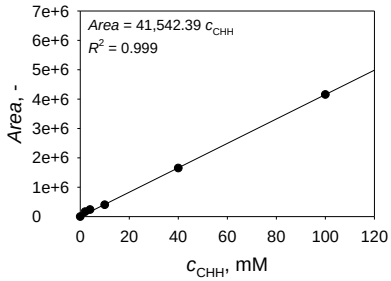

Appendix figure 13 Calibration curve for 3,5-dihidroxyhexanal (DHH). HPLC analysis using Method 2. Retention time: 10.2 minutes. The DHH standard was provided by Prof. W.-D. Fessner, PhD from Technische Universität Darmstadt (Germany).

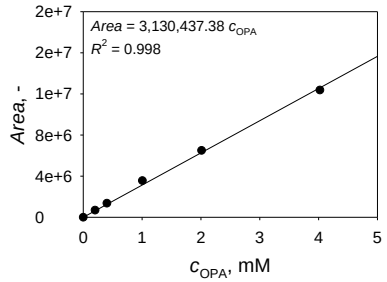

Appendix figure 14 Calibration curve for *N*-(3-oxopropyl)-2-phenylacetamide (OPA). HPLC analysis using Method 3. Retention time: 13.1 minutes. OPA was produced in the lab following a standard operating procedure provided by the CarbaZymes partners. Larger quantities of OPA were provided by M. Fekete, PhD from Enzymicals AG (Germany).

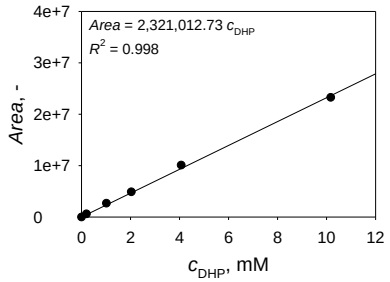

Appendix figure 15 Calibration curve for *N*-(2-((2*R*,4*R*)-4,6-dihydroxytetrahydro-2*H*-pyran-2-yl)ethyl)-2-phenylacetamide (DHP). HPLC Method 3. Retention time: 14.4 minutes. DHP was produced in lab following the procedure described in Chapter 4.2.4.1.

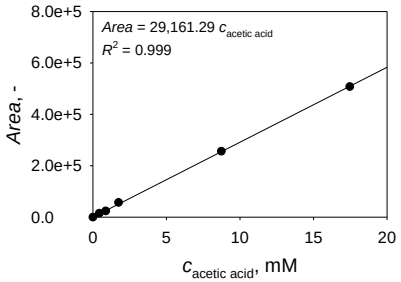

Appendix figure 16 Calibration curve for acetic acid. HPLC Method 3. Retention time: 1.9 minutes. Acetic acid is commercially available.

7.2 HPLC and LC-MS chromatograms

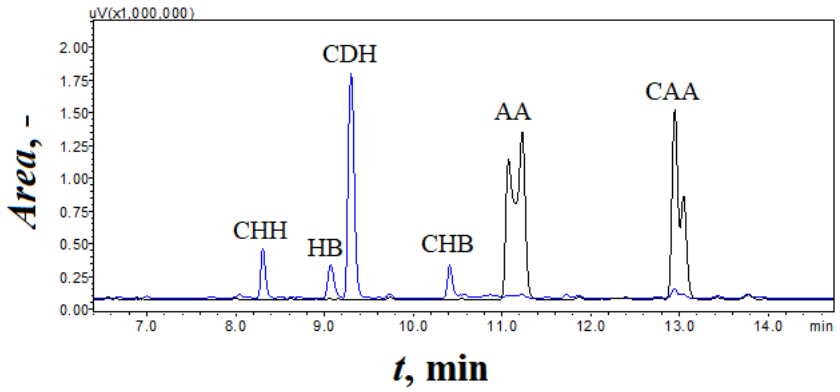

Appendix figure 17 Overlapped HPLC chromatograms that show 3,5-dihydroxyhexanal (DHH), 3-hidroxybutanal (HB), 6-chloro-3,5-dihydroxyhexanal (CDH), acetaldehyde (AA) and chloroacetaldehyde (CAA). The chromatograms represent experimental data obtained from a DERA-catalyzed aldol addition of AA with CAA. The black-colored chromatogram represents the CDH sample taken at the beginning of the reaction (t = 0 min), when only AA and CAA were present. The blue-colored chromatogram represents the DHP sample taken during the aldol addition, when certain amounts of DHH, HB, CDH and CHB were present. The retention times of AA, CAA, CHB and CDH were 11.1, 12.9, 10.4 and 9.3 minutes, respectively. The retention time of HB was 9.1 minutes, while of DHH 8.3 minutes.

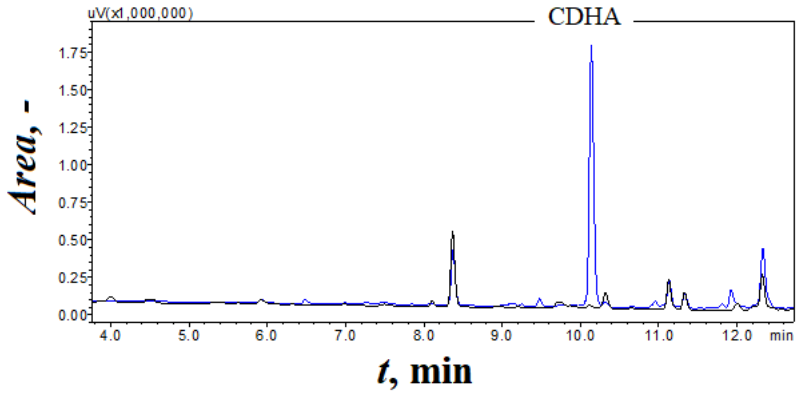

Appendix figure 18 Overlapped HPLC chromatograms that show 3-chloro-3,5-dihidroxyhexanoic acid (CDHA). The chromatograms represent experimental data obtained from a AlDH-catalyzed CDH oxidation. The black-colored chromatogram represents the CDHA sample taken at the beginning of the reaction (t = 0 min). The blue-colored chromatogram represents the CHDA sample taken during the oxidation. The retention time of the CDHA acid was 9.9 minutes.

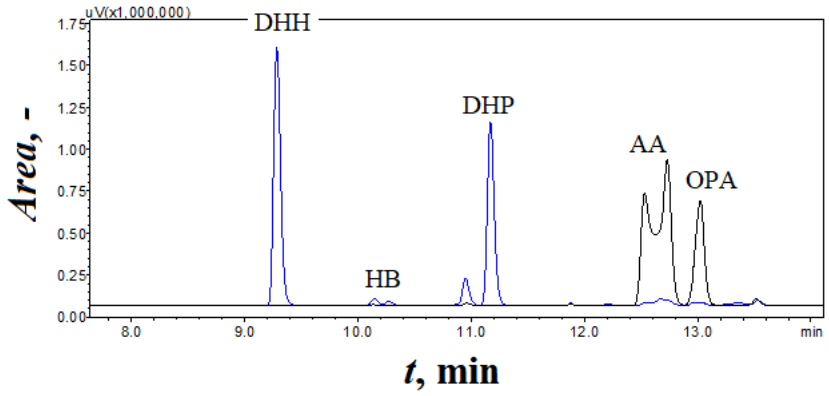

Appendix figure 19 Overlapped HPLC chromatograms that show 3,5-dihydroxyhexanal (DHH), 3-hidroxybutanal (HB, double-peak), *N*-(2-((2*R*,4*R*)-4,6-dihydroxytetrahydro-2*H*-pyran-2-yl)ethyl)-2-phenylacetamide (DHP), acetaldehyde (AA) and *N*-(3-oxopropyl)-2-phenylacetamide (OPA). HPLC analysis using Method 2. The chromatograms represent experimental data obtained from a DERA^{062}-catalyzed aldol addition of AA with OPA. The black-colored chromatogram represents the DHP sample taken at the beginning of the reaction (t = 0 min), when only AA and OPA were present. The blue-colored chromatogram represents the DHP sample taken during the aldol addition, when certain amounts of DHH, HB (double-peak) and DHP were present. The retention time of AA, OPA, DHP, HB and DHH were 12.6, 13.0, 11.2, 10.2 and 9.2 minutes, respectively.

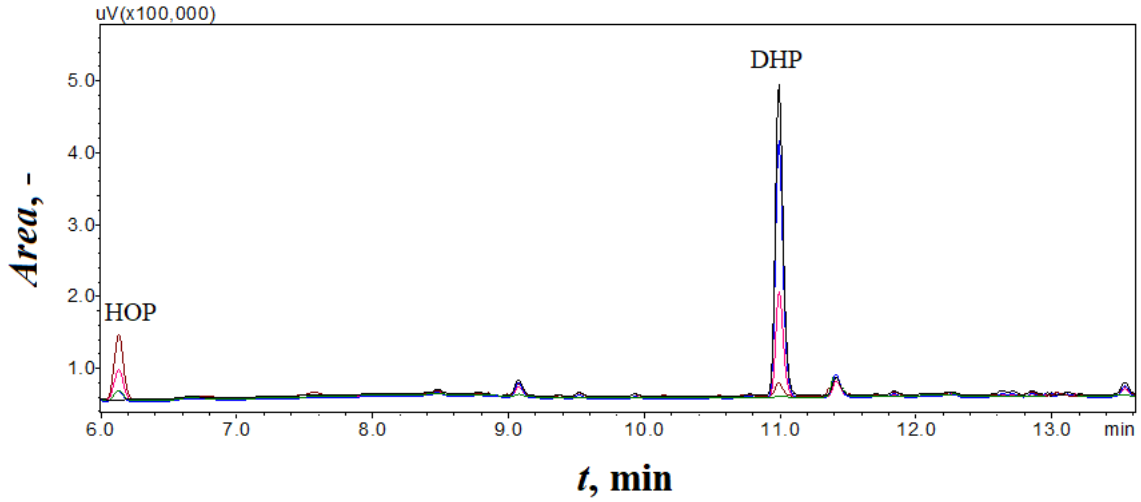

Figure 106 Appendix figure 20 Overlapped HPLC chromatograms that show *N*-(2-((2*R*,4*R*)-4,6-dihydroxytetrahydro-2*H*-pyran-2-yl)ethyl)-2-phenylacetamide (DHP) and *N*-(2-((2*R*,4*R*)-4-hydroxy-6-oxotetrahydro-2*H*-pyran-2-yl)ethyl)-2-phenylacetamide (HOP). HPLC analysis using Method 2. The chromatograms represent experimental data obtained from a KRED^{354}-catalyzed DHP oxidation. The black-colored chromatogram represents the HOP sample taken at the beginning of the reaction (t = 0 min), when only DHP was present. The remaining chromatograms, shown in color represent, the HOP samples taken during the DHP oxidation into HOP. The retention time of the HOP was 6.2 minutes, while of DHP was 11.2 minutes.

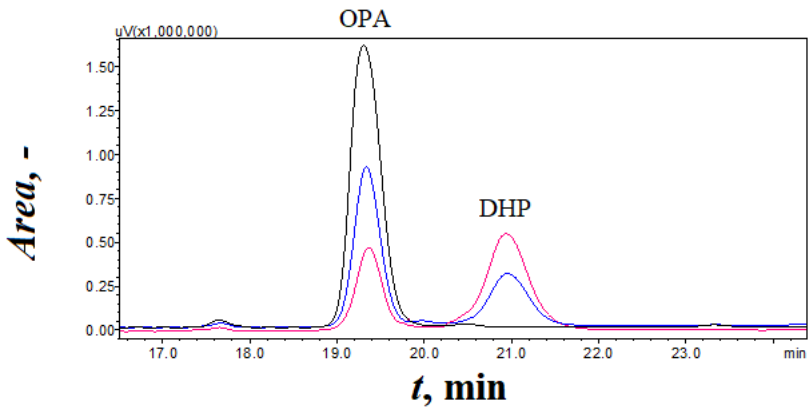

Appendix figure 21 Overlapped HPLC chromatograms that show *N*-(3-oxopropyl)-2-phenylacetamide (OPA) and *N*-(2-((2*R*,4*R*)-4,6-dihydroxytetrahydro-2*H*-pyran-2-yl)ethyl)-2-phenylacetamide (DHP). HPLC analysis using Method 3. The chromatograms represent experimental data obtained from a DERA^{062}-catalyzed aldol addition of AA onto OPA. The black-colored chromatogram represents the DHP sample taken at the beginning of the reaction (t = 0 min), when only OPA was present. The remaining blue- and pink-colored chromatograms show the DHP samples taken during the DHP synthesis. The retention time of OPA and DHP were 19.5 and 21.0 minutes, respectively.

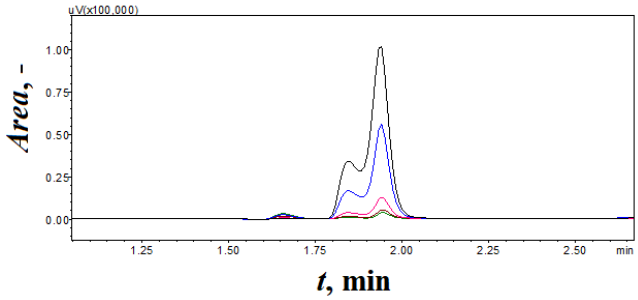

Appendix figure 22 Overlapped HPLC chromatograms for different concentrations of acetic acid visible as a double-peak. HPLC analysis using Method 3. Retention time .1.9 minutes.

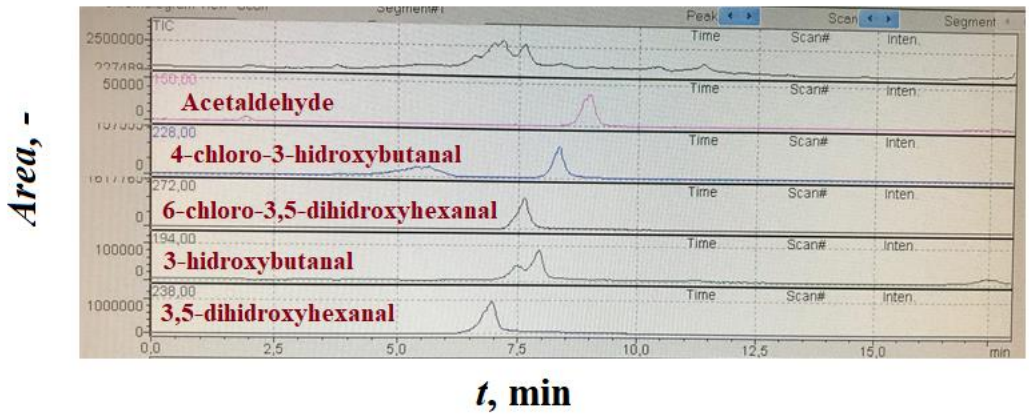

Appendix figure 23 LC-MS chromatograms for acetaldehyde, 4-chloro-3-hydroxybutanal, 6-chloro-3,5-dihydroxyhexanal, 3-hydroxybutanal and 3,5-dihydroxyhexanal. The LC-MS analysis of the derivatized products was done using the LC-MS analysis (Phenomenex Kinetex Core shell C18 column, 2.6 µm, 100 x 4.6 mm). HPLC with DAD and MS detection (Shimadzu LCMS-2020 single quadrupole liquid chromatograph mass spectrometer) was used. The selected ion monitoring method was used to confirm molecular weight of the derivatized peaks of formed products. The mobile phase consisted of solvent A (0.1% v/v formic acid in water) and solvent B (0.1% v/v formic acid in acetonitrile) with gradient elution from 90 to 19 %A for the first 10 minutes and from 19 to 90 %A from minute 14 to 16. The flow rate was 0.5 mL/min, the column temperature was set at 30 °C, and the UV detection at 215 nm. The mass spectrophotometer was equipped with electrospray ionization (ESI) source and operated in positive polarity mode. ESI conditions were capillary voltage 4 kV, nebulizing gas flow 1.5 L/min, drying gas flow 15 L/min, temperature 300 °C.

8 ABBREVIATIONS AND SYMBOLS

8.1 Abbreviations

AA	acetaldehyde
ACE	acetone
ACN	acetonitrile
AlDH	aldehyde dehydrogenase
API	active pharmaceutical ingredients
ATP	adenosine triphosphate
BSA	albumin from bovine serum
BY	substrate-to-enzyme ratio, g/g
CAA	chloroacetaldehyde
CDH	(3*R*,5*S*)-6-chloro-3,5-dihydroxyhexanal
CDHA	(3*R*,5*S*)-6-chloro-3,5-dihydroxyhexanoic acid
CFE	cell-free extract
CFU	Amicon ultra-centrifugal filter units
CHB	(*S*)-4-chloro-3-hydroxybutanal
CYDHA	(3*R*,5*S*)-6-cyano-3,5-dihydroxyhexanoic acid
DCM	dichloromethane
DERA	deoxyribose-phosphate aldolase (e.g. DERA^{Tm}, DERA^{024}, DERA^{062})
DH	dehydrogenase
DHH	(3*R*,5*R*)-3,5-dihydroxyhexanal

DHP	*N*-(2-((2*R*,4*R*)-4,6-dihydroxytetrahydro-2*H*-pyran-2-yl)ethyl)-2-phenylacetamide
DRP	2-deoxyribose 5-phosphate sodium salt
EC	enzyme commission (number)
EtOAc	ethyl acetate
EtOH	ethanol absolute
FAD	flavin adenine dinucleotide
FDF	final delivery form
FMN	flavin mononucleotide
GDH	glucose dehydrogenase
GDH	α-glycerophosphate dehydrogenase from rabbit muscle
HB	(*R*)-3-hydroxybutanal
HHDH	halohydrin dehalogenase
HMG-CoA	3-hydroxy-3-methylglutaryl coenzyme A
HOBA	(*R*)-3-hydroxy-4-((*S*)-oxiran-2-yl)butanoic acid
HOP	*N*-(2-((2*R*,4*R*)-4-hydroxy-6-oxotetrahydro-2*H*-pyran-2-yl)ethyl)-2-phenylacetamide
HPLC	high performance liquid chromatography
IPA	isopropanol
KRED	ketoreductase (e.g. $KRED^{332}$, $KRED^{354}$, $KRED^{011}$)
LDL-C	low-density lipoprotein cholesterol
MetOH	methanol
NAD^+	nicotinamide adenine dinucleotide, oxidized form
NADH	nicotinamide adenine dinucleotide phosphate, reduced form

$NADP^+$	nicotinamide adenine dinucleotide phosphate, oxidized form
NADPH	nicotinamide adenine dinucleotide phosphate, reduced form
NOX	NAD(P)H-dependent oxidase (e.g. NOX^{009}, NOX^{001})
NOX(AlDH)	NOX-acting enzymes in the AlDH CFE
NOX($KRED^{332}$)	NOX-acting enzymes in the $KRED^{332}$ CFE
NOX($KRED^{354}$)	NOX-acting enzymes in the $KRED^{354}$ CFE
OPA	*N*-(3-oxopropyl)-2-phenylacetamide
PA	propionaldehyde
R&D	research and development
STY	space-time yield, g/(L·day)
TEA-HCl	triethanolamine hydrochloride
TFA	trifluoroacetic acid
TPI	triosephosphate isomerase from rabbit muscle
Tris	tris(hydroxymethyl)aminomethane

8.2 Symbols

% *n*/*n*	molar percentage
% *v*/*v*	volume percentage
a	parameter of a polynomial model, mM^{-2} min^{-1} or min^{-1}
A_S	specific enzyme activity, U/mg
b	parameter of a polynomial model, mM^{-1} min^{-1}
c	molar concentration
d	parameter of a polynomial model, min^{-1}

d	diameter, mm
E_A	activation energy, J/mol
ee	enantiomeric excess, %
k	reaction rate constant, mL/(mg·mM·min) or mL/(mg·min)
K_A	activation constant, -
k_d	deactivation rate constant, min^{-1}
K_i	inhibition constant, mM ($mmol/dm^3$)
K_m	Michaelis constant, mM ($mmol/dm^3$)
m	mass, g
q	volumetric flow rate, mL/min
r	reaction rate, U/mL (mmol/mL·min)
R^2	coefficient of determination, -
T	temperature, °C
t	time, min or h
V	volume, mL
V_e	volume of the added enzyme, mL
V_m	maximum rate of reaction, U/mg (mmol/mg·min)
V_r	reactor volume, mL
V_{rn}	reaction volume, mL
w/*w*	mass fraction for mass percent, %
X	substrate conversion, %
Y	product yield, %

8.3 Greek alphabet letters and symbols

ρ density, g/mL

σ standard deviation, -

γ mass concentration, mg/mL

9 BIOGRAPHY

Anera Švarc [redacted] Showing strong keenness towards natural science, in 2009 she finished Fifth Gymnasium that is specialized in science and mathematics in Zagreb. Same year she enrolled at Faculty of Chemical Engineering and Technology, University of Zagreb and obtained her master's degree in 2014. While pursuing her studies, she was among top 10 % students which for she was honored with the *magna cum laude* diploma. During the period between 2012 and 2014 she was awarded with three Dean's Awards for her scientific work, was two-times granted with the academic merit scholarship from the City of Zagreb and in 2014 she participated with her teammates at the INOVA-Mladi winning the first place for their project prototype. During her studies she was awarded with the SIPGA and CEEPUS scholarships which enabled her to gain additional hands-on skills and knowledge by working as a research assistant intern at Institute for Molecular and Cell Biology (Singapore) and at the Department of Environmental Chemistry and Bioanalytics, Faculty of Chemistry, Nicolaus Copernicus University (Toruń, Poland).

In year 2015 she started working at the Department of Reaction Engineering and Catalysis at the Faculty of Chemical Engineering and Technology, University of Zagreb on the Horizon 2020's project CarbaZymes (coordinator: Prof. Wolf-Dieter Fessner, PI: Prof. Zvjezdana Findrik Blažević) involving processes based on a C-C bond-forming enzyme platform, where she became a PhD research assistant by enrolling in the PhD studies at the parent Faculty under the mentorship of prof. Vrsalović Presečki the same year. While pursuing her PhD and working on the CarbaZymes project, in order to widen her know-how and laboratory skills, she obtained a COST fellowship which enabled her to work as a PhD research assistant intern at the Institute for Biochemistry, Biotechnology and Bioinformatics, Technical University Braunschweig (Germany), and has finishing three biocatalysis-related summer schools abroad: two in Italy and one in Spain.

She currently works as a scientist, medicinal chemist at Fidelta Ltd.

She is fully proficient in English and German and has basic proficiency in Spanish.

At the time of writing (2019), she has published six papers in CC journals, one abstract in a CC journal and one paper in an open-access journal. She has participated at several national and international scientific conferences in the form of oral and poster presentations.

Journal articles:

1. **Švarc, Anera**; Skendrović, Dino; Vrsalović Presečki, Ana. Biocatalysis for the Production of Pharmaceutical Intermediates: The Statin Precursors, Kemija u industriji 68(9-10): 469-476 (2019)
2. **Švarc, Anera**; Findrik Blažević, Zvjezdana; Vasić-Rački, Đurđa; Szekrenyi, Anna; Fessner, Wolf-Dieter; Charnock, Simon J.; Vrsalović Presečki, Ana. 2-Deoxyribose-5-phosphate aldolase from *Thermotoga maritima* in the synthesis of a statin-side chain precursor: characterization, modelling and optimization, Journal of Chemical Technology and Biotechnology 94(6): 1832-1842 (2019)
3. Vrsalović Presečki, Ana; Pintarić, Lela; **Švarc, Anera**; Vasić-Rački, Đurđa. Different strategies for multi-enzyme cascade reaction for chiral *vic*-1,2-diol production, Bioprocess and Biosystems Engineering 41(6): 793-802 (2018)
4. **Švarc, Anera**; Valinger, Davor; Vasić-Rački, Đurđa; Vrsalović Presečki, Ana. Stereoselective synthesis of (1*S*,2*S*)-1-phenylpropane-1,2-diol by cell-free extract of *Lactobacillus brevis*, Green Processing and Synthesis 5(2): 153-161 (2016)
5. **Švarc, Anera**; Valinger, Davor; Vasić-Rački, Đurđa; Vrsalović Presečki, Ana. Stereoselective synthesis of phenylpropane 1,2-diols from (*S*)-2-hydroxypropiophenone by NADH-dependent oxidoreductases, Biochemical Engineering Journal 103: 250-255 (2015)
6. Grčić, Ivana; Kristan, Ekatarina, **Švarc, Anera**; Krčelić, Maja; Stefanović, Maja; Ježovita, Oskar; Vujević, Dinko; Anić Vučinić, Aleksandra; Koprivanac, Natalija. Methodology of strategic environmental assessment in Croatian radioactive management sector, The Holistic Approach to Environment 5(2): 83-103 (2015)
7. **Švarc, Anera**; Ukić, Šime; Radojević Lacković, Sandra; Đuričić, Biljana; Novak, Mirjana; Bolanča, Tomislav. Influence of ultrasonic and microwave irradiation on cation exchange properties of clay material, Chemical and Biochemical Engineering Quarterly 27(1): 29-35 (2013)

Published peer-reviewed conference abstracts in CC journals:

1. Vrsalović Presečki, Ana; Pintarić, Lela; **Švarc, Anera**; Vasić-Rački, Đurđa. Stereoselective diol production by multi-enzyme system, Abstracts / Journal of Biotechnology 256S (2017), pp S5–S16; European Biotechnology Congress 2017, Dubrovnik, Croatia, 25 - 27 May 2017

Published peer-reviewed conference abstracts:

1. Vrsalović Presečki, Ana; **Švarc, Anera**; Vasić-Rački, Đurđa; Hernandez, Karel; Clapés, Pere; Findrik Blažević, Zvjezdana. Model optimization of DERA-catalyzed double aldol addition. 9th International Congress on Biocatalysis, Hamburg, 2018.
2. **Švarc, Anera**; Vasić-Rački, Đurđa; Findrik Blažević, Zvjezdana; Hernandez, Karel; Clapés, Pere; Vrsalović Presečki, Ana. Mathematical modeling of DERA-catalyzed statin side-chain intermediate production. 9th International Congress on Biocatalysis, Hamburg, 2018.
3. **Švarc, Anera**; Gašpar, Kristina; Vasić-Rački, Đurđa; Findrik Blažević, Zvjezdana; Vrsalović Presečki, Ana. Modelling of lactol oxidation catalyzed by oxidoreductases. 12th Meeting of Young Chemical Engineers, Zagreb, 2018.
4. **Švarc, Anera**; Vasić-Rački, Đurđa; Findrik Blažević, Zvjezdana; Vrsalović Presečki, Ana. Mathematical modeling of lactone synthesis catalyzed by aldehyde dehydrogenase. 13th International Symposium on Biocatalysis and Biotransformations, Budapest, 2017.
5. Vrsalović Presečki, Ana; **Švarc, Anera**; Vasić-Rački, Đurđa; Findrik Blažević, Zvjezdana. Selection of optimal proccess design in the synthesis of statin intermediate. 13th International Symposium on Biocatalysis and Biotransformations, Budapest, 2017.
6. **Švarc, Anera**; Vasić-Rački, Đurđa; Findrik Blažević, Zvjezdana; Vrsalović Presečki, Ana. Mathematical modelling of lactol synthesis catalyzed by 2-deoxyribose-5-phosphate aldolase. 25th Croatian meeting of chemists and chemical engineers, Poreč, 2017.
7. **Švarc, Anera**; Česnik, Morana; Sudar, Martina; Vrsalović Presečki, Ana; Vasić-Rački, Đurđa; Findrik Blažević, Zvjezdana. The investigation of the stability of 2-deoxyribose-5-phosphate aldolase. 11th Meeting of Young Chemical Engineers, Zagreb, 2016.
8. Česnik, Morana; **Švarc, Anera**; Sudar, Martina; Vrsalović Presečki, Ana; Vasić-Rački, Đurđa; Findrik Blažević, Zvjezdana. Intermediate isolation in the synthesis of statin side chains. 11th Meeting of Young Chemical Engineers, Zagreb, 2016.
9. **Švarc, Anera**; Valinger, Davor; Vasić-Rački, Đurđa; Vrsalović Presečki, Ana. Stereoselective synthesis of chiral 1,2-diols from (S)-2-hydroxypropiophenone by alcohol and glycerol dehydrogenases with coenzyme regeneration. 24th Croatian meeting of chemists and chemical engineers, Zagreb, 2014.
10. **Švarc, Anera**; Studzińska, Sylwia; Bolanča, Tomislav; Buszewski, Bogusław. Quantitative structure-retention relationship models for prediction of antisense oligonucleotides retention times in ultra-high performance liquid chromatography. X Konferencja

Chromatograficzna „Chromatografia – niezbędne narzędzie w nauce i technice”, Lublin, 2014.

11. **Švarc, Anera**, Vasić-Rački, Đurđa; Vrsalović Presečki, Ana. Application of various *Lactobacillus brevis* cell disruption methods in order to obtain maximal alcohol dehydrogenase activity. 8th International Conference on Breath Research & Cancer Diagnosis, Toruń, 2014.
12. **Švarc, Anera**; Valinger, Davor; Vasić-Rački, Đurđa; Vrsalović Presečki, Ana. 8th International Conference on Breath Research & Cancer Diagnosis. Mathematical modelling of production of (1*S*,2*S*)-1-phenylpropane-1,2-diol catalysed by alcohol dehydrogenase from *Lactobacillus brevis*. 8th International Conference on Breath Research & Cancer Diagnosis, Toruń, 2014.
13. **Švarc, Anera**; Valinger, Davor; Vasić-Rački, Đurđa; Vrsalović Presečki, Ana. Mathematical modelling of production of (1*S*,2*S*)-1-phenylpropane-1,2-diol catalysed by alcohol dehydrogenase from *Lactobacillus brevis*. 10th Meeting of Young Chemical Engineers, Zagreb, 2014.
14. **Švarc, Anera**; Đuričić, Biljana, Radojević Lacković, Sandra; Novak, Mirjana; Ukić, Šime; Bolanča, Tomislav. Determination of clay ion exchange capacity treated by ultrasonic and microwave irradiation. 9th Meeting of Young Chemical Engineers, Zagreb, 2012.
15. Bolanča, Tomislav; Ukić, Šime; Radojević Lacković, Sandra; Đuričić, Biljana; **Švarc, Anera**; Novak, Mirjana. Influence of ultrasonic and microwave irradiation on cation exchange properties of clay material. 3rd International Symposium on Environmental Management, Zagreb, 2011.

Master’s Thesis:

Švarc, Anera. Mathematical modelling of optically active diol production catalyzed by alcohol dehydrogenase in cell-free extract of *Lactobacillus brevis*. Faculty of Chemical Engineering and Technology, Department of Reaction Engineering and Catalysis, supervisor: Prof. Ana Vrsalović Presečki, PhD, Zagreb, 2014.

Bachelor’s Thesis:

Švarc, Anera. Development of artificial neural network model for prediction of microwaves and ultrasound clay activation. Faculty of Chemical Engineering and Technology, Department of Analytical Chemistry, supervisor: Prof. Tomislav Bolanča, PhD, 2012.